Hyaluronan (HA)-Regulation of Vascular Smooth Muscle Cell Phenotype and Vascular Calcification in Chronic Kidney Disease

Shrea Roy BTech MSc

Thesis presented for the degree of Philosophiae Doctor

2023

Cardiff University

Institute of Nephrology

School of Medicine

Heath Park

CF14 4XN

DEDICATION

I would like to dedicate this thesis to my family. They have always shown me unconditional love and support in everything I pursue in life.

ACKNOWLEDGEMENTS

First and foremost, I am extremely grateful to my supervisory team; Dr. Soma Meran, Professor Donald Fraser, and Dr. Anne-Catherine Raby for mentoring me throughout my PhD career. You have provided proper support and guidance in the conception and the development of this thesis. Soma, you have been both strict and caring when needed. I have learnt so much during the course of this PhD and my time in the UK, thank you for giving me the opportunity to be a part of your wonderful group. Thank you for shaping me into a scientist I am today. I will always remember the time I called you after returning from my secondment to give you the news of my stolen slides and because of a bad phone connection we could hear each other as chipmunks, and you thought I had been kidnapped (which thankfully you did not consider to be the better scenario).

Besides my supervisors, I would like to thank Dr. Robert Steadman for your insightful comments on my work, much needed guidance, kind-heartedness, and consistent encouragement which have helped me through this journey. I would remember all your stories from America and your swimming stories which I always eagerly awaited to hear from you every week. You would always guess what I would have for lunch, and I knew your after-swimming snacks because it would rarely change (I also know your favourite Weatherspoon's order!). Thank you for being there for me for every abstract and every poster and being so humble and kind to me always.

I would like to thank Dr. Irina Grigorieva, you were dependable for advice of all natures and your academic input to my work and personal life was hugely appreciated. Your treasured support which was really influential in shaping my experiment methods and critiquing my results. You are one of the best scientists I know, and you have inspired me every day, from your organisational skills to your scientific way of looking at things. I loved that fact that I could talk to you about everything from serious to fun conversations. I don't think I have bugged anyone so much in my life as much as I have bugged you and you were always so patient and helpful!

I would also like to thank Dr. Emma Woods; you have been a friend and guide from the very first day and was always there to help me with my stress. Having been so encouraging when my experiments would not work, although you were more stressed than me at times. I loved chatting with you on anything and everything and wished you stayed in WKRU though the whole length of my PhD. You were terribly missed!

I would also like to thank Professor. Timothy Bowen, Dr. Mario Labeta and Dr. Usman Khalid I am grateful for the advice you have provided me along the way whenever I presented in the lab meetings.

I would like to thank my research team of WKRU Esra, Morgane, Kim, Cheryl, Kate, Lucy, Dan, Lex, Leah, Chantal, Bnar, Yuehan, Sarah, Aeliya, Tanya, Shrinivas, Paolo, and Charlie for a cherished time spent together in the lab, and in social settings.

I am also grateful to Dr. Etto Eringa, Dr. Marc G Vervleot, Jamie from VU University of Amsterdam and Professor Leon Schurgers from MU Maastrict for their excellent *in vivo* models and for training me and giving me the opportunity to do my secondment in their respective labs. It was such an opportunity to learn, and you made me feel so welcomed during my stay in the Netherlands.

I had an enormous backing from both my dad (Sujit Roy), mom (Chaitalee Roy) and love from my brother (Sagnik Roy) and sister (Srishti Roy). You have provided me with unconditional support throughout my entire time in research, even if you didn't quite know what I was doing most of the time, you were patient when I rambled on the phone. You also nurtured me throughout the times I did not quite know what I was doing myself. You supported me through all my failures and encouraged me to try again in life. Thank you for always encouraging the best and reinforcing the importance of having a bit of time off work and your immense love. I would not be where I am today without you guys. Thanks for bringing the best out of me. Love you all loads!

My husband, Joshua Gibian, you have shared the journey with me, being my unrelenting source of encouragement. You have celebrated with me after each successful experiment and mourned with me with every failure. You have listened to my presentations and when I talk about my work and have made a huge effort to communicate with me about this research.

By this time, I am sure you will be able to take a quiz on calcification and hyaluronan. You have always provided a guided and objective source of calm throughout my times of doubt and a source of motivation when I became overwhelmed. I am forever grateful.

Last but not the least I would like to thank Marie Sklodowska Curie - IMPROVE PD ITN Scholarship for providing me with the funding, secondment, and training opportunities for the research. It also provided me with the opportunity to meet other PhD students and inspirational scientists and it has been a great privilege to be a part of this amazing collection of wonderfully talented people.

Summary

Vascular calcification (VC) is a powerful predictor of cardiovascular mortality and is prevalent among patients with chronic kidney disease (CKD), including those on dialysis, yet it lacks effective treatment. It can occur in two anatomical locations: intimal and medial layers. The transformation of vascular smooth muscle cells (VSMCs) into an osteoblastic phenotype within arterial walls is a key factor in the development of medial VC. Previous research has shown that the glycosaminoglycan hyaluronan (HA) in the extracellular matrix plays a vital role in cell phenotype regulation, in the contexts of cancer biology, stem cell biology, and epithelial-mesenchymal transition. While previous studies have shown increased expression of HA in non-CKD related VC, its role in controlling VSMC phenotype and osteogenic differentiation has not been explored.

This study aimed to investigate the role of HA in medial calcification. Both *in vivo* and *in vitro* models of medial calcification revealed a decrease in HA levels during VSMC osteogenic differentiation. Experiments involving HA degradation indicated that HA has an inhibitory effect on calcification. Additionally, the study examined HA-binding proteins such as TSG-6 and Versican, uncovering their roles in modulating HA and influencing VSMC differentiation. The research emphasized the significance of HAS isoenzymes in HA synthesis, with HAS1 and HAS2 overexpression demonstrating protective effects against calcification. However, HAS3 displayed complex effects on calcification, necessitating further exploration.

Inflammation plays a pivotal role in VC associated with CKD-related cardiovascular disease. In both in vivo and in vitro inflammation models, increased HA expression was observed, aligning with previous findings in atherosclerosis. Moreover, the study identified altered expression patterns of HA-binding proteins under inflammatory conditions.

In summary, this research illuminates the role of HA and its associated proteins in arterial calcification within CKD. It suggests that certain forms of HA in the media may have a protective effect, whereas consistently in the intima, HA is associated with exacerbated disease. This underscores the significance of specific HA-binding proteins and underscores the

need for further investigation into the intricate interplay between inflammation and calcification in CKD-related cardiovascular disease.

Presentations

Roy S., Grigorieva I., Steadman R., Fraser D., Raby A-C., Meran S. Hyaluronan (HA)- Dependent Regulation of Vascular Smooth Muscle Cell Phenotype and Vascular Calcification in Chronic Kidney disease patients, IMPROVE Peritoneal Dialysis, Cardiff, UK, 2020

Roy S., Grigorieva I., Steadman R., Fraser D., Raby A-C., Meran S. Hyaluronan (HA)- Dependent Regulation of Vascular Smooth Muscle Cell Phenotype and Vascular Calcification in Chronic Kidney disease patients, Infection and Immunity Meeting, Cardiff, UK, 2020

Roy S., Grigorieva I., Steadman R., Fraser D., Raby A-C., Meran S. Hyaluronan (HA)- Dependent Regulation of Vascular Smooth Muscle Cell Phenotype and Vascular Calcification in Chronic Kidney disease patients, IMPROVE Peritoneal Dialysis, Vienna, Austria, 2020 (remote)

Roy S., Grigorieva I., Steadman R., Fraser D., Raby A-C., Meran S. Hyaluronan (HA)- Dependent Regulation of Vascular Smooth Muscle Cell Phenotype and Vascular Calcification in Chronic Kidney disease patients, UK Kidney Week, Glasgow, UK, 2021 (poster, remote)

Roy S., Grigorieva I., Steadman R., Fraser D., Raby A-C., Meran S. Hyaluronan (HA)- Dependent Regulation of Vascular Smooth Muscle Cell Phenotype and Vascular Calcification in Chronic Kidney disease patients, Infection and Immunity Meeting, Cardiff, UK, 2021

Roy S., Grigorieva I., Steadman R., Fraser D., Raby A-C., Meran S. Hyaluronan (HA)- Dependent Regulation of Vascular Smooth Muscle Cell Phenotype and Vascular Calcification in Chronic Kidney disease patients, IMPROVE Peritoneal Dialysis, Heidelberg, Germany, 2021

Roy S., Grigorieva I., Steadman R., Fraser D., Raby A-C., Meran S. Hyaluronan (HA)- Dependent Regulation of Vascular Smooth Muscle Cell Phenotype and Vascular Calcification in Chronic Kidney disease patients, International Society for Hyaluronan Sciences, US, 2021 (poster, remote)

Roy S., Grigorieva I., Steadman R., Fraser D., Raby A-C., Meran S. Hyaluronan (HA)- Dependent Regulation of Vascular Smooth Muscle Cell Phenotype and Vascular Calcification in Chronic Kidney disease patients, IMPROVE Peritoneal Dialysis, Amsterdam, Netherlands, 2022

Roy S., Grigorieva I., Steadman R., Fraser D., Raby A-C., Meran S. Hyaluronan (HA)- Dependent Regulation of Vascular Smooth Muscle Cell Phenotype and Vascular Calcification in Chronic Kidney disease patients, Infection and Immunity Meeting, Cardiff, UK, 2022

Roy S., Grigorieva I., Steadman R., Fraser D., Raby A-C., Meran S. Hyaluronan (HA)- Dependent Regulation of Vascular Smooth Muscle Cell Phenotype and Vascular Calcification in Chronic Kidney disease patients, IMPROVE Peritoneal Dialysis, Keele, UK, 2022

Roy S., Grigorieva I., Steadman R., Fraser D., Raby A-C., Meran S. Hyaluronan (HA)- Dependent Regulation of Vascular Smooth Muscle Cell Phenotype and Vascular Calcification in Chronic Kidney disease patients, UK Proteoglycan and Glycosaminoglycan Meeting 2023 Leeds, UK, 2023

Roy S., Grigorieva I., Steadman R., Fraser D., Raby A-C., Meran S. Hyaluronan (HA)- Dependent Regulation of Vascular Smooth Muscle Cell Phenotype and Vascular Calcification in Chronic Kidney disease patients, International Society for Hyaluronan Sciences, Portland, USA, 2023

Roy S., Grigorieva I., Steadman R., Fraser D., Raby A-C., Meran S. Hyaluronan (HA)- Dependent Regulation of Vascular Smooth Muscle Cell Phenotype and Vascular Calcification in Chronic Kidney disease patients, UK Kidney Week, Bristol, UK, 2023 (poster)

Table of Contents

Abbreviations

α-SMA	A-smooth muscle actin
ACR	Albumin to creatinine ratio
agLDL	Aggregated low-density lipoprotein
ALPL	Alkaline phosphatase
APO E	Apolipoprotein E
ARS	Alizarin Red Standards
ATF4	Activating transcription factor 4
BHABP	Biotinylated hyaluronan binding protein
BMP-7	Bone morphogenic protein 7
BSA	Bovine serum albumin
Ca	Calcium
Ca/Ph	Calcium/Phosphate
CAC	Coronary artery calcium
Cbfa-1	Core binding factor-α1 gene
CD44	Cell surface adhesion receptor
CD44v7/8	Cell surface adhesion receptor variant 7/8
CEMIP	Cell migration inducing protein
CFM	Confocal microscopy
CKD	Chronic kidney disease
Col1a1	Type I collagen
CPP	Calciprotein particles

CRF	Chronic renal failure
CT	Threshold cycle
CVD	Cardiovascular disease
Da	Daltons
DMSO	Dimethyl sulphoxide
DNA	Deoxyribonucleic acid
ECM	Extracellular matrix
EDTA	Ethylenediaminetetraacetic acid
EGF	Epidermal growth factor
EMT	Epithelial-to-mesenchymal transition
ESRD	End stage renal disease
ESRF	End stage renal failure
ESKD	End stage kidney disease
eGFR	Estimated glomerular filtration rate
F-Actin	Filamentous actin
FBS	Fetal bovine serum
FCS	Fetal calf serum
FGF23	Fibroblast growth factor 23
g	Gravitational force
ga	Gauge
GAG	Glycosaminoglycan
GDP	Glucose degradation products

GFP	Green Fluorescent Protein
GFR	Glomerular filtration rate
GPI	Glycosylphosphatidylinositol
HA	Hyaluronan
HABP	Hyaluronan binding protein
HARE	HA receptor for endocytosis
HAS	Hyaluronan Synthase
HAS2AS1	HAS2 antisense-1
HD	Haemodialysis
HDL	High-density lipoprotein
HEK293	Human Embryonic Kidney cell line
HMW-HA	High molecular weight hyaluronan
HRP	Horseradish peroxidase
Hyal	Hyaluronidase
kDa	Kilo dalton
K/DOQI	Kidney Disease Outcomes Quality Initiative
I-α-I	Inter-alpha inhibitor
ICC	Immunocytochemistry
IgG	Immunoglobulin G
IFN-γ	Interferon gamma
IL-1β	Interleukin-1 beta

IL-6	Interleukin-6
LDL	Low-density lipoprotein
LMW-HA	Low molecular weight hyaluronan
LV	Left ventricular
LYVE-1	Lymphatic vessel endothelial HA receptor 1
MAPK	Mitogen-activated protein kinase
MGP	Matrix gla protein
mins	minutes
mL	millilitre
mM	Milli Molar
mmol/L	Millimoles per litre
MMP9	Matrix metallopeptidase 9
mRNA	Messenger RNA
MSC	Mesenchymal stem cell
Msx2	Msh Homeobox 2
Na+/K+ pumps	Sodium-potassium pumps
NEFRONA	National Observatory of Atherosclerosis in Nephrology
NFκβ	Nuclear factor kappa beta
ng	Nanograms
OC	Osteocalcin
OD	Optical density

OM	Osteogenesis induction medium
OPG	Osteoprotegerin
OPN	Osteopontin
ORF	Open reading frame
P	Phosphate
PBS	Phosphate buffered saline
PCR	Polymerase chain reaction
PD	Peritoneal dialysis
PDGF	Platelet-derived growth factor
PFA	Paraformaldehyde
Pit-1	Sodium-dependent phosphate cotransporter-1
Pit-2	Sodium-dependent phosphate cotransporter-2
PPi	Pyrophosphate
PTH	Parathyroid hormone
Q-PCR	Quantitative polymerase chain reaction
RANKL	Receptor activator of nuclear factor kappa beta
RHAMM	Hyaluronan-mediated motility receptor
RNA	Ribonucleic acid
RRT	Renal replacement therapy
RT	Reverse transcription
RT-qPCR	Real Time – quantitative polymerase chain reaction

RunX2	Runt-related transcription factor 2
S. D	Standard deviation
secs	seconds
SM-1/2	Smooth muscle myosin isoform 1/2
SM22α/β	Smooth muscle 22 alpha / beta
SMMHC	Smooth muscle myosin heavy chain
Sox9	SRY-Box transcription factor 9
SPAM1	Sperm adhesion molecule 1
SP7	Osterix
Src kinase	Proto-oncogene tyrosine-protein kinase Src
Strep-Hyal	Streptococcus hyaluronidase
TGF-β	Transforming growth factor beta
TMEM2	Transmembrane protein 2
TNF-α	Tumour necrosis factor alpha
TNFIP6	Tumour necrosis factor-α-induced protein 6
TSG-6	Tumour necrosis factor-α-stimulated gene/protein-6
VC	Vascular calcification
VCAN	Versican
VLDL	Very low-density lipoprotein
VSMC	Vascular smooth muscle cells
Vit K	Vitamin K

v/v	Volume by volume
w/o	With or without
w/v	Weight per volume
°C	Degree celsius
µL	Micro liter
µM	Micro molar
µm	micrometre
µg	microgram
%	Percentage
4MU	4-Methylumbelliferone

List of Figures

List of Table

Chapter 1

General Introduction

1.1 Overview of Chronic Kidney Disease

15% of the world's population is affected by chronic kidney diseases (CKD), making it a significant challenge for health organizations worldwide[1-3]. CKD has become a major health burden both in developing and developed countries due to the prevalence of diabetes, hypertension, and obesity and has been reported to increase by 32% in the last 10 years[1,4,5]. The prevalence of CKD is rising and is predicted to rise further. Cardiovascular disease (CVD) is the leading cause of mortality in CKD patients where patients often die of cardiovascular complications before they even reach End-Stage Renal Failure (ESRF)[6,7]. Even early and moderate CKD patients, as well as patients on dialysis, have markedly increased levels of cardiovascular morbidity and mortality compared with age-matched counterparts in the general population[8,9]. CVD is the most common cause of death in CKD and even early-stage CKD is associated higher risks of CVD[10].

The indicators of kidney damage are proteinuria (commonly using albumin to creatinine ratio, ACR and/or protein to creatinine ratio) and decreased renal function (below thresholds of GFR estimated from serum creatinine concentration). The National Kidney Foundation Kidney Disease Outcomes Quality Initiative introduced the classification and definition of CKD in 2002[11]. CKD is defined as a progressive decline in kidney function that persists for more than 3 months[11] and it is conventionally divided into 5 main stages Error! Not a valid bookmark self-reference. based on GFR (Glomerular Filtration Rate) measured[12,13]. Normal GFR is 130-120ml/min in adults and GFR lower than 60 ml/min indicates loss of normal kidney function[14].

Stage 1: - Reduced eGFR (>90ml/min) and structural abnormality in the kidney are observed. Signs of kidney damage could be protein in the urine (proteinuria) or blood in the urine (hematuria)[15-17]. Urea and creatinine levels are normal. This stage is diagnosed by kidney damage markers e.g., albuminuria (ACR > 3 mg/mol).

Stage 2: - More kidney damage with reduced function (60-89ml/min). Generally eGFR between 60-89ml/min means that the kidneys are healthy but in Stage 2 CKD suggests that there are other signs of kidney damage such as albuminuria or other physical damage[12]. Urea and creatinine levels, which affect GFR (the parameter which defines the kidney function for

clinicians), are mildly elevated. In this stage creatinine level, blood pressure is monitored, and damage markers are observed.

Stage 3: - This stage is characterized by moderately increased kidney damage and reduced GFR (30-59ml/min). As kidney function declines waste products can build up in the blood causing a condition known as “uremia.” In stage 3, a person is more likely to develop complications of kidney disease such as high blood pressure, anaemia (a shortage of red blood cells) and/or early bone disease[18].

Stage 4: - In this stage the kidney damage is severe with significant loss of function (GFR 15-29ml/min). Complications of kidney disease such as high blood pressure, anaemia, early bone disease, heart disease and other cardiovascular diseases are prevalent[12,18,19].

Stage 5: - End-Stage Renal Disease (ESRD) where the kidney function is severely impaired (GFR <15ml/min), where the kidneys are not working sufficiently to filter waste or extra fluid out of the blood. At this point, if appropriate the patient will need to be guided towards renal replacement therapies such as kidney transplantation and dialysis.

Prognosis of CKD by GFR and albuminuria categories: KDIGO 2012				Persistent albuminuria categories description and range		
				A1 Normal to mildly increased	A2 Moderately increased	A3 Severely increased
				<30 mg/g <3 mg/mmol	30–300 mg/g 3–30 mg/mmol	>300 mg/g >30 mg/mmol
GFR categories (mL/min/1.73 m²) description and range	G1	Normal or high	≥90			
	G2	Mildly decreased	60–89			
	G3a	Mildly to moderately decreased	45–59			
	G3b	Moderately to severely decreased	30–44			
	G4	Severely decreased	15–29			
	G5	Kidney failure	<15			

Table 1 CKD Classification based on Glomerular Filtration rate and Albuminuria

Green: low risk, Yellow: moderately increased risk, Orange: high risk, Red: very high risk[11,12]. The classification gives five GFR levels and three albuminuria levels. A diagnosis of CKD can be made in the presence of a glomerular filtration rate (GFR) <60 mL/min per 1.73 m^2 or in the presence of albuminuria >30 mg/24 h (marked in red)[20]. A person with G1 and G2 and A1 is indicated with green is considered to have low risk of kidney failure. A person at G5 with A3 is indicated with red and is at high-risk kidney failure. Figure taken from here[18] Andrassy KM et al. *Kidney International*. 2013.

1.2 End Stage Renal Disease (ESRD)

ESRD (CKD stage 5) indicates the requirement of Renal Replacement Therapy (RRT) to sustain life is imminent[18]. The RRT treatment options available to ESRD patients are Haemodialysis (HD), Peritoneal Dialysis (PD) and kidney transplantation. According to UK data in 2015, 67.3% of the patients were on HD, 18.4% on PD and 8.6% had a functioning transplant and 5.7% had died or stopped treatment by 90 days[21].

Dialysis remains the mainstream treatment for most ESRD patients. The patients are informed about the dialysis treatment options available to them so that they can make a choice of the

treatment they wish to receive depending on their lifestyles[22,23]. This is guided by their medical needs and background. Although kidney transplantation is the most desired and cost-effective outcome for patients with ESRD, there are several limitations to the access to transplantation worldwide mainly due to the supply of healthy kidney donors and suitability of recipients[24,25]. Not all patients are medically fit enough to have a transplant, so transplant is not an appropriate option for all patients, hence, many patients with ESRD will require treatment with dialysis. Patients with CKD as well as patients on HD and PD, have a high risk of cardiovascular morbidity and mortality; with cardiovascular health being one of the main barriers to an individual's suitability for kidney transplantation[26].

1.3 Peritoneal Dialysis (PD)

18% of ESRD patients in UK are using Peritoneal Dialysis (PD), as it is a well-established and effective form of treatment of RRT for ESRD patients[27]. Although studies have shown no survival differences between PD and HD, PD offers benefits in terms of being a modality that promotes better patient autonomy. It is also described as better preserving residual renal function which has been linked to linked to better survival[28]. PD is also more cost effective than HD and can be safely delivered at home as well as in other locations outside clinical environments and can be done as continuous dialysis throughout the day or overnight while the patient is asleep. The studies show that it is mostly opted for by Caucasians[29]. It is also seen as a common choice of patients with higher educational background, married, employed and cohabitating patients[30]. However, PD is underused compared to HD in UK, and there is a concerted effort to improve recruitment to PD programs in many areas of the country including in Wales[31-33].

During the coronavirus pandemic, PD was of particular relevance as a home therapy for ESRD. People with ESRD are often elderly with a multitude of comorbid conditions and also immunocompromised. Their mortality from Covid19 has been reported to be as high as 30%, and facilitating a home therapy that does not involved congregation of patients in haemodialysis facilities was protective to patients in terms of reducing virus transmission and allowing better opportunities for shielding and isolation[34].

Peritoneal Dialysis (PD) uses the peritoneal membrane for dialysis. This is a thin, naturally occurring membrane that surrounds the abdominal organs. It is highly vascular and therefore is ideal as a membrane through which biological by-products, water and electrolytes can be exchanged between the blood and any fluid infused into the peritoneal cavity. A permanent in-dwelling catheter allows sterile dialysis fluid to be instilled into the peritoneal cavity and this fluid removes water, solutes, and other by-products that are no longer filtered by the kidneys and diffuse into the fluid from the blood flowing through the peritoneal membrane. The dialysis fluid is eventually drained and replaced by fresh dialysate to repeat the process. Though PD is a popular technique, it has some limitations which can cause the technique to fail. The effectiveness of the treatment depends on the gradient concentration, membrane surface and permeability. Peritoneal fibrosis is one of the most serious complications among PD patients and it is caused by repeated infections and high levels of inflammation in the peritoneal membrane[35]. The use of bioincompatible PD solutions which are high in glucose, also play a role to alter the structure of peritoneal membrane and drive inflammation and peritoneal fibrosis[36]. Ultimately, ongoing peritoneal fibrosis leads to damage to the peritoneal membrane such that PD is no longer viable for that patient as a renal replacement therapy.

1.4 Systemic Inflammation in PD

Patients with CKD (and particularly patients on peritoneal dialysis) are well known to have elevated levels of systemic inflammation, with particularly elevated levels of the cytokines TGF-β1 and IL-6. Furthermore, numerous studies have shown a link between systemic inflammation and cardiovascular disease; and there are specific links between IL-6 and cardiovascular pathology in PD[37,38]. TGF-β1 and IL-6 are described as elevated in CKD and PD patients as in PD you get repeated peritoneal infection[39-42]. Recent reports suggest that systemic inflammation in CKD drives CVD[43,44].

1.5 Cardiovascular Pathology in patients with CKD

CVD and CKD are closely inter-related, where one organ causes dysfunction in the other. The mortality from CVD is 10 to 20 times higher in ESRD patients than in the general population[45]. These patients have a high prevalence of arrythmias and sudden cardiac death[46,47]. CKD also coexists with other cardiovascular factors such as dyslipidaemia, hypertension, and diabetes.

CKD is a powerful independent predictor of adverse prognosis following myocardial infarction[48,49], and coronary diseases[50,51]. Heart failure develops in patients even with low degree of CKD[52]. According to The National Observatory of Atherosclerosis in Nephrology (NEFRONA) at even early stages of CKD, there is increased the risk of atheromatous plaques[53]. ESRD patient also shows exaggerated atherosclerosis[54,55] and vascular calcification in arteries[56]. Hence, according to the Kidney Disease Outcomes Quality Initiative (K/DOQI) guidelines in 2005, all patients, regardless of symptoms, should undergo assessment for cardiovascular disease and risk factors for cardiovascular disease at the initiation of dialysis[57]. In addition, both intimal and medial arterial calcification was found in young and middle-aged dialysis patients who did not have any traditional risk factors for atherosclerosis[58].

Several studies in animal models also shows the link between CVD in CKD patients. Renal mass ablation in rats showed severe CVD complications by triggering left ventricular hypertrophy, fibrosis, and defective capillarization[59]. Apolipoprotein-E is the major cholesterol carrier; thus, apolipoprotein deficient mice are predisposed to atherosclerosis. In uremic apolipoprotein E–deficient (APO E −/−) mice[60,61] calcified lesions, plaque formation, and severe arterial damage was observed. In addition to this, CKD, enhanced the development of atherosclerosis and excessive calcification of atheromatous lesions[62]. In another study, it was shown that in uninephrectomised rats, myocardial infarction triggered a marked rise in albumin excretion rate and a simultaneous increase in focal glomerulosclerosis[63]. Cardiac function was impaired in an animal model of renal failure (5/6 nephrectomy) in rat[64]. Furthermore, microvascular abnormalities were observed in the heart, such as, aorta thickenings[65] and reduced capillary supply[59] in sub-totally nephrectomised rats.

Established treatments for atherosclerotic disease include: a) antiplatelet therapy, which helps to reduce risks of myocardial infarction by influencing the mechanisms that contribute to atherosclerosis b) lipid-lowering therapy (lowering of LDL to slow down or even reverse the cholesterol deposition in arteries) and c) percutaneous coronary angioplasty (intervention to open up narrow or blocked artery thus restoring coronary blood flow)[66,67]. Whilst these therapies work for atherosclerotic vascular disease in the general population, they appear to be less effective in managing cardiovascular disease in patients with CKD, and this is partly related to the prevalence of vascular calcification (VC) present in medial layer of arteries in CKD patients[68,69]. At the present time, there are no pharmacological therapies designed expressly for the treatment of VC, largely due to our limited understanding of the underlying disease mechanisms. Statins initially appeared promising as a means of preventing or reversing calcification in patients, based on the ability of these lipid-lowering drugs to reduce valve calcification in vitro[70,71] and in animal models[72-74]. However, unfortunately, that promise has not translated to a significant improvement in prospective clinical trials[75-77]. Specifically for VC, lowering calcium and therapy with phosphate binders do not work to mitigate the effects of artery calcification[78]. This strongly suggests that there must be 'missing links' in the disease connection between the heart and the kidney and is primarily thought to be because patients with CKD have a distinct underlying cardiovascular pathology different from that in the general population. My studies are going to focus on arterial pathology relevant to CKD patients on PD. The two main pathologies that exist in this context are exaggerated atherosclerosis and VC of arteries. As there is already a lot of literature on atherosclerosis as well as some treatments for atherosclerosis, my thesis will focus on understanding the mechanisms that drive VC as this is poorly understood and has no available therapies.

1.6 Types of VC (based on site and size)

VC is classified based on the site of calcification. Clinically, calcification of the blood vessels as well as cardiac tissues is classified into two different categories: Atherosclerotic or intimal calcification, and Medial artery calcification.

The cardiovascular disease present in the general population is characterized by lipid dysregulation, endothelial dysfunction and atherosclerotic plaque formation leading to narrowed blood vessels and myocardial ischaemia[79] **Figure 1 [A]**. Intimal calcification often coincides with atherosclerosis as both are pathological processes affecting the intimal layer of the vessel wall and initiate luminal narrowing. Intimal calcification refers to the build-up of calcified areas within atherosclerotic lesions.

In CKD, in addition to intimal calcification, there is prominent medial calcification. This is characterized by Vascular smooth muscle cells (VSMC) in the arterial media differentiating to osteoblast-like cells which release matrix vesicles containing calcium and phosphate into the stroma. This leads to deposition of a calcified matrix in the arterial media causing arterial stiffness[80,81], and in time, this leads to LVH [82-85] **Figure 1 [B]**.

In PD patients, medial calcification can often be found along the entire vascular tree and is worse in patients who are also diabetic[10,86]. Medial calcification is linked to aging and commonly found in peripheral arteries[87,88] and is prevalent in patients with diabetes and/or CKD. Interestingly, earlier literature suggests that medial remodelling or calcification precedes atherosclerosis at certain sites[89], and more recent data indicate an interaction between medial and intimal calcification, with both potentially impacting each other[90,91].

VC is further classified depending on the size of calcification. Intimal calcification involves the accumulation of different sizes of calcium deposits within atherosclerotic lesions, which can exist in micro- and macrocalcification forms. Microcalcification (<50 µm in diameter) are small calcium deposits that occur within the intima. Microcalcifications are often linked to reduced plaque stability making it prone to rapture, thus potentially promoting thrombus formation[92]. Conversely, macrocalcification, referring to large, calcified areas (>50 µm in diameter) that can occur in both the intima and the media. Macrocalcifications are typically seen in more advanced stages of atherosclerosis and has been associated with enhanced plaque stability, possibly influenced by statins that promote both plaque stabilization and increased intimal calcification[93-96].

Clinically, distinguishing between micro- and macrocalcification is challenging due to limited resolution in computed tomography (CT), which is around 200 µm[97]. The pattern of calcification in the intimal plaque is of importance: small, frequent, spotty calcifications are more often found in patients with an acute myocardial infarction or with unstable angina pectoris (chest pain or discomfort due to coronary heart disease), whereas the presence of extensive calcifications was highest in those with stable angina pectoris[98]. Additionally, VC's impact extends beyond size and pattern, with factors like density and location contributing to cardiovascular disease's pathogenesis. For instance, coronary artery calcium (CAC) volume is associated with CVD risk, while CAC density shows an inverse correlation with CVD risk[99]. Moreover, the location of calcium deposits within atherosclerotic plaques determines the plaque's vulnerability to rupture; deposits in the fibrous cap region may lead to plaque rupture whereas, calcium deposits that are located in the necrotic core do not seem to have significant an impact on plaque stability[100].

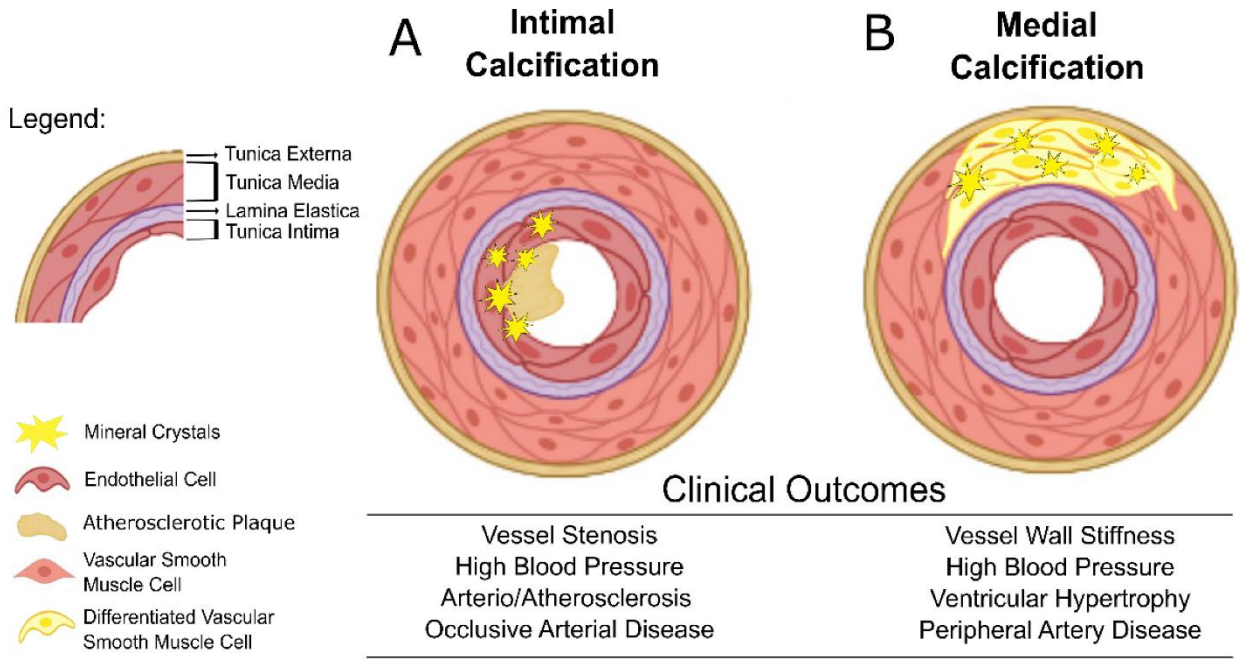

Figure 1 Intimal and medial Calcification

(A) Intimal Calcification is confined to the endothelium of the vessel and associated with atherosclerosis. Intimal calcification is characterised by microcalcification deposits within the fibrous caps of the atherosclerotic plaque, weakening the structure of the arterial wall and increasing the risk of plaque rupture[101,102]. (B) Medial Calcification affects the tunica media, the layer mainly composed of VSMCs, and it is strongly associated with CKD, aging and diabetes[103]. It is a

concentric process distinguished by macrocalcification, medial fibrosis, and arterial stiffness. Contractile, VSMCs exhibit a marked decrease in expression for VSMC-specific contractility markers but express more bone markers[104]. Figure taken from here[105] Marreiros C et al. *International Journal of Molecular Sciences*. 2022.

1.7 Anatomy of arteries and intimal and medial calcification

Arteries deliver oxygenated blood to tissue, and veins circulate deoxygenated blood back to the heart. Veins have thinner walls and deform more easily than arteries. Veins also lack the distinct molecular and tissue organization of arteries.

Arterial tissue is characterized by three distinct layers of tissue **Figure 2**. The arterial intima is composed of endothelial cells that form epithelium tissue on a basement membrane made of connective tissue and matrix molecules. This layer is in contact with blood and important for preventing thrombosis. Endothelial cells produce elastin molecules that contribute some elasticity to the vessel. Endothelial cells also produce laminin that functions in structural and organizational stability. The extracellular matrix of the intima consists of fibrillin microfibrils and collagen fibers. The intima is separated from the media by the internal elastic lamina. In atherosclerotic disease, it is generally the arterial intima that is distorted caused by endothelial dysfunction and intimal plaque formation.

The arterial media is the middle layer in arteries and contains a dense population of VSMCs organized concentrically with bands of elastic tissue. It contains the most elastin within the vessel and is rich in proteoglycans and other matrix molecules. The media maintains the structure of blood vessels, confers mechanical properties to blood vessels, including high elasticity and strength, and functions in the tolerance and regulation of blood pressure. These mechanical properties are important for the overall function of a vessel. The media is separated from the adventitia by the external elastic lamina.

The arterial adventitia is composed of multiple types of connective tissue. It contains a highly collagenous extracellular matrix that helps prevent vessel rupture at high pressure, fibroblasts, blood vessels, adipocytes, preadipocytes and nerves. Small blood vessels called

the vasa vasorum provide nourishment and oxygen to cells within the vessel wall. Adventitia also contributes rigidity and form to the blood vessel. In the event of serious arterial damage, mechanisms within the adventitia should cause coagulation. The collagen confers thrombogenic properties, leading to platelet adhesion and thrombus formation. Fibronectin, laminin, and thrombospondin can also promote platelet 4 adhesion. The expression of antithrombin III is reduced when the sub endothelium is exposed to blood components.

VC can occur in two areas in arteries. In the intima VC is associated with endothelial dysfunction and atherosclerotic plaque formation and this occurs in the general population as well as in CKD patients. VC can also occur in the arterial media, and this is specific to and highly prevalent in patients with CKD and therefore, the focus of this thesis will be the study of medial VC.

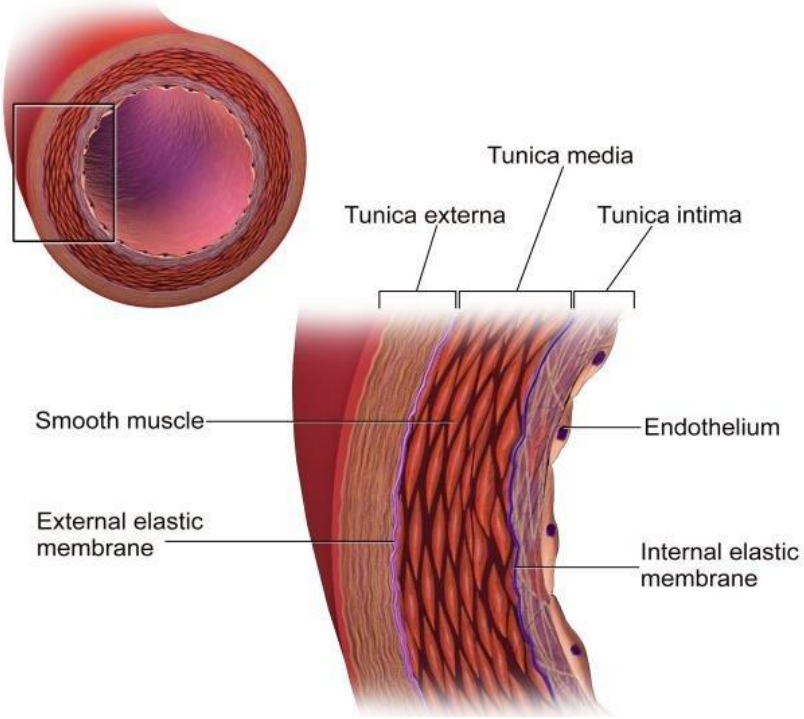

Figure 2 Multilayer anatomy of an arterial wall with tunica intima, media, and adventitia

Tunica Intima consists of endothelium, which is a single layer of squamous epithelium resting on a basement membrane. Tunica media or middle layer is composed of smooth muscle and elastic fibers. Tunica adventitia consists of fibroblasts and collagen fibers. The figure has been taken from here[106] Tyson J et al. *Bioengineering (Basel)*. 2020.

1.8 Medial vascular calcification

Vascular calcification (VC) in the arterial media is a controlled process where VSMCs change into bone-like cells, leading to the pathological deposition of calcium and phosphate in the arterial wall and resulting in vessel calcification[107]. This phenomenon is not limited to blood vessels and can also occur in other soft tissues like connective, cartilage, tendons, and epithelial tissues. Although VC is regarded as part of the normal aging process, certain pathological processes such as diabetes, hypertension, CKD, and or rare hereditary disorders can also precipitate the condition[108].

Serum levels of calcium and phosphate are tightly regulated by the digestive, endocrine, skeletal, and urinary systems. Calcium and phosphate are absorbed in the small intestine and stored in bones, cartilage, teeth, and other parts of the body. The skeletal system plays a significant role as a reservoir for calcium and phosphate, undergoing active bone turnover through osteoblastic (bone formation) and osteoclastic (bone resorption) activities. The kidneys play a significant role in regulating serum calcium and phosphate levels through active reabsorption or secretion[109,110]. Hormonal regulation by parathyroid hormone (PTH) and cholecalciferol (active vitamin D) also tightly controls these levels[111,112]. When there is dysregulation of calcium and phosphate, the ions can deposit on the extracellular matrix, forming crystals. This can lead to changes in cell phenotype, with VSMCs losing markers like SM22α and expressing osteogenic or chondrogenic markers[113]. Phosphate ions act as triggers for these changes in gene transcription, resulting in VSMC mineralization[114]. Elevated calcium levels can also induce mineralization by affecting VSMC phenotype through changes in phosphate sensitivity[107,115].

Many studies have shown the importance of VC in terms of cardiovascular mortality and morbidity. VC is seen early in the course of CKD[116], and is a strong predictor of cardiovascular mortality[117,118]. The phenomenon of VC, which includes calcification of intimal atheromatous plaque, medial calcification, and calcification of the aortic valve or mitral annulus, is a frequent consequence of CKD[119-122]. A meta-analysis found that patient with VC are at a 3-4 fold greater risk of cardiovascular events and all cause of cardiovascular mortality than patient with no VC[1]. The arterial stiffening associated with medial calcification promotes systolic

hypertension, increased pulse pressure, and ventricular hypertrophy[123]. Arterial stenosis of the aortic valve reflecting calcification put major load on the heart, which has been linked to stroke and cardiovascular mortality and this association needs further investigation[124-127]. In CKD patients, atherosclerotic lesions in the tunica intima are aggravated. They have increased in number and the lesions have a distinct morphology demonstrating a thicker and more calcified appearance than in the general population.

1.9 Molecular mechanism of VC

Throughout much of the 20th century, it was believed that VC was a passive process, involving the mere deposition of calcium phosphate products due to elevated levels circulating in the body. However, a significant shift in understanding has occurred over the past three decades, leading to a new consensus that VC is, in fact, an actively orchestrated biological phenomenon. Recent research has provided confirmation that VC can manifest even at normal serum levels of calcium and phosphate in individuals with diabetes[128], CKD[129], and/or atherosclerosis[55]. Nonetheless, the specific events that trigger calcification under these conditions remain largely unknown.

In light of clinical and basic studies, there have emerged four potential mechanisms of calcification that may be at play, and these mechanisms are not necessarily mutually exclusive[130]. They involve: 1) the reduction of inhibitory proteins and/or an increase in promoters of calcification, 2) induction of bone formation, 3) the presence of circulating nucleating complexes, and 4) apoptosis or programmed cell death. The next section provides a summarized overview of these mechanisms and their potential roles in VC. The Molecular mechanism of VC is summarised in the **Figure 3** and explained in detail in the later sections.

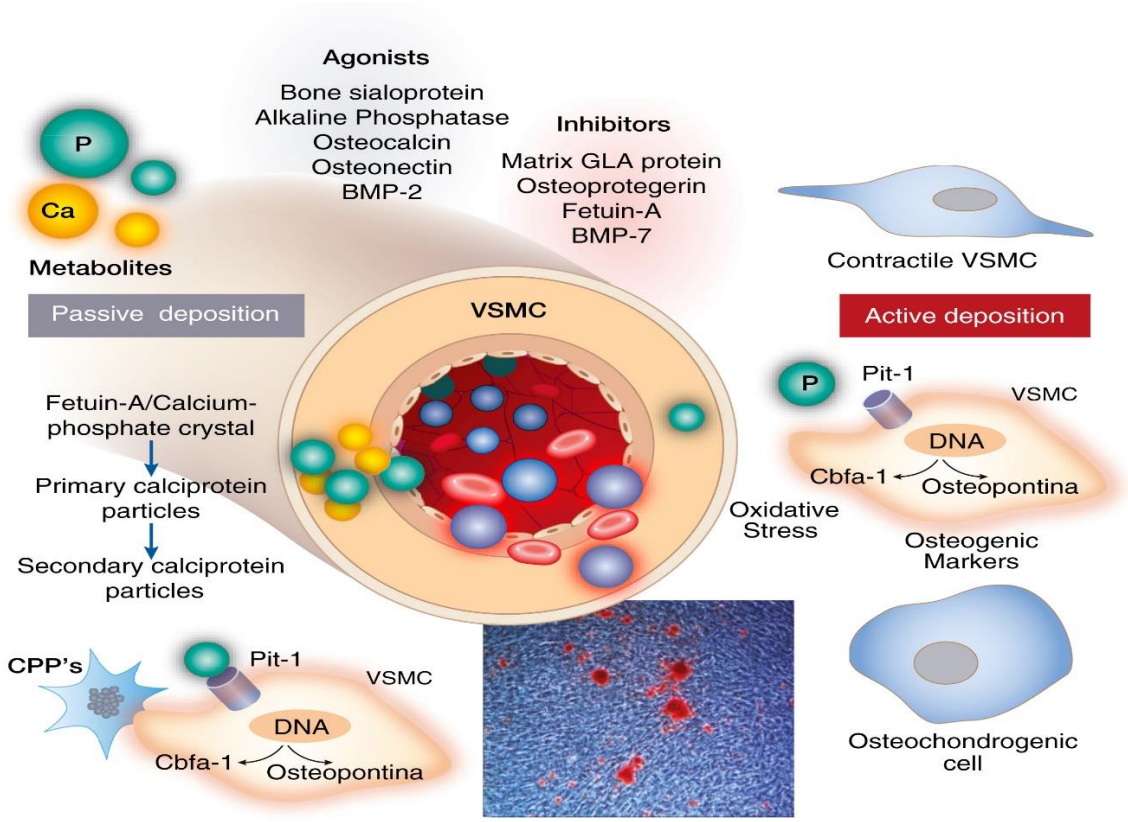

Figure 3 VSMC to osteoblasts

VSMCs become synthetically active and under stress factors, like elevated calcium and phosphate levels or uremic toxins (e.g., during CKD), switch to a dedifferentiated synthetic phenotype and later become osteoblast li.ke cells[131,132].In VC, the deposition of hydroxyapatite crystals along the vessel, decreases vessel flexibility, impairs proper blood flow and is associated with CVD mortality[133].In this figure, a schematic diagram (in the middle) of artery carrying red blood cells (in red) and leucocytes (in blue) along with the initiating ions, calcium (yellow) and phosphate (in green) is shown. The agonist and the inhibitors of vascular calcification process are shown on top of the artery. Bottom of the figure is a histological image of an arterial wall where the calcification is shown (in dark pink). On the right side, the contractile VSMC transforms into osteoblasts in the presence of osteoblastic markers, phosphate ions, oxidative stress and this shows active formation of calciprotein particles. Here phosphate is shown to enter through Pit-1 which promotes differentiation by upregulating core factor binding alpha-1 or RunX2 and osteopontin. On the left-hand side, the accumulation of calcium-phosphate crystal is mediated by Fetuin-A, which later forms primary calcium particles and later, secondary calcium particles and thus passive formation of calciprotein particle occurs. The figure is taken from here[130] Vervloet M et al. *Kidney Int*. 2017.

1.9.1 Loss of calcification Inhibitors

To prevent spontaneous calcification, the body contains inhibitors of calcification present in both the circulation and the vasculature. Two significant proteins with strong ion-binding capacity are fetuin-A and matrix Gla protein (MGP)[134,135].

a) Role of Feutin -A

Fetuin-A is a plasma protein primarily synthesized in the liver, playing a critical role in stabilizing protein-mineral complexes known as calciprotein particles (CPPs). The formation of CPPs helps prevent pathological deposition of calcium and phosphate in tissues, provided they are efficiently cleared from the circulation. Clearance of CPPs is attributed to liver Kupffer cells, and if this process is impaired, it may lead to particle-induced inflammation and VC[136]. Fetuin-A deficient mice on a DBA/2 genetic background exhibit extensive extraosseous calcification, especially in brown adipose tissue, skin, heart, lung, and kidney[137,138]. Mice lacking Fetuin A experience soft tissue and intravascular calcification, especially when exposed to Vitamin D[138]. A recent cross-sectional study in stable haemodialysis patients revealed that fetuin concentrations were significantly lower in those on dialysis and correlated with an increased risk of cardiovascular death[139]. Hence, fetuin deficiency may contribute to the excessive vascular calcification observed in patients with ESRD.

b) Role of MGP

Another essential protein associated with calcification is MGP, highly expressed in cartilage and VSMCs. It is a vitamin K-dependent protein, requiring vitamin K for its biological activity[135]. Studies in mice shows that when MGP is knocked out or when its activity is reduced in VSMCs, VC occurs in medial layers[140,141]. Moreover, overexpression of MGP in the APO E−/− mouse model of atherosclerosis reduced both intimal and medial calcification of atherosclerotic plaques whereas gene deletion of MGP in APO E−/− mice accelerated intimal calcification of plaques[142]. In an experimental mouse model of VC using MGP−/− mice, spontaneous VC occurs in mice older than 2 weeks of age[143]. Additionally, in older MGP−/− mice with advanced vascular calcification, clusters of cells with chondrocytes features were observed causing their death within the first two months of age[140,143]. Similarly, in patients,

the use of vitamin K antagonists has been linked to VC. MGP expression is increased in human atherosclerotic lesions and VSMCs are predominantly involved in intimal calcification[144,145].

Understanding these calcification inhibitors and their interactions is crucial for elucidating the complex mechanisms involved in vascular calcification and may have implications for developing potential therapeutic approaches to manage this process and associated cardiovascular conditions.

1.9.2 Induction of Bone formation

(a) VSMC Phenotyping Differentiation under high phosphate environments

Hyperphosphatemia refers to an abnormally high level of phosphate in the blood. It is often observed in patients with kidney disease, particularly those with ESRD[146]. Elevated serum phosphate poses a significant risk for VC and cardiovascular mortality in these patients[146,147]. While the thermodynamic relationship between Ca × P may contribute to calcification, emerging evidence suggests that the direct impact of elevated phosphate on vessel wall cells plays a more crucial role in regulating calcification propensity.

Studies have shown that heterogeneous, uncloned populations of VSMCs do not spontaneously mineralize in culture. However, when exposed to elevated phosphate levels similar to those found in hyperphosphatemic individuals (>2 mmol/L), these VSMCs can be induced to mineralize[148-151]. Under such conditions, the extracellular matrix surrounding the VSMCs undergoes calcification, exhibiting features similar to those seen in bone and pathological vascular calcification in vivo[139]. These features include the presence of calcifying collagen fibers, matrix vesicles, and bioapatite.

The change in VSMCs from a contractile state to an osteochondrogenic state due to elevated phosphate levels is different from the phenotypic alterations seen in arteries damaged by chemicals, disease, or trauma[152]. The osteochondrogenic state might be specifically designed to repair and adapt to a mineralizing microenvironment, involving the upregulation of mineral

regulating molecules like Osteopontin. Other molecules, that promote or inhibit VC such as elevated calcium and BMP-7, might also influence VSMC phenotypic changes[111,140].

Treatment with elevated phosphate leads to VSMCs undergoing a significant change in phenotype, where they lose smooth muscle lineage markers like smooth muscle (SM) α-actin and SM22α, and gain osteochondrogenic markers such as osteopontin, Cbfa-1/Runx2, alkaline phosphatase, and osteocalcin[150,153]. This pattern of gene expression is also observed in biopsy specimens from ESRD patients with calciphylaxis (calcium accumulates in small blood vessels of the fat and skin tissues) and calcified inferior epigastric arteries[153].

The phenotypic transition in response to elevated phosphate in VSMCs depends on the activity of sodium-dependent phosphate cotransporters in the cells. Sodium-dependent phosphate cotransporters use the sodium gradient to actively transport phosphate into the cell. Three types of these cotransporters have been identified, with type I and type II being expressed in the intestine and the kidney[154,155], whereas type III cotransporters, represented by Pit-1 and Pit-2, being expressed in human VSMCs[140]. These proteins are more ubiquitously expressed in tissues including kidney, heart, lung, brain, liver, and bone[156]. Inhibition of sodium-dependent phosphate transport, elevated phosphate-induced mineralisation, and the expression of RunX2 and ALPL[140,157,158]. Suppressing endogenous Pit-1 expression inhibits mineralization, while overexpressing either Pit-1 or Pit-2 rescues phosphate-induced mineralization in Pit-1-deficient cells[114]. Vasopressin has also been shown to induce VSMC mineralization through the enhancement of Pit-1's phosphate transport activity[84]. These findings highlight the crucial role of Pit-1 and phosphate transport in VSMC mineralization and phenotypic modulation due to elevated phosphate levels.

(b) Role of transforming growth factor-β1 (TGF-β1)

Evidence supporting the transdifferentiation of VSMCs was demonstrated by Schulick et al. in an animal model[159]. In this study, an in vivo gene delivery model was used, employing an adenoviral vector expressing active TGF-β1. The researchers found that rat arterial VSMCs lost their lineage markers when exposed to active TGF-β1. Approximately 10-25% of all intimal and medial cells exhibited characteristics resembling chondrocytes, leading to cartilaginous

metaplasia due to the local accumulation of active TGF-β1. It's worth noting that cartilage is a precursor to bone formation through a process called endochondral bone formation, which is a crucial developmental mechanism for the formation of long bones. Additionally, TGF-β1 was found to be present in calcified aortic valves and was observed to colocalize with calcification and bone formation in atherosclerotic lesions[160,161].

(c) Fibroblast Growth Factor 23 (FGF23)-Klotho

FGF23 is mainly produced by osteocytes, responding to changes in phosphate levels[162]. Its actions are closely linked with the transmembrane protein Klotho, acting as a cofactor. Together, they regulate phosphate resorption in the proximal renal tubule, as well as intestinal phosphorus absorption, achieved by reducing calcitriol synthesis in the kidney[163,164]. It's worth noting that these functions are only effective in the presence of Klotho. In the absence of Klotho, even high levels of circulating FGF23 cannot adequately regulate systemic phosphate homeostasis[165]. As a result, when serum phosphate levels are elevated, FGF23 levels rise as a compensatory response, making them an indirect surrogate marker of VC.

FGF23 has further impacts on calcium and vitamin D metabolism. Vitamin D is also involved in calcium uptake and bone mineralization. FGF23 accelerates the breakdown of vitamin D[163]. Consequently, serum FGF23 levels are positively correlated with parathyroid hormone (PTH) and phosphate levels and negatively correlated with 1,25(OH)2D (active form of vitamin D), GFR, and tubular phosphate reabsorption[166]. During the early stages of CKD, FGF23 levels increase significantly and play a pivotal role in mineral ion changes and bone metabolic disorders[167]. In mice lacking FGF23, hyperphosphatemia, hypercalcemia, elevated 1,25(OH)2D levels, and reduced PTH levels have been observed, collectively indicating impaired skeletal mineralization[167].

Furthermore, as renal function declines, FGF23 levels progressively rise and peak in end-stage renal disease. Moreover, FGF23 has emerged as a useful predictor of mortality in CKD patients[168]. These findings underscore the role of FGF23 in both osseous mineralization and extraosseous (soft tissue) mineralization processes.

(d) Role of RunX2

RunX2, also known as core-binding factor alpha 1, plays a crucial role as a master regulator of osteoblastic differentiation. It serves as the most upstream transcription factor essential for osteoblastic differentiation in VSMCs[169]. RunX2 protein is detected in preosteoblasts and the expression is upregulated in immature osteoblasts and downregulated in mature osteoblasts. Notably, RunX2 expression has been observed in calcified arterial tissues of patients with CKD, indicating its selective presence in these calcified regions[170,171].

Inorganic phosphate, a major contributor to VC, also induces the expression of RunX2[172]. Acting as a transcription factor, RunX2 increases the expression of various osteogenic genes, including osteocalcin (OC), osteopontin (OPN), osterix, alkaline phosphatase (ALPL), and type-1 collagen[173]. Of particular importance, osterix is a direct target of RunX2 and plays an essential role in the RunX2-mediated calcifying phenotype of VSMCs.

(e) Role of ALPL

ALPL is one of the osteoblastic phenotype markers and is considered essential in the VC process. It has been detected in vascular and heart valve calcifications. ALPL is expressed on the surface of cells that can act on phosphate liberators. It a membrane bound glycoprotein serves as a significant phenotypic marker of both bone formation and VC, making it an essential component in these processes[174,175]. It is the earliest marker of bone formation and bone calcification[176]. Inflammatory cytokines and vitamin D induce its up-regulation and mineralization[111,177].

During bone formation and growth, osteoblasts actively produce ALPL, and its levels in the blood can serve as an indicator of bone formation and turnover[178]. As bones undergo remodeling and repair, ALPL activity increases, reflecting an increase in bone formation activity[179].

Its activity is crucial for hydroxyapatite formation during endochondral ossification in bone development[179]. Interestingly, ALPL plays a similar role in the vasculature during ectopic calcification, where it degrades pyrophosphate (PPi).

1.9.3 Circulating Nucleation Complexes

There is growing evidence suggesting a connection between bone remodelling, specifically the activity of osteoclasts, and VC. Studies have revealed the involvement of osteoprotegerin (OPG) in this relationship. OPG is a soluble protein belonging to the TNFα family, expressed by osteoblasts, which inhibits osteoclastogenesis. For instance, mice lacking OPG exhibit both osteoporosis and VC, suggesting that OPG and its regulators may play a crucial role in explaining the link between CVD and osteoporosis[180]. There is a study that has shed light on OPG's significance as an osteoblast-derived inhibitor of osteoclast differentiation and function. It exerts this effect by binding to receptor activator of NFκB ligand (RANKL), thus blocking the function of receptor activator of NFκB (RANK)[181].

Although the impact of OPG on VSMCs is not as well understood[182], studies by Price et al. have demonstrated that OPG, can inhibit arterial calcification in rats treated with warfarin and/or vitamin D[183,184]. What's intriguing is that the doses used to inhibit bone resorption are also effective in preventing vascular calcification.

In another study, they utilized a specific inhibitor of osteoclastic V-H+-ATPase, using SB 242784 (an enzyme required for the secretion of protons by osteoclasts), to successfully prevent both VC and osteoclastic resorption in rats treated with toxic doses of vitamin D[185]. Based on these findings, it has been proposed that VC might be linked to osteoclastic resorption. According to another study, crystal nuclei generated during bone resorption may travel in the bloodstream and become lodged in soft tissue, thereby inducing tissue mineralization[182]. Interestingly, under certain conditions, a complex consisting of a calcium phosphate mineral and two proteins, Fetuin and MGP, is released from bone and detected in the blood. This release of the complex can be inhibited by blocking osteoclastic activity[186].

The exact mechanism by which such a circulating nucleating complex crosses the endothelial barrier remains is unknown. Furthermore, if bisphosphonates and other osteoclastic inhibitors prove to be effective against CVD therapy it will pave towards therapy associated with negative impacts on cardiovascular health.

1.9.4 Cell Death

Cell death has long been recognized as a significant mechanism for VC, particularly in dystrophic calcification observed in atherosclerotic lesions, where extensive necrotic areas are commonly seen. When cells undergo apoptosis, they become highly permeable to calcium and phosphate, leading to the accumulation of these ions beyond their solubility product. This accumulation facilitates the homogeneous nucleation of crystals, potentially contributing to calcification.

Phospholipid membranes within dying cells may also serve as sites for heterogeneous nucleation and/or epitactic growth of calcium phosphate crystals[157]. Interestingly, matrix vesicles, known as the nucleation sites for calcium phosphate crystal formation in cartilage and bone, have been observed in calcifying vascular lesions[187]. These vesicles appear to originate from dying VSMCs.

In vitro studies on cultured VSMC nodules have further supported the link between cell death and VSMC calcification. Apoptosis was found to occur before the onset of nodular calcification in VSMCs. Moreover, when apoptosis was stimulated or inhibited in these nodules, VSMC calcification increased or decreased, respectively. Additionally, researchers found that apoptotic bodies isolated from VSMC cultures accumulated calcium, and similar to matrix vesicles, the calcium inside the apoptotic bodies was in crystallized forms[188].

These findings provide evidence that apoptotic bodies derived from cultured VSMCs can act as sites for initiating and nucleating calcium phosphate deposition, potentially contributing to VC. However, the exact relationship between apoptotic bodies and matrix vesicles requires further investigation.

Research efforts in the past decade have improved understanding the factors involved in medial VC, the mechanisms that regulate the process of trans-differentiation to osteoblast-like cells remain unclear. This study will focus on trying to understand the mediators of medial VC that are specific to CVD in CKD.

1.10 Vascular Smooth Muscle Cells

VSMCs are located in tunica media are the principal mediators of medial VC. These non-striated, non-voluntary, contractile cells can be found in various tissues, including blood vessels, the trachea, iris, urinary bladder, and the digestive tract[189]. These are highly specialized cells in the blood vessel whose primary function is contraction, maintaining the blood vessel diameter, blood flow distribution and blood pressure[190]. In addition to their contractile function, VSMCs are essential for maintaining and remodeling the ECM of blood vessels[191]. They have more plasticity than any other cells for carrying out contraction, differentiation, and synthesis of extracellular matrix[192]. In healthy adult tissues, VSMCs typically exhibit a contractile phenotype, characterized by slow proliferation, and responsiveness to signals like acetylcholine and norepinephrine. These cells also express a variety of contractile proteins, including α-SMA, SM-22α, SM myosin heavy chains SM-1 and SM-2, calponin, and smoothelin.

VSMCs differ from other myocytes as they display phenotypic plasticity and are not terminally differentiated[193]. When faced with local cues, such as injury, VSMCs can alter their phenotype, exhibiting a transition from a contractile state to what is known as a 'synthetic' state. In this synthetic state, VSMCs down-regulate contractile proteins, increase proliferation, and remodel the ECM to facilitate migration and repair. Traditionally, this phenotypic transition was perceived as a binary process, with cells reverting to the contractile state after completing the repair. However, recent studies have unveiled that VSMCs can maintain a spectrum of phenotypes and express characteristics of various cell types, including osteoblasts, chondrocytes, adipocytes, and macrophage foam cells[194]. The shift from a contractile to an osteo/chondrogenic phenotype involves the development of calcifying vesicles, decreased expression of mineralization inhibitory molecules, and the production of

a matrix prone to calcification[195]. As this phenotypic change occurs, VSMCs lose markers associated with smooth muscle (SM22α and α-SMA) and gain osteochondrogenic markers, such as RunX2, SP7, osteopontin, osteocalcin, and ALPL, as well as Sox9, Type II, and X collagen (Col II and Col X).

In vitro studies have played a significant role in classifying VSMC phenotypes by stimulating the cells to differentiate along various lineages. When VSMCs are cultured with aggregated low-density lipoprotein (agLDL), they exhibit downregulated elastogenic capacity and an increase in macrophage foam cell markers, including LGALS3/Mac2, CD11b, F4/80, and CD68[196,197]. Similarly, VSMCs grown in apidogenic differentiation media display adipocyte markers such as adipsin, adipocyte fatty acid-binding protein, C/EBPalpha, peroxisome proliferator-activated receptor gamma (PPAR-c), and leptin[198]. The plasticity of VSMCs, allowing them to take on different phenotypes, is widely recognized, but the spectrum of phenotypes and their relative importance in VC remains a subject of debate. Current understanding suggests that VSMC phenotype switching during calcification may vary depending on the location of calcification, with inflammatory phenotypes developing during intimal rather than medial calcification e.g., macro and microcalcification and plaque stability will depend upon the location and the osteogenic stimuli. In vivo attempts to investigate this phenomenon using lineage tracing experiments face challenges due to changes in cellular marker expression, such as the loss of SM22α and α-SMA, necessitating the use of advanced genetic fate mapping techniques[192,199]. Moreover, the presence of other cell types, such as multipotential vascular stem cells, adipose cells, fibroblasts, and macrophages, capable of differentiating and acquiring VSMC marker expression, adds complexity to the picture[200]. Recent studies have revealed that approximately 40% of foam cells found in advanced human coronary artery lesions express both the VSMC marker α-SMA and the macrophage marker CD68. However, the exact nature of these cells remains unclear. It is uncertain whether they represent VSMC-derived cells that have activated macrophage markers, or they are macrophages that have activated VSMC markers, or neither[201]. Many of these phenotypic transitions are pathological and actively contribute to driving vascular disease processes. Therefore, comprehending the environmental factors, transcriptional programs, and signaling pathways responsible for driving these phenotypic changes is critical in developing future therapeutic strategies.

1.10.1 VSMC osteogenic differentiation

Osteo/chondrogenesis, the process of differentiating into bone or cartilage, is under the control of specific transcriptional programs influenced by physiological and mechanical cues. Initially, mesenchymal precursors express both Sox9 and RunX2, key transcription factors marking the onset of osteogenic and chondrogenic differentiation. The balance between RunX2 and Sox9 expression determines the lineage fate, with RunX2 driving the osteogenic phenotype while Sox9 binds to RunX2, repressing its actions[202]. In the osteogenic phenotype, RunX2 acts as a transcription factor, binding to downstream genes involved in bone development, including ALPL, Type 1 collagen, osteopontin, MMP9, and SP7[203] **Table 2**. Other drivers of the osteogenic phenotype include activating transcription Factor 4 (ATF4), expressed in more mature osteocytes, and the bone morphogenic proteins (BMPs)[204]. The BMPs, members of the transforming growth factor (TGF)-β family of proteins, play critical roles in activating RunX2 in various cell types and are pivotal in bone repair[204].

The evidence supporting the osteochondrogenic differentiation of VSMCs in VC comes from genetic lineage tracing studies in mouse models[145,205]. These studies have revealed compelling findings, showing that the majority of the osteochondrogenic precursor-like cells (around 75-88%) and nearly all of the chondrocyte-like cells (approximately 98%) observed in atherosclerotic lesions originate from VSMCs[145]. These findings strongly implicate VSMCs as crucial mediators of Intimal calcification. Moreover, the locations of these VSMC-derived cells in the atherosclerotic lesions of these animal models closely mirror the locations of VC seen in human atherosclerotic lesions[206,207]. These VSMC-derived cells are predominantly found in the fibrous cap of atheromas and regions exhibiting cartilaginous metaplasia and calcification. Similar to human VC, these cells show a loss of SMC marker protein expression, including SMMHC, SM22α, and α-SMA, except for a few cells on the lumen side of the fibrous cap. Interestingly, at early time points, VSMC-derived cells are frequently observed to cluster in the deep intimal and inner medial layers, adjacent to breaks in the elastic lamina, suggesting that they likely originated from medial VSMCs. These lineage tracing studies align with an electron microscopy study that identified cells with hybrid characteristics of both VSMCs and chondrocytes, termed 'myochondrocytes,' in human atherosclerotic lesions[208]. Together,

these findings provide compelling evidence for the involvement of VSMCs in the osteochondrogenic differentiation process that drives atherosclerotic intimal calcification, shedding light on the complex mechanisms underlying this process in vascular pathologies.

Apart from the transcription factors and genes, VC process is controlled by other stimuli including inflammation, oxidative stress, and changes in ECM (extracellular matrix) composition. The ECM provides structural support and contributes to the integrity and function of blood vessels. However, when the balance between calcification-promoting and calcification-inhibiting factors in the ECM is disrupted, vascular calcification can occur. Understanding the complex interactions between the ECM and VC is critical for developing targeted therapeutic interventions to prevent or reverse this pathological process. By modulating the ECM environment and its interactions with cells, it may be possible to mitigate the development and progression of VC and its associated CVD complications.

MSC	Immature Osteoprogenitor	Mature Osteoprogenitor	Preosteoblast	Differentiated osteoblast	Osteocyte
Alkaline Phosphatase (ALP)	–	+	++	+++	–
Phex	–	–	–	+++	+++
Osteocalcin (OCN)	–	–	–	–→+++	–
Osteopontin (OPN)	–/+	–/+	–→+	–→+++	–→+++
Runx2	+	+	++	+++	+++
Osterix	–	–	++	++	?
Collα1	–	++	++	++	–
Bone sialoprotein (BSP)	–↔++	++↔–	–→+++	–→+++	–→+++

Table 2 Well-established markers of the osteoblast during developmental sequencing

There are three major stages of osteoblastogenesis: - proliferation, matrix maturation and mineralization, which are characterized by different molecular markers[209]. The most frequently used markers of the osteoblast differentiation process are alkaline phosphatase (ALPL), type I collagen (Col1a1), osteopontin (OPN), bone sialoprotein (BSP), osteocalcin (OCN). In general, ALPL, BSP and Col1a1 are early markers of osteoblast differentiation, while OCN appear late, concomitantly with mineralization. OPN peaks twice, during proliferation and then again in the later stages of differentiation. RunX2 is the most upstream transcription factor essential for osteoblast differentiation. This shows some important categories of molecules in the lineage and their utility

to help define transitions in osteoblast differentiation. −, no detectable expression; −/+, +, ++, +++, expression ranging from detectable to very high; −→+++, heterogeneous expression in individual cells[209]. Figure is taken from here[209] Pittenger MF et al. *Science*. 1999.

1.11 The Extracellular Matrix

The ECM in animals is a complex network of proteins, glycoproteins, and proteoglycans that organizes cells into tissues and enables them to respond to mechanical forces. This intricate matrix provides structural support to various body parts, including the skeletal system (bones, teeth, tendons, ligaments, and cartilage), blood vessels, hollow organs (bladder, lung), and skin.

It was originally believed to serve no function other than to act as a scaffold providing structural support. However, the ECM has now been implicated in the modulation of crucial biochemical and molecular cues that are required for cellular processes such as migration, differentiation, proliferation, and cell-cell adhesion[210].

The diverse composition of the ECM allows tissues to perform distinct functions through interactions between matrix molecules, growth factors, and cell surface receptors, which facilitate cell adhesion to ECM components. For instance, cartilage ECM, rich in collagen II and proteoglycans, is well-suited for resisting compression, whereas the basement membrane ECM is enriched in laminin and non-fibrillar collagen, creating a separating interface between different tissue layers. In the kidney, the ECM acts as a molecular filter[211-213].

Collagen, the most abundant structural protein in the ECM, exists in over 20 genetically distinct types. All types share a common structure—a right-handed triple helix formed by three individual collagen chains intertwined[214]. Among them, collagen type I is prevalent in mammalian tissue and is ubiquitous across the animal and plant kingdoms. It has been extensively studied and well-characterized[215]. Fibrillar collagens, including collagen type I, provide tissues with stability and tensile strength.

In the body, elastin serves as another vital structural protein, found in tissues capable of stretching, such as the skin, bladder, and blood vessels. Its function lies in permitting tissue

deformation and subsequent recoil in response to mechanical stress, providing essential structural integrity. This elastic property complements the role of collagen fibers, which offer rigidity and tensile strength, making them the primary contributors to the mechanical properties of the ECM[216,217]. The balance between the synthesis and degradation of elastic fibers and collagen fibers determines their abundance in the ECM, which is regulated by various proteases[218].

Glycosaminoglycans (GAGs) play a supporting role in the biomechanical functions of collagens and elastin. These GAGs contribute to the gel-like properties of the ECM and are often components of proteoglycans. Proteoglycans consist of GAGs arranged in a bottle brush-like structure, grafted onto a protein core. GAGs are highly anionic polymers that have a remarkable ability to absorb water, imparting compressive strength to the tissue. Moreover, they are involved in regulating water uptake, sequestering growth factors, and facilitating cell migration[219].

Among the GAGs, Hyaluronan (HA) holds a unique position as a non-sulfated type. Its presence contributes to frictional resistance against interstitial fluid flow and serves as an important lubricant in joints. In cartilage tissue engineering, hyaluronic acid is commonly used as a scaffold component, highlighting its significance in the field[220-222].

Within the ECM, certain proteins like fibronectin and laminin play a critical role in cell adhesion, earning them the nickname "ECM glue." Fibronectin, the second most abundant protein in the ECM after collagen, is a large glycoprotein with diverse binding domains. It exists in two forms: a soluble form found in the blood and an insoluble form present in the ECM[223,224]. On the other hand, laminin is a key component of the basement membrane, an ECM structure that separates the epithelium from underlying layers of connective tissue and muscle. Laminin is involved in various cellular processes such as cell differentiation, migration, proliferation, and importantly, angiogenesis[225,226].

The assembly of many ECM proteins occurs outside the cell, forming structural scaffolds tailored to specific tissue functions. Their biosynthesis is a complex process that involves numerous specific post-translational modifications, both intra- and extracellularly[227,228].

1.12 Hyaluronan (HA)

HA is a non-sulphated, negatively charged, linear matrix glycosaminoglycan that is ubiquitously expressed in somatic tissues during health and is altered during many pathologies. The properties of HA were first determined by the work of Karl Meyer and John Palmer in the 1930s[229] and the chemical structure was defined in 1954. They purified 'a polysaccharide of high molecular weight' from bovine vitreous humor and termed it 'hyaluronic acid'[229]. It is made up of two sugar units of alternating N-acetyl-D-glucosamine and D-glucuronic acid linked by β (1-4) and β (1-3) bonds[230] **Figure 4**. HA is synthesized in humans by the HA synthase (HAS) enzymes 1, 2, and 3, which are encoded by the corresponding HAS genes[231,232]. Several hyaluronidases have been identified; however, recent studies have cast doubt on the specificity or potency of the hyaluronidase activity of some of these proteins[233]. Among the most studied are Hyal1, Hyal2, and PH20. HA-binding proteins have been grouped together as a family termed hyaladherins and further subdivided in matrix and cell-surface hyaladherins (receptors). Specific hyaluronan-hyaladherin interactions affect cell behaviour.

Unlike other glycosaminoglycans, HA is unique in being unsulfated and contains no epimerized uronic acid residues. To transport HA to the ECM, HAS enzymes act as glycosyltransferases and combine N-acetyl-D-glucosamine and D-glucuronic acid to form HA. HA is extruded through the membrane into the extracellular space simultaneously as synthesis proceeds. This mode of biosynthesis is unique among macromolecules since nucleic acids, proteins, and lipids are synthesized in the nucleus, endoplasmic reticulum/Golgi, cytoplasm, or mitochondria. The extrusion of the growing chain into the extracellular space allows unconstrained polymer growth, thereby achieving the exceptionally large size of HA. Confinement of synthesis within the Golgi or post-Golgi compartment could limit the overall amount or length of the polymers formed[231,232]. HA polymers are thus synthesized at the HAS active site on the intracellular side of the membrane and exported simultaneously as linear, unaltered polymers[232].

In humans, HA exists in many tissues during health and is abundant in the vitreous of the eye, the umbilical cord, synovial fluid, heart valves, skin, and skeletal tissues. The number of

disaccharide units varies within a tissue and in theory, an infinite number of can be added to a HA polymer and the number can reach 30,000 in some tissues[234]. The 3D structure of HA suggests that it is an overall coiled structure irrespective of size and it forms a rigid, helical confirmation in physiological solution[235,236]. However, in biological tissues the macromolecular structure of HA is dependent on its molecular weight and its interactions with receptors/proteins at the cell surface as well as other intracellular and extracellular hyaladherins.

HA was first thought to be just a space filler of the extracellular matrix, because of its presence in cartilage and in the vitreous of the eye and was labelled as an "extracellular goo" because of its viscoelastic properties[234] . Over the last two decades however, HA has been increasingly found to have multifunctional roles in biology[237]. These encompass roles in embryonic development and tissue regeneration[238,239], tumour invasion[240], transformation by oncogenes[241] and in cytokine responses to injury[242-244]. At a cellular level, cell associated HA matrix has been shown to have multiple complex roles ranging from mechanochemical support, to regulation of cell division influencing tumour growth and metastasis[245]. HA interacts with various cell surface receptors to initiate intercellular signalling and regulate cell-cell adhesion, migration, proliferation and differentiation[231]. Therefore, elevated HA levels have been described in both health and disease contexts, thus a lot of research has been directed towards dissecting the beneficial versus pathogenic forms of HA in biology[246].

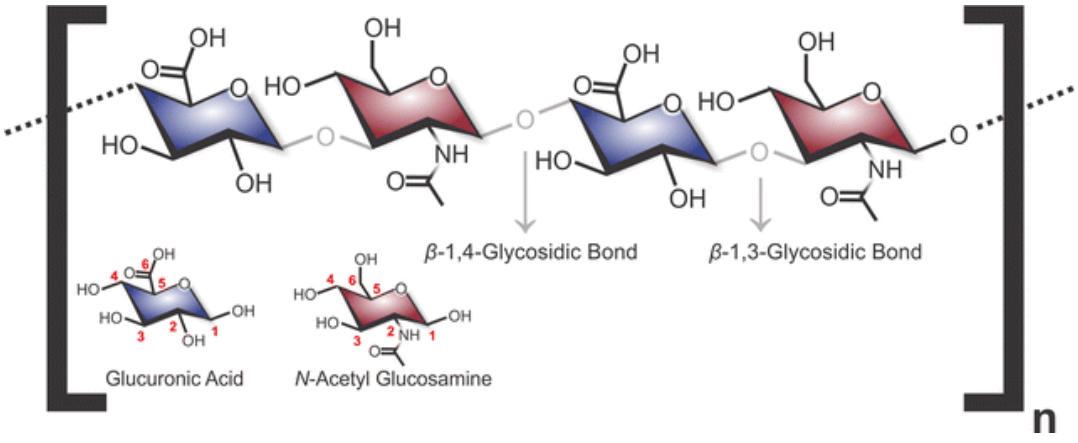

Figure 4 Chemical Structure of HA

Hyaluronic Acid is made up of two sugar units of alternating N-acetyl-D-glucosamine and D-glucuronic acid linked by β (1-4) and β (1-3) bonds[230]. Its structure is reported to be a stiffed helical

confirmation that gives the molecule an overall coiled coil structure. The figure has been taken from[247] de Oliveira JD et al. *Microbial Cell Factories*. 2016.

1.12.1 HA Synthesis

HA is synthesized in humans by HA synthase (HAS) enzymes located within the plasma membrane. Three mammalian genes have been identified which encode the HAS enzymes and are termed HAS 1, 2, and 3[231,232]. These 3 genes have been located on different chromosomes, the different HAS enzymes have been reported to have different levels of activity, different expression patterns and thus have been proposed to have distinct biological roles in HA synthesis[248-250]. Each of the three HAS genes is known to be expressed at different times during embryogenesis[251]. Cell-specific variations of HAS expression have also been observed and support the theory of specific functions of individual HAS genes[251]. Although the specific functions of the HAS isoenzymes are unclear, it is known that cytokines and growth factors like IL-1β, TGF- β1, IL-6, EGF and PDGF differentially influence the transcription of HAS genes[252-254]. Numerous transcription binding sites, such as CCAAT box, CAGA, Sp1 and NF-κB in the promoter region of the distinct HAS genes have been identified[255-257]. In addition, a natural anti-sense mRNA of mouse and human HAS2 has been described and termed HAS2 antisense-1 (HAS2AS1), suggesting that there may be further transcriptional modification of HAS2[258]. HAS2AS1 has an alternate splice site for both human and mouse[258]. Furthermore, it has been suggested that post transcriptional regulation of HAS expression occurs due to the fact that levels of HAS mRNA do not always correspond with the levels of HA secretion[259].

HAS1 is thought to be the least active, while HAS2 is more catalytically active than HAS1 and HAS3 is described as the most catalytically active of the three and it is expressed late in embryonic development in adult tissues. HAS1 and HAS2 ($>2*10^6$ Da) both reportedly synthesize high molecular weight HA ($2*10^6$ Da and ($>2*10^6$ Da respectively), while HAS3 produces lower molecular weight HA ($2*10^5$ Da)[251,260,261]. However, the studies reporting the differences in molecular weight generation are old and need to be updated using more modern technological advances.

The functional relationship of the HAS proteins has been assessed in studies by generation of a knockout mouse for each HAS gene[261,262]. Loss of HAS2 is embryonically lethal as deletion of HAS2 in mice leads to a failure of heart development and results in death at day 10 of embryonic development. These embryos had multiple developmental defects, including yolk sac and cardiac defects with no formation of cardiac jelly or cardiac cushion, and contain virtually no HA, suggesting that HAS2 is required for HA biosynthesis during normal embryonic development. However, deletion of HAS1 and HAS3 does not affect embryonic development and animals are viable and fertile[263-265] supporting the central role of HAS2 during normal embryonic development.

There is evidence suggesting that HAS isoforms play important roles in cellular differentiation and altered cell phenotype[266]. Overexpression of HAS2 promotes epithelial to mesenchymal transition and fibroblast to myofibroblast differentiation[266-272]. Overproduction of HA by expression of HAS genes generates transgenic mice with increased tumour metastasis and proliferation of transformed cells, supporting the role of HA in tumorigenesis[260,273]. HA biosynthesis has been shown to increase during cell proliferation and migration and it decreases at high cell densities when cell proliferation is low[274]. HAS activity also influences the organization of pericellular and extracellular structures. HAS3 overexpression in proximal tubular epithelial cells leads to formation of elongated pericellular HA cable-like structures, whereas HAS2 overexpression in the same cells inhibits HA cable formation but promotes formation of HA pericellular coats instead[275,276]. As the organization of pericellular HA is related to cellular function, it is therefore possible that HAS enzymes play a role in the regulation of cell function[277,278]. HA can form coats around cells and can interact with cell-surface receptors to prevent immune cell recognition and block phagocytosis by macrophages[279]. In inflammatory settings, HA has been shown to form cable-like structures that differ from HA pericellular coats, as they serve as attachment-ligands for receptors on inflammatory cells and are partly responsible for leukocyte recruitment and retention[280,281]. The presence of HA cables is not exclusive to inflammatory settings. Organisation of HA into cables has been shown to have anti-inflammatory roles as well. For example, monocytes have been shown to adhere tightly to HA cables in clusters whilst inactive, mainly through CD44 expression on their cell surface. Therefore, cables in this context prevented monocyte

interactions with resident cells, and abrogated monocyte dependent inflammatory cytokine production[275,276,282,283].

1.12.2 HA Degradation

The synthesis of HA is balanced by catabolism, thereby maintaining a relatively constant concentration in the tissue under normal conditions. The half-life of HA varies amongst tissues ranging from several minutes in circulating blood (2–5 min), (1–2 days) in the epidermal compartment, (1–3 weeks) in the cartilage to approximately 70 days in the vitreous humor of the eye[230]. A 70-kg individual has 15 g of HA, approximately a third of HA within the human body is degraded and resynthesized daily[251].

HA degradation can also take place outside cells due to the presence of extracellular enzymes. Hyaluronidases are also present inside the cells in endoscopes and lysosomes that further degrade HA inside the cells[230]. Extracellular high molecular weight HA is thought to bind to the plasma membrane either thought the HA receptors (CD44)[251,284,285], Lymphatic Vessel Endothelial HA Receptor-1 (LYVE-1)[286] as well as HARE (HA receptor for endocytosis)[287]. HA can then be internalized through HA-CD44 mediated endocytosis transported to the lysosomes that contain hyaluronidases and/or two exoglycosidases (β-glucuronidase and β-N-acetyl glycosaminidases) that further degrade[288]. This degradation is caused by a group of enzymes called Hyaluronidases (HYALs). Several hyaluronidases have been identified; however, recent studies have cast doubt on the specificity or potency of some of these proteins[233]. In the human, three genes (HYAL1, HYAL2, and HYAL3) are found tightly clustered on chromosome[289] 3p21.3, coding for hyaluronidase-1 (HYAL1), HYAL2, and HYAL3[289,290]. Another three genes HYAL4, PHYAL1 (a pseudogene), and SPAM1 (Sperm Adhesion Molecule 1), clustered in a similar fashion on chromosome 7q31.3, are unlikely to have major roles in HA degradation. They code, respectively, for Hyal4, transcribed but not translated in the human, and PH-20. PH-20 is relatively specific for testes, the enzyme facilitating penetration of sperm through the cumulus mass that surrounds the ovum. The enzyme is also necessary for fertilization[291]. From the cluster on chromosome 3p, the HYAL 1, 2 and 3 enzymes vary in the optimum pH, as does the relative activity, and localization[292-295].

HYAL1, the first hyaluronidase purified from human plasma, is widely expressed in both plasma and urine[296]. It is found in major parenchymal organs such as the liver, kidneys, spleen, and heart. HYAL2 is also expressed in somatic tissues but has much lower enzymatic activity compared to HYAL1. Hyal2-/- mice show extremely high plasma levels of HA and develop skeletal abnormalities, and severe cardiopulmonary dysfunction[297,298]. In both humans and mice, mutations in the HYAL2 gene have been associated with severe heart defects[299].

HYAL1 is found predominantly intracellularly, whereas HYAL2 can be found both intracellularly and at the cell surface[300,301]. HYAL1 degrades high molecular weight HA into small oligosaccharides. HYAL2 is anchored to the plasma membrane by a glycosylphosphatidylinositol (GPI) link, though a portion of 2 also occurs in a soluble form. HYAL2 at the cell surface degrades HMW-HA into intermediate HA fragments of about 20 kDa in size (50 disaccharides)[300]. It has been speculated that HYAL1 and HYAL2 work in succession to degrade HA, with the hypothesis that HYAL2 generates HA fragments of about 20 kDa, which is then internalized and further degraded to tetrasaccharides by lysosomal HYAL1/HYAL2[300,302,303]. Enzymatic activity of HYAL3 has not been reported on[304-306], but there is some evidence that HYAL3 may support and augment the activity of HYAL1[307]. Knockout of HYAL3 alone in mice however leads to subtle differences in ECM architecture with little change in phenotype, fertility and viability of the mice suggesting limited sole function[307,308].

Recently another hyaluronidase CEMIP (Cell Migration Inducing Protein) was discovered. This hyaluronidase in the earliest step of HA depolymerization. CEMIP is a crucial HA-binding protein responsible for HA-specific depolymerization. Knockdown of CEMIP resulted in the complete loss of HA-degrading activity, establishing CEMIP as an essential factor for HA depolymerization in human skin and synovial fibroblasts[309]. CEMIP system operates through clathrin-coated endocytic vesicles, degrading incorporated HA in early endosomes, and releasing HA molecules of intermediate size into the extracellular space[309]. Additionally, its expression is regulated by a range of cytokines[310,311]. TGF-β, a pro-fibrotic protein and inducer of cell proliferation, can regulate CEMIP expression in dedifferentiated chondrocytes[312].

In addition to CEMIP and the HYAL family molecules, another novel cell surface hyaluronidase, transmembrane protein 2 (TMEM2), has been reported. CEMIP and the extracellular domain of TMEM2 share 48% amino acid sequence identity[313]. Studies in mice also showed that TMEM2 is more highly expressed at the transcriptional level than CEMIP, both during development and in adult tissues[313]. Experiments with overexpressed HEK293 cells and in vitro reactions using recombinant TMEM2 proteins have verified its hyaluronidase activity[313]. CEMIP and TMEM2 expressions together with HA depolymerisation appeared to be tightly regulated by the action of TGF-β1[314]. TGF-β1 enhanced TMEM2 levels and decreased both CEMIP and HA processing. Treatment of human skin fibroblasts with IL-β1 increased TMEM2 expression but suppressed both CEMIP and HA depolymerization[314]. In zebrafish, mutations in the TMEM2 homologue result in cardiac development defects[315,316]. TMEM2 has been reported to regulate HA turnover and promote developmental angiogenesis in zebrafish[316].

1.12.3 Hyaladherins

HA exerts its wide-ranging biological function through its interactions with a number of different HA binding proteins termed hyaladherins. Over 40 hyaladherins have been identified, and HA enacts its wide-ranging cellular functions, through specific HA-hyaladherin interactions, which in turn affect HA macromolecular structure and subsequent cell responses[317-320]. Hyaladherins have been grouped together according to their location: cellular and extracellular[321] **Figure 5**.

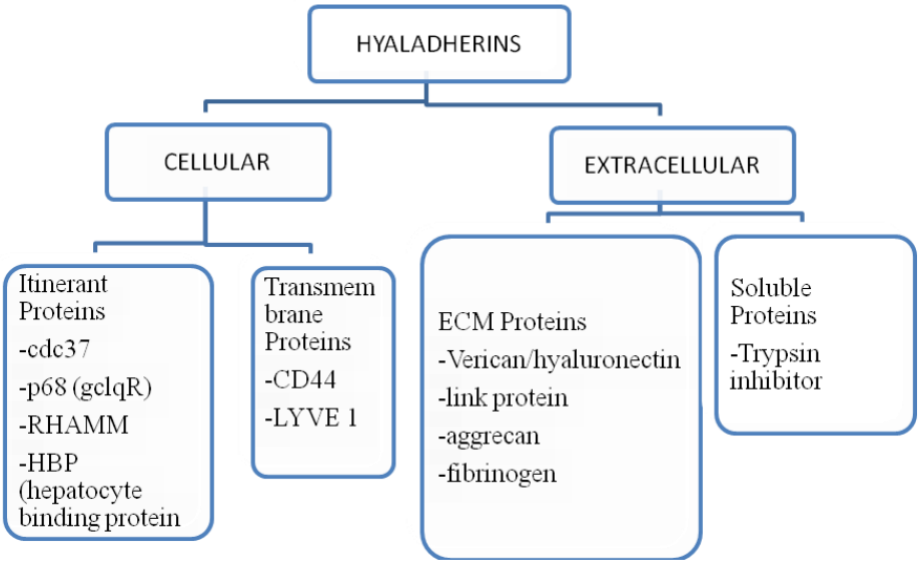

Figure 5 Hyaladherin family of proteins

Hyaladherins can be divided into cellular and extracellular proteins. The cellular proteins can be further divided into itinerant and transmembrane proteins. Extracellular can be further divided into ECM proteins and soluble proteins. This has been taken from here[322] Entwistle J et al. *J Cell Biochem*. 1996.

Among the cellular hyaladherins (HA receptors), CD44 is the main HA receptor and can be present as multiple isoforms due to alternative RNA splicing[323,324]. CD44 plays an important role in cell-cell adhesion, retention of pericellular matrix and cell proliferation[284,285,325,326]. CD44 can interact with the actin cytoskeleton and has roles in activation of signalling pathways[327-330] (such as MAP kinases, Src kinase, Rho GTPases, tyrosine kinase and protein kinases C) and regulation of matrix remodeling[284,285,331]. Interaction of CD44 with HA also has an important role in inflammation, embryonic development, T-cell activation, and oncogenic signalling and metastasis[328,332]. Transcriptional regulation can be influenced by pro inflammatory cytokines such as IL-1 and growth factors like EGF, TGF-β and BMP-7 (bone morphogenetic protein-7)[333-335]. CD44 also interacts and co-localizes with TGF-β receptors and modulates the intercellular pathways involved in TGF-β signaling[336,337]. Furthermore, CD44 can be shed from plasma and thereafter, exists in the plasma which can interfere with the HA and membrane bound CD44 interaction[337].

A unique hyaladherin, which can be present at the cell surface, within the cytoplasm or in the nucleus is RHAMM (the Receptor for HA-Mediated Motility). Like CD44, RHAMM also goes

through alternative RNA splicing. Depending on the RHAMM isoform present, it plays a role in cytoskeletal organization, intracellular signal transduction or HA mediated migration[338]. RHAMM regulates migration and cytoskeletal reorganization. Intracellular RHAMM is localized in the centromere and has the ability to regulate the cell cycle[335]. Studies have shown that that RHAMM compensates for the loss of CD44 resulting in increased HA accumulation which allows increased HA signalling through RHAMM[339]. This compensation occurs due to loss of CD44 and not because of enhanced RHAMM expression. There is evidence of over-expression of RHAMM in response to injury in macrophages, fibroblasts, epithelial and VSMCs[340-342].

Versican and tumour necrosis factor stimulated gene 6 (TSG-6) are examples of extracellular hyaladherins, which are present in soft tissues and are involved in crosslinking HA to other matrix structures and inflammatory cells and regulate matrix remodelling[343-347]. Versican interacts with TSG-6, HA and organize into discrete ECM filaments or cables that emanate from cell surface that bind leukocytes[281,282,348].Versican, which binds to HA, can also bind to CD44[344] suggesting that both versican and HA may stabilize CD44-dependent interactions and subsequent CD44-dependent signalling in inflammatory cells. On the other hand, Versican binding to HA may interfere with the binding of HA to CD44[349]. HA and Versican are greatly involved in vascular remodeling[350,351]. Normally Versican is present in low amounts, but it increases dramatically in most diseases[347,352-354]. During inflammation, versican is also differentially expressed in macrophages as they differentiate from monocytes[355-357].

Tumour necrosis factor-stimulated gene-6 (TSG-6), also called TNFα-induced protein 6 (TNFIP6). The rapid upregulation of TSG-6 in the presence of proinflammatory cytokines such as TGFβ, TNFα and IL-6 is consistent with its involvement in inflammatory processes[358]. TSG-6 is one of ∼20 genes that are significantly upregulated (∼two-fold induction) in human microvascular endothelial cells suggests that it might be involved in the pathology of vascular diseases[359]. TSG-6 is widely documented to be involved in the formation of HA peri-cellular matrices and maintains myofibroblast phenotype[269]. Further, silencing TSG-6 mRNA in proximal tubular cells, prevented the formation of HA cables and hence controlling the EMT of these cells[360]. These HA cables are commonly associated with the immune response and bind leukocytes to HA in a process that is CD44-dependent[276,361]. The ability of TSG-6 to

interact with HA and its upregulation in inflammatory situations suggests that it might somehow influence the formation of complexes with HA and thus be important for regulating ECM modelling and/or assembly.

1.12.4 HA and regulation of cell phenotype

HA in association with various hyaladherins described above, has been implicated in biological processes such as embryogenesis, cell adhesion, migration, and proliferation. HA-rich matrices are essential for cell migration and proliferation during embryonic development and organogenesis[362].

In VSMCs, HA promote the proliferative and migratory phenotype[363,364]. In a study, antisense inhibition of HAS2 inhibits proteoglycan retention and matrix assembly[365]. HA may be critical for tissue volume space and creation of cell-free spaces[237]. HA stimulates cell migration indirectly by binding with the proteoglycan versican and providing an extracellular or pericellular environment and facilitate migration by diminishing cell surface adhesivity[363,366]. HA has also been shown to stimulate migration of endothelial cells and organize the capillary basal lamina and stabilize the capillary wall of growing capillaries, which serve to link proliferating and migrating endothelial cells to the extracellular matrix[367]. Has2 knockout mouse embryos lack the characteristic transformation of cardiac endothelial cells into mesenchyme[362]. In another study, loss of HAS2 function during mouse development resulted in embryonic lethality and major reduction in cell-free, matrix defined spaces[362].

HA-rich matrices are characteristic for many tumours and seem to be critically involved in tumour cell migration and invasion[368]. Angiogenesis, formation of new blood vessels, has been shown as a property of HA[369]. HA is shown to modify the properties of other matrices, such as collagen and fibrin and thereby stimulating tumour cell migration[370].

Our research group has previously focused on investigating the role of HA in fibrotic diseases and its impact on regulating pro-fibrotic cell phenotypes, particularly the fibroblast to myofibroblast differentiation and Epithelial Mesenchymal Transition (EMT). In fibroblasts and

epithelial cells this is driven by the cytokine, TGF-β1 and is dependent on HAS2-mediated HA assembly into pericellular coats[371,372]. During injury, fibroblasts proliferate and migrate to the site of injury and differentiate to their activated form myofibroblasts which drives effective wound healing and is dependent on TGF-β1. In myofibroblasts, HA is found in an organized pericellular matrix or 'coat,' which is associated with cell migration[363,373]. Additionally, it can form pericellular HA cable-like structures that modulate interactions with mononuclear leukocytes through CD44 receptors[271,272,371,374-376]. The observed differences between these structures are thought to be mediated through differences in the binding of distinct hyaladherins such as TSG-6. TSG-6 affects HA macromolecular structure and CD44-dependent triggering of cell responses. TSG-6 also mediates the mechanism of EMT in renal epithelial cells and thereby contributes to changes in cell phenotype. TSG-6-mediated formation of inter-alpha inhibitor (I-α-I) heavy chain-HA complexes is critical for the formation of the peri-cellular HA matrix and knockout of TSG-6 produced loose HA-pericellular coats resulting in slowed cell migration[376].

Overexpression of HAS2 in renal proximal tubular epithelial cells induces a migratory phenotype and the accumulation of an HA pericellular matrix and led to enhanced cell migration[275]. Whereas overexpression of HAS3 favours the accumulation of HA in cables between and across cells and has no effect on cell phenotype[276]. Exogenous HA, through engagement with its principle receptor CD44, increases migration[326].

HA mediate myofibroblast resistance phenotype, through cell surface receptor (CD44v7/8) internalization of HA coat[268]. Cells that can internalize HA by means of this cell surface receptor (CD44v7/8) are resistant to EMT and myofibroblast differentiation[377]. Additionally, HA is known to have an established link with osteogenesis in bone[378-380], which will be further discussed in the subsequent section.

HA and its binding proteins regulate the expression of inflammation by promoting to attenuating inflammatory responses and it is dependent on how HA is synthesized, degraded, and organized within the peri-cellular matrix. The focus of my project is to investigate the role of HA in regulating the phenotype of VSMCs.

1.12.5 HA in Osteogenesis and Chondrogenesis

Bone has separate cell types for matrix synthesis (osteoblasts), matrix degradation (osteoclasts) and mechanosensory functions (osteocytes)[381,382]. The formation and resorption of bone is coordinated within remodeling, or basic multicellular units[382] and an imbalance in bone formation and resorption causes many diseases. We know that there is an established link between HA and Osteogenesis in bone[378-380]. One potential function of HA in bone is as a regulator of mineralization. HA binds hydroxyapatite (with a weak affinity) in calcified cartilage and bone, and although it does not modify mineral growth, it might have a regulatory role in mineralization[383]. HMW-HA increases osteoblast proliferation and mineralization, whereas LMW-HA (60 kDa) increases proliferation but not mineralization[384].

HA helps in the growth and development of joint cartilage and bone by promoting growth of new cells and tissues[385]. HA regulates bone remodeling by controlling osteoclasts, osteoblasts, and osteocyte behavior[386]. HA has an effect on bone formation in in vitro models of osteogenesis, as cultures with LMW-HA dosage showed bone colonies at the bases of fibroblasts[387]. Furthermore, calvarial (top part of the skull)-derived mesenchymal stem cells in rats showed HMW-HA facilitates cell proliferation and differentiation with alkaline phosphatase activity (early marker of bone formation)[384]. In another study, rat calvarial osteoblast cultured with high concentration of HA showed enhanced alkaline phosphatase activity[388]. Exogenous HA stimulates endogenous HA, and also promotes bone marrow stromal cell proliferation and osteogenic gene expression[389]. HA reduces urinary markers of bone resorption indicating that HA inhibits bone resorption and provides a protective effect on bone density of rats[390]. In contrast, HA fragments >8000 Da induce osteoclastic bone resorption via interaction between RANK (receptor activator) and RANKL (RANK ligand)[391]. Moreover, HA synthesis and bone resorption seems to be well coordinated as seen calcium release in dental bacteria was correlated with the synthesis of HA in bone culture[392]. On the contrary, addition of plaque extract to the culture media stimulated both the synthesis and release of hyaluronic acid to the culture media, while stimulating calcium release[392].

HA production by means of the HAS2 gene expression is essential for survival. Mice processing no HAS2 expression in chondrocytes died near birth and displayed abnormalities throughout

their skeletal[239]. HYAL1 is upregulated during osteoclastogenesis[393]. HA receptors also have an important role in bone formation. The main HA receptor, CD44-/- mice show destruction of joints and progressive crippling which suggests CD44 has an important role in bone formation[394]. HA-CD44 plays an important role in osteoclastogenesis by facilitating binding of adhesion molecules on osteoblasts to macrophage like cells[395]. CD44-/- mice exhibit thicker cortical bone and a smaller medullary cavity, suggesting that CD44 is essential for HA to bind with RANKL[396]. Another HA receptor, RHAMM shows enhanced mRNA is associated with osteolytic bone lesions[397]. HA binding proteins show a critical role in osteogenesis. A cDNA microarray study analyzing ligament cells from patients with an ectopic bone formation disease further suggests a role for HA in bone remodeling. TSG-6 was down-regulated during osteoblast differentiation and that overexpression of TSG-6 could not restrict mesenchymal stem cell differentiation. Overexpression of TSG-6 did not protect osteoarthritis but increased ectopic bone formation, suggesting TSG-6 is a target for therapeutic intervention for ectopic ossification[398,399]. Versican is present in the early stages of bone formation in the development of rat jaw bones and hindlimbs and has an important role in bone remodeling[400,401].

The extensive involvement of HA in various aspects of bone calcification, mineralization, and osteogenesis strongly suggests its potential role in osteogenesis within blood vessels. Given its wide-ranging functions in skeletal tissues, it is plausible that HA may also exert important effects on osteogenesis processes within vascular structures. Further exploration and understanding of HA's role in vascular osteogenesis could lead to novel insights into the pathophysiology of VC and potentially uncover new therapeutic targets to mitigate its adverse effects on cardiovascular health.

1.12.6 Role of HA in Vascular diseases

Vascular diseases are pathological conditions of arteries. that can be triggered by various factors, including pathogens, oxidized LDL particles, and inflammatory stimuli, that trigger endothelial cell activation. This activation leads to the synthesis of proinflammatory molecules, such as cytokines and chemokines, and the expression of adhesion molecules on

the cell surface. Consequently, circulating immune cells, such as monocytes and lymphocytes, are recruited and infiltrate the vessel wall.

Observations have indicated that HA is likely to be involved in the development of vascular diseases such as atherosclerosis, restenosis (reduction in the diameter of the vessel lumen after angioplasty), and diabetic angiopathy (disease of the blood vessels)[402-404]. These observations show that the levels of HA are altered in these arterial disease conditions. In heart valves, HA has been found to be the largest single contributor to the content of GAG content in heart valves, comprising ~35% of total GAGs in the aortic valves[405]. Notably, HA's role in vascular diseases extends beyond its contribution to the glycosaminoglycan content in the ECM. It has been implicated in the regulation of chronic inflammation, a key process underlying the formation and progression of atherosclerotic plaques. During the development of atherosclerosis, inflammatory processes involving immune cells and cytokines promote the accumulation of lipid-rich plaques within the arterial walls. HA exhibits unique abilities to interact with lipids and lipoproteins, suggesting an additional potential role in lipid retention and lipid-driven immune responses during atherosclerosis[406]. Furthermore, HA has been shown to accumulate locally in certain areas during the build-up of atherosclerotic plaques[407-409]. This localized HA accumulation raises questions about its possible involvement in plaque formation and progression, warranting further investigation into its exact role in shaping the disease pathophysiology. Intriguingly, HA's versatility becomes evident in its role as an effective medium for delivering bone morphogenic protein 2 (BMP2)[410,411]. BMP2 is a signalling molecule responsible for both normal bony ossification and abnormal heterotopic ossification in various tissues, including blood vessels. In this context, HA has been associated with promoting hyperplastic VSMC phenotypes, indicating a potential role in driving tissue remodeling and pathogenic changes in the vascular walls.

The role of HA in atherosclerosis and vascular remodeling has been investigated by manipulating HA levels, revealing distinct effects on disease progression. Inhibition of HA synthesis using 4MU facilitate leukocyte adhesion, subsequent inflammation, and progression of atherosclerosis[412]. This suggests that HA may have an atheroprotective function. In contrast, knockout of the HAS3 gene in mice showed that it inhibited VSMC remodeling and atherosclerosis[413,414]. This indicates that HAS3 may have an atherogenic role, contributing to the development and progression of atherosclerosis. Moreover, in APO E-/-

mice HAS3 expression was found to increase early during lesion formation, particularly when macrophages enter atherosclerotic plaques. Interestingly, APO E-/- mice lacking HAS3 (HAS3/APO E-/-mice) developed less atherosclerosis, providing further evidence that HAS3 promotes atherosclerosis[413]. Similarly, the overexpression of HAS2 in VSMCs of APO E-/-mice was shown to increase atherosclerosis[415], suggesting that elevated levels of HA in the vascular wall promote the progression of atherosclerotic lesions, and that HAS2 may also have an atherogenic role. Overall, these studies indicate that different isoforms of HAS, specifically HAS2 and HAS3, play distinct roles in atherosclerosis. While inhibition of HA synthesis appears to exacerbate the disease, indicating an atheroprotective effect, increased expression of HAS2 and HAS3 is associated with promoting atherosclerosis.

Vascular diseases, particularly atherosclerosis, are influenced by the crucial involvement of hyaladherins. Among them, the CD44 cell adhesion molecule has garnered significant attention in numerous studies, as it appears to promote atherosclerosis by mediating the recruitment of inflammatory cells into platelets and activating vascular cells[416,417]. Studies in CD44-deficient mice further support its critical role in atherosclerosis, with a substantial reduction in aortic lesions observed in CD44-/- mice compared to wild-type counterparts[417]. Human studies have provided valuable insights into CD44's relevance in vascular pathology. The accumulation of both HA and its receptor CD44 at sites of plaque erosion, highlighting their relevance in atherosclerosis[418,419]. In mouse models lacking CD44 (APO E-/-. CD44-/-), there was a notable reduction in inflammation and enhanced formation of fibrous caps within the plaques[416]. Moreover, in the mouse model of atherosclerosis[417,420], and in human atherosclerotic plaques[421,422], the expression of CD44 in vascular tissues was highest in plaques that were rich in macrophages and susceptible to rupture. This finding indicates that CD44 expression is associated with inflammatory processes and potential plaque instability. Another fascinating aspect of CD44 is its association with the accumulation of ligands, such as Osteopontin, during the progression of atherosclerotic plaques[415,423]. This accumulation of ligands appears to be a significant factor in the advancement of atherosclerosis. Moreover, CD44 was shown to be a driver of calcification of valve interstitial cells as knockdown of CD44 resulted in reduced calcification of aortic valve[424]. This suggests that CD44 plays a key role in the calcification processes associated with atherosclerosis. RHAMM, another receptor for HA, was found to be strongly expressed on intimal blood vessels but absent from other regions of

the vessels[425]. This observation suggests that RHAMM may have specific roles in regulating processes within intimal blood vessels, potentially affecting vascular function and pathology.

Several animal studies have investigated the expression of TSG-6 in atherosclerotic lesions, both in vivo[426-428] and in rabbit atherosclerotic plaques[428]. These studies revealed that TSG-6 levels were increased in the fibrous cap of the plaques, indicating TSG-6 could potentially play a role in stabilizing the plaque[426]. Furthermore, in another study using APO E-deficient mice, TSG-6 was found to be expressed in atherosclerotic plaques in the aorta and neointimal lesions following injury. The presence of TSG-6 in these locations aligns with the presence of vascular inflammation and macrophages, indicating its involvement in processes linked to atheromatous plaques[429]. Enhanced expression of TSG-6 is present in both plasma and aortic wall, mostly tunica media of patients with aortic aneurysms[430]. Moreover, Versican appears to be one of the main components of the ECM that binds to LDL during the progression of atherosclerosis in the arterial intima[431]. Versican is prominent in advance lesions of atherosclerosis, at the border of lipid filled necrotic cores as well as the plaque thrombus surface, suggesting a role in lipid accumulation, inflammation, and thrombosis[432]. Additionally, proinflammatory stimulants, such as hypoxia, seem to increase Versican expression, further implicating its involvement in inflammation-related processes[433,434]. Elevated expression of Versican is seen in myeloid cells in autoimmunity, in cardiovascular diseases such as coronary stenosis, myocardial infraction[433,435,436]. Thus, the existing literature on HA and its role in atherosclerosis is extensive. However, relatively little is known about the association between HA and VC. Further research and investigation are needed to better understand the potential link between HA and the process of VC, as this area remains relatively unexplored.

1.12.7 Role of HA in Diabetes

Diabetes is a significant comorbidity that contributes to VC, and HA plays a crucial role in this process. The association between diabetes and VC has been well-established, with diabetes being a major risk factor for accelerated calcification in blood vessels. In the context of diabetes, HA's role becomes particularly relevant in the context of diabetes, as studies have

shown that HA levels are altered in diabetic conditions, impacting the vascular microenvironment.

In diabetic patients, there is an accumulation of HA around VSMCs in the tunica media of blood vessels[437]. This accumulation is considered a crucial element in a series of diffuse matrix changes in the vessel walls[402,438], leading to increased vessel wall thickness, especially in juvenile patients with a diabetes[439,440]. Structural changes in the arterial walls associated with altered HA metabolism further suggest its involvement in accelerated atherogenesis[441]. Acute increase in plasma HA was found to coincide with endothelium perturbation, increasing vascular vulnerability[442]. Inhibiting HA synthesis and shedding in response to inflammation, smoking, or diabetes mellitus accelerates atherosclerosis[443]. Both HA and HYAL1 are increased in the plasma levels in patients with diabetes and HYAL1 contributes to vessel wall dysfunction[444].

Accumulation of HA is seen in the glomeruli of diabetic rats[445]. In diabetic rats, increased HYAL activity has been observed, correlating with increased intima-media thickness[415,446,447]. In in-vivo studies, HAS2 transgenic mice show arterial stiffness and atherosclerosis, whilst knock down of the HA receptor, CD44, attenuates arterial diseases[448-450]. CD44-HA is involved in the development of diabetes and Injection of anti-CD44 monoclonal antibody or administration of hyaluronidase showed reduction in diabetes-mellitus in mice[451].

Emerging evidence suggests that HA levels are elevated in diabetes. Diabetes is a complex disease associated with various complications, including cardiovascular issues and vascular dysfunction. If uncontrolled, diabetes can progress to CKD, and we observed similar changes in HA both in diabetes and CKD. Given this intricate relationship, regulating alteration in HA will be crucial in slowing down the process of CKD and hence VC.

1.12.8 HA and VSMCs

In healthy arteries, VSMCs reside in the medial layer, where they actively express contractile proteins (i.e., α-SMA) and account for ECM macromolecules deposition, including elastin, collagens, and proteoglycans. These specialized functions enable VSMCs to play significant roles in maintaining the elasticity of large arteries, regulating the diameter of muscular arteries and arterioles, and facilitating the elastic recoil of arteries in response to changes in hemodynamic conditions[452]. Interestingly, HA has a significant role in the onset and progression of atherosclerotic pathology and can induce VSMCs phenotypic switching.

The interplay between HA and VSMCs has been implicated in several crucial aspects of the disease, including VSMC proliferation and migration. In advanced atherosclerosis, intimal lesions show an increased mass of VSMCs, indicating enhanced proliferation and/or migration of these cells[453]. This coincides with the upregulation of HA production in both migrating and proliferating VSMCs, suggesting that HA is involved in disease progression[454]. Notably, in vitro studies have confirmed the upregulation of HA synthesis in proliferating VSMCs[455,456]. In a study of distribution of HA in different layers of human aorta in association to proliferation and migration, the highest concentration of HA in the human aorta was found in the tunica media, which mainly consists of VSMCs[408]. Treatments using 4MU blocked VSMC proliferation and migration and induced apoptosis[457]. However, rescuing with HMW-HA restored cell viability by inhibiting cell death[458]. CD44, a receptor for HA, is widely distributed in the proteoglycan layer of the ECM. It is associated with VSMC functions such as migration, proliferation, and cellular activation. Studies have shown that CD44 directly regulates VSMC proliferation in vitro[459]. LMW-CD44 interactions stimulate VSMC proliferation, while HMW-CD44 interactions inhibits it[417,460]. HA mediates VSMC migration through both CD44 and RHAMM receptors and VSMC proliferation only through the CD44 receptor[460,461]. Interestingly, VSMCs produce versican[462], which binds to HA[463,464]. The synthesis of versican is also upregulated during VSMC proliferation in vitro, further indicating the intricate relationship between HA and VSMCs in atherosclerosis[465]. In contrast, TSG-6 suppresses migration and proliferation of human VSMCs via NF-κB pathways[358].

The interplay between HA and VSMCs has been implicated as a significant factor in various aspects of vascular diseases. In particular, genetic factors also play a role in this relationship, as different isoforms of HAS genes produce distinct HA types in VSMCs. For instance, overexpression of HAS1 and HAS2 in arterial VSMCs results in the production of predominantly HMW-HA, while HA produced by HAS3 and control VSMCs were LMW-HA[466]. HAS1 transduced VSMCs accumulated greatest amount of HA and increased monocyte binding compared to other transduced VSMCs, and, all transduced cells alters VSMC phenotype[466]. Furthermore, the HAS2 gene has been identified as the major isoform in VSMCs[364,467,468], exerting a substantial influence on VSMC phenotype. When human arterial VSMCs were stimulated with iloprost, a medication for arterial hypertension, there was enhanced pericellular formation of HA coats, and by knocking down HAS2 by siRNA, total HA in response to the medication was markedly decreased[407] suggesting HAS2 has a strong influence of VSMC phenotype. Overexpression of HAS2 in mouse VSMCs showed increased neointimal hyperplasia[415,469]. Overexpression of individual HAS isoforms differentially regulates VSMC migratory and monocyte-adhesive cell phenotypes, whilst constitutive over-expression of hyaladherin TSG-6 confers a growth advantage to these cells and cause vascular remodelling[427,466,470].

In the context of tissue injury and damage, HA plays a significant role in VSMC responses. Studies have shown that during vascular injury, there is an increase in HA synthesis. This increase in HA has been observed to be particularly significant around proliferating VSMCs during the early stages of neointimal formation in injured arteries[427]. In response to tissue damage, over expression of HAS1 and HAS2 is seen in VSMCs[471]. Additionally, CD44, is upregulated in VSMCs after lesions of atherosclerosis, *in vivo*[417]. This upregulation of CD44 has been linked to proliferating responses of VSMCs to HA, as its expression increases in a similar temporal pattern after the lesion[460]. Moreover, research involving bovine VSMCs demonstrated that vascular damage leads to an increase in the expression of RHAMM. This receptor was localized in VSMCs at the edge of the lesion after a scratch wound assay[472]. In this context, blocking HA binding with RHAMM using specific antibodies abolished VSMC migration, suggesting that HA-RHAMM interactions play a role in VSMC movement after injury[472]. Furthermore, studies have shown enhanced expression of TSG-6 in VSMCs after

injury in the rat neointima[358]. TSG-6 is an important mediator in HA-related inflammation and tissue repair processes.

Overall, the interplay between HA and VSMCs is essential in the context of atherosclerosis. HA affects VSMC behaviour by regulating proliferation, migration, and cellular activation, while VSMCs produce molecules that interact with HA, adding to the complexity of their relationship in vascular disease development. These findings provide valuable insights into potential therapeutic targets for managing atherosclerosis and related vascular diseases. However, little is known about the role of HA in VSMC transdifferentiation to osteoblast like cells.

1.12.9 HA and Medial VC

HA plays a crucial role in regulating inflammation and is often abundant in areas of inflammation. It accumulates in the ECM and in serum during various inflammatory states, and often the serum level correlates with the degree of inflammation[473,474]. In a study, HA was shown to remodel the ECM expression in human VSMCs during development of fibroproliferative lesion, potentially accelerating vascular disease[475]. Additionally, the induction of HAS and HA production can lead to complications in the kidney in response to morphogenetic cytokines, highlighting HA's pivotal role in inflammatory responses and its influence on cellular behaviour and the lymphocyte recruitment injury sites[476-478]. Once leukocytes enter the inflamed tissue, they encounter a myriad of ECM and cell surface components. HA has several functions relative to inflammation, and the interactions of leukocytes with HA may be involved in their capture and retention within areas of inflammation. HA has emerged as an important ligand for leukocyte recruitment. It plays an important role in trafficking of leukocytes to and from an inflamed tissue[479,480]. HA and the receptor CD44 facilitate leukocyte margination and emigration from the blood into the vessel wall[481,482]. During inflammation, certain defined stimuli promote HA dependent leukocyte adhesion by stimulating the synthesis of HA cable-like structures that bind monocyte[283,361,483]. Several studies have shown that leukocytes can bind to VSMC via HA cables[278,361].

In CKD, elevated inflammation is associated with high levels of medial VC and related cardiovascular morbidity/mortality. As HA is elevated and involved in mediating inflammation, along with its role in regulating cell differentiation, the thesis will explore the hypothesis that systemic inflammation modulates HA, influencing VSMCs to undergo transdifferentiation into bone-like cells that deposit a calcifying matrix in arteries.

1.13 Hypothesis

Alterations in hyaluronan (HA) regulates medial vascular calcification in chronic kidney disease through regulation of vascular smooth muscle cell phenotype and function.

1.14 Aims

VC is highly prevalent in patients with CKD. It strongly predicts cardiovascular mortality and has no effective treatment. The trans-differentiation of VSMC to an osteoblast-like phenotype within the arterial wall is central to the pathogenesis of VC. Previous work has shown that the extracellular matrix glycosaminoglycan HA is a critical regulator of cell phenotype in the context of cancer biology, stem cell biology and epithelial-mesenchymal transition. Increased expression of HA is also seen in non-CKD related vascular disease. However, the role of HA in regulating VSMC phenotype and osteogenic differentiation in VC has not been previously investigated. My project aims to investigate the hypothesis that the systemic inflammation that is prevalent in patients with CKD drives alterations in HA synthesis and assembly in arteries that promotes VSMCs to differentiate into osteoblast-like cells. These bone-like cells subsequently deposit calcium/phosphate in the vessel walls causing VC, arterial stiffness, and CKD-specific heart disease.

My specific objectives were:

1. To set up an in vitro model of VC and identify the role of cytokines elevated in CKD in driving VC.

2. To characterise alterations in HA before and after osteogenic differentiation and to identify the role of cytokines elevated in CKD in modulating HA in VSMCs. Furthermore, to investigate a functional link between alterations in HA and VSMC osteogenic transdifferentiation.

3. To relate the role of systemic inflammation and uremia with alterations in arterial HA *in vivo*; and correlate this with development of arterial VC.

Chapter 2

Materials and Methods

2.1 Materials

All general and tissue culture reagents were purchased from Sigma-Aldrich (Poole, Dorset, UK), Thermo Fischer Scientific (Waltham, Massachusetts, USA), BD Biosciences (San Jose, USA) or GIBCO/Life technologies (Paisley, UK) unless otherwise stated. PCR and qPCR primers were purchased from Thermo Fischer Scientific. The source of any other reagents used is described in the following sections.

2.2 Human Aortic Vascular Smooth Muscle Cells (VSMCs) Cell Culture

Cryopreserved VSMCs were purchased from Thermofischer (Gibco, UK) and grown in T25 flasks in smooth muscle complete growth medium (Sigma-Aldrich, UK) containing smooth muscle growth supplements: Fetal Calf Serum: 0.05 ml/ml, Epidermal Growth Factor (recombinant human): 0.5 ng/ml, Basic Fibroblast Growth Factor (recombinant human): 2 ng/ml, Insulin (recombinant human): 5 µg/ml). It is a low-serum (5% V/V) medium developed to establish and maintain vascular smooth muscle cell cultures. Primary cells were maintained at 37 °C in 5 % CO_2, and 95 % air in a humidified incubator and routinely passaged at confluency. The medium was replaced every 3 days. Cells between passages four to nine were used for all the experiments. On reaching 80% confluence, the cells were split at a 1:3 ratio using Trypsin/EDTA (Gibco, UK) solution (0.025% trypsin and 0.01% EDTA) in Phosphate Buffered Saline (PBS) (Gibco, UK). The cells were utilized for experiments, or cryo-preserved. All experiments were performed on cells seeded 24-48 hours in advance, allowing the cells to attach to the surface of the tissue culture plate and to reach a cell density appropriate for the experiment.

2.2.1 Cellular Sub-culture

VSMCs were grown to confluent monolayers in 75cm^2 tissue culture flasks. Cells were then treated with a phosphate buffer saline solution (PBS), containing 0.025% trypsin, 0.01 % EDTA and incubated at 37 °C for 1-2 minutes, until cells became detached from the flask. An equal

volume of FBS was then used to neutralise the trypsin and the cell suspension was centrifuged for 5 min at 1500 rpm, at room temperature. The subsequent pellet was suspended in 50 ml of smooth muscle complete growth medium containing 10% FBS. To continue culture expansion, the cell suspension was split with a 1:3 ratio into sterile 75cm^2 tissue culture flasks. The cells were grown to a high density in 75 cm^2 tissue culture flasks. To expand the culture, the cell suspension was diluted 1 in 10, using fresh smooth muscle complete growth medium, before being placed into a sterile 72 cm^2 tissue culture flask. Any remaining unused cells were cryogenically frozen and stored, as described.

2.2.2 Induction of VSMC calcification

In vitro calcification of VSMCs was induced by culturing cells in growth medium 231 (Gibco, UK), supplemented with Osteogenesis Medium (OM). Three different types of OM were initially used to investigate the medium promoting the best VSMC osteogenic differentiation (**Table 3**):

OM1: This contained Ascorbic Acid 2-Phosphate Solution (0.2mM), Glycerol 2-Phosphate (10 mM) and Dexamethasone (50nM) (**Table 3**).

OM2: A commercially bought osteogenic medium supplement, OM2 (Thermo Fischer, UK) which contains fetal bovine serum, 1 % v/v and heparin, 30 µg/ml (**Table 3**).

OM3: Sodium orthophosphate (10mM) was added to the existing media of OM1 (**Table 3**).

The 6-well plates were coated with bovine Fibronectin (PromoCell, Germany), final concentration (1 mg/ml) in PBS. The coated 6-well plates were incubated at Room temperature (RT) for 60 mins till it dried out and then the cells were seeded. Unstimulated control VSMCs were incubated in fresh complete smooth muscle growth medium at the time of stimulation unless otherwise stated. The cells were cultured in 100 units/ml penicillin (Gibco), 100 µg/ml Streptomycin. The cells were cultured until they were 85-90% confluent using the smooth muscle growth medium and replacing the culture medium every 48 hours. When the cells were confluent, the medium was replaced by Osteogenesis Induction Medium.

Three different media were trialed for their effectiveness at inducing differentiation. This medium change corresponded to differentiation Day 0. The medium was replaced by 2 ml of fresh Osteogenic medium every 48 hours. The rate of calcification was determined by Alizarin Red staining and RNA was extracted for analysis of gene expression by PCR, as described.

Normal Medium	Osteogenic Medium 1	Osteogenic Medium 2	Osteogenic Medium 3
1. Fetal Calf Serum: 0.05 ml/ml	1. Ascorbic acid 2-Phosphate (0.2 mM)	Commercially Purchased (fetal bovine serum, 1 % v/v; and heparin, 30 µg/ml)	1. Ascorbic acid 2-Phosphate (0.2 mM)
2. Epidermal Growth Factor (recombinant human): 2 ng/ml	2. B glycerol 2- Phosphate (10 mM)		2. B glycerol 2- Phosphate (10 mM)
3. Basic Fibroblast Growth Factor (recombinant human): 2 ng/ml	3. Dexamethasone (50 nM)		3. Dexamethasone (50 nM)
4. Insulin (recombinant human): 5 µg/ml			4. Sodium Orthophosphate (10 mM)

Table 3 Normal and Osteogenic Induction Media

Normal media is the growth media for vascular smooth muscle cells. For inducing differentiation of the VSMCs, three types of Osteogenic Mediums were used: - OM1, OM2, and OM3. OM1 containing Ascorbic Acid 2-Phosphate Solution (0.2mM), Glycerol 2-Phosphate (10 mM) and Dexamethasone solution (50nM) and OM3, where sodium orthophosphate (10mM) was added to the existing media of OM1. OM2 was commercially purchased osteogenic media.

2.2.3 Cell Storage and Retrieval

Cells that were not required for subsequent experiments were cryogenically stored. Briefly, following subculture, cells were centrifuged to form a pellet. The pellets of VSMC cultures were taken from a 75 cm^2 flask and re-suspended in 1 ml of a solution containing 10% dimethyl sulphoxide (DMSO), 30 % FBS and 60 % smooth muscle complete growth medium, respectively. 1 ml of solution was then transferred to a cryogenic vial (Thermo-Fisher

Scientific) and stored at 80 °C for 24 h. Cells were stored long-term in liquid nitrogen at -196 °C.

2.2.4 Cell Counting and Viability Assay

Cells were counted using a LUNA-FL™ Automated Fluorescence Cell Counter (Logos Biosystem). For each cell count, 10 µl of the cell sample was mixed with 10 µl 0.4% Trypan Blue Stain gently in a microcentrifuge tube by pipetting up and down. 10-12 µl of the mixed cell sample was loaded into the inlet of one chamber of the counting slide LUNA™ Reusable Slide (Cat # L12008 Logos Biosystem). The loaded slide was inserted into the slide port and "Bright Field Cell Counting" button on the home screen was selected. After adjusting the focus of the cells displayed on the screen, "count" was selected and this generated data (Total, Live, and Dead cell concentrations, Viability, Average Cell Size, Actual number of Total, Live and Dead cells) was displayed on the screen.

2.3 Animal Experiments

This collaborative project involved the University of Amsterdam and the University of Maastricht. Animal experiments were conducted in the respective labs. The collaborators transported the tissues for analysis. The two different animal models are: -

a. Medial VC model with no uraemia [A, B], and

b. Atherosclerotic model with uraemia and PD fluid [C-E].

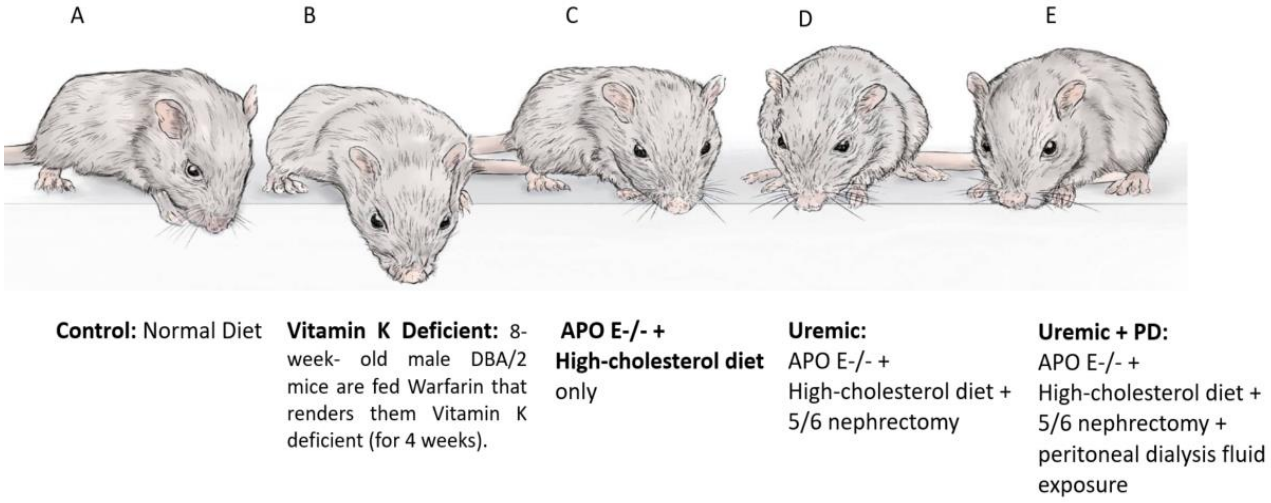

Figure 6 In vivo model of arterial disease – Medial Vascular calcification and Atherosclerosis in mice with CKD.

The two in vivo model are shown here are the Medial Vascular Calcification Model - Control [A], Vitamin K deficient [B], and the Atherosclerosis model - APOE knockout + high fat diet [C], APOE knockout + high fat diet + 5/6th Nephrectomy [D] and APOE knockout + high fat diet + 5/6th Nephrectomy + Peritoneal Dialysis fluid infusions [E].

2.3.1 Induction of Vascular Calcification

DBA/2 mice were bought from Charles River Laboratories Inc ('s-Hertogenbosch, The Netherlands). Mice were kept in a temperature-controlled environment (20°C) with a regular day & night cycle. All animal experiments were conducted under a protocol approved by the ethics committee for animal experiments of Maastricht University. Warfarin (a vitamin K antagonist; VKA) diet was prepared. In brief, warfarin (3 mg/g; Sigma, Zwijndrecht, The Netherlands) was mixed with normal chow diet (Arie Blok diets, Woerden, The Netherlands). Regular Western type diet (WTD) was bought directly from the supplier (0.25% cholesterol; Arie Blok diets, Woerden, The Netherlands). Mice were placed on warfarin diet for either 0 week (control), 1-, 2- or 4-weeks **Figure 6**.

At sacrifice, blood was collected in 3.2% sodium citrate by vena cava puncture and the aorta was flushed with 100 µM sodium nitroprusside in phosphate buffered saline (PBS). The aortic arch, its main branches as well as other organs, were excised and fixated in 1% paraformaldehyde overnight and embedded in paraffin. Aortic arch and aortic root were

sectioned and stained for calcium deposits (Alizarin red and Von Kossa stains) and for HA matrix and HA-related proteins by Immunofluorescence.

2.3.2 Atherosclerosis Model

ApoE$^{-/-}$ mice were purchased from Janvier Labs (Le Genest-Saint-Isle, Laval, France) and bred and housed according to institutional guidelines. All animal experiments were approved by the local Animal Experimental Ethics committee (VU Medical Centre, Amsterdam, the Netherlands) and the Dutch National Central Committee on animal experimentation (AVD11400020209344), in conformation with directive 2010/63/EU of the European Parliament.

2.3.3 Induction of Chronic Kidney Diseases in APOE-/- mice

Twelve-week-old male and female mice were subjected to a 5/6 nephrectomy**.** In brief, mice were placed under isoflurane anaesthesia (0.2 L/min O_2 and air, 4% induction, 2-3% maintenance) after receiving pre-operative analgesia (0.05 mg/kg s.c. Buprenorphine (Temgesic); Schering-Plough, Kenilworth, New Jersey, USA). An abdominal midline incision was made after which the capsule of the left kidney was removed. The upper and lower lobes were then cut away and cauterised (High temperature fine tip cautery pen (Bovie Medical, Clearwater, Florida, USA; #AA01)). Next, during the same procedure the right kidney was decapsulated followed by total ligation of the renal blood vessels and ureter. The right kidney was then removed in its entirety. Soluble sutures were applied to the muscle and skin layers. Mice received twice daily injections of 0.05mg/kg buprenorphine for two days following surgery. Sham surgeries only included the incision and removal of the capsule from both kidneys.

2.3.4 Peritoneal Dialysis Infusions

14 days after the nephrectomy an access port was installed in mice due to undergo peritoneal dialysis fluid exposure (MousePort with 4 French catheter (UNO Roestvaststaal BV, Zevenaar, the Netherlands; #MMP-4S)). One week after surgery, once daily infusions of 2mL of warmed Physioneal (Physioneal 3.86% (Baxter Healthcare Ltd, Thetford, UK)) were started via the port using specialised needles (PosiGrip HuberPoint Needle, 25ga x 1/2" (UNO Roestvaststaal BV, Zevenaar, the Netherlands; #PG25-500)) and continued for 67 consecutive days. At the same time as the port installations, all mice were placed on a high-cholesterol (0.15%) diet (Altromin, Lage, Germany; #C1000 mod) for 9-weeks until the end of experimental period **Figure 7**.

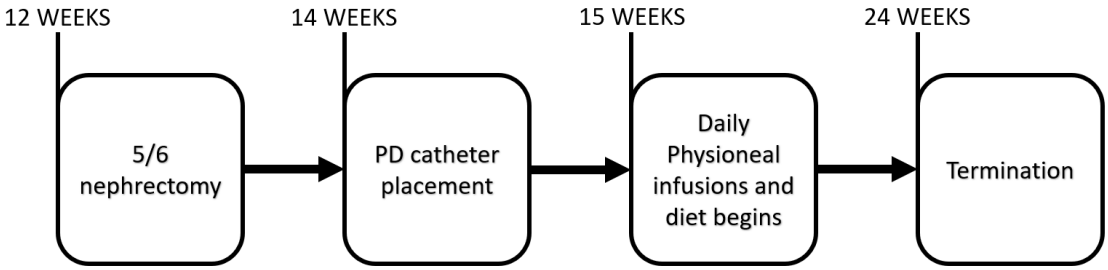

Figure 7 Experimental setup for Atherosclerosis Model

99 *ApoE-/- C57BL6/J* male and female mice are quickly susceptible to plaque development with high-cholesterol/fat diet. Three long term inflammatory hits to establish a new model of Atherosclerosis secondary to 5/6th nephrectomy and dialysis fluid infusions.

2.3.5 Histology of APO E-/- mice

Mice were terminated via CO_2 gassing after which the heart was exposed, and blood collected via right ventricular puncture. 8 ml of ice-cold phosphate-buffered saline (PBS) was then perfused through the system via the left ventricle. The heart, arterial tree, and lymph nodes were fixed in 1% paraformaldehyde (PFA), whilst all other organs and tissues were fixed in 4% PFA. All tissues were then dehydrated and embedded in paraffin and prepared as 4 µm tissue sections.

2.4 Calcium Staining

2.4.1 Calcium Assay: Alizarin Red-Cell Staining

Alizarin red staining was used as a determinant of calcium in the cell matrix. The cells were fixed with 4 % paraformaldehyde for 15 mins. After removing the fixative, the cells were rinsed three times with distilled water. Water was removed and 1 ml/well Alizarin red solution was added. It was incubated at room temperature for at least 20 mins. The excess dye was removed, and cells washed 4 times with deionized water by gentle rocking for 5 mins for each wash. 1.5 ml of water was added to each well to prevent the cells from drying. Each plate was inspected with a standard inverted light microscope (Leica DMLA Light Microscope). Representative images were taken using an Olympus DP27 Microscope Digital Camera.

2.4.2 Quantitative analysis for Alizarin Red staining

The dyed cells were analysed quantitatively for their calcium concentration by comparing OD_{405} values of acetic acid extracts with a panel of standard concentrations. 400 µl of 10% acetic acid was added to each well and incubated for 30 mins with shaking. When the monolayer was loosely attached, a cell scraper was used to gently scrape the cells and transfer the suspension to a microcentrifuge tube. The samples were vortexed before heating them at 85 °C for 10 mins. The tubes were then transferred to ice for 5mins and then centrifuged at 20,000 x g for 15 mins. 400 µl of the supernatant was transferred into a new microcentrifuge tube and the pH was neutralized using 10% Ammonium Hydroxide. Alizarin red standards (ARS) were made by diluting 10X ARS dilution buffer. 1:10 in distilled water to obtain a 1X working ARS dilution buffer. 40 mM Alizarin Red solution was diluted to 1:20 in 1X ARS dilution buffer to get a 2 mM working stock. Standards were constructed in a ‘high range’ set by diluting the 2 mM working stock in 2-fold serial dilutions in 1.5 ml microcentrifuge tubes. The blank consisted of just the 1X ARS dilution buffer. 150 µl of the

standard samples were added in duplicates to the wells of an opaque-wall, transparent bottom 96-well plate and absorbance measured at OD_{405}.

2.4.3 Calcium Assay: Alizarin Red -Tissue Staining

Alizarin Red S, an anthraquinone derivative, used to identify calcium in tissue sections. Slides of mouse aorta sections were placed in a Techne Hybridisation Incubator (HB-1D) for 30 minutes at 60 °C until the wax had melted. Sections were deparaffinised using three xylene (Merck) immersions (5 mins each), agitating gently at each stage. Sections were then rehydrated using reducing concentrations of ethanol (Merck); initially three immersions in 100% ethanol (5 mins each), followed by three immersions in 96%, 70% and 50% ethanol respectively (1 min each). Sections were rinsed in distilled water before being placed into a sodium citrate buffer with tween (10 mM, 0.05% Tween, pH 6.0). Antigen retrieval was performed by autoclaving the sections immersed in sodium citrate buffer (Astell AMB240 Autoclave, Liquid Programme) at 120°C for 20 mins. Slides were then rinsed twice in 1 x Phosphate Buffered Saline (PBS), pH 7.4. Wax Pen (Vector Laboratories) was used to outline the aorta section on each slide. Slides were placed in a moistened slide chamber. 2 g of Alizarin Red S was mixed with 100 mL of distilled water and the pH was adjusted to 4.3 with 10% ammonium hydroxide. Fresh Alizarin Red solution was added to the tissue section for 5 minutes at room temperature. This produced a red-orange staining of the calcium in the aorta. The excess dye was blotted off the sections and was dehydrated in acetone, 20 dips. Then in Acetone-Xylene (1:1) solution, 20 dips. The sections were then dehydrated through distilled water x2, ethanol 50%, ethanol 70%, ethanol 96%, ethanol 100% x3, xylene x3 (20 dips each), before being mounted with Cytoseal (ThermoFisher) and covered with a cover slip. The tissue sections were inspected with a standard inverted light microscope (Leica DMLA Light Microscope). Representative images were taken using an Olympus DP27 Microscope Digital Camera.

2.4.4 Calcium Assay: Von Kossa staining

Von Kossa staining is used in histological visualization of calcium deposits in paraffin or frozen sections. The tissue sections were deparaffinized as described above. The slides were incubated in 50 µl Silver Nitrate Solution (5%) and was exposed to UV light or 100-watt bulb for 1 hour. The sections were rinsed 3 times in distilled water. 50 µl of 2% Sodium Thiosulphate was added to the sections and incubated for 5 minutes. The sections were washed in tap water x2 and then with distilled water x2. The sections were counterstained with Nuclear Fast Red solution and were incubated for 5 minutes. The sections were again washed in tap water x2 and then with distilled water x2. The sections were then dehydrated with distilled water, water, ethanol 50%, ethanol 70%, ethanol 96%, ethanol 100% x3, xylene x3 (20 dips each), before being mounted with Cytoseal (ThermoFisher) and covered with a cover slip. The stains were visualised using Leica DMLA Light Microscope.

2.5 Cytokine stimulation

VSMCs were induced with 10 ng/mL human recombinant TGF-β1 (R & D Systems, Abingdon, UK) or 10 ng/ml IL-6 (R & D Systems, Abingdon, UK) for 0, 7, 14 and 21 days. VSMCs were grown to 85% confluence before the medium was replaced with control medium or osteogenic medium containing 10 ng/ml of TGF-β1 or IL-6. The experimental cell system used to observe the effects of stimulation with TGF-β1 or IL-6 on VSMC osteogenic differentiation.

2.6 Chemical Treatments to modulate HA

4-Methylumbelliferone (4MU) (Sigma-Aldrich) was used to inhibit HA synthesis in VSMCs. 4MU is a coumarin derivative that is known to inhibit HA synthesis. This agent inhibits global HA synthesis by depletion of cellular Uridine diphosphate glucuronic acid (UDP-GlcUA) by enzymatic conjugation to glucuronic acid. Confluent monolayers of VSMCs were incubated for 48 hours in smooth muscle complete growth medium containing 1 mM of 4MU in 0.1%

(v/v) DMSO. Control cells were incubated for 48 hours in smooth muscle complete growth medium containing 0.1% (v/v) DMSO. Following 48 hours, the medium was replaced by either smooth muscle complete growth medium (control) or fresh OM (treated) and analysed as previously described. Treatment with 4MU was assessed by RT-qPCR and the Alizarin-Red assay.

Hyaluronidase from Streptococcus hyaluronidase (Sigma-Aldrich) was used to provide a HA depleted state around cells for an extended period of time. Hyaluronate lyase cleaves HA at the β-D-GalNAc-(1-4)-β-D-GlcA bond yielding 3-(4-deoxy-β-D-gluc-4-enuronosyl)-N-acetyl- D-glucosamine tetra- and hexasaccharides. Unlike other hyaluronidases, this enzyme is specific for HA and is inactive with chondroitin and chondroitin sulphate. Cells were treated with 1iU Streptococcus hyaluronidase for 1 hour prior to stimulation with Osteogenic medium.

2.7 Plasmid Generation

2.7.1 HAS1/HAS2 Overexpression Vector

The HAS1 and HAS2 vectors were purchased (New England Biolabs). Amplification of the cloned vector was achieved via bacterial transformation into one-shot competent Escherichia coli (New England Biolabs) and subsequently grown overnight on ampicillin containing agar. Single colonies were extracted, sub-cultured and DNA purified, according to the Miniprep Kit protocol (Sigma-Aldrich). Negative RT experiments were performed alongside HAS1 and HAS2 mRNA QPCR, to ensure pCR 3.1-HAS1/HAS2 vectors were not conveying false positive overexpression. All samples were RQ1 DNAse treated (Promega) prior to RT to prevent amplification of open reading frame DNA.

2.8 Transient Transfection

2.8.1 Plasmid Transfection

Transient transfection was performed with the aid of the Lipofectamine LTX Transfection Kit according to manufacturer's protocol (Life Technologies). Briefly, for one 12-well cell culture plate; 375ng plasmid DNA, 0.5 µl PLUS reagent and 1 µl Lipofectamine LTX were added to 200 µl OPTIMEM transfection medium, mixed well and incubated at room temperature for 15 minutes. Following incubation, 200 µl of transfection solution was then added to the well containing 800 µl supplemented smooth muscle complete growth medium. Cells were incubated for 72 hours before the medium was replaced with Osteogenic medium for further experimentation or analysis. As a negative control, an empty pCR 3.1 plasmid (containing no open reading frame sequence) was also transfected into cells. VSMCs were grown to 70% confluence prior to transfection.

2.8.2 Small Interfering RNA (siRNA) Transfection

Transient transfection was carried out using a specific siRNA to HAS3 (ID 119475). VSMCs were grown to 80% confluence in 6-well plates in complete smooth muscle growth medium. Two solutions were made for transfection, the first contained 100 µl per sample of OPTIMEM transfection medium and the specific target siRNA (33 nm; final concentration.). The second contained 100 µl of OPTIMEM transfection medium and Lipofectamine 2000 (1:50 dilution; Invitrogen). The two solutions were incubated at room temperature for 45 min, combined and mixed thoroughly. 800 µl of OPTIMEM transfection media was added to the solution for each sample, this gave a final transfection solution volume of 1 ml per well. 1 ml of fresh smooth muscle complete growth medium/ Osteogenic Medium was then added to each well and samples were incubated for 48 hours. Following transfection, the medium was removed, and fresh smooth muscle complete growth medium/Osteogenic Medium was added 2 ml/well and was replaced every 48 hours. A negative control scrambled siRNA I.D. AM4613 (Ambion) was carried out simultaneously for all transfection experiments (a nonsense sequence, bearing no resemblance to known human mRNA sequence).

2.9 Collagen Gel Analysis

Collagen type I (5mg/ml) sourced from rat tails (Gibco) was diluted to 4mg/ml. Briefly, 8 ml of collagen was added to (1ml) 10xPBS, (0.20 ml) 1M NaOH, and 0.8 ml (dH_2O). The subsequent solution was then slowly mixed to achieve the optimal pH 7.0. The gel was pipetted into 6-well plates and incubated at 37 °C for 40 min, until the gel was firm. The gels were then washed using culture medium before VSMCs were seeded and left to adhere in smooth muscle complete growth medium. Following 48 hours growth period, VSMCs were stimulated with Osteogenic Medium. Control (non-stimulated) VSMC cultures were used as experimental controls.

2.10 RNA Analysis

2.10.1 RNA Extraction

VSMCs were lysed in TRIzol Reagent (Thermo Fischer Scientific, UK) and RNA was extracted as per manufacture's recommended protocol with TRIzol Plus RNA Purification Kit (Thermo Fischer, UK). The growth medium was removed from the culture wells and 1 ml of TRIzol™ Reagent was added per 1×10^5—10^7. The lysate was pipetted up and down several times to homogenize. The lysate was centrifuged for 5 minutes at 12,000 × g at 4–10°C, then the clear supernatant was transferred to a new tube and was incubated at RT for 5 minutes to permit complete dissociation of the nucleoproteins complex. 0.2 mL of chloroform was added per 1 ml of TRIzol™ Reagent and incubated for 2–3 minutes. followed by centrifugation of the sample for 15 minutes at 12,000 × g at 4°C. The mixture separated into a lower red phenol-chloroform phase, an interphase, and a colourless upper aqueous phase. Approximately, 600 µl of the colourless, upper aqueous phase containing the RNA was transferred to a new tube and an equal volume of 70% ethanol was added, then mixed by vortexing. Up to 700 µl of the sample was transferred to a spin cartridge (with collection tube) and centrifuged at 12,000 ×

g for 15 seconds. The flow-through was discarded then the spin cartridge was reinserted into the same collection tube. 700 µl of Wash Buffer I was added to the spin cartridge and centrifuged at 12,000 × g for 15 seconds. The flow-through was discarded and then the spin cartridge was reinserted into the same collection tube. 500 µl of Wash Buffer II was added to the spin cartridge and centrifuged at 12,000 × g for 15 seconds. The flow-through was discarded and then the spin cartridge was reinserted into the same collection tube. Centrifuged again at 12,000 × g for 1 minute to dry the membrane and the collection tube was discarded, the spin cartridge was inserted into a recovery tube and 30 µl of RNase-free water (Thermo Fischer Scientific) was added to the centre of the spin cartridge and centrifuged at >12,000 × g for 2 minutes. The spin cartridge was discarded. The recovery tube contained the purified total RNA. This was stored on ice if used within a few hours. For long-term storage, the purified RNA was stored at - 80 °C. The quality and quantity of the purified RNA was determined by UV absorbance at 260 nm using Nanodrop 3300 (Thermo Scientific).

2.10.2 Reverse Transcription (RT)

Reverse transcription polymerase chain reaction (RT-PCR) was employed to detect specific changes in gene expression. mRNA reverse transcription and resultant cDNA generation was performed using a High-capacity cDNA Reverse Transcription Kit with RNase Inhibitor (Thermo Fischer Scientific, UK). The RT was conducted using a final volume of 20 µl per reaction, containing: 1 µg RNA (diluted in 10 µl RNase free distilled H_20), 2 µl of 10* RT random primers, 2 µl of 10 * RT buffer, 0.8 µl of 25* 100 mM dNTPs (deoxynucleotide triphosphates; mixed nucleotides: dATP, dCTP, dGTP and dTTP), 1 µl of 50 U/µl Reverse Transcriptase, 0.5 µl of 20 U/µl RNase Inhibitor (Promega) and 3.7 µl RNase Free distilled H_2O. RT non template control (RT-NTC) or negative control reaction contained an equal volume of water instead of diluted RNA. Thermal cycling conditions were: 10 minutes at 25°C, 2 hours at 37°C and 5 minutes at 85°C, followed by a cooling step at 4°C. Generated cDNA was stored at -20°C until further use.

2.10.3 Real Time – quantitative polymerase chain reaction (RT-qPCR)

RT-qPCR was used to determine mRNA expression of Osteopontin (SPP1), Runt-related transcription factor 2 (RunX2), Alkaline phosphatase (ALPL), α-SMA (ACTA2), HAS Synthases (HAS1, HAS2, HAS3), Hyaluronidases (HYAL1 and HYAL2), HA receptors (CD44 and RHAMM), and HA binding proteins (TSG6 and Versican). Primers were purchased from Thermo Fisher Scientific and were either custom designed or commercially available (see **Table 4** and **Table 5**). Experiments were carried out in 6 well plates. Briefly, cells were washed with PBS and total RNA was extracted using TRIzol. RT-qPCR was carried out using either TaqMan Fast Universal PCR master mix (x2 No AmpErase ® UNG) or Power SYBR Green PCR Master Mix (Thermo Fisher Scientific) according to the manufactures' protocols. 1 µl of cDNA was used for all qPCR reactions. A negative control containing RNase-free de-ionised H2O in the place of the cDNA was included in each experiment. Endogenous controls, β-actin (TaqMan) or β-actin (SYBR green) that were not affected by the treatments used were amplified simultaneously with the gene target to be used as a reference gene. Expression analysis was carried out using the ViiA-7 real time PCR system from Thermo Fisher Scientific. The amplification program for SYBER green used a cycle of 95 °C for 15 s and 60 °C for 1 min for 40 cycles, followed by a melt-curve stage at 95 °C for 15 s, 60 °C for 1 min, and a final dissociation step of 95 °C for 15 s. Relative quantification used the comparative CT method. The CT value (the threshold cycle where the amplification is in the linear range of the amplification curve) of the standard endogenous control reference gene was subtracted from the CT value of the target gene to obtain a ΔCT value. The mean ΔCT was then calculated for control experiments. The relative quantification (RQ) for the experimental target genes was then calculated using the mean of the control experiments with the following equation (2^ − (Δ($Experimental\ Target$) − ΔCT($Mean\ Control\ Grup$)) .

Gene Target	TaqMan® Gene Expression assay
RUNX2	Hs01047973_m1
SPP1	Hs00959010_m1
ALPL	Hs01029144_m1
ACTA2	Hs00426835_m1
HAS1	Hs00987418_m1
HAS2	Hs00193435_m1
HAS3	Hs00193436_m1
HYAL1	Hs00537920_g1
HYAL2	Hs01117343_g1
CD44	Hs00153304_m1
RHAMM	Hs00234864_m1
TSG-6	Hs00200180_m1
VCN	Hs00171642_m1
B-Actin	Hs01060665_g1

Table 4 Applied Biosystems™ TaqMan® gene expression assay mixes.

Catalogue and assay IDs are provided *in lieu* of primer sequences, as Applied Biosystems™ do not supply this information.

Gene Target	Custom-design Primer Sequence
B-Actin	Forward: GACAGGATGCAGAAGGAGATTACT Reverse: TGATCCACATCTGCTGGAAGGT

Table 5 Applied Biosystems™ SYBR™ Green gene expression assay primers.

On delivery, primer efficiencies were optimised by group members through use of a 10-fold dilution series (90 - 100 % efficiency accepted).

2.11 Hyaluronan Enzyme-Linked Immunosorbent Assays

An ELISA-like assay (HA ELISA) was commercially purchased (Corgenix, Broomfield, CO, USA) and used to assess the concentrations of HA in HASMC cultures, and cells stimulated with Osteogenic Medium. Cells were grown in 6-well plates and were maintained at 37°C in a 5% CO_2/95% air atmosphere, for the duration of the experiment. The samples were collected at 0, 7, 14 and 21 days. VSMCs were grown to 85% confluence before the medium was replaced with control medium or osteogenic medium. To investigate the changes in soluble HA in media (extracellular HA), cell culture medium was removed and transferred into Eppendorf microcentrifuge tubes and kept on ice. To investigate changes in pericellular HA, cells were then washed with PBS before adding 500 µl trypsin-EDTA (0.01%) solution for 5 min at room temperature. The samples were centrifuged, at 4000 x g for 5 mins at 4 °C. The supernatant was transferred to Eppendorf microcentrifuge tubes, and trypsin was deactivated by heating to 95 °C for 5 min then kept on ice, which was used to investigate pericellular HA. The cell pallet was re-suspended in 100 µl of Lysis Buffer [1 ml of RIPA lysis buffer (Promega, Wisconsin) and 10 µl Protease Inhibitor Cocktail (Santa Cruz Biotech)] and kept on ice for 10 min. This extract was used to investigate the changes in intracellular HA.

All the samples (extracellular, pericellular, and intracellular) were centrifuged at 1000 x g for 10 mins at room temperature. HA was then quantified by ELISA, according to the manufacturer's protocol. All of the reagents, buffers, controls, and reference solutions were provided (In Kit), which were warmed to room temperature before use. Immediately before use, wash buffer was prepared using 33X concentrate PBS wash (30 ml; In Kit), made up to 1 L with dd-H_2O (0.01 M final concentration, pH 7.35).

The assay used micro wells coated with a highly specific HA binding protein (HABP) from bovine cartilage to capture HA and an enzyme-conjugated version of HA to detect and measure HA in samples. Once at room temperature, all HA reference solutions, HA controls and samples of extracellular, pericellular, and intracellular HA were briefly vortexed and centrifuged for 30 s. Each of these was subsequently diluted in fresh 1.5 ml tubes by adding 10 parts reaction buffer to 1 part solution/control/sample. All dilutions were vortexed and centrifuged as before, and 100 µl of each were added to the appropriate wells of the HABP-coated 96-well plate Diluted samples and HA reference solutions were incubated in the micro wells allowing HA to bind to immobilized HABP for 1 hour. Post incubation, wells were emptied carefully to avoid cross-contamination and washed using wash buffer (x4) to remove non-bound molecules. Wells were inverted between each wash and any excess buffer was removed by blotting plates on absorbent paper. After residue removal, HABP conjugated with Horseradish Peroxidase (HRP) (100 µl/well) was added to the wells and incubated for 30 mins at room temperature, allowing complex formation with bound HA. Following a second wash, a chromogenic substrate (TMB/H_2O_2) (100 µl/well) was subsequently added for 30 min, under darkness, at room temperature, was added to develop a coloured reaction. Stopping solution (100 µl/well) was added to the wells and the intensity of the colorimetric signal was measured using a Fluostar Optima Meter spectrometer at 450 nm wavelength and its incorporated analysis software, MARS™. HA concentrations were analysed by comparing the absorbance of the samples against a reference curve prepared from five reference solutions (50, 100, 200, 500 and 800 ng/ml) and a reagent blank (0 ng/ml) included in the kit. The assay was sensitive to 10 ng/ml, with no cross-reactivity reported with other GAG components. Mean concentrations of HA (ng/ml) and the SEM values were calculated for each condition/sample group. Each of the experiments were performed independently, at n = 3.

2.12 Protein Analysis

2.12.1 Immunocytochemistry and Confocal Microscopy

Immunocytochemistry (ICC) and Confocal microscopy (CFM) were used to analyse α-SMA stress fibre, F-actin formation, and the localization of Hyaluronan. Immuno-fluorescent visualisation of HAS Synthases (HAS1, HAS2, HAS3), Hyaluronidases (HYAL1 and HYAL2), HA receptors (CD44 and RHAMM), HA binding proteins (TSG6 and Versican) protein expression and interaction were performed. Cells were sub-cultured from 75 cm^2 flasks, seeded in 8 well Permanox chamber slides (Nunc; Thermo Fisher Scientific) and grown to 80% confluence. Cells were fixed using 4 % (w/v) paraformaldehyde solution for 15 mins at room temperature. For intracellular analysis cells were treated with 0.1 % (v/v) Triton X-100 for 5 min at room temperature and then washed 3 times with PBS. For blocking the endogenous background of HA, one drop of Avidin (from ready-to-use bottle) was added to each cell chamber and incubated for 15 mins. The cells were then washed with PBS and followed by 1 drop of biotin (from ready-to-use bottle) to each well chamber and again incubated for 15 mins. The cells were washed with PBS and then blocked using 200 µl 0.1% (w/v) BSA/PBS for HA and 10% goat serum for appropriate primary antibody (**Table 6**) per well for 1 h, at RT to prevent non-specific binding. Samples were then washed and treated with 200 µL of the appropriate primary antibody for 1 hour at RT or overnight at 4 °C. When visualising HA, bHABP was used in place of primary antibody and for visualising F-actin, a phalloidin conjugate Alexa Fluor® 555 (Sigma-Aldrich) was used. Following 3 PBS washes, a secondary antibody conjugated to a fluorescent tag (**Table 7**) was added to the well for 1 h, at RT. Avidin-FITC was used in place of secondary antibody when visualising HA. Incubation of secondary and nuclear staining was performed whilst covered to avoid photobleaching. Wells were washed 3 times with PBS and stained with DAPI (1:1000) stain (Vector laboratories Inc. Birlingane) for nuclear staining. The cells were then washed 3 times with PBS. The slides were then mounted with cover slips using Fluroschield mounting media for fluorescence. Samples were visualized and examined under UV- light using a Leica Dialux 20 fluorescent microscope or Zeiss LSM880 upright confocal microscope with Airyscan.

Indirect immuno-fluorescent identification of Phalloidin was used to visualise F-actin as assessment of Osteogenic differentiation using a different staining protocol. After incubation in 1% (w/v) bovine serum albumin (BSA) and washes, cells were incubated with Phalloidin toxin conjugated to FITC (Sigma) diluted in 0.1% BSA in PBS for 2 hours at room temperature.

After a further washing step, cell nuclei were stained with Hoechst / DAPI solution (Sigma). Cells were then mounted and analysed by fluorescent microscopy as before.

Antibody	Host and Type	Dilution
Anti-α-SMA	Polyclonal - Mouse/ IgG2a	1:25
Phalloidin – Conjugate Alexa Fluor 555 (Sigma)	N/A	1:25
Hyaluronan Binding Protein (HABP) (Merck Lifesciences)	N/A	1:100
Anti-HAS1 (Abcam)	Monoclonal - Rabbit	1:100
Anti-HAS2 (Santa Cruz)	Monoclonal - Rabbit	1:100
Anti-HAS3	Polyclonal - Rabbit/ IgG	1:100
Anti-HYAL1	Polyclonal - Rabbit/IgG	1:100
Anti-HYAL2	Monoclonal - Goat	1:100
Anti-CD44	Monoclonal - Rabbit	1:100
Anti-RHAMM	Polyclonal - Rabbit/ IgG	1:100
Anti-TSG-6	Polyclonal - Rabbit/ IgG	1:100
Anti-VCAN	Polyclonal - Mouse/IgG	1:100

Table 6 Primary antibodies for Immunofluorescence

Antibody	Host and Type	Dilution
Anti-Mouse-IgG2b (Alexa Fluor 488)	Polyclonal-Goat	1:500
Anti-Rat-IgG1 (Alexa Fluor 488)	Polyclonal-Goat	1:500
Anti-Rabbit-IgG (Alexa Fluor 488)	Polyclonal-Goat	1:500
Anti-Mouse-IgG2a (Alexa Fluor 594)	Polyclonal-Goat	1:500
Anti-Rat-IgG (Alexa Fluor 594)	Polyclonal-Goat	1:500
Anti-Rabbit-IgG (Alexa Fluor 594)	Polyclonal-Goat	1:500
Streptavidin 488	N/A	1:200
Streptavidin 594	N/A	1:200

Table 7 Secondary antibodies for Immunofluorescence

2.12.2 Immunofluorescence

Immunohistochemistry was used for visualisation of HA matrix, HAS Synthases (HAS1, HAS2, HAS3), Hyaluronidases (HYAL1 and HYAL2), HA receptors (CD44 and RHAMM), HA binding proteins (TSG6 and Versican) protein expression and interaction in tissue sections of mouse aorta. Slides preparation till antigen retrieval step were same as mentioned above in **Section 2.5.3**. Slides were then rinsed twice in 1 x Phosphate Buffered Saline (PBS), pH 7.4. Wax Pen (Vector Laboratories) was used to outline the aorta section on each slide. Slides were placed in a moistened slide chamber. Endogenous peroxidase activity was blocked by applying 3% hydrogen peroxide/methanol to each section for 10 minutes at room temperature. Slides were then rinsed twice in 1 x PBS. Normal Goat Serum Blocking Solution (Vector Laboratories) 10% was applied to each section for 20 minutes at room temperature. Slides were then rinsed twice in 1 x PBS. Avidin/Biotin Blocking Kit (Vector Laboratories) was used as the final blocking stage when visualising HA. Avidin Blocking Reagent was applied to each section for 15 minutes at room temperature, prior to rinsing twice in 1 x PBS. Biotin Blocking Reagent was then applied to each section for 15 minutes at room temperature, prior to rinsing twice in 1 x PBS.

Primary antibodies (**Table 6**) were diluted with 1% Goat Serum (Vector Laboratories). 50 µl of primary antibody solution was applied to each section and slides were left overnight at 4°C in a moistened slide chamber. Slides were then rinsed three times in 1 x PBS. Secondary antibodies (**Table 7**) were diluted with 1% Goat Serum (Vector Laboratories). 50 µl of secondary antibody solution was applied to each section and slides were left at room temperature for 30 minutes in a moistened slide chamber. Slides were then rinsed three times in 1 x PBS. DAPI solution was applied to each section and slides were left at room temperature for 5 minutes in a dark, moistened slide chamber. Slides were then rinsed twice in 1 x PBS before being mounted with Fluoroshield (Merck) and covered with a cover slip. Tissue sections were analysed by confocal microscopy.

2.13 Statistical Analysis

Statistical analysis was performed using Microsoft® 365 Excel or GraphPad Prism 9.0. Graphical data were expressed as mean ± Standard Deviation (S.D). For statistical analysis of multiple experimental conditions, Kruskal-Wallis test was used to identify statistical differences across groups, followed by Dunn's post-test to identify statistical significance. A p value of less than 0.05 was considered statistically significant (ns = $p>0.05$, * = $p\leq0.05$, ** = $p\leq0.01$, *** = $p\leq0.001$, **** = $p\leq0.0001$).

2.14 Image J analysis

The fluorescent microscopy image was opened using ImageJ software. The region of interest (ROI) was selected for measuring the fluorescence intensity. Background fluorescence was subtracted by measuring a nearby region without fluorescence as the background, and then subtracting its Mean Gray Value from the ROI's Mean Gray Value. For multiple ROI, this was repeated for each image to calculate the mean. The results were obtained from the result window in ImageJ software. The formulae used was corrected total cell fluorescence (CTCF) = *Integrated Density – (Area of Selected Cell x Mean Fluorescence of Background readings).*

Chapter 3

Development and characterization of in vitro experimental model of VSMC osteogenic differentiation

3.1 Introduction

3.1.1 VSMCs osteogenic differentiation

The intricate interplay of VSMCs and their osteogenic transdifferentiation process represents a complex yet vital aspect of understanding and combating VC. In this chapter, we explore the intricacies of VSMC behaviour during osteogenic differentiation, with a focus on uncovering the mechanisms driving this transformation. VSMCs predominantly reside in the medial layer of blood vessels, enduring mechanical stress and exposure to blood flow. VSMCs are not terminally differentiated and can change their phenotype in response to environmental cues including growth factors/inhibitors, mechanical influences, cell-cell and cell-matrix interactions, extracellular lipids and lipoproteins, and various inflammatory mediators in the injured artery wall[190,484,485]. Under normal conditions, VSMCs exhibit an elongated, spindle-shaped morphology and express a low proliferative rate and maintain a stable phenotype[486]. VSMCs are defined by the presence of specific genes and markers that serve as indicators of their identity as smooth muscle cells. Among these key genes and markers is α-SMA, a well-recognized marker that plays a crucial role as a cytoskeletal protein, essential for the contractile function of VSMCs. Additional markers include, Smooth Muscle Myosin Heavy Chain (SMMHC), calponin, SM22α, Smoothelin, Caldesmon, Myocardin, Smooth Muscle Protein 22 Beta (SM22β), Smooth Muscle Cell Actin (SMCA)[199,487-489].

During their *in vitro* transformation into mature osteoblasts, VSMCs exhibit reduced proliferation alongside decreased contractility[490]. During VSMC osteogenic differentiation, VSMCs are thought to shift to an osteoblast-like state. While several genes are known to be upregulated during this transformation, the precise mechanism triggering this shift remains elusive[491]. Some of the key genes associated with this transition encompasses RunX2, Osteopontin, Alkaline phosphatase (ALPL), collagen type I, bone morphogenic proteins (BMPs), SRY-Box Transcription Factor 9 (Sox9) and Msh Homeobox 2 (Msx2)[114,491-493]. Intriguingly, these osteoblastic markers are found to be elevated in the vasculature of both uremic rats and CKD patients[494,495]. It is important to note that the specific gene expression profile may vary depending on experimental conditions and the stage of differentiation[496].

Collectively, these genes serve as molecular markers that aid in assessing and confirming the osteogenic differentiation of VSMCs. As VSMCs differentiate into an osteoblast-like state, they undergo various changes in behaviour and characteristics. One significant change is the initiation of matrix mineralization[88,492,497]. Key developmental steps include the secretion of an organic extracellular matrix and subsequent mineralization through hydroxyapatite deposition[498]. Numerous studies explored this transformation to gain insights into calcification. When VSMCs undergo osteogenic differentiation, there are both similarities and differences between calcified VSMC cells and osteoblasts[499]. For instance, genes associated with osteogenesis such as RunX2, Osteopontin and Alkaline Phosphatase were found to be upregulated in calcified VSMCs. However, the mRNA levels of these genes were considerably lower than what is typically seen in osteoblasts, suggesting an early osteoblast-like stage in calcified VSMCs[499]. Another intriguing finding is that while there are indication of reduced expression of α-SMA in calcified VSMCs supporting the phenotypic switch concept[500], there are also evidences suggesting that VSMC calcifications are not dependent necessarily depend on the downregulation of α-SMA. In fact, in some cases α-SMA expression was upregulated in these osteogenic-like VSMCs[501]. This suggests that VSMCs can undergo transdifferentiation without completely losing their contractile charecteristics[501]. VSMCs kept their own identity while using mechanisms that osteoblasts use to mineralize[501]. Though the exact mechanism of calcification remains unclear, the literature consistently indicates that VSMCs assume an intermediary identity between VSMCs and osteoblasts during this process. This highlights the complexity of their transformation. Existing literature provide evidence that an active inhibition of calcification and the prevention of pro-osteogenic gene expression is crucial for retention of the VSMC phenotype[88,502]. Conversely, it was found that VSMC-mediated calcification is enhanced in an inflammatory environment, under conditions of oxidative stress, hypercalcaemia, and hyperphosphatemia, and in cases of apoptosis[156,494,495,503]. Indeed, numerous studies in both animal models and humans have consistently demonstrated a strong positive correlation between hyperphosphatemia, hypercalcemia, and VC. In experimental settings, conditions such as high serum phosphate levels play a pivotal role in triggering VSMC transdifferentiation. In vitro study have illustrated that elevated phosphate levels actively encourage the deposition of calcium within the arteries[503]. Prior research has shed light on how increased phosphate levels prompt phenotypic changes in VSMCs, leading to enhanced osteochondrogenic protein expression[504,505]. Furthermore,

accelerated calcification of VSMCs has been observed in ESRD patients[129]. Additionally, *in vitro* studies involving the exposure of VSMCs to elevated phosphate and calcium concentrations have demonstrated a dose-dependent increase in mineralization[129,506].

3.1.2 Role of inflammatory cytokines elevated in CKD patients

Cytokines play critical roles in regulating cellular processes, including proliferation, differentiation, survival, and gene expression. However, during chronic inflammatory conditions, the finely tuned control of the immune response is lost, leading to disease progression. In patients with CKD, CVD risk is a complex issue[507] and systemic inflammation is common particularly in those patients with ESRD[508,509]. The reasons behind the increased inflammation risk in ESRD patients are multifaceted, stemming from factors related to both non-dialysis as well as dialysis-related aspect[510-512]. The combination of a compromised immune response and persistent immune activation contributes to the low-grade systemic inflammation and disrupted cytokine balance typical in the uremic state. This imbalance is associated with an elevated risk for vascular disease[512]. The accelerated atherosclerotic process in ESRD involves various interconnected processes, including oxidative stress, endothelial dysfunction, and VC[508,512]. All of these occur in an environment of ongoing low-grade inflammation, with impaired functions of immune cells like neutrophils and T cells, as well as a dysregulated cytokine network[511].

In individuals with CKD, inflammatory cytokines such as IL-6 and TGF-β1 become elevated, sparking an inflammatory response[39,41,513]. Elevated IL-6 levels exhibit a robust correlation with forthcoming cardiac events and cardiovascular mortality in patients with myocardial infarction[514]. Patients with cardiomyopathy and higher serum IL-6 levels demonstrate a lower ejection fraction and worse prognosis[515]. Clinical observations reveal elevated serum IL-6 levels in dialysis patients and CKD patients with VC[516,517]. The perpetuation of vascular inflammation is driven by IL-6, which in turn stimulates VSMC proliferation and migration[518,519]. IL-6 contributes to VC by prompting the differentiation of VSMCs into cells

resembling osteoblasts. IL-6/STAT3 pathway upregulates RunX2 gene expression, which is an important transcription factor of the differentiation of osteoblast[520]. The activation of IL-6-mediated receptor activator of NF-κB ligand (RANKL) significantly influences VC's progression[521,522], and inhibiting IL-6 has been shown to reduce VC[523]. Lee, Guan-Lin et al. further substantiate this by demonstrating that restraining IL-6 can attenuate VC[524].

TGF-β1 is a versatile cytokine associated with VC. In VSMCs, phosphate triggers an increase in TGF-β1 levels, which in turn governs osteogenic differentiation[525,526]. TGF-β1 also regulates VSMC calcification and valve calcification in the heart[526,527]. A noteworthy finding is that while TGF-β1 reduces the expression of VSMC markers like α-SMA, it concurrently amplifies the expression of osteogenic markers and facilitates calcification within aortic segments[528]. TGF-β1 plays a pivotal role in the production of bone matrix, yet its influence does not extend to calcium deposition within VSMCs under high-phosphate conditions[527]. In this context, TGF-β1 prompts an augmented expression of the osteoblast-specific transcription factor RunX2, thereby promoting bone matrix generation in VSMCs exposed to a high-phosphate environment[527]. However, neutralization of TGF-β1 could not inhibit high-phosphate-induced VSMCs calcification, indicating that TGF-β1 was not necessary for the deposition of calcium[527].

In conclusion, the intricate process of VC involves a convergence of factors, with high phosphate levels and the presence of inflammatory cytokines, such as IL-6 and TGF-β1, emerging as key contributors. The elevated phosphate environment triggers molecular cascades that promote osteogenic differentiation, ultimately leading to the deposition of calcium and phosphate within VSMCs. Whilst TGF and IL-6 have been shown in many studies to be correlated with worse VC in clinical studies, the direct relationship between these cytokines and VSMC differentiation has not been explored and you will do this in this chapter.

This chapter will centre on examining the contribution of elevated phosphate levels on VSMC differentiation and explore the culture conditions required to promote optimal VSMC osteogenic differentiation. Furthermore, the work in this chapter explores the direct role of the cytokines IL-6 and TGF- β1 in promoting VSMC osteogenic transformation.

3.2 Results

3.2.1 Establishing an *in vitro* model of VSMC Osteogenic differentiation

Initial experiments were performed on primary cultures of VSMCs to assess and optimize osteogenic differentiation. VSMCs were treated with each osteogenesis induction medium (see methods **Table 3**) for up to 21 days. The VSMCs were then assessed on day 0, day 7, day 14, and day 21 following stimulation. As a control, cells were stimulated with smooth muscle cell growth medium alone. The present study had the purpose to try to mimic *in vitro*, the modification that occurs in CKD patients, to study its effect on VSMC calcification. In order to determine the most optimum conditions to promote VSMC osteogenic differentiation, we used three different types of osteogenic media, OM1, OM2 and OM3 and characterized the changes for each independently.

To demonstrate if incubation of VSMCs with osteogenic medium led to calcium crystal deposition [$Ca_{10}(PO_4)_6(OH)_2$] in the VSMC matrix a commercially available Alizarin Red staining assay was used. The cells were fixed and stained with Alizarin Red and viewed under confocal microscope. To explore the ability of different media to calcify the media, the cells were stimulated with OM1, OM2 and OM3.

Stimulation with OM1, the results demonstrated no Alizarin Red staining at day 0, early evidence of small, typically round, or oval-shaped structures are seen at day 7, and increased sized nodules are observed on day 14 and day 21 **Figure 8 [A-D]**. These oval-shaped structures are called calcified nodules and have a role in mineralization in VSMCs[529,530].

OM2 stimulation did not show any Alizarin red staining in any time points. There was an evident change in morphology from spindle-shaped cells at day 0 to more cobble stone-like structures from day 7 – day 21 **Figure 8 [E-H]**.

Stimulation with OM3, demonstrated no Alizarin Red staining at day 0, early evidence of calcification at day 7, moderate sporadic calcification at day 14 and widespread calcification at day 21 **Figure 8 [I-L]**.

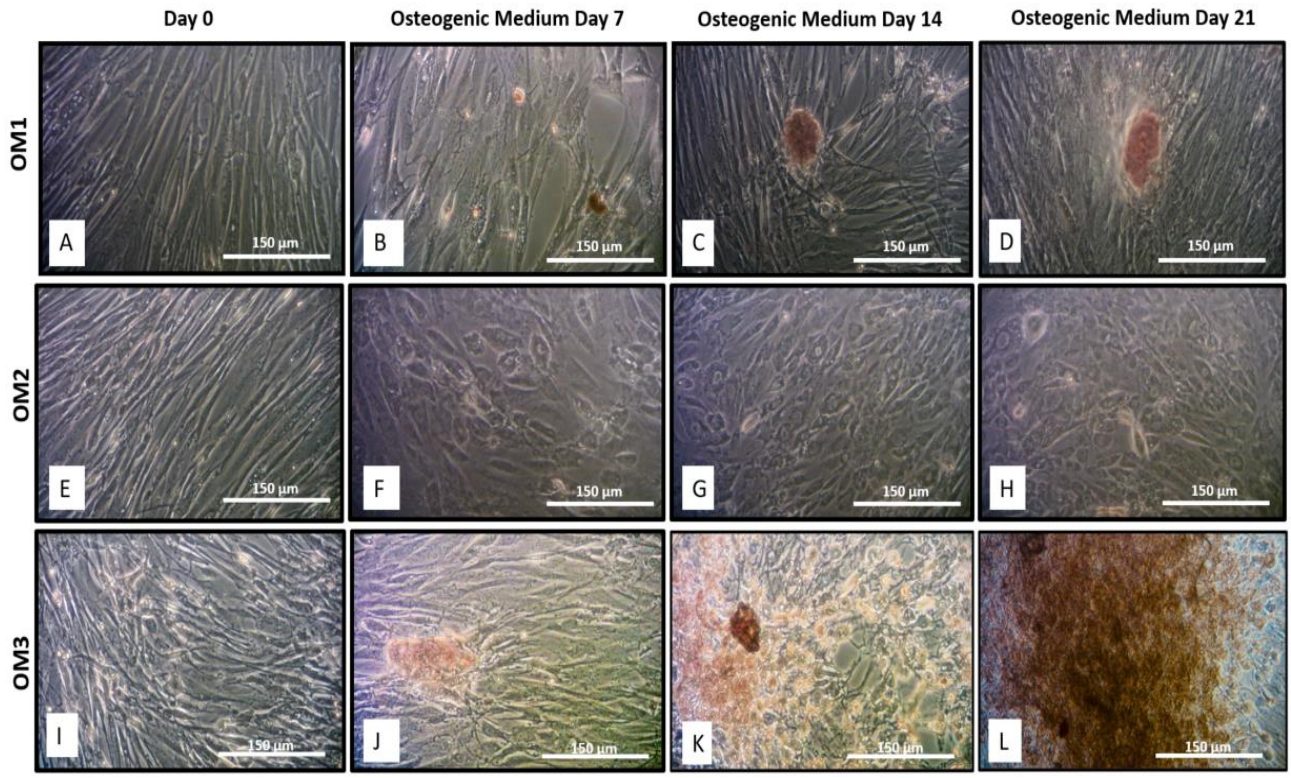

Figure 8 Alizarin red experiment when VSMCs stimulated with OM

Human aortic vascular smooth muscle cells were grown in Osteogenic Medium 1 (OM1), Osteogenic medium 2 (OM2) or Osteogenic medium 3 (OM3). The confluent monolayers were grown for up to 21 days in these media. They had been analysed at four different time points, day 0, 7, 14 and 21. The cells were fixed and stained with Alizarin Red which picks up calcium deposition in the matrix. The cells were analysed under a light microscope at magnification 100X. A digital eyepiece microscope camera was used to take pictures of the cells. Representative photographs of one of four independent experiments giving similar results.

To quantify levels of calcification and investigate the osteogenic medium that led to the most prominent osteogenic differentiation, an absorbance assay was used following Alizarin Red staining. Comparisons were made between osteogenic media 1 and 3 as OM2 did not show any calcification. As a control, cells were also stimulated in normal VSMC growth medium as described in the methods. For quantification, supernatants from cell cultures were assessed on a plate reader to measure absorbance following Alizarin Red staining as described in the

methods. The results demonstrated that osteogenic medium 3 led to a significant increase in calcium deposition at day 14 and 21 compared to control cells and cells stimulated with osteogenic medium 1 **Figure 9 [A]**. This was also evident on observation with naked eye as demonstrated in pictures of cell culture plates **Figure 9 [B]**.

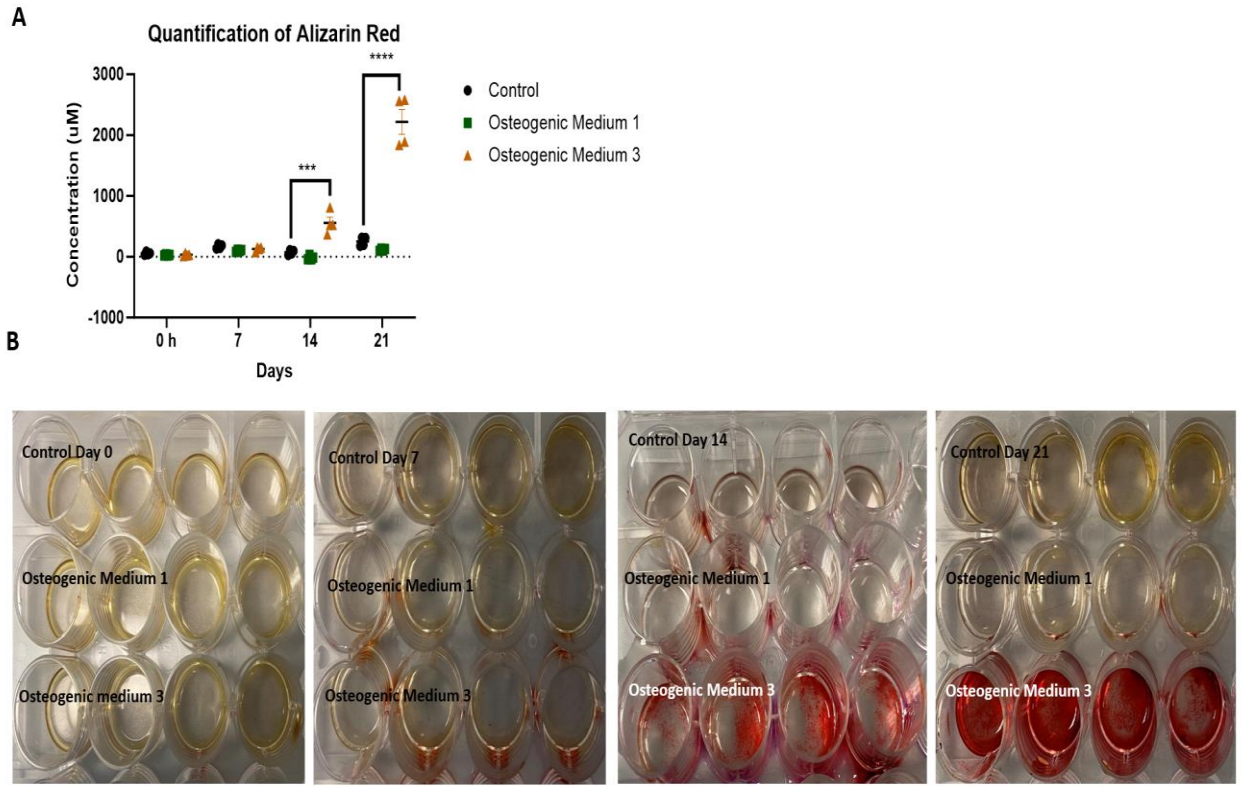

Figure 9 Quantification of Alizarin Red staining showing calcium deposition in human aortic VSMCs cultured under calcifying conditions

Vascular smooth muscle cells were grown in two media: OM1 consisting of Ascorbic Acid 2-Phosphate Solution (0.2mM), Glycerol 2-Phosphate (10 mM) and Dexamethasone solution (50nM) and OM3, where sodium orthophosphate (10mM) was added to the existing OM1. The confluent monolayers were grown for up to 21 days in these media. The monolayers of cells were then stained with alizarin red (B) and extracted for quantitative measurement of absorbance at OD405 (A). (B) Representative photographs of one of four independent experiments giving similar results. Data was analysed by Kruskal-Wallis test followed by Dunn's post hoc analysis (* = p≤0.001, **** = p≤0.0001). The data is expressed as mean ± S.D.**

RT-qPCR was subsequently used to determine the effects of the different osteogenic media outlined in **Table 3** on the transcriptional regulation of osteogenic genes including RunX2, Osteopontin, and bone-specific Alkaline Phosphatase[531 532,533].

Upregulation of RunX2 was observed following treatment with OM1, OM2 and OM3 up to day 21 **Figure 10 [A-C]** compared to control cells at 0 h. This is in line with previous research which has shown RunX2 to have an increased expression in osteoblasts and trans-differentiated VSMCs[533,534]. Stimulation with OM3 demonstrated the most prominent increase in RunX2 expression in VSMCs at day 14 and day 21 **Figure 10 [C]**.

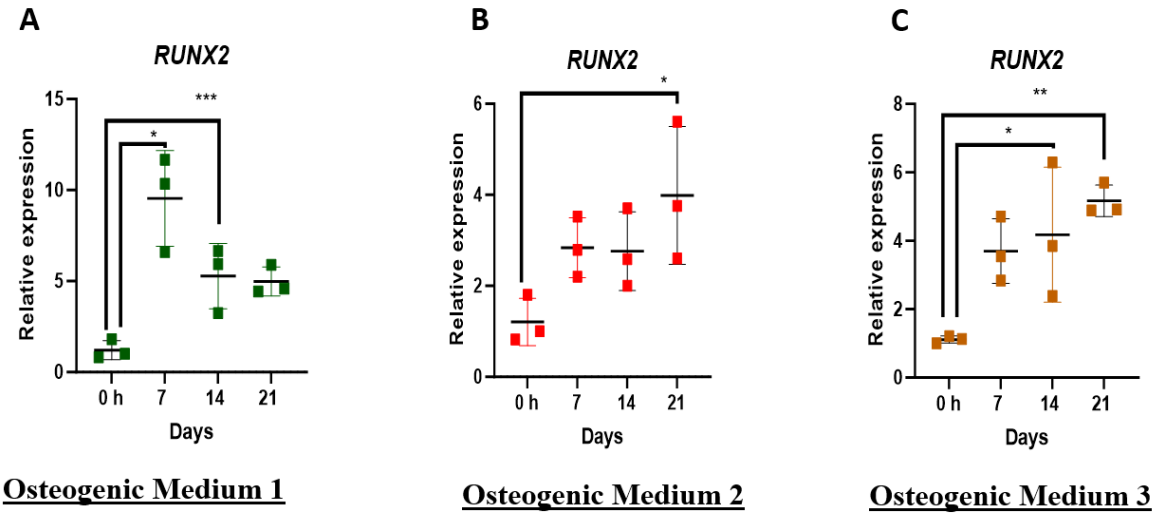

Figure 10 RunX2 mRNA expression in VSMCs incubated with Osteogenic Media

Human aortic vascular smooth muscle cells were grown in Osteogenic Medium 1 (OM1), Osteogenic medium 2 (OM2) or Osteogenic medium 3 (OM3). Control cells were treated with VSMC growth medium. The media were replaced every 3 days. mRNA was extracted at 0 hour, 7 days, 14 days, and 21 days. *RunX2* expression was assessed by RT-qPCR. β-actin was used as a standard reference gene and gene expression was assessed relative to control samples at 0 h. The comparative C_T method was used for relative quantification of gene expression and the results were represented as mean ± S.D. Each point in the scatter dot plot denotes a single biological replicate. Data was analysed by Kruskal-Wallis test followed by Dunn's post hoc analysis (ns = p>0.05, * = p≤0.05, ** = p≤0.01, *** = p≤0.001).

Similarly, Osteopontin an ECM protein highly expressed by osteoblasts[535,536] had an increased mRNA expression by VSMCs treated with OM1 at day 21 compared to control cells at 0 h. However, as previously observed with RunX2 the mRNA expression of Osteopontin had no increase at day 7 or day 14 **Figure 11 [A]**. Using OM2 to stimulate VSMCs had no effect on the mRNA expression of osteopontin at any time point throughout the experiment **Figure 11 [B]**. VSMCs that were stimulated with OM3 had an increased expression of Osteopontin compared to control VSMCs at day 21 **Figure 11 [C]**.

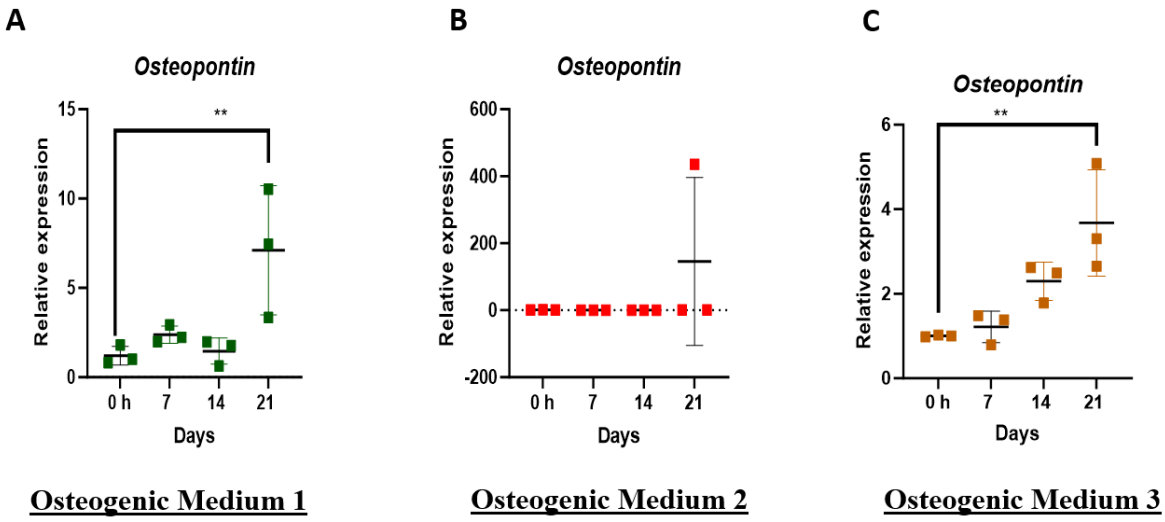

Figure 11 Osteopontin mRNA expression in VSMCs incubated with Osteogenic Media

Human aortic vascular smooth muscle cells were grown in OM1, OM2 or OM3. Control cells were treated with VSMC growth medium. The media were replaced every 3 days. mRNA was extracted at 0 hour, 7 days, 14 days, and 21 days. *Osteopontin* expression was assessed relative to control samples at 0 h. The comparative C_T method was used for relative quantification of gene expression and the results were represented as mean ± S.D. For the scatter dot plot, the median value obtained from each dot, are represented by a line. Each point in the scatter dot plot denotes a single biological replicate. Data was analysed by Kruskal-Wallis test followed by Dunn's post hoc analysis (ns = p>0.05, ** = p≤0.01).

Bone-specific Alkaline Phosphatase (ALPL) is a regulator of bone mineralization. Therefore, an increase in ALPL mRNA expression is indicative of VSMC differentiation to a more osteogenic phenotype[537,538]. Treating VSMCs with OM1 and OM2 increased ALPL expression at day 7 but this was not sustained at the later time points of days 14 and 21 **Figure 12 [A-B]**. Stimulation with OM3 increased the mRNA expression of ALPL at all timepoints from day 7 through too day 21 **Figure 12 [C]**. These data combined corroborate the findings of the Alizarin Red assay that OM3 is the best media for promoting VSMC osteogenic differentiation *in vitro*.

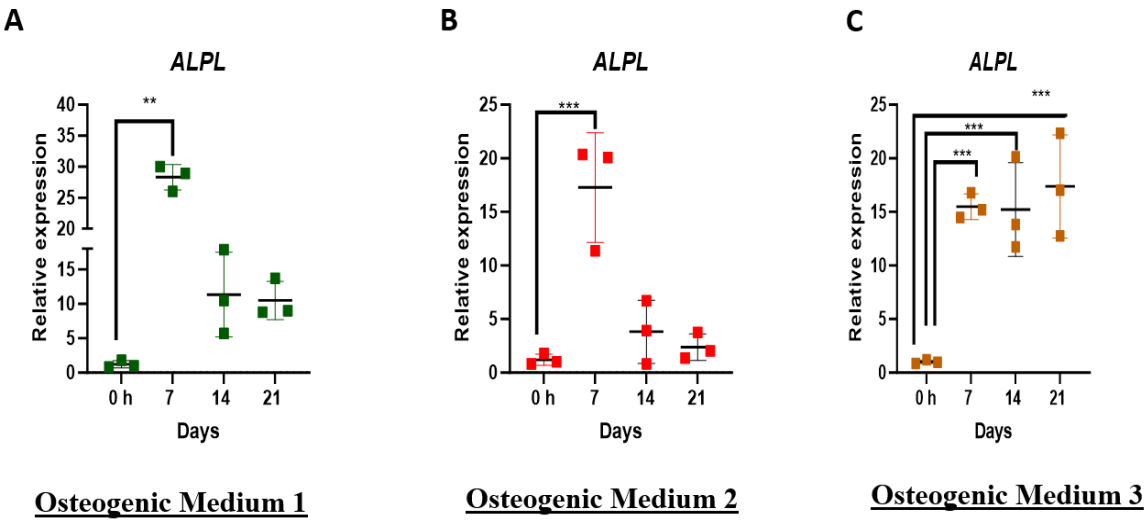

Figure 12 ALPL mRNA expression in VSMCs incubated with Osteogenic Media

Human aortic vascular smooth muscle cells were grown in OM1, OM2 or OM3. Control cells were treated with VSMC growth medium. The media were replaced every 3 days. mRNA was extracted at 0 hour, 7 days, 14 days, and 21 days. *ALPL* expression was assessed relative to control samples at 0 h. The comparative C_T method was used for relative quantification of gene expression and the results were represented as mean ± S.D. For the scatter dot plot, the median value obtained from each dot, are represented by a line. Each point in the scatter dot plot denotes a single biological replicate. Data was analysed by Kruskal-Wallis test followed by Dunn's post hoc analysis (= p≤0.01, *** = p≤0.001).**

α-SMA is a characteristic marker of VSMCs. It is an actin protein involved in the contractile phenotype of smooth muscle[539,540]. α-SMA is also present in non-muscle cells, like myofibroblasts where its contribute to cell contractility[541]. However, α-SMA is not expressed by osteoblasts. Therefore, changes in expression of α-SMA may also be important as VSMCs undergo phenotypic change [542]. The expression of α-SMA was analysed at the mRNA level using qPCR and at the protein level using immunocytochemistry. Cells were stimulated with either OM1, OM2 or OM3, and compared to control cells. To assess the gene expression and the protein expression of α-SMA the timepoints used were as previous: 0 h, 7, 14 and 21 days.

Stimulating VSMCs with OM1 and OM2, showed an increased expression of α-SMA mRNA expression at 7 days, compared to control cells. However, there was no change in α-SMA mRNA expression on day 14 and 21 **Figure 13 [A-B]**. Interestingly, cells stimulated with OM3 also had a higher mRNA expression of α-SMA at the day 7 and 14 timepoints, whereas there is an upward trend at day 21 compared to control cells **Figure 13 [C]**.

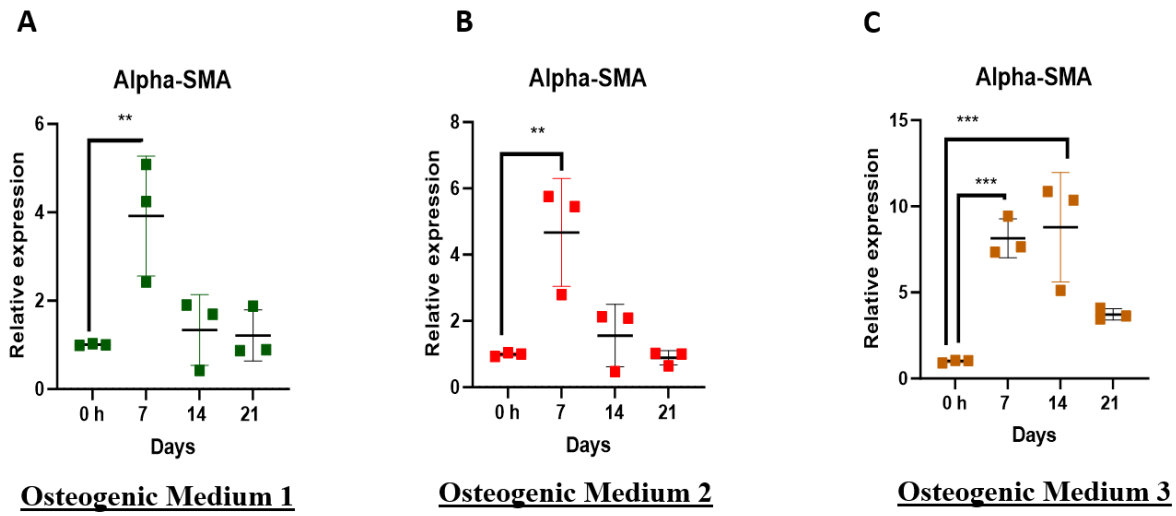

Figure 13 α-SMA mRNA expression in VSMCs incubated with Osteogenic Media

Human aortic vascular smooth muscle cells were grown in OM1, OM2 or OM3. Control cells were treated with VSMC growth medium. The media were replaced every 3 days. mRNA was extracted at 0 hour, 7 days, 14 days, and 21 days. α-SMA expression was assessed relative to control samples at 0 h. The comparative C_T method was used for relative quantification of gene expression and the results were represented as mean ± S.D. For the scatter dot plot, the median value obtained from each dot, are represented by a line. Each point in the scatter dot plot denotes a single biological replicate. Data was analysed by Kruskal-Wallis test followed by Dunn's post hoc analysis (= p≤0.01, *** = p≤0.001).**

To visualize α-SMA protein expression VSMCs stimulated with control medium **Figure 14 [A, C, E, G, I & K]** were compared to VSMCs stimulated with OM3 **Figure 14 [B, D, F, H, J & K]**. Cells were stained for α-SMA as described in the methods. The images were taken at time points day 0, day, 7, day 14, and day 21. VSMCs stimulated with control medium alone had a diffuse expression of cytoplasmic α-SMA throughout the cell at all timepoints **Figure 14 [A, C, E, G & I]**, respectively. The addition of OM3 did not alter this expression at day 0 and there is no change between the control and the differentiated cells **Figure 14 [B]**. Stimulation with OM3 for 7 days increased the cellular expression of stress fibers in some cell populations, **Figure 14 [D] (white arrows)**. However, there were still cells present that exhibited the diffuse cytoplasmic α-SMA expression that was observed in control cells **Figure 14 [D] (white Arrows)**. Following, 14 days of stimulation with OM3 the population of cells that expressed α-SMA stress fibers increased, **Figure 14 [F]**. Nearly all the cells expressed cortical α-SMA stress fibers by day 21 of OM3 stimulation and the intensity of α-SMA staining was significantly increased **Figure 14 [H, J & K]**.

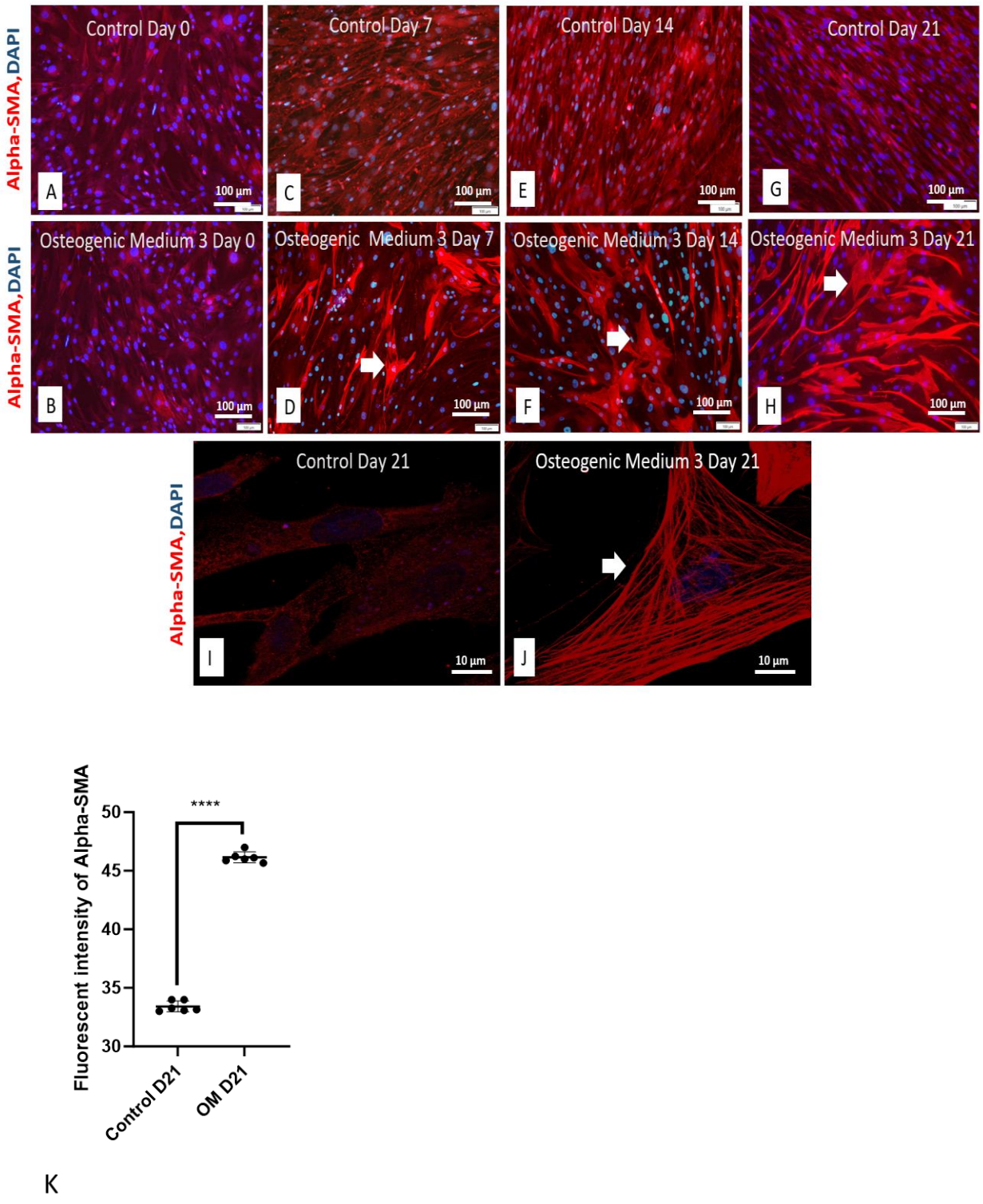

Figure 14 α-SMA (red) protein expression in VSMCs incubated with OM3.

Sub-confluent monolayers of human aortic vascular smooth muscle cells were grown on 8-well chamber slides and treated with OM3. The control cells were grown in smooth muscle growth medium. Cells were fixed using 4 % paraformaldehyde at day 0 (CT), day 7, day 14 and day 21. Cells

were then and stained for α-SMA (red stain), control cells [A, C, E, G and I] osteogenic cells [B, D, F, H and J]. The cells were analysed by confocal microscopy, magnification x100 and x400. Increased α-SMA stress fibres were observed at days 14 and 21 following osteogenic treatment, depicted by white arrows [D, F, H and J]. The fluorescent intensity was measured using the ImageJ software [K]. For the scatter dot plot, the median value obtained from each dot, are represented by a line. All the values are expressed as means ± SD from 6 biological replicates in each group. Data was analysed by Mann-Whitney test followed by Dunn's post hoc analysis (** = p≤0.0001).**

Filamentous actin (F-actin) is a global contractile marker. It can assemble and disassemble, allowing cells to dynamically change their shape and respond to external cues[543]. The orchestration of actin filaments experiences significant shifts during cellular differentiation[544]. To visualize morphological changes for F-actin protein expression, VSMCs stimulated with control medium **Figure 15 [A, C, E, G, I & K]** were compared to VSMCs stimulated with OM3 **Figure 15 [B, D, F, H, J & K]**. The images were taken at time points day 0, day 7, day 14, and day 21. Thin and long actin filaments extend parallel to the long axis in control cells at all timepoints **Figure 15 [A, C, E, G & I] (white arrows)**. The addition of OM3 did not alter this expression at day 0 **Figure 15 [A-B]**. Stimulation with OM3 for 7 days increased the cellular expression of stress fibers in some cell populations and the morphological changes initiated. Distinct individual VSMCs adopt a star-like spread, showcasing a spindle or polygonal shape **Figure 15 [D] (white arrows)**. In these cells, the periphery displays prominently thick bundled fibers. F-actin is evident on the cell's plasma membrane and also appears in intermittent bundles spanning the cell's length. Following 14 days and 21 days of stimulation with OM3 the population of cells that expressed F-actin stress fibers increased coupled with distinct phenotypic shifts. VSMCs transition to a larger polygonal form, accompanied by a substantial reorganization of F-actin into dense bundles that traverse the cell's entire length **Figure 15 [F, H, J & K] (white arrows)**.

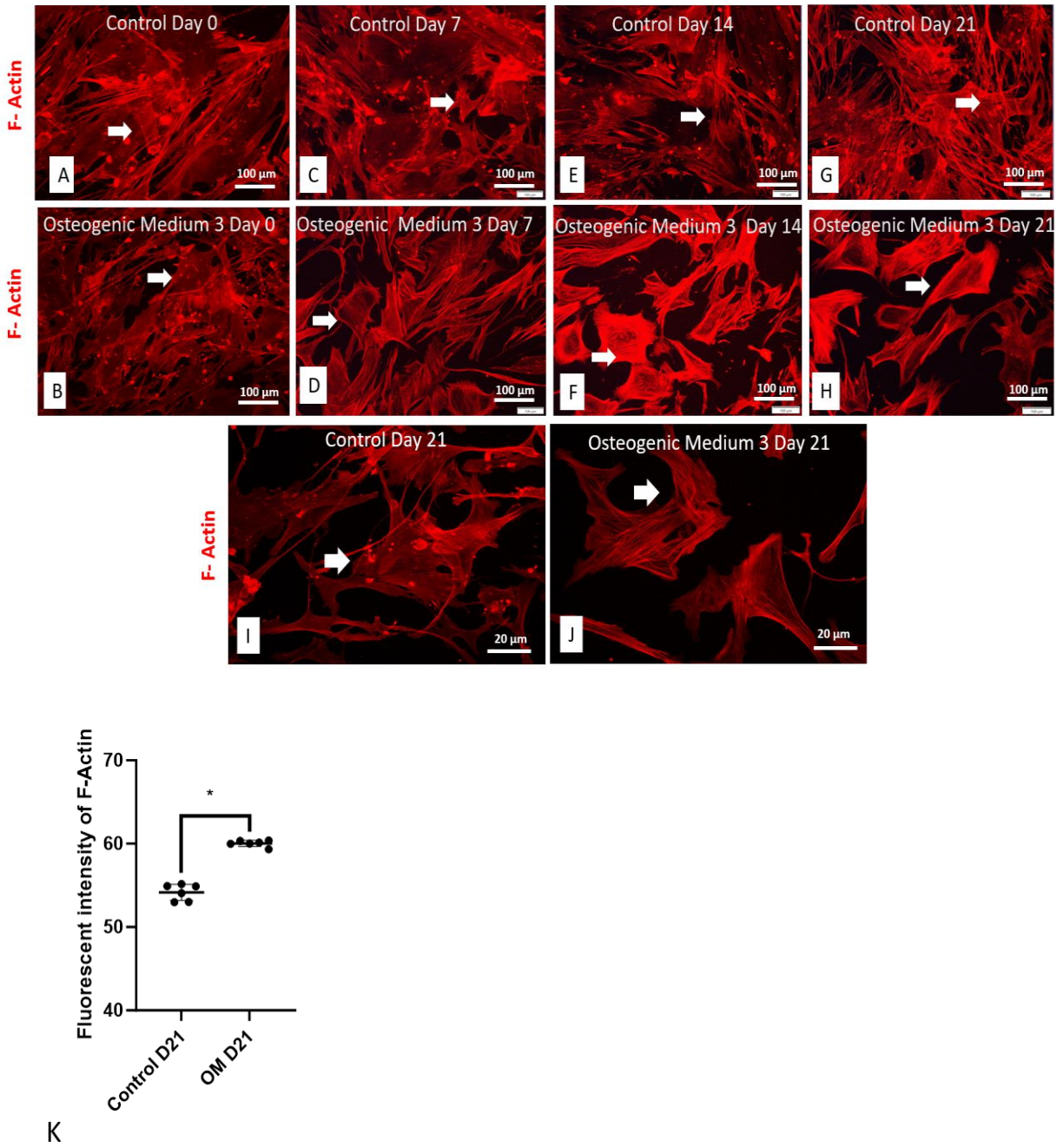

Figure 15 F-actin (red) protein expression in VSMCs incubated with OM3 (phalloidin Staining)

Sub-confluent monolayers of human aortic vascular smooth muscle cells were grown on 8-well chamber slides and treated with osteogenic or control medium. Cells were fixed using 4 % paraformaldehyde at day 21 and F-Actin [Phalloidin] were added. The cells were analysed by confocal microscopy, magnification x100 and x400. Increased α-SMA stress fibres were observed at day 21 following osteogenic treatment, depicted by white arrows [D, E, H]. The fluorescent intensity was measured using the ImageJ software [K]. For the scatter dot plot, the median value obtained from each dot, are represented by a line. All the values are expressed as means ± SD from 6

biological replicates in each group. Data was analysed by Mann-Whitney test followed by Dunn's post hoc analysis (* = p≤0.05).

VSMCs are highly contractile, however when they undergo osteogenic differentiation, they become less contractile. By 72 h, an evident reduction in contractility was observed VSMCs **Figure 16 [A & C]**. In contrast, despite the above α-SMA results, cells subjected to OM3 exhibited no discernible contractile capacity at the same 72 h interval **Figure 16 [B & C]**.

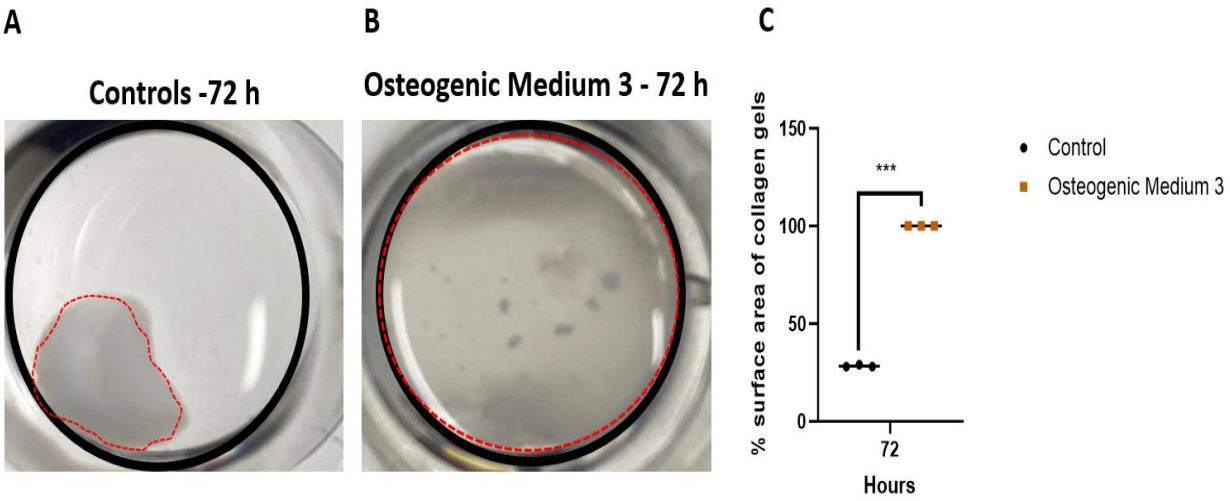

Figure 16 Collagen gel contractility assay

To assess the contraction ability of VSMCs when stimulated with osteogenic medium 3, VSMCs were seeded into pre-made collagen gels and grown to 50-60% confluence. Control cells were treated with VSMC growth medium. The collagen gels were photographed at 72 h. (A & B) Representative photographs of one of three independent experiments giving similar results (C). The black circle shows the circumference of the well and the red dotted circle shows the circumference of the gels. Statistical Data was analysed by Mann-Whitney test followed by Dunn's post hoc analysis (* = p≤0.001).**

Viability assays are crucial in evaluating the effects of treatments. To confirm that the above presented results were not related to increased cell death in the treated groups, viability of the VSMCs in response to OM3 was accessed. A slight decrease in the viability of VSMCs treated with Osteogenic Medium was observed when compared to the viability of the control group at the same 21-day interval **Figure 17**.

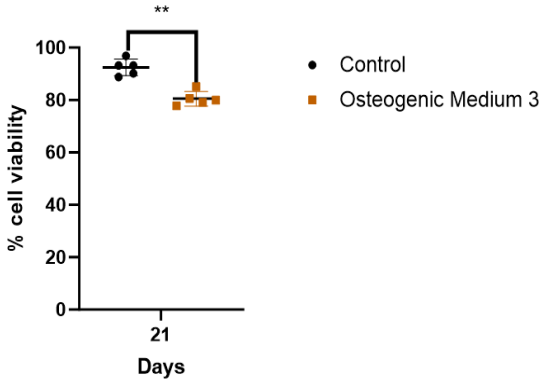

Figure 17 Viability assay

Cells viability assessed with cell counter. VSMCs were grown in OM3. Control cells were treated with VSMC growth medium. The media were replaced every 3 days. For the scatter dot plot, the median value obtained from each dot, are represented by a line. Each point in the scatter dot plot denotes a single biological replicate. Data was analysed by Mann-Whitney test followed by Dunn's post hoc analysis (= p≤0.01).**

3.2.2 Role of cytokines relevant in CKD on VSMC osteogenic differentiation: IL-6 and TGF-β1

IL-6 is an indicator of severity of the chronic inflammatory process and TGF-β1 is an immune biomarker involved in the regulation of calcification[38]. Many studies have identified increased IL-6 and TGF-β1 in the blood serum of both CKD and PD patients[38,545,546]. This increased presence of IL-6 and TGF-β1 correlates with increased VC in these patients[547-549]. Thus, here I will explore the direct effects of these cytokines on VSMC osteogenic differentiation.

To demonstrate if incubation of VSMCs with IL-6 and TGF-β1 led to calcium crystal deposition [$Ca_{10}(PO_4)_6(OH)_2$] in the VSMC matrix a commercially available Alizarin Red staining assay was used as above. The cells were fixed and stained with Alizarin Red and viewed under light microscopy. The results demonstrated no Alizarin Red staining at day 0, 7, 14 or 21. Incubated VSMCs stimulated with cytokines (IL-6 and TGF-β1) demonstrated a slight increase in absorbance but this was not statistically significant, and the values were only marginally different from the controls **Figure 18**.

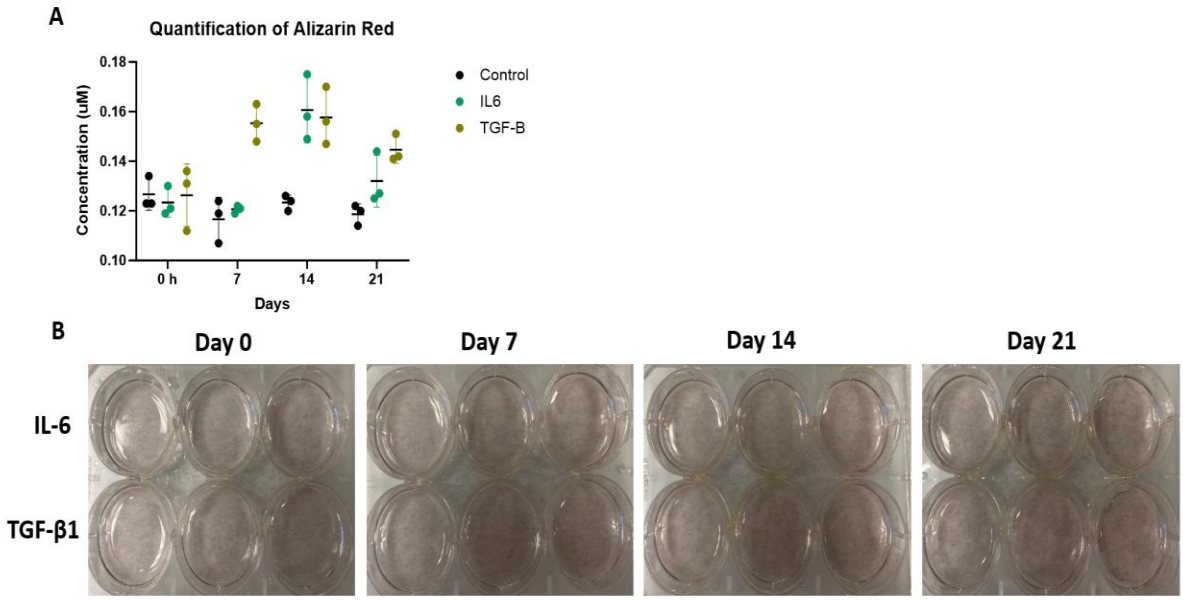

Figure 18 Quantification of Alizarin Red when stimulated with IL-6 and TGF-β1

Vascular smooth muscle cells were grown in normal growth medium with 10 ng/mL of IL-6 and TGF-β1 for up to 21. The monolayers of cells were stained with alizarin red (B) and then extracted for quantitative measurement OD absorbance at OD405 (A). (B) Representative photographs of one of three independent experiments giving similar results (A). Data was analysed by Kruskal-Wallis test followed by Dunn's post hoc analysis. The data represents mean ± S.D.

To assess the role of TGF-β1 **Figure 19** and IL-6 **Figure 20** on osteogenic gene expression, VSMCs were stimulated with either TGF-β1 or IL-6 alone in normal media. The results were analysed by qPCR at 0 h and 7 days, 14 days, and 21 days following stimulation with IL-6 and TGF-β1. RTqPCR was used to determine the effect of TGF-β1 alone on the transcriptional regulation of the osteogenic markers RunX2, Osteopontin, Bone-specific Alkaline Phosphatase and the smooth muscle marker, α-SMA.

The results demonstrated that stimulation with TGF-β1 (10 ng/mL) led to an increase in expression of Osteopontin and α-SMA mRNA expression at days 14 and 21 **Figure 19.**

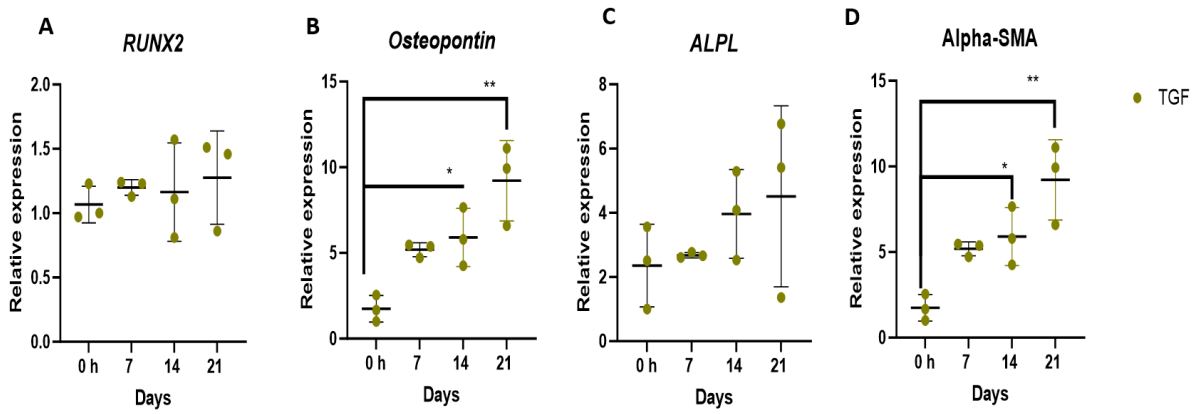

Figure 19 Effects of TGF-β1 on markers of osteogenic differentiation in VSMC

VSMCS were stimulated with normal growth medium with 10 ng/mL of TGF-β1 for up to 21 days and osteogenic marker expression was assessed by RT-qPCR. β-actin was used as a standard reference gene. The comparative C_T method was used for relative quantification of gene expression and the results were represented as mean ± S.D. For the scatter dot plot, the median value obtained from each dot, are represented by a line. Each point in the scatter dot plot denotes a single biological replicate. Data was analysed by Kruskal-Wallis test followed by Dunn's post hoc analysis (= p≤0.01).**

To investigate the effect of the of IL-6 alone, VSMCs were treated with normal growth medium and was stimulated with cytokine IL-6 (10 ng/mL) for up to 21 days under serum-free conditions. The VSMCs were then assessed on day 0, day, 7, day 14, and day 21 following stimulation.

When VSMCs were stimulated with normal growth medium with IL-6 (10 ng/mL), an upward trend in RunX2 expression was observed but there were no significant changes at any timepoints compared to control at 0 h **Figure 20 [A]**.

There was a gradual increase of Osteopontin expression from day 7 to day 21 when stimulated with IL-6 **Figure 20 [B]**. The increase of Osteopontin at day 21 is similar as previously observed with stimulation with TGF-β1 with normal growth medium.

VSMCs had an increased Alkaline Phosphatase expression when stimulated with IL-6 at day 14 and day 21 **Figure 20 [C]**. An increase in α-SMA mRNA expression at day 14 and day 21 was observed when stimulated with IL-6 **Figure 20 [D]**, and this was previously observed with stimulation with TGF-β1 in normal growth medium.

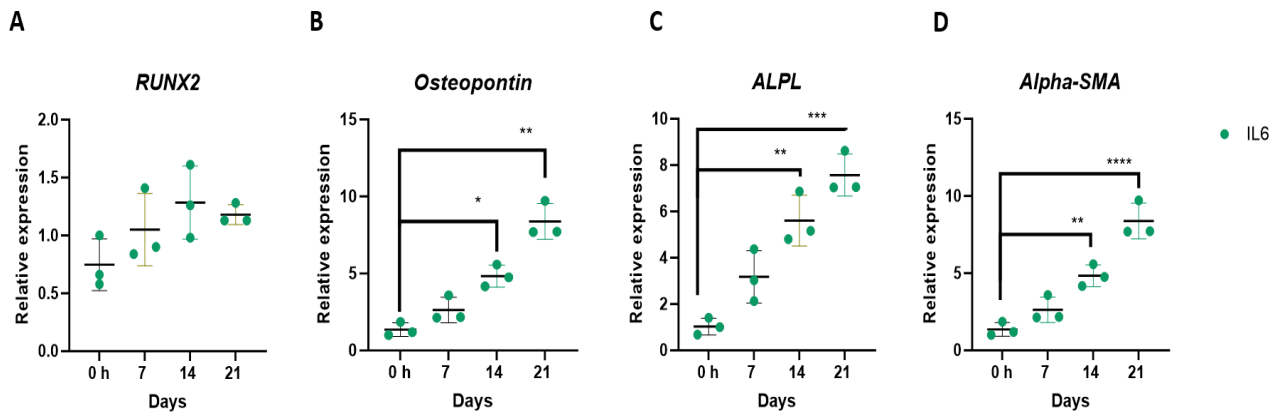

Figure 20 Effects of IL-6 on osteogenic differentiation markers in VSMCs

VSMCS were stimulated with normal growth medium with 10 ng/mL of IL-6 for up to 21 days and osteogenic markers expression was assessed by RT-qPCR. β-actin was used as a standard reference gene. The comparative C_T method was used for relative quantification of gene expression and the results were represented as mean ± S.D. For the scatter dot plot, the median value obtained from each dot, are represented by a line. Each point in the scatter dot plot denotes a single biological replicate. Data was analysed by Kruskal-Wallis test followed by Dunn's post hoc analysis (= p≤0.01, *** = p≤0.001, **** = p≤0.0001).**

3.3 Discussion

The main aims of the work in this chapter were to: - a) establish and characterize an in vitro model of VSMC-osteogenic differentiation and b) to characterise the effects of IL-6 and TGF-β1 on VSMC-osteogenic differentiation.

Vascular calcification is an active gene regulated process which resembles osteogenesis and this is an important driver in morbidity and mortality in renal disease[56]. Achieving control over this process requires understanding mechanisms underlying VC so that therapeutic strategies can be designed to prevent and treat VC. The present study had the purpose to try to mimic *in vitro*, the modification that occurs in CKD patients in order to be able to study its effect on VSMC calcification. To determine the optimum conditions to drive VSMC osteogenic differentiation *in vitro*, we used 3 types of osteogenic media, OM1, OM2 and OM3 and characterized the changes for each. OM1 was induced in the VSMCs with use of dexamethasone, β-glycerophosphate, and ascorbic acid-2-phosphate. OM2 on the other hand, served as a commercially acquired osteogenic medium which was initially used as a positive control. OM3 closely resembled OM1 but featured the addition of sodium orthophosphate. Phosphate ions are pivotal in biological calcification processes such as bone formation, tooth mineralization, and soft tissue calcification, with high phosphate levels being particularly influential in VSMC trans-differentiation in vitro. This trans-differentiation phenomenon mirrors clinical observations in CKD patients, where elevated phosphate levels correlate with adverse cardiovascular outcomes. Various experimental protocols induce VC *in vitro* by elevating extracellular phosphate levels in the culture medium, typically through the addition of compounds like β-glycerophosphate[550,551] or sodium phosphate[552,553]. In this context, OM1 employed a combination of two types of phosphates (Ascorbic acid-2-Phosphate and β-glycerophosphate), while OM3 featured a combination of three phosphate varieties (Ascorbic acid-2-Phosphate, β-glycerophosphate and sodium orthophosphate) resulting in distinct outcomes. There are three types of phosphate which have been used in this thesis are described as follows: -

Sodium orthophosphate is a simple inorganic salt that provides a direct source of phosphate ions to the body. These phosphate ions readily combine with calcium ions, forming insoluble

calcium phosphate minerals, which are the foundation components of calcification. Unlike sodium orthophosphate, β-glycerophosphate is an organic compound comprising glycerol and phosphate. Because of its organic nature, it necessitates additional cellular processes to release phosphate ions. Existing literature suggests β-glycerophosphate not only accelerates calcification but also contributes to the initiation of phenotypical transdifferentiation in VSMCs[554,555]. Derived from vitamin C (ascorbic acid) through phosphorylation, ascorbic acid 2-phosphate differs from the other two compounds in that it doesn't directly supply phosphate ions for calcification. Instead, it is commonly used in conjunction with β-glycerophosphate to stimulate cell growth and collagen synthesis[556]. Collagen is a critical component of bone and tissue, and ascorbic acid 2-phosphate indirectly supports calcification by aiding in the production of this extracellular matrix[557]. Beyond these phosphates, we also utilized dexamethasone in our study. Dexamethasone enhances the calcification process by promoting cell proliferation and differentiation[558,559].

The major form of the calcium phosphate is hydroxyapatite this is what that gives bones their rigidity. Stimulation with OM1, VSMCs produced oval-shaped structures referred to as calcified or mineralised nodules. Existing literature indicates that these nodules are characteristic of VSMCs when cultured in calcified medium[529,560,561] and they serve as nucleation sites for calcium crystal formation[562]. In other studies electron microscope revealed that the composition of calcium deposits within these nodules closely resembles hydroxyapatite, and RT-qPCR analysis revealed these calcified nodules in VSMCs express high level of smooth muscle markers (α-SMA, SM22α)[115]. In context of this thesis, although the VSMCs were able to form these nodules, they did not deposit minerals outside of these structures within the matrix. It appeared as though they were on the right path but missing a crucial factor for proper calcification—a process mimicking VSMC osteogenic differentiation. In contrast, cells stimulated with OM2 showed an inability to calcify. Notably, in this study, stimulation with OM3 resulted in significant calcium precipitation in the matrix, as well as induction of osteogenic gene markers. My findings strongly suggest that sodium orthophosphate, also known as trisodium phosphate, plays a pivotal role in VSMC osteogenic differentiation. In some cells, phosphate uptake is facilitated by sodium-coupled transporters. These transporters harness the energy generated by the movement of sodium ions across the cell membrane to facilitate the uptake of phosphate ions[563]. The sodium gradient established

by sodium-potassium pumps (Na+/K+ pumps) can provide the necessary energy for this co-transport[564]. In this study, the addition of sodium orthophosphate to the culture medium caused an immediate increase in pH, making it more alkaline. This rise in pH has a significant impact on calcium and phosphate precipitation. At higher pH levels, phosphate ions become more negatively charged, increasing their likelihood of reacting with positively charged calcium ions to form insoluble calcium phosphate minerals, like hydroxyapatite[565]. This precipitation is a critical step in the calcification process. Existing research shows that bone-forming cells are sensitive to pH changes and alkaline pH may promote their differentiation and activity, thereby facilitating calcification[566]. In OM1, while β-glycerophosphate can also contribute phosphate ions, its role in mineralization is less direct compared to sodium orthophosphate, which may not be as efficient in inducing calcification.

This model was further validated by characterising alterations in osteogenic gene expression. RunX2, Osteopontin and Alkaline phosphatase are key markers of osteogenic differentiation, and they are found in osteoblasts[531,534,567]. All the osteogenic marker demonstrated increased expression by day 21. The commercial purchased medium (OM2) did not significantly promote osteogenic gene expression or matrix calcification. Although the gene expression of medium OM1 was not poor, demonstrated little calcium staining in the matrix. VC is a two-way process which occurs on genetic level and mineral level and OM3 was excellent in both. Henceforth, we will refer to OM3 simply as 'OM,' as it will be the osteogenic medium used in the subsequent chapters.

In light of these findings, we further explored the impact of VSMC osteogenic differentiation, particularly on cell viability. VSMCs undergoing osteogenic differentiation exhibit a slight decrease in cell viability. Existing literature suggests that in vitro VC in human is tightly regulated by apoptosis[91,562]. It is theorized that physiological cell death is a useful mechanism for liberation of intracellular stores of calcium[188]. It is theorized that in a calcifying environment, apoptosis can be induced, leading to the formation of VSMC-derived apoptotic bodies that serve as nucleation sites for hydroxyapatite formation[188]. Consistent with these observations, our study revealed that VSMC calcification was associated with a slightly elevated level of cell death compared to control VSMCs. The exact reasons behind this phenomenon remain unclear. It's possible that the cells don't receive adequate nutrients from the culture medium, or perhaps cell death is orchestrated as part of the mechanism that

ultimately leads to calcification. Previous research has shown that inhibiting apoptosis can result in a reduction in VSMC calcification[551,568].

In continuation of our investigation into VSMC behaviour during osteogenic differentiation, we observed an unexpected phenomenon related to α-SMA, a critical marker defining VSMCs' contractile properties. Conventionally, one might anticipate a decrease in α-SMA expression following osteogenic differentiation. However, in our experiments, both α-SMA mRNA and protein expression exhibited an increase by day 21. The literature suggests that when VSMCs differentiate into osteoblast-like cells, they do not lose all their VSMC properties. Instead, they gain some osteogenic phenotype while still retaining some properties of their own[562,569,570] and are thus termed osteogenic-like VSMCs. However, why their α-SMA expression increased as they underwent osteogenic differentiation is not clear. One possibility may be that the cells sense the increased rigidity in their environment as a consequence of the Ca/Ph matrix deposition and respond to this by trying to improve their contractility to improve the flexibility/reduce the stiffness of their surrounding tissues and hence increasing α-SMA gene and protein expression. During the process of VSMC osteogenic differentiation, the emergence of stress fibers comprised of F-actin also became more pronounced. These stress fibers, which bundle actin filaments together, contribute to the cell's mechanical stability and generate contractile forces. The presence of these stress fibers seemed interconnected with the heightened rigidity and mineralization characteristic of osteogenically differentiated VSMCs. However, similar to the results with α-SMA, the increase in stress fibers was unexpected and is postulated to be a compensatory mechanism by the cells to improve their contractility. Numerous investigations have elucidated the profound impact of the actin cytoskeleton and cell shape on mesenchymal stem cell (MSC) differentiation and in our study VSMCs come from MSC lineage[571]. For instance, during adipogenic differentiation, MSCs adopt a flower-like configuration, while osteogenic lineage commitment leads to a star-like morphology[567,572]. My results show the star-shaped, polygonal morphology when VSMCs become more osteogenic. Notably, star-shaped cells exhibit a pronounced density of stress fibers[572].

As a result of the α-SMA and F-actin results, the next steps were to quantitatively assess the contractility changes during VSMC osteogenic differentiation, and a contractility assay was therefore undertaken. In this assay, VSMCs that underwent osteogenic differentiation had

significantly attenuated (if any) ability to contract a collagen gel. Interestingly, previous literature suggests that decrease in contractility of VSMCs is coupled with dramatically increase of their proliferation capacity and secretion of matrix metalloproteinases to promote ECM remodelling[543]. Hence, the results indicate that as VSMCs undergo osteogenic differentiation, deposit calcium in the matrix and upregulate expression of osteogenic marker genes, they also have markedly reduced contractility. The exaggerated expression of α-SMA and formation of F-actin fibres might be an attempted (but failed) compensatory mechanism of the cells to try to improve their contractile ability.

In the latter part of this chapter, the role cytokines circulating in high levels during CKD and PD were investigated, and the direct impact of these cytokines of VSMC phenotype was explored. IL-6 is a marker of severity of chronic inflammatory processes and TGF-β1 is a biomarker involved in VC[38]. Both cytokines are elevated in CKD and in PD. In CKD patients, upregulation in IL-6 gene expression strongly correlates with increased VC in clinical studies[573]. IL-6 in clinical studies is strongly predictive of VC and our data supports that this might be because it is a potent inducer of osteogenic gene expression in VSMCs[520]. Similar to IL-6, TGF-β1 is promotes aortic calcification[574] and regulates VC and osteoblastic differentiation in VSMCs[575,576]. Although IL-6 and TGF-β1 did not in isolation promote calcification in the matrix, that it is likely that in a clinical setting in the presence of hyperphosphatemia that this would promote the calcification process, and indeed our studies showed a trend towards increased calcification although the results were not statistically significant.

In summary, this chapter's findings pinpoint successfully established an in vitro model of VSMC osteoblast differentiation that can be used to study the mechanisms that regulate VC in subsequent chapters and that these cells are functionally distinct in their reduced contractile ability. OM3 (referred to as OM in subsequent chapters) as the superior osteogenic medium among the three options, as evidenced by its effectiveness in promoting calcium deposition and osteogenic marker expression. We have also identified that IL-6 and TGF-β1 can in isolation also increased markers of osteogenic gene expression.

The next chapter will explore the mediators of VSMC osteogenic differentiation, with a specific focus on the ECM component HA because of the large body of literature supporting its role in cell differentiation in other biological contexts.

Chapter 4

The role of hyaluronan (HA) in VSMC osteogenic transdifferentiation

4.1 Introduction

VC is a complex pathological process associated with CKD disorders[87]. Understanding the molecular mechanisms underlying VC is of paramount importance, as it can inform the development of therapeutic strategies to combat these debilitating conditions. A novel area of interest within VC research is the role of HA, a key component of the extracellular matrix known for its multifaceted roles in various pathological processes.

HA has long been recognized for its contributions to its involvement in vascular diseases, osteogenesis, and regulation of cell phenotype[271,387,448]. However, recent studies have uncovered intriguing links between HA and VC, suggesting that HA negatively regulates VC[577]. Intriguingly, the relationship between HA and VC appears to be multifaceted and dependent on various factors, including the molecular weight of HA, its distribution within the cellular microenvironment, and the expression levels of key enzymes involved in HA metabolism (HAS and HYALs), its related proteins (CD44 and RHAMM) and binding partner such as TSG-6 and Versican. Moreover, the precise mechanisms by which HA influences the differentiation of VSMCs into an osteogenic phenotype, a hallmark of VC, remain incompletely understood.

To shed light on these intricate relationships, this chapter delves into the effects of HA on VSMC differentiation and VC through a series of comprehensive in vitro experiments. My research aims in this chapter is to decipher whether HA acts as a protector or promoter of VSMC osteogenic differentiation and VC. In the subsequent sections, I present the experimental findings, discussing the effects on HA during osteogenic differentiation, influence of inflammatory cytokines on HA during VSMC osteogenic differentiation, HA degradation methods, such as 4MU and Strep-Hyal, on VSMC behaviour and highlighting the differential roles of specific HAS isoenzymes. Ultimately, this investigation strives to contribute to our understanding of the intricate interplay between HA and VC, potentially uncovering novel therapeutic avenues for combatting VC.

4.2 Results

4.2.1 Characterising alterations in HA and related HAS isoenzymes, Hyaluronidases and Hyaladherins following VSMC osteogenic differentiation

To visually investigate alterations in HA matrix in VSMCs, Immunocytochemistry (ICC) was used. Initial experiments were carried out using OM to stimulate VSMCs for 7, 14 and 21 days. A fluorescent biotinylated HABP was used to stain (green) for HA in VSMCs.

Control VSMCs and OM treated VSMCs (day 0) had a diffuse expression of cytoplasmic HA (white arrows) and an accumulation of HA within the nucleus of each cell (white block arrows) **Figure 21 [A, B & I]**. Incubation with normal control media for VSMCs did not change the expression of HA at any of the later timepoints **Figure 21 [A, C, E, G & I]**. However, following incubation with OM, the cells visibly demonstrated a change in morphology and became larger and more "poach egg" shaped **Figure 21 [D, F & H]**. At Day 7 and Day 14 of OM treatment the cells exhibited reduced levels of cytoplasmic HA and increased pericellular HA **Figure 21 [D & F]**. Furthermore, HA was present in newly forming cell-cell contact spindles, resembling previously described HA cables. There was attenuated expression, punctate intracellular HA staining, and long linear structures that connect different cells **Figure 21 [H, J & K] (white arrows)**. At higher magnification, the overall intensity of HA staining went down as cells underwent osteogenic differentiation and punctate staining with long linear structures interconnecting different cells were evident **Figure 21 [J & K] (white arrows).**

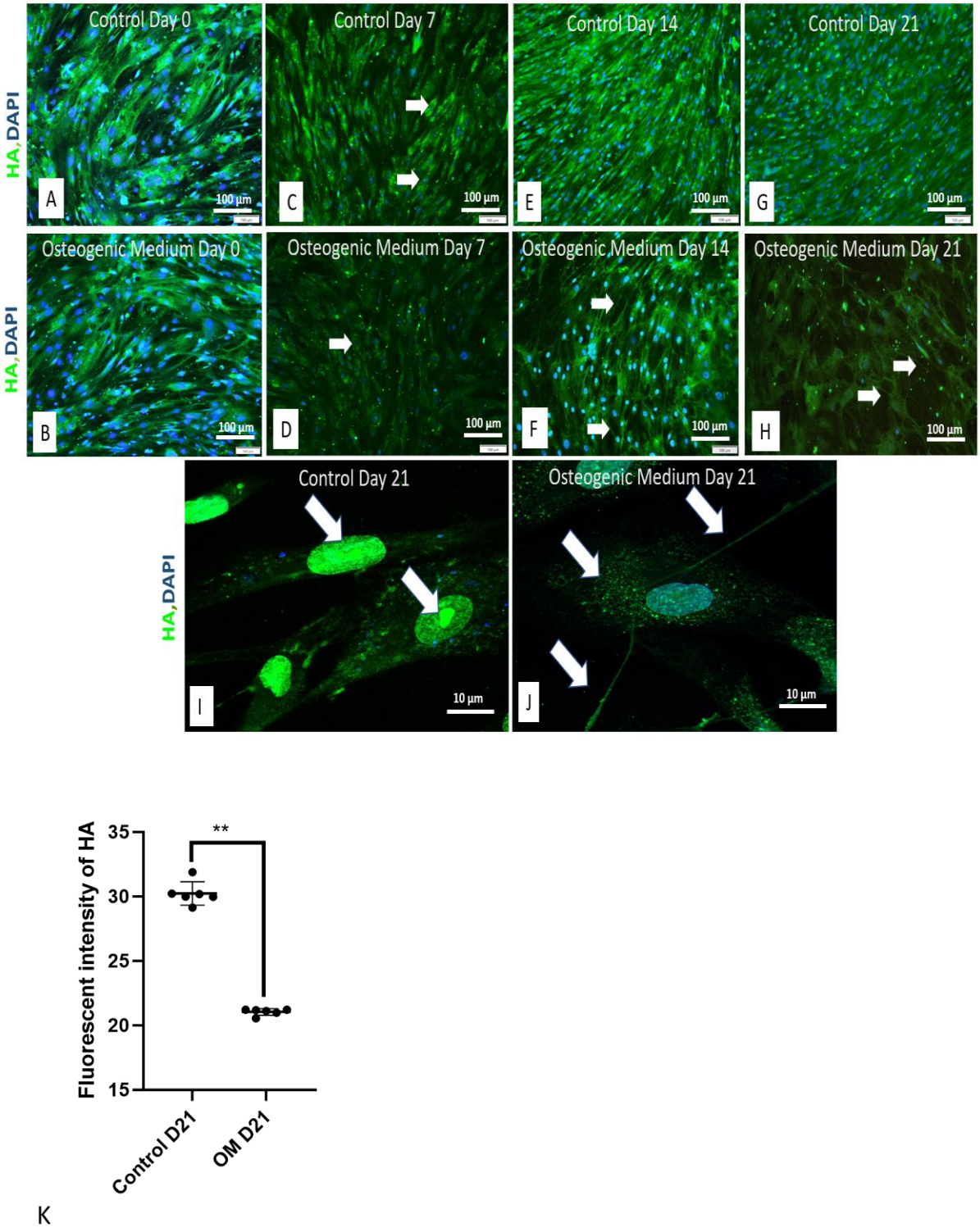

Figure 21 HA (green) expression in differentiated VSMCs when stimulated with OM.

Sub-confluent monolayers of human aortic vascular smooth muscle cells were grown on 8-well chamber slide and treated with osteogenic medium. The control cells were grown in smooth muscle growth medium. Cells were fixed using 4% paraformaldehyde at the following timepoints day 0 (CT), day 7, day 14 and day 21. Cell were then and stained for (bHABP) (green), control cells [A, C, E, G and I] osteogenic cells [B, D, F, H and J]. The cells were analysed by confocal microscopy,

magnification x100 [A-H] and x630 [I-J]. The images were taken at 4 different time points along the course of osteogenic differentiation. The fluorescent intensity was measured using the ImageJ software [K]. For the scatter dot plot, the median value obtained from each dot, are represented by a line. All the values are expressed as means ± SD from 6 biological replicates in each group. Data was analysed by Mann-Whitney test followed by Dunn's post hoc analysis (= p≤0.01).**

Specific HA ELISA was subsequently performed to quantify HA levels and distribution in OM treated VSMCs. Control cells were incubated with normal growth medium. Treatment with OM showed an overall attenuation of extracellular HA **Figure 22 [A]** and intracellular HA **Figure 22 [B]** at all time points as cells underwent osteogenic differentiation. Whilst there was a significant increase in pericellular HA at day 7 when VSMCs were treated with OM **Figure 22 [C]**. The increase in pericellular HA suggests that this could be influencing membrane receptor rearrangement leading to intracellular signalling phenotypes.

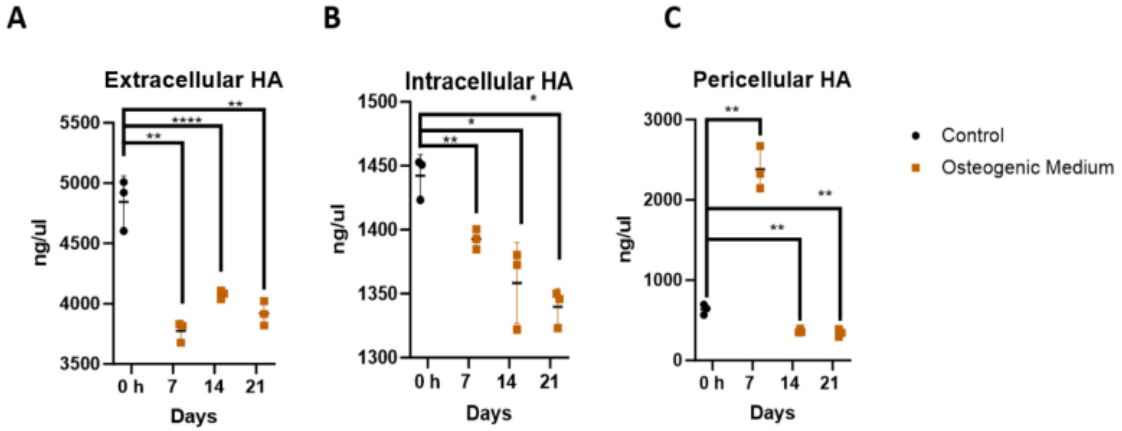

Figure 22 Characterization of the HA distribution during VSMC osteogenic differentiation using HA ELISA

Human aortic vascular smooth muscle cells were grown in Osteogenic Medium (addition of ascorbic acid-2-phosphate, glycerol-2-phosphate, dexamethasone, and sodium orthophosphate 10mM). Quantification of extracellular, intracellular, and pericellular HA by HA-ELISA at time points, 0 h, 7 days, 14 days, and 21 days. [A] conditioned cell culture media, [B] individual concentrations of HA in intracellular lysates and [C] cell surface trypsinates. Each point in the scatter dot plot denotes a single biological replicate, the line and whiskers represent mean and Standard Deviation. Data was analysed by Kruskal-Wallis test followed by Dunn's post hoc analysis (= p≤0.01, *** = p≤0.001, **** = p≤0.0001).**

Dysregulation of HA synthases has previously been associated with vascular disease[577]. To determine if alternation in expression of HAS enzymes were responsible for HA changes observed above in the context of VC, qPCR was used to confirm the mRNA expression of HAS1, HAS2 and HAS3 in VSMCs following stimulation with OM. Cells were extracted at 0, 3, 16, 24, 48, and 72 h.

The mRNA expression of all 3 HAS isoenzymes decreased compared to control at all early time points (0-72 h) following stimulation with OM **Figure 23 [A-B]**.

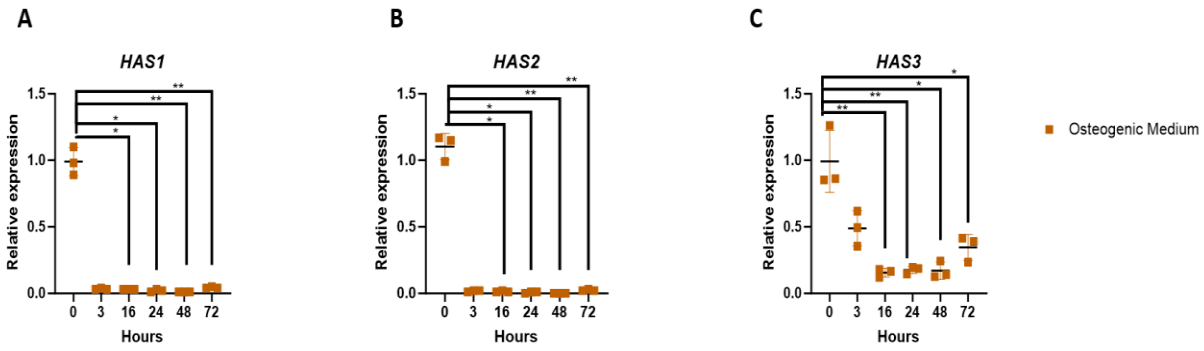

Figure 23 HAS Synthases mRNA expression in VSMCs incubated with Osteogenic Medium in early time points

Human aortic vascular smooth muscle cells were grown in Osteogenic Medium up to 72 hours. Control cells were treated with VSMC growth medium. mRNA was extracted at 0, 3, 16, 24, 48, and 72 h. HAS Synthases expression was assessed relative to control samples at 0 h. The comparative C_T method was used for relative quantification of gene expression and the results were represented as mean ± S.D. For the scatter dot plot, the median value obtained from each dot, are represented by a line. Each point in the scatter dot plot denotes a single biological replicate. Data was analysed by Kruskal-Wallis test followed by Dunn's post hoc analysis (ns = p>0.05, * = p≤0.05, ** = p≤0.01).

RT-qPCR was then conducted to determine mRNA expression of the HAS isoenzymes at later timepoints of 0 h, 7-, 14-, and 21-days. The mRNA expression of HAS1 consistently decreased compared to control following 7, 14 and 21 days of stimulation with OM **Figure 24 [A]**. Similarly, stimulating VSMCs with OM led to a significant decrease in HAS2 expression at all time points from day 7 to day 21 **Figure 24 [B]**. HAS3 mRNA was slightly more complex in that there was an initial decrease in expression followed by increased expression at day 21 **Figure 24 [C]**.

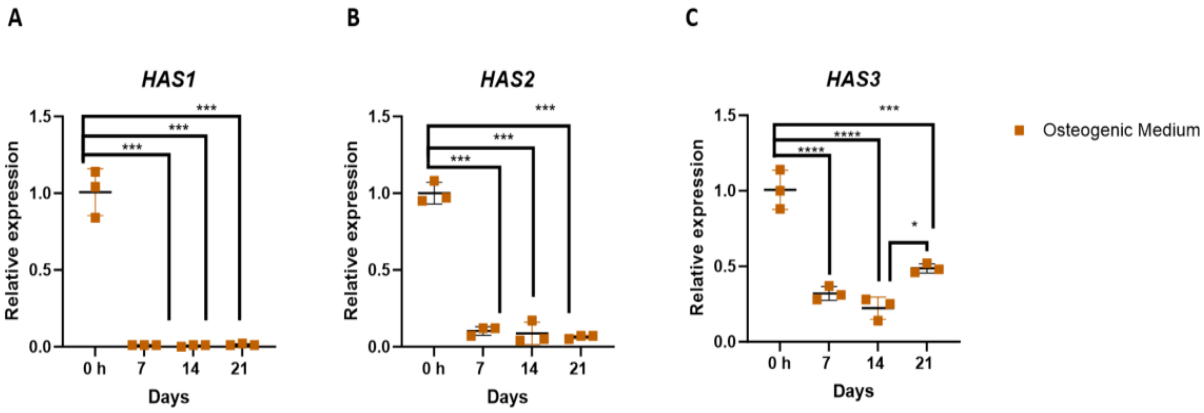

Figure 24 HAS Synthases mRNA expression in VSMCs incubated with Osteogenic Medium

Human aortic vascular smooth muscle cells were grown in Osteogenic Medium. Cellular HAS 1/2/3 expression normalized to beta actin was measured by RT-qPCR at time points, 0 h, 7 days, 14 days, and 21 days. Each point in the scatter dot plot denotes a single biological replicate, the line and whiskers represent mean and Standard Deviation. Data was analyzed by Kruskal-Wallis test followed by Dunn's post hoc analysis (ns = p>0.05, * = p≤0.05, ** = p≤0.01, *** = p≤0.001, **** = p≤0.0001).

To visualize HAS1 protein expression VSMCs stimulated with normal (control)medium **Figure 25 [A, C, E, G, I & K]** were compared to VSMCs stimulated with OM **Figure 25 [B, D, F, H, J & K]**. The images were captured at four specific time points day 0, day, 7, day 14, and day 21. VSMCs stimulated with control medium exhibited a diffuse cytoplasmic distribution of HAS1 protein throughout the cell at all examined timepoints **Figure 25 [A, C, E, G & I],** and had an accumulation of nuclear HAS1 in control cells, which was evident only at the higher magnification image **Figure 25 [I]**. There were no changes at day 0 **Figure 25 [B]**. Stimulation with OM for 7 days led to a reduction of HAS1 protein expression **Figure 25 [D],** and this reduction was more pronounced by day 14 and day 21 **Figure 25 [F, H, J & K]**. At higher magnification, cytoplasmic punctate staining of HAS1 around the nucleus was observed in both control and osteogenic-differentiated cells **Figure 25 [I & J]**.

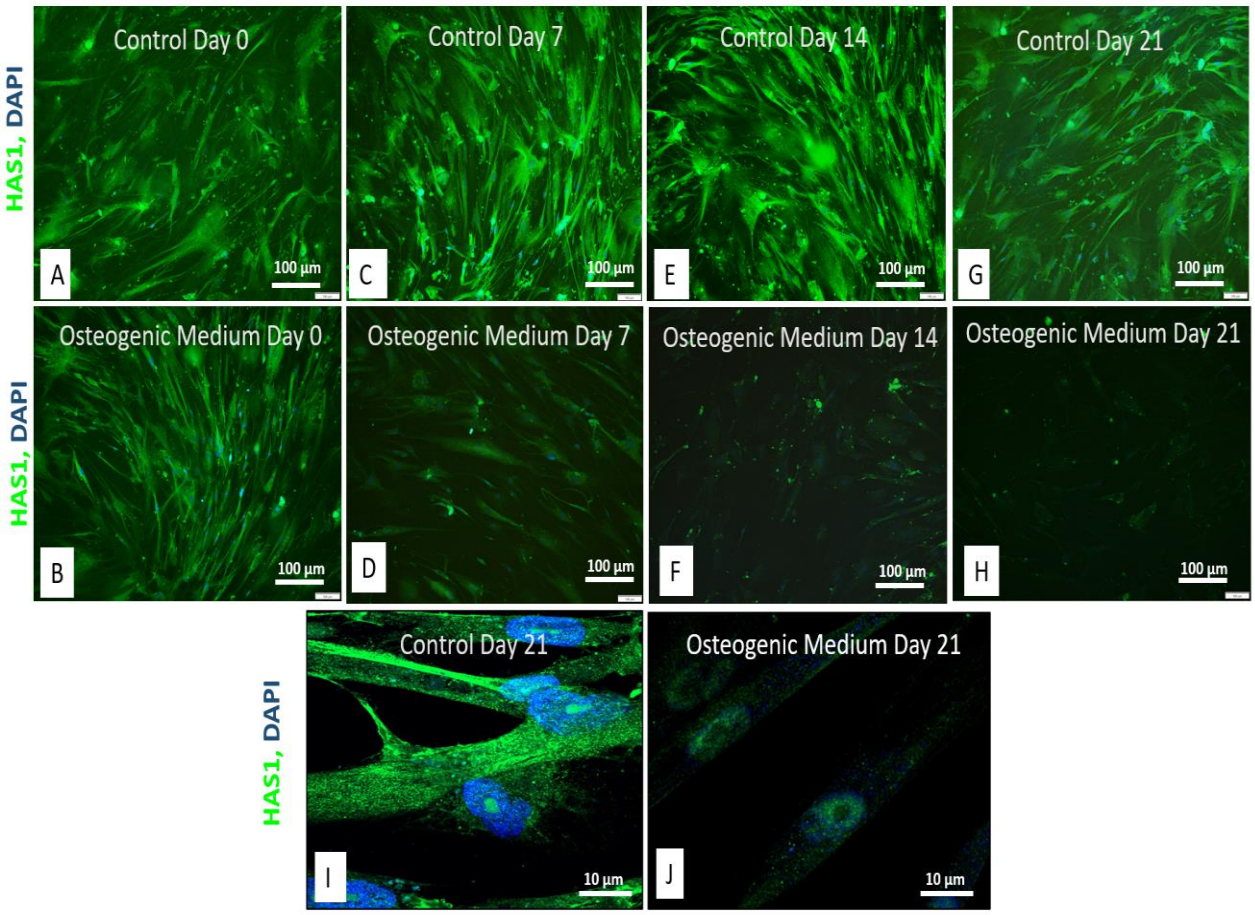

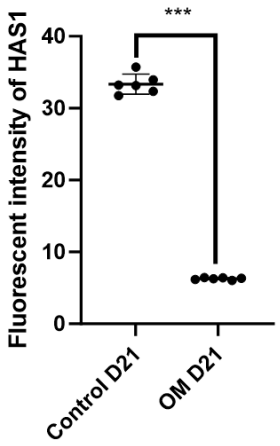

K

Figure 25 HAS1 (green) expression in differentiated VSMCs when stimulated with OM.

Sub-confluent monolayers of human aortic vascular smooth muscle cells were grown on 8-well chamber slide and treated with osteogenic medium. The control cells were grown in smooth muscle growth medium. Cells were fixed using 4% paraformaldehyde at the following timepoints day 0 (CT), day 7, day 14 and day 21. Cells were then and stained for (HAS1) (green), control cells [A, C, E, G and I] osteogenic cells [B, D, F, H and J]. The cells were analysed by confocal microscopy, magnification x100 [A-H] and x630 [I-J]. The images were taken at 4 different time points along the course of

osteogenic differentiation. The fluorescent intensity was measured using the ImageJ software [K]. For the scatter dot plot, the median value obtained from each dot, are represented by a line. All the values are expressed as means ± SD from 6 biological replicates in each group. Data was analysed by Mann-Whitney test followed by Dunn's post hoc analysis (* = p≤0.001).**

To visualize HAS2 protein expression VSMCs stimulated with control medium **Figure 26 [A, C, E, G, I & K]** were compared to VSMCs stimulated with OM **Figure 26 [B, D, F, H, J & K]**. The images were taken at time points day 0, day, 7, day 14, and day 21. VSMCs stimulated with control medium alone had a pronounced expression of cytoplasmic HAS2 spanning the entire cell at all timepoints **Figure 26 [A, C, E, G & I]**. There were no changes at day 0 **Figure 26 [B]**. Similar to HAS1, HAS2 protein expression was decreased when stimulated with OM for 7 days **Figure 26 [D],** and this attenuation continued at 14 days and 21 days **Figure 26 [F, H, J & K]**. Higher magnification images revealed the punctate staining of HAS2 and confirmed this **Figure 26 [I & J].**

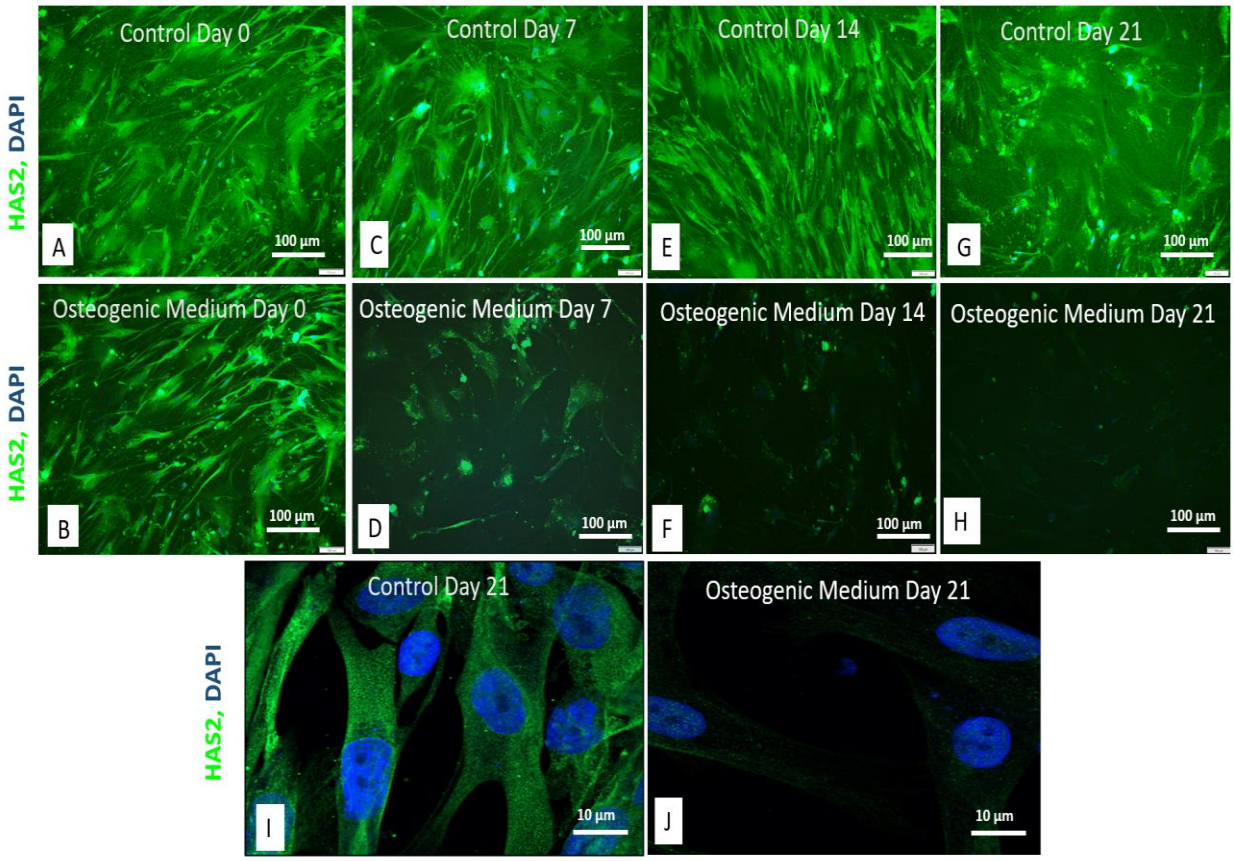

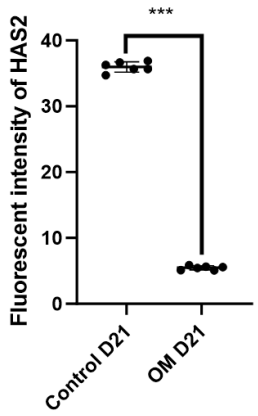

K

Figure 26 HAS2 (green) expression in differentiated VSMCs when stimulated with OM.

Sub-confluent monolayers of human aortic vascular smooth muscle cells were grown on 8-well chamber slide and treated with osteogenic medium. The control cells were grown in smooth muscle growth medium. Cells were fixed using 4% paraformaldehyde at the following timepoints day 0 (CT), day 7, day 14 and day 21. Cells were then and stained for (HAS2) (green), control cells [A, C, E, G and I] osteogenic cells [B, D, F, H and J]. The cells were analysed by confocal microscopy, magnification x100 [A-H] and x630 [I-J]. The images were taken at 4 different time points along the course of osteogenic differentiation. The fluorescent intensity was measured using the ImageJ software [K]. For the scatter dot plot, the median value obtained from each dot, are represented by a line. All the values are expressed as means ± SD from 6 biological replicates in each group. Data was analysed by Mann-Whitney test followed by Dunn's post hoc analysis (* = p≤0.001).**

The protein expression of HAS3 was visualised next. VSMCs stimulated with control medium **Figure 27 [A, C, E, G, I & K]** were compared to VSMCs stimulated with OM **Figure 27 [B, D, F, H, J & K]**. The images were captured at four distinct time points day 0, day, 7, day 14, and day 21. HAS3 was consistently detectable in VSMCs stimulated solely with control medium at all examined time points **Figure 27 [A, C, E, G & I]**. In contrast to HAS1 and HAS2, the stimulation with OM from day 7 to day 21 resulted in an upregulation of cellular HAS3 protein expression **Figure 27 [D, F, H & J]**, which was notably evident in the higher magnifying image **Figure 27 [J & K]**.

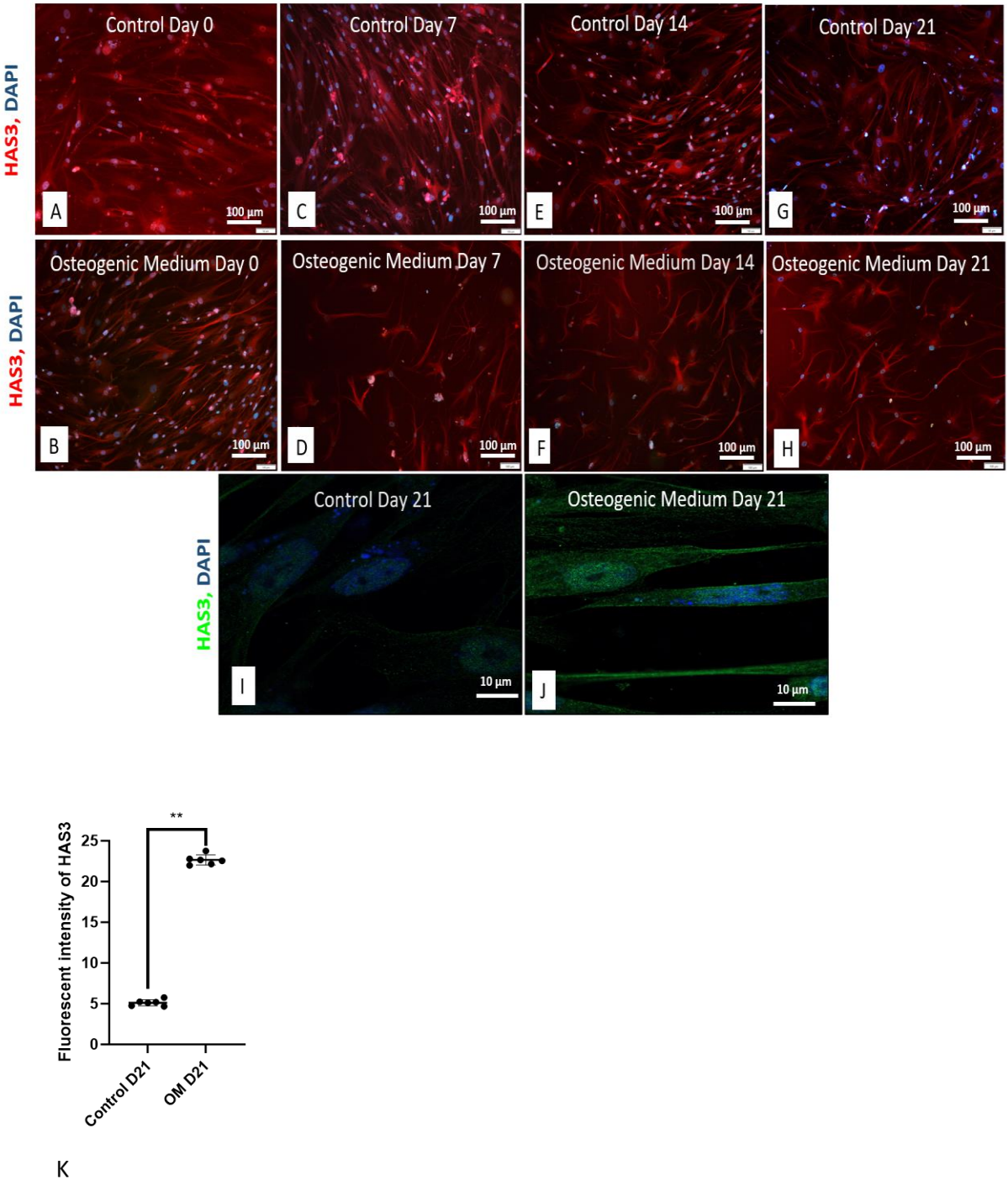

Figure 27 HAS3 expression in differentiated VSMCs when stimulated with OM.

Sub-confluent monolayers of human aortic vascular smooth muscle cells were grown on 8-well chamber slide and treated with osteogenic medium. The control cells were grown in smooth muscle growth medium. Cells were fixed using 4% paraformaldehyde at the following timepoints day 0 (CT), day 7, day 14 and day 21. Cells were then and stained for (HAS3), control cells [A, C, E, G and I] osteogenic cells [B, D, F, H and J]. The cells were analysed by confocal microscopy, magnification x100 [A-H] and x630 [I-J]. The images were taken at 4 different time points along the course of osteogenic differentiation. The fluorescent intensity was measured using the ImageJ software [K]. For the scatter dot plot, the median value obtained from each dot, are represented by a line. All the

values are expressed as means ± SD from 6 biological replicates in each group. Data was analysed by Mann-Whitney test followed by Dunn's post hoc analysis (= p≤0.01).**

To characterize the expression of HYAL1 and HYAL2 in VSMCs following treatment with OM qPCR was carried out at 0, 3, 16, 24, 48, and 72 h. Similar to the expression of HA Synthases, the mRNA expression of HYAL 1/2 decreased compared to control levels following 3, 16, 24, 48, and 72 h of stimulation with OM **Figure 28 [A-B]**.

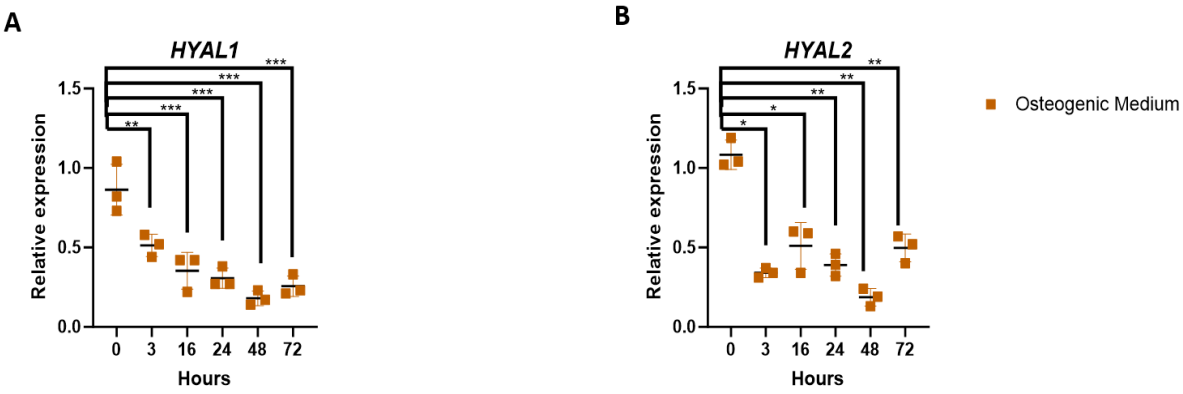

Figure 28 Hyaluronidases mRNA expression in VSMCs incubated with Osteogenic Medium in early time points

Human aortic vascular smooth muscle cells were grown in Osteogenic Medium up to 72 hours. Control cells were treated with VSMC growth medium. mRNA was extracted at 0, 3, 16, 24, 48, and 72 h. Hyaluronidases expression was assessed relative to control samples at 0 h. The comparative C_T method was used for relative quantification of gene expression and the results were represented as mean ± S.D. For the scatter dot plot, the median value obtained from each dot, are represented by a line. Each point in the scatter dot plot denotes a single biological replicate. Data was analysed by Kruskal-Wallis test followed by Dunn's post hoc analysis (ns = p>0.05, * = p≤0.05, ** = p≤0.01, *** = p≤0.001).

To assess the expression of HYAL1 and HYAL2 at late time points in VSMCs following treatment with OM, qPCR was performed at 0 hours, 7 days, 14 days, and 21 days. Similar to the pattern observed with HAS isoenzymes, treatment with OM lead to a consistent decrease in HYAL1 mRNA expression at all examined timepoints from day 7 to day 21 **Figure 29 [A]**. Stimulation with OM also resulted in a reduced HYAL2 mRNA expression at day 14 compared

to controls at 0 h **Figure 29 [B]**. However, HYAL2 expression returned to its basal levels at day 21 **Figure 29 [B]**.

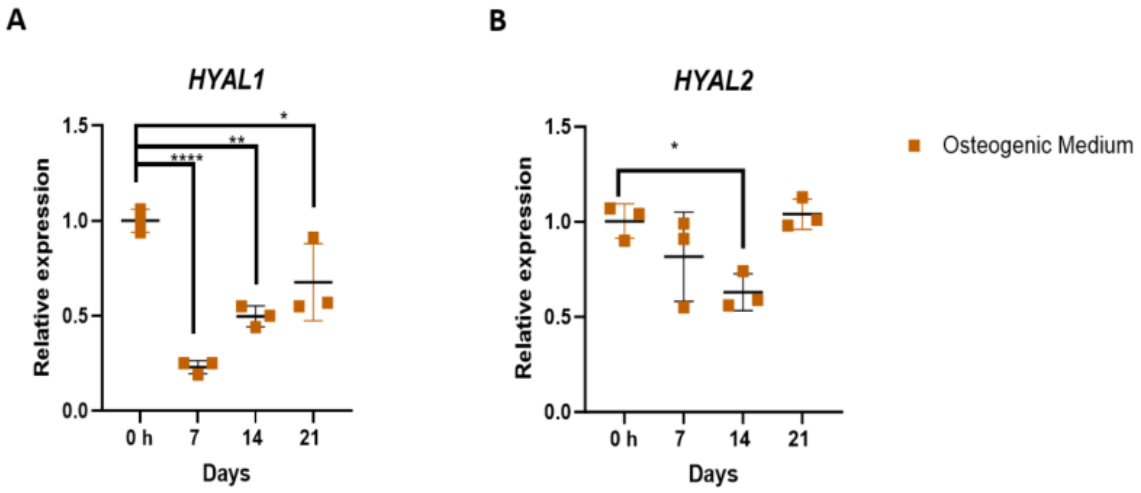

Figure 29 Hyaluronidases mRNA expression in VSMCs incubated with Osteogenic Medium

HYAL1/2 expression was assessed by RT-qPCR. β-actin was used as a standard reference gene and gene expression was assessed relative to control samples for each time point. The comparative C_T method was used for relative quantification of gene expression and the results were represented as mean ± S.D. For the scatter dot plot, the median value obtained from each dot, are represented by a line. Each point in the scatter dot plot denotes a single biological replicate. Data was analysed by Kruskal-Wallis test followed by Dunn's post hoc analysis (ns = p>0.05, * = p≤0.05, ** = p≤0.01, *** = p≤0.001).

To visualize HYAL1 protein expression VSMCs stimulated with control medium **Figure 30 [A, C, E & G]** were compared to VSMCs stimulated with OM **Figure 30 [B, D, F & H]**. The images were taken at time points day 0, day, 7, day 14, and day 21. VSMCs stimulated with control medium alone demonstrated strong expression of HYAL1 throughout the entire cell at all timepoints **Figure 30 [A, C, E & G]**. There were no changes at day 0 **Figure 30 [B]**. Stimulation with OM for 7 to 14 days significantly reduced the cellular expression of HYAL1 **Figure 30 [D & F]**. By day 21, HYAL1 was undetectable in the osteogenic-treated cells **Figure 30 [H]**.

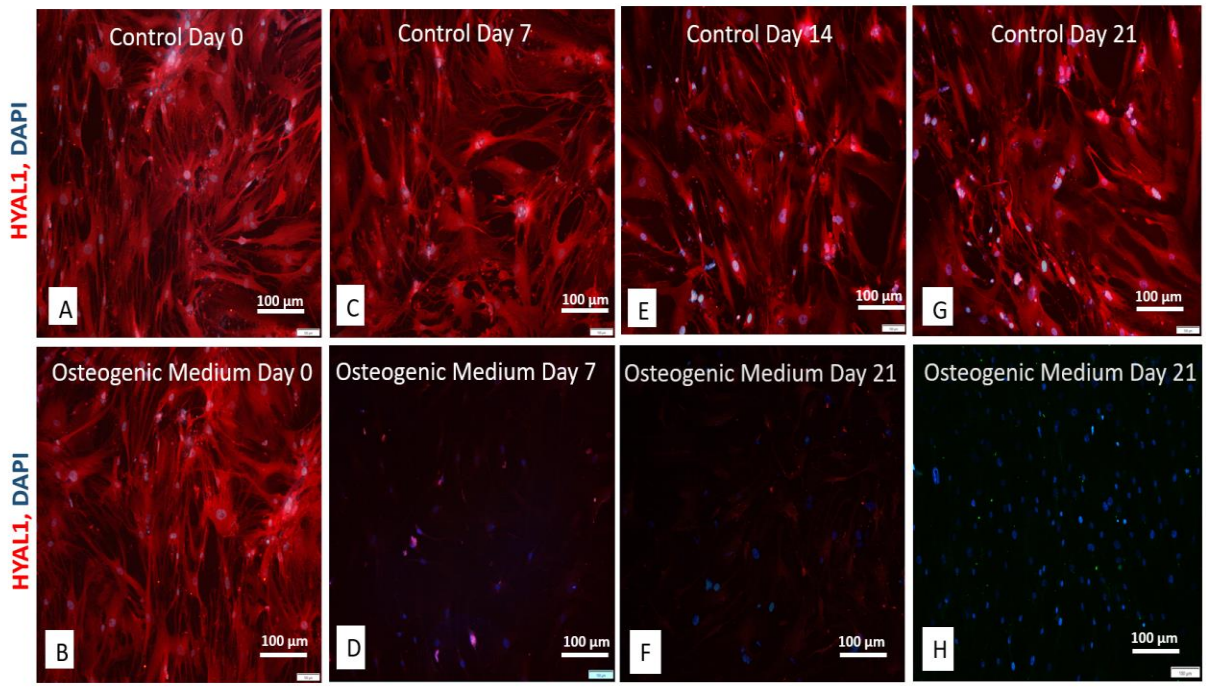

Figure 30 HYAL1 (red) expression in differentiated VSMCs when stimulated with OM.

Sub-confluent monolayers of human aortic vascular smooth muscle cells were grown on 8-well chamber slide and treated with osteogenic medium. The control cells were grown in smooth muscle growth medium. Cells were fixed using 4% paraformaldehyde at the following timepoints day 0 (CT), day 7, day 14 and day 21. Cells were then and stained for (HYAL1) (red), control cells [A, C, E, and G] osteogenic cells [B, D, F, and H]. The cells were analysed by confocal microscopy, magnification x100. The images were taken at 4 different time points along the course of osteogenic differentiation (n=6).

To visualize HYAL2 protein expression VSMCs stimulated with control medium **Figure 31 [A, C, E, G, J & K]** were compared to VSMCs stimulated with OM **Figure 31 [B, D, F, H, I & K]**. The images were taken at time points day 0, day, 7, day 14, and day 21. VSMCs treated solely with control medium displayed a diffuse cytoplasmic expression of HYAL2 spanning the entire cell at all examined time points **Figure 31 [A, C, E, G & I]**, respectively. Although the addition of OM did not induce noticeable changes between the control and differentiated cells at any time point, **Figure 31 [A-H]**, closer inspection at higher magnification revealed a slight reduction in protein expression in OM-treated cells at day 21 **Figure 31 [J & K]**.

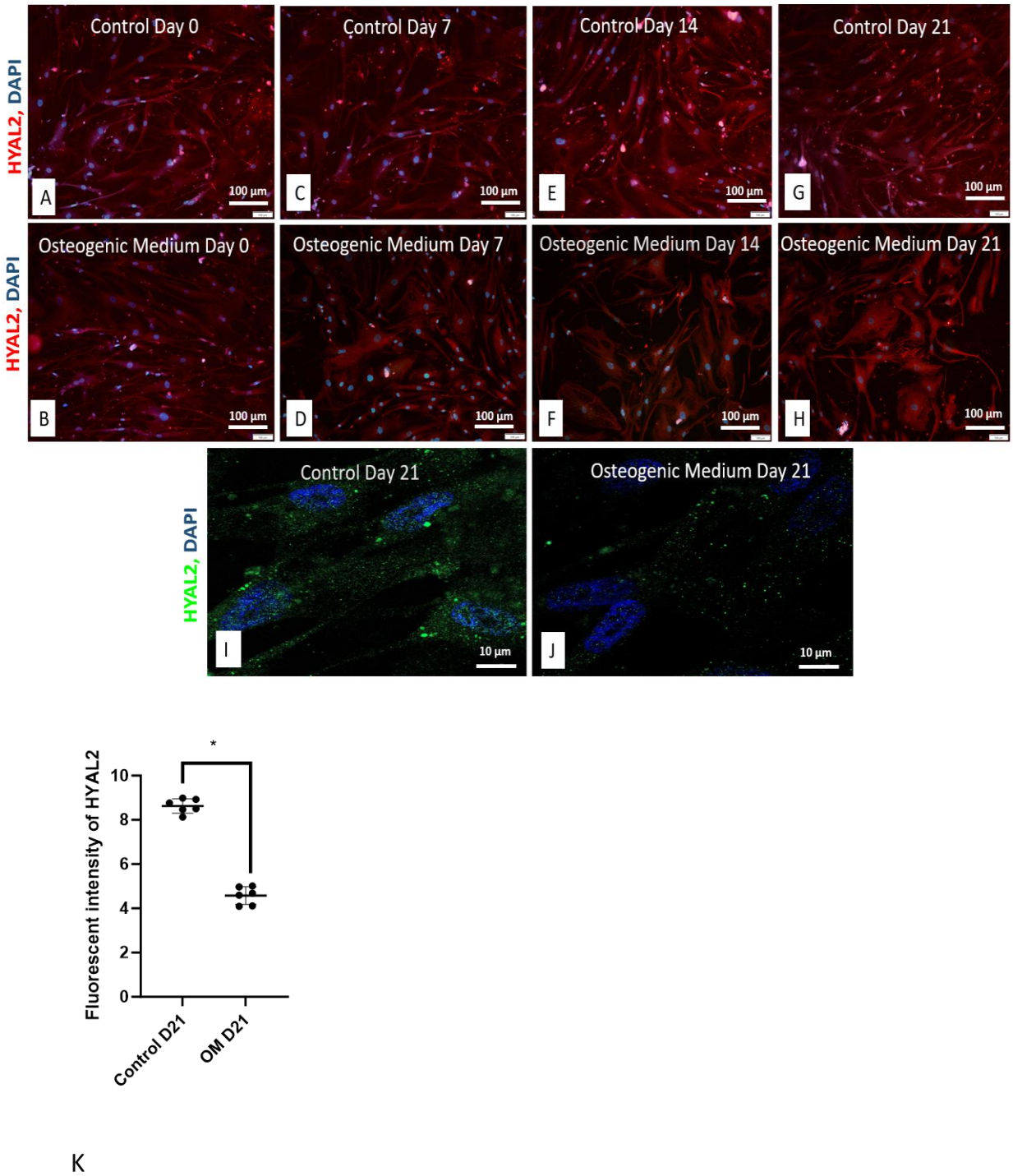

Figure 31 Hyaluronidases protein expression in VSMCs incubated with Osteogenic Medium

Sub-confluent monolayers of human aortic vascular smooth muscle cells were grown on 8-well chamber slide and treated with osteogenic medium. The control cells were grown in smooth muscle growth medium. Cells were fixed using 4% paraformaldehyde at the following timepoints day 0 (CT), day 7, day 14 and day 21. Cells were then and stained for (HYAL2) (red), control cells [A, C, E, G and I] osteogenic cells [B, D, F, H and J]. The cells were analysed by confocal microscopy, magnification x100 [A-H] and x630 [I-J]. The images were taken at 4 different time points along the course of osteogenic differentiation. The fluorescent intensity was measured using the ImageJ software [K].

For the scatter dot plot, the median value obtained from each dot, are represented by a line. All the values are expressed as means ± SD from 6 biological replicates in each group. Data was analysed by Mann-Whitney test followed by Dunn's post hoc analysis (* = p≤0.05).

Next, we sought to gain an understanding of the mRNA expression the principal HA receptors, CD44 and RHAMM in VSMCs stimulated with osteogenic media. RT-qPCR was carried out at 0, 3, 16, 24, 48, and 72 h initially. Similar to HA Synthases and HYALs, the mRNA expression of CD44 and RHAMM decreased below control levels at all the time points compared to 0 h **Figure 32 [A-B]**.

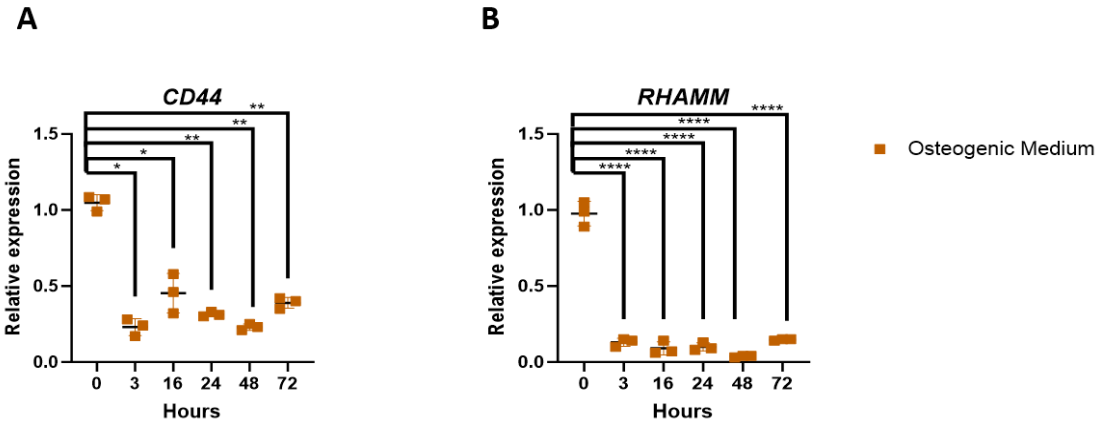

Figure 32 HA receptors mRNA expression in VSMCs incubated with Osteogenic Medium in early time points

Human aortic vascular smooth muscle cells were grown in Osteogenic Medium up to 72 hours. Control cells were treated with VSMC growth medium. mRNA was extracted at 0, 3, 16, 24, 48, and 72 h. HA receptors expression was assessed relative to control samples at 0 h. The comparative C_T method was used for relative quantification of gene expression and the results were represented as mean ± S.D. For the scatter dot plot, the median value obtained from each dot, are represented by a line. Each point in the scatter dot plot denotes a single biological replicate. Data was analysed by Kruskal-Wallis test followed by Dunn's post hoc analysis (ns = p>0.05, * = p≤0.05, ** = p≤0.01, *** = p≤0.001, **** = p≤0.0001).

To characterize the later expression of the HA receptors, CD44 and RHAMM in VSMCs stimulated with OM, mRNA was collected at 0 hr, 7 days, 14 days, and 21 days. Treating VSMCs with OM attenuated the mRNA expression of CD44 at all timepoints from day 7 days

to 21 days, compared to control cells **Figure 33 [A]**. VSMCs that were stimulated with OM also had reduced expression of RHAMM at day 7 and a downward trend was observed at the later time points at day 7 to day 21 compared to control VSMCs **Figure 33 [B].**

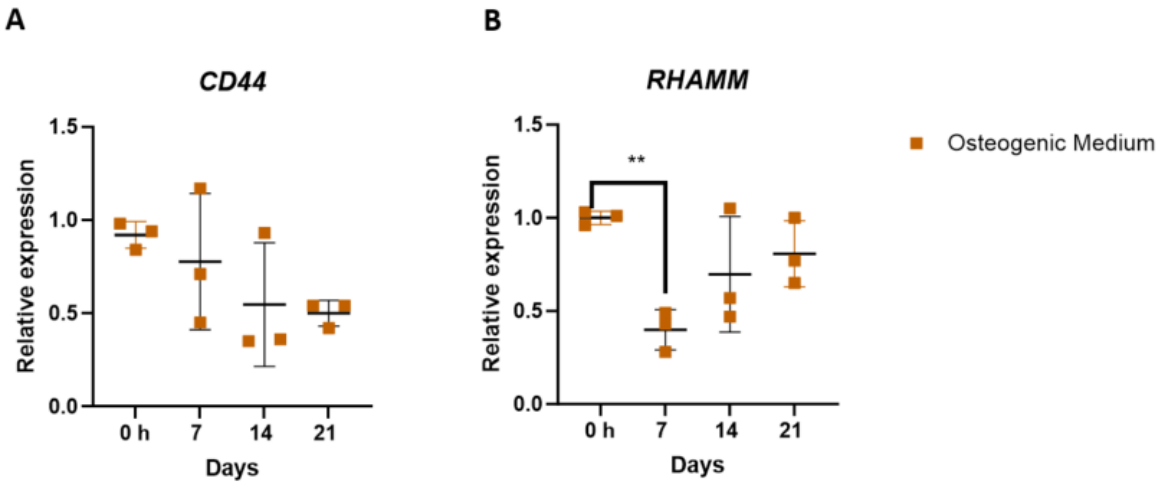

Figure 33 HA receptor* CD44 *and RHAMM mRNA expression in VSMCs incubated with Osteogenic Medium

Human aortic vascular smooth muscle cells were grown in OM. Control cells were treated with VSMC growth medium. CD44 and RHAMM expression was assessed relative to control samples. The comparative C_T method was used for relative quantification of gene expression and the results were represented as mean ± S.D. For the scatter dot plot, the median value obtained from each dot, are represented by a line. Each point in the scatter dot plot denotes a single biological replicate. Data was analysed by Kruskal-Wallis test followed by Dunn's post hoc analysis (ns = p>0.05, ** = p≤0.01, *** = p≤0.001, **** = p≤0.0001).

To visualize the protein expression of CD44, VSMCs stimulated with control medium **Figure 34 [A, C, E, G & I]** were contrasted with those exposed to OM **Figure 34 [B, D, F, H & I]**. The images were taken at time points day 0, day, 7, day 14, and day 21. The addition of OM did not bring about any recognisable alteration in this expression pattern at any time point compared to control cells **Figure 34 [A-I]**.

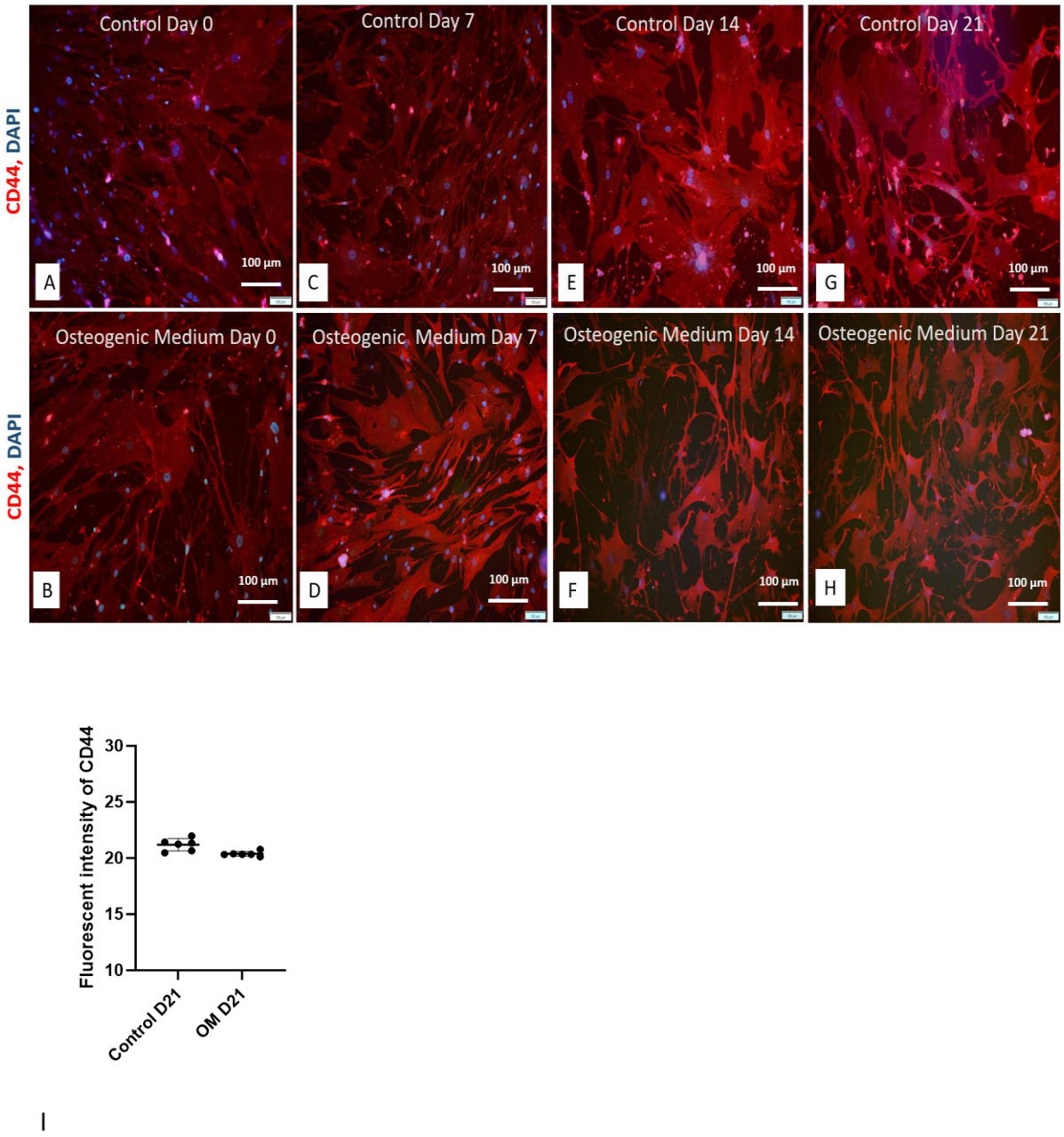

Figure 34 CD44 (red) expression in differentiated VSMCs when stimulated with OM.

Sub-confluent monolayers of human aortic vascular smooth muscle cells were grown on 8-well chamber slide and treated with osteogenic medium. The control cells were grown in smooth muscle growth medium. Cells were fixed using 4% paraformaldehyde at the following timepoints day 0 (CT), day 7, day 14 and day 21. Cells were then and stained for (CD44) (red), control cells [A, C, E and G] osteogenic cells [B, D, F and H]. The images were taken at 4 different time points along the course of osteogenic differentiation. The fluorescent intensity was measured using the ImageJ software [I]. For the scatter dot plot, the median value obtained from each dot, are represented by a line. All the values are expressed as means ± SD from 6 biological replicates in each group.

To visualize RHAMM protein expression VSMCs stimulated with control medium **Figure 35 [A, C, E & G]** were compared to VSMCs stimulated with OM **Figure 35 [B, D, F & H]**. Imaging was conducted at distinct time points: day 0, day 7, day 14, and day 21. After 7 days of OM stimulation, VSMCs displayed reduced expression of RHAMM compared to control cells **Figure 35 [D]**. By the 14- and 21-day marks, RHAMM expression was no longer detectable via immunocytochemistry **Figure 35 [F and H]**.

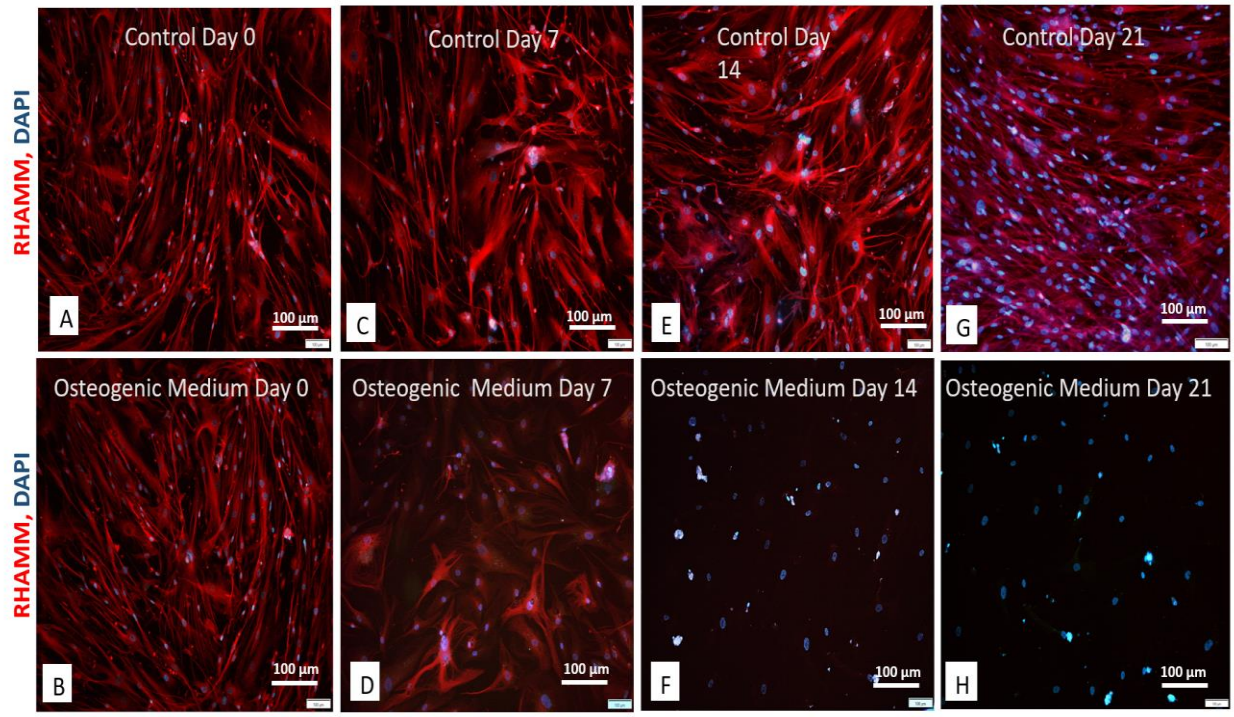

Figure 35 RHAMM (red) expression in differentiated VSMCs when stimulated with OM.

Sub-confluent monolayers of human aortic vascular smooth muscle cells were grown on 8-well chamber slide and treated with osteogenic medium. The control cells were grown in smooth muscle growth medium. Cells were fixed using 4% paraformaldehyde at the following timepoints day 0 (CT), day 7, day 14 and day 21. Cells were then and stained for (RHAMM) (red), control cells [A, C, E, and G] osteogenic cells [B, D, F, and H]. The cells were analysed by confocal microscopy, magnification x100. The images were taken at 4 different time points along the course of osteogenic differentiation (n=6).

TSG-6 is one of the principal and most widely studied hyaladherins. It plays important roles in inflammation, HA coat formation, inflammatory cell migration, cell proliferation, developmental processes, and tissue remodeling[578]. In these studies, when stimulated with OM at short time points, there was a decrease at 3, 16, 24, and 48 h followed by an increase in TSG-6 expression at 72 h **Figure 36**.

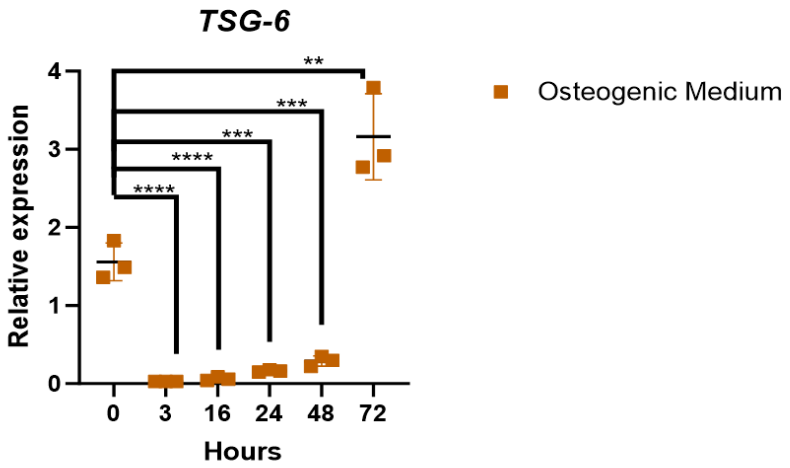

Figure 36 HA binding protein TSG-6 mRNA expression in VSMCs incubated with Osteogenic Medium in early time points

Human aortic vascular smooth muscle cells were grown in Osteogenic Medium up to 72 hours. Control cells were treated with VSMC growth medium. mRNA was extracted at 0, 3, 16, 24, 48, and 72 h. HA binding proteins expression was assessed relative to control samples at 0 h. The comparative C_T method was used for relative quantification of gene expression and the results were represented as mean ± S.D. For the scatter dot plot, the median value obtained from each dot, are represented by a line. Each point in the scatter dot plot denotes a single biological replicate. Data was analysed by Kruskal-Wallis test followed by Dunn's post hoc analysis (ns = p>0.05, * = p≤0.05, ** = p≤0.01, *** = p≤0.001, **** = p≤0.0001).

When stimulated with OM at latter timepoints however, TSG-6 mRNA expression decreased compared to control samples at all timepoints **Figure 37**.

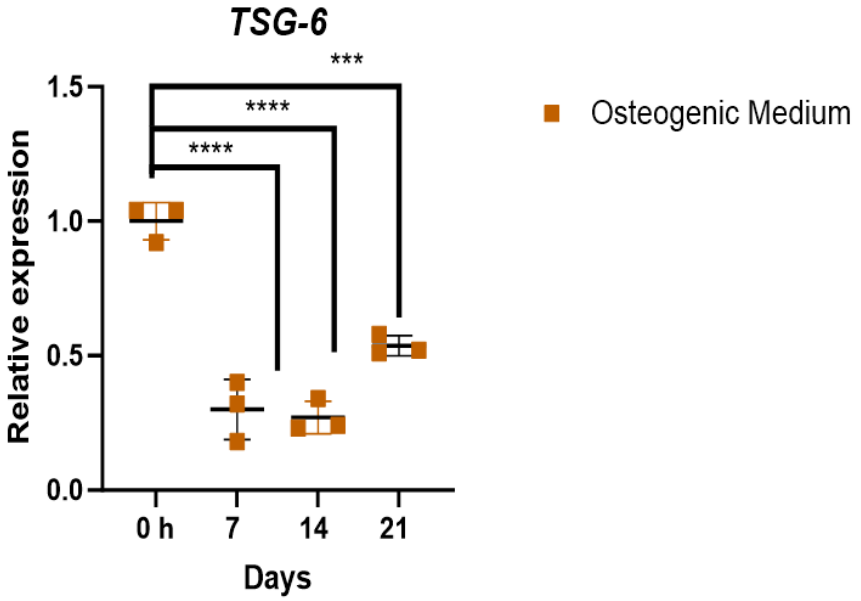

Figure 37 HA binding protein TSG-6 mRNA expression in VSMCs incubated with Osteogenic Media

Human aortic vascular smooth muscle cells were grown in OM. Control cells were treated with VSMC growth medium. TSG-6 expression was assessed relative to control samples at 0 h. The comparative C_T method was used for relative quantification of gene expression and the results were represented as mean± S.D. For the scatter dot plot, the median value obtained from each dot, are represented by a line. Each point in the scatter dot plot denotes a single biological replicate. Data was analysed by Kruskal-Wallis test followed by Dunn's post hoc analysis (ns = p>0.05, * = p≤0.05, ** = p≤0.01, *** = p≤0.001, **** = p≤0.0001).

To visualize TSG-6 protein expression VSMCs stimulated with control medium **Figure 38 [A, C, E, G, I & K]** were compared to VSMCs stimulated with OM **Figure 38 [B, D, F, H, J & K]**. These observations were made at four time points: day 0, day 7, day 14, and day 21. VSMCs stimulated solely with control medium exhibited a diffuse cytoplasmic distribution of TSG-6 throughout the cell at all time points **Figure 38 [A, C, E, G & I]**. There was no change at day 0 **Figure 38 [B]**. However, at 7, 14, and 21 days of OM stimulation, the cellular expression of TSG-6 diminished **Figure 38 [D, F, H & J]**. This was also evident in the higher power images shown **Figure 38 [I, J & K]**.

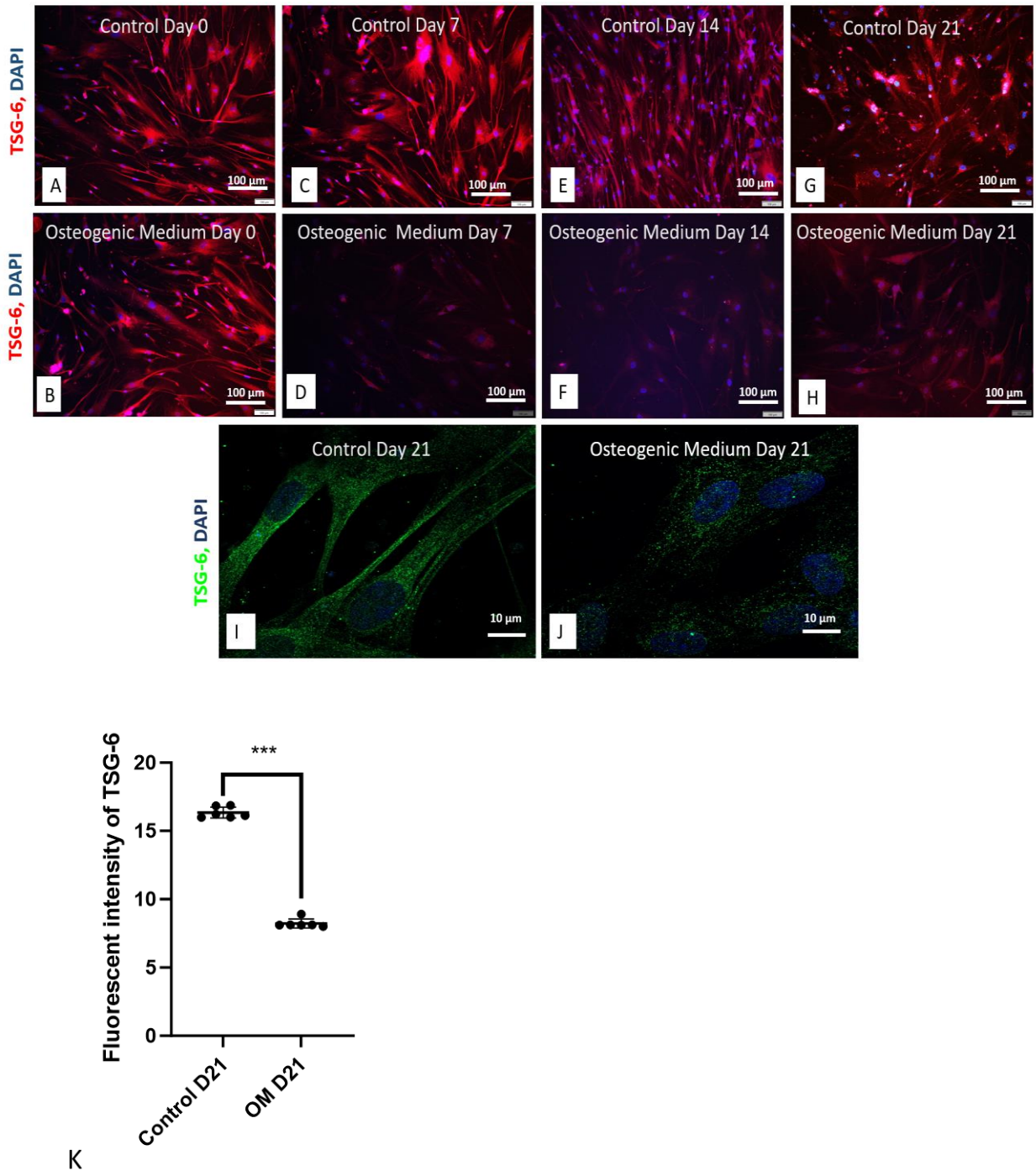

Figure 38 TSG-6 expression in differentiated VSMCs when stimulated with OM.

Sub-confluent monolayers of human aortic vascular smooth muscle cells were cultivated on 8-well chamber slide and subjected to treatment with osteogenic medium. Control cells were cultivated in smooth muscle growth medium. At specific time points (day 0, day 7, day 14, and day 21), cells were fixed using 4% paraformaldehyde. Following fixation, the cells were stained to visualize TSG-6 expression. Control cells were represented in images [A, C, E, G and I], while osteogenic cells were depicted in images [B, D, F, H and J]. Analysis was carried out using confocal microscopy at magnifications of x100 [A-H] and x630 [I-J]. These images were captured at four distinct time points

during the osteogenic differentiation process. The fluorescent intensity was measured using the ImageJ software [K]. For the scatter dot plot, the median value obtained from each dot, are represented by a line. All the values are expressed as means ± SD from 6 biological replicates in each group. Data was analysed by Mann-Whitney test followed by Dunn's post hoc analysis (* = p≤0.001).**

Versican (VCAN) is another hyaladherin, which is an extracellular matrix proteoglycan which has a role in cell adhesion, migration, and proliferation. It crosslinks with HA and regulates ECM remodelling[343,363,579]. Similar to all HAS, HYALs, and HA receptors when stimulated with OM, there was a decrease in VCAN mRNA expression at all time points up to 72 h **Figure 39**.

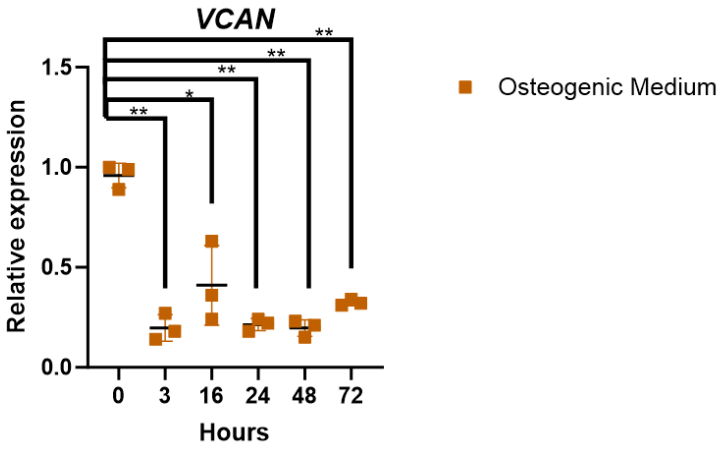

Figure 39 HA binding protein Versican (VCAN) mRNA expression in VSMCs incubated with Osteogenic Medium in early time points

Human aortic vascular smooth muscle cells were grown in Osteogenic Medium up to 72 hours. Control cells were treated with VSMC growth medium. mRNA was extracted at 0, 3, 16, 24, 48, and 72 h. HA binding proteins expression was assessed relative to control samples at 0 h. The comparative C_T method was used for relative quantification of gene expression and the results were represented as mean ± S.D. For the scatter dot plot, the median value obtained from each dot, are represented by a line. Each point in the scatter dot plot denotes a single biological replicate. Data was analysed by Kruskal-Wallis test followed by Dunn's post hoc analysis (ns = p>0.05, * = p≤0.05, ** = p≤0.01, *** = p≤0.001, **** = p≤0.0001).

The mRNA expression of VCAN showed no change in expression from the control VSMCS when stimulated with OM at the examined later time points **Figure 40**.

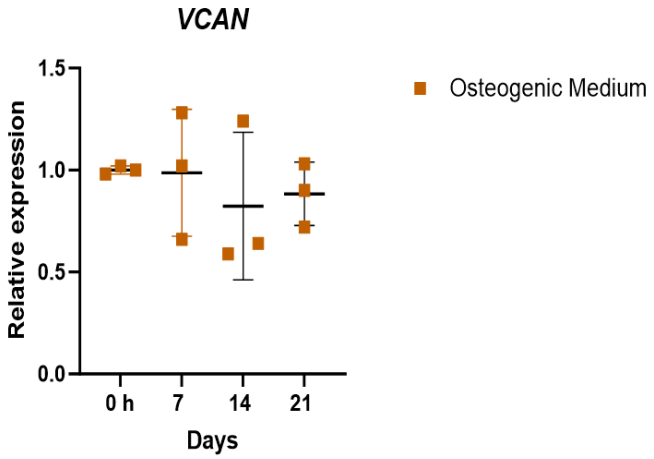

Figure 40 HA binding protein Versican mRNA expression in VSMCs incubated with Osteogenic Media

Human aortic vascular smooth muscle cells were grown in OM. Control cells were treated with VSMC growth medium. Versican (VCAN) expression was assessed relative to control samples at 0 h. The comparative C_T method was used for relative quantification of gene expression and the results were represented as mean± S.D. For the scatter dot plot, the median value obtained from each dot, are represented by a line. Each point in the scatter dot plot denotes a single biological replicate. Data was analysed by Kruskal-Wallis test followed by Dunn's post hoc analysis (ns = p>0.05, * = p≤0.05, ** = p≤0.01, *** = p≤0.001, **** = p≤0.0001).

To visualize VCAN protein expression, VSMCs stimulated with control medium **Figure 41 [A, C, E, G, I & K]** were compared to VSMCs stimulated with OM **Figure 41 [B, D, F, H, J & K]**. Images were captured at four different time points: day 0, day, 7, day 14, and day 21. At day 0, VSMCs stimulated solely with control medium exhibited a diffuse expression of cytoplasmic VCAN **Figure 41 [A]**. However, the stimulation with OM significantly enhanced both the intensity and of VCAN staining from day 7 to day 21 **Figure 41 [D, F, H, J & K]**, compared to the control cells **Figure 41 [C, E, G, I & K]**.

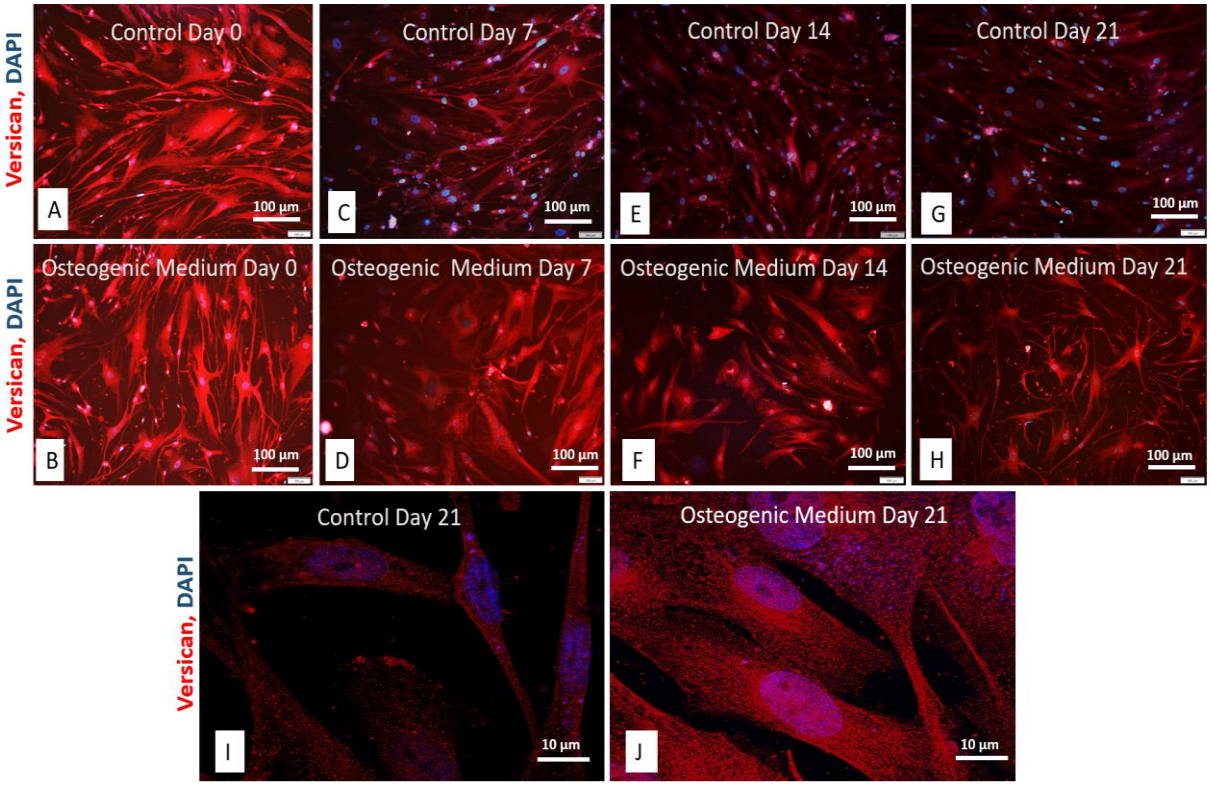

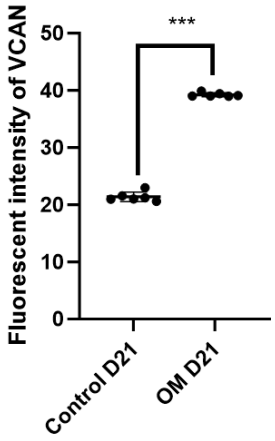

K

Figure 41 VCAN (red) expression in differentiated VSMCs when stimulated with OM.

Human aortic vascular smooth muscle cells were cultivated as sub-confluent monolayers on 8-well chamber slides. These cells were then subjected to osteogenic medium treatment, while control cells were grown in smooth muscle growth medium. At specific time points (day 0, day 7, day 14, and day 21), cells were fixed using 4% paraformaldehyde. Subsequently, the fixed cells were stained to visualize VCAN (red). Control cells were represented in images [A, C, E, G, and I], while osteogenic cells were depicted in images [B, D, F, H, and J]. The analysis was performed using confocal microscopy at magnifications of x100 [A-H] and x630 [I-J]. The images were taken at 4 different time

points spanning the osteogenic differentiation process. The fluorescent intensity was measured using the ImageJ software [K]. For the scatter dot plot, the median value obtained from each dot, are represented by a line. All the values are expressed as means ± SD from 6 biological replicates in each group. Data was analysed by Mann-Whitney test followed by Dunn's post hoc analysis (* = p≤0.001).**

4.2.2 Alterations in HA following stimulation with cytokines relevant in CKD

HA has been reported to meditate the inflammatory environment, and both regulates and is regulated by inflammatory cells, genes and cytokines[279]. However, it is not understood what the role of HA is in VC, it is also not known if there is an association between the increased expression of these cytokines and alterations in HA related to VC in VSMCs. The role of IL-6 and TGF-β1 on HA synthesis, turnover, and HA receptor/hyaladherin expression was therefore assessed. VSMCs were stimulated with either TGF-β1 or IL-6 alone **Figures 42-43** (TGF-β1) and **Figures 44-45** (IL-6). The impact of TGF-β1 in HAS isoenzymes was assessed in short time points. All the HAS isoenzymes showed an initial increase followed by attenuation. There is an increased mRNA expression of HAS1 at 3 and 24 h compared to the controls at 0 h **Figure 42 [A]**. HAS2 demonstrated an increased expression at 3 h **Figure 42 [B]** while HAS3 showed attenuation at 16 and 72 h compared to the controls at 0 h **Figure 42 [C]**. Next, we assessed the impact of TGF-β1 in HYALS. The expression of HYAL1 was underdetermined. Expression of HYAL2 mRNA showed attenuation at 72 h compared to the controls at 0 h **Figure 42 [D]**. We then proceeded to study how TGF-β1 impacts the receptors associated with HA. Stimulation with TGF-β1, CD44 demonstrated attenuation at 48 h followed by increase in expression at 72 h **Figure 42 [E]**. RHAMM displayed increased expression at 16 and 24 h **Figure 42 [F]**. Following that we delved into examining how TGF-β1 affects HA-binding protein. Notably, TSG-6 expression remains unchanged at all time points **Figure 42 [G]**, while VCAN exhibited increased expression at 24 h compared to control cells at 0 h **Figure 42 [H]**.

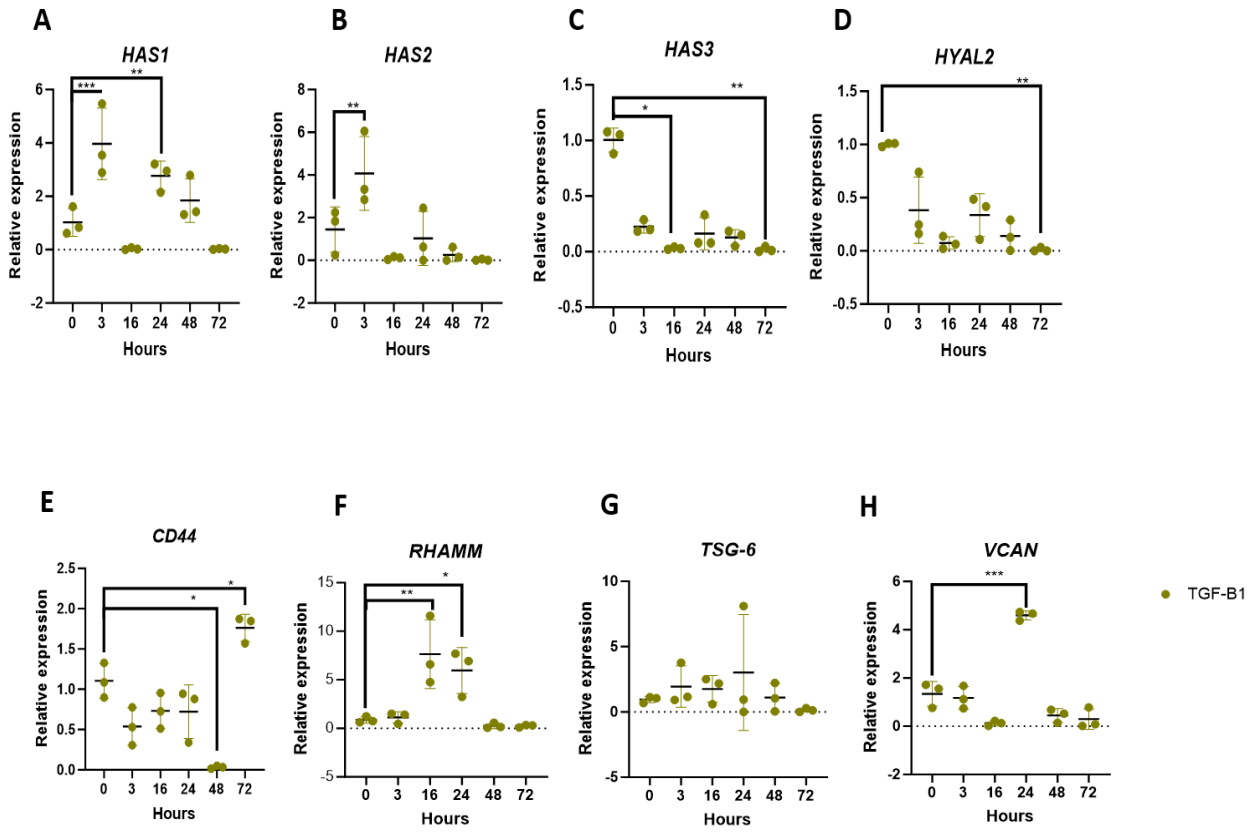

Figure 42 HA and related proteins mRNA expression in VSMCs stimulated with TGF-β1 in early time points

VSMCS were stimulated with normal medium with 10 ng/mL of TGF-β1 for up to 72 hours. mRNA was extracted at 0, 3, 16, 24, 48, and 72 h and HA and related proteins expression was assessed by RT-qPCR. β-actin was used as a standard reference gene. The comparative C_T method was used for relative quantification of gene expression and the results were represented as mean ± S.D. For the scatter dot plot, the median value obtained from each dot, are represented by a line. Each point in the scatter dot plot denotes a single biological replicate. Data was analysed by Kruskal-Wallis test followed by Dunn's post hoc analysis (ns = p>0.05, * = p≤0.05, ** = p≤0.01, *** = p≤0.001).

In the analysis of late time point expression of HAS isoenzymes, the results indicated increased mRNA expression of HAS1 at 7 days compared to the controls at 0 h **Figure 43 [A]**. Stimulating VSMCs with normal growth medium + TGF-β1 displayed an upward trend in both HAS2 and HAS3 mRNA expression at all time points from day 7 to day 21, compared to the controls at 0 h **Figure 43 [B-C]**. HYAL1 also demonstrated an upward trend in expression in VSMCs when stimulated with TGF-β1 **Figure 43 [D]**. However, the expression of HYAL2 mRNA showed no significant changes at any time points compared to the controls at 0 h **Figure 43 [E]**. Stimulation with TGF-β1 did not induce significant changes in the expression of CD44 and VCAN at any timepoints from days 7 to 21 **Figure 43 [F and I]**. Conversely, RHAMM exhibited

attenuation at all timepoints from day 7 days to 21 days **Figure 43 [G]**. TSG-6 displayed increased expression at day 14 and 21 compared to control cells at 0 h **Figure 43 [H]**.

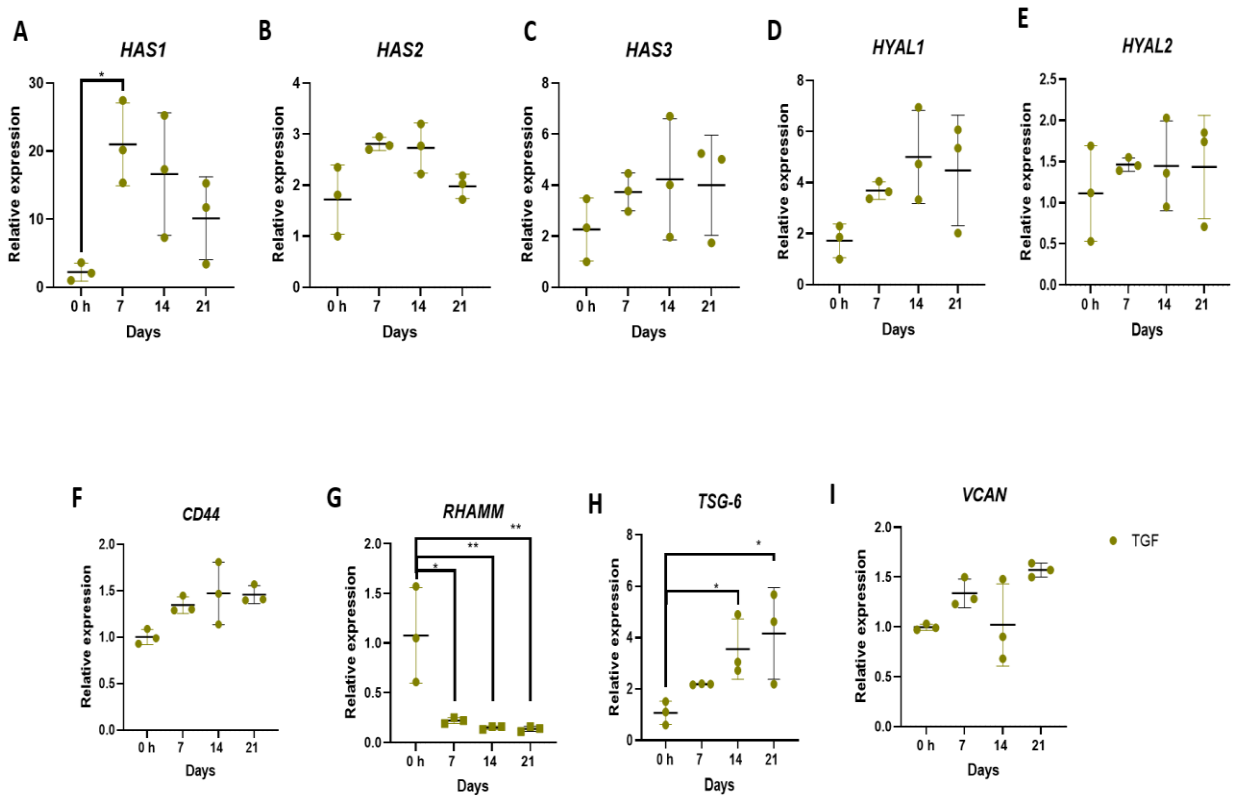

Figure 43 HA and related proteins mRNA expression in VSMCs stimulated with TGF-β1

VSMCS were stimulated with normal medium with 10 ng/mL of TGF-β1 for up to 21 days and HA and its related proteins expression was assessed by RT-qPCR. β-actin was used as a standard reference gene. The comparative C_T method was used for relative quantification of gene expression and the results were represented as mean ± S.D. For the scatter dot plot, the median value obtained from each dot, are represented by a line. Data was analysed by Kruskal-Wallis test followed by Dunn's post hoc analysis (ns = p>0.05, * = p≤0.05, ** = p≤0.01).

Early time point expression of HAS isoenzymes were investigated at up to 72 h when stimulated with IL-6. There was an increased mRNA expression of HAS1 and HAS2 at 3 h **Figure 44 [A-B]**, and an increased expression of HAS3 at 72 h, compared to the controls at 0 h **Figure 44 [C]**. HYAL1 expression did not exhibit any significant changes at any time points **Figure 44 [D]**. The expression of HYAL2 mRNA showed attenuation at 48 h compared to the controls at 0 h **Figure 44 [E]**. Similar to stimulation with TGF-β1, stimulation with IL-6 displayed an attenuation at 48 h followed by an increase in expression at 72 h **Figure 44 [F]**. Similar to stimulation with TGF-β1, stimulation with IL-6 showed an increased expression of RHAMM at 16 and 24 h **Figure 44 [G]**. Moreover, there was an increased mRNA expression of TSG-6 at 72 h **Figure 44 [H]**, and VCAN had exhibited attenuation at 48 h, followed by an increased expression at 72 h, compared to control cells at 0 h **Figure 44 [I]**.

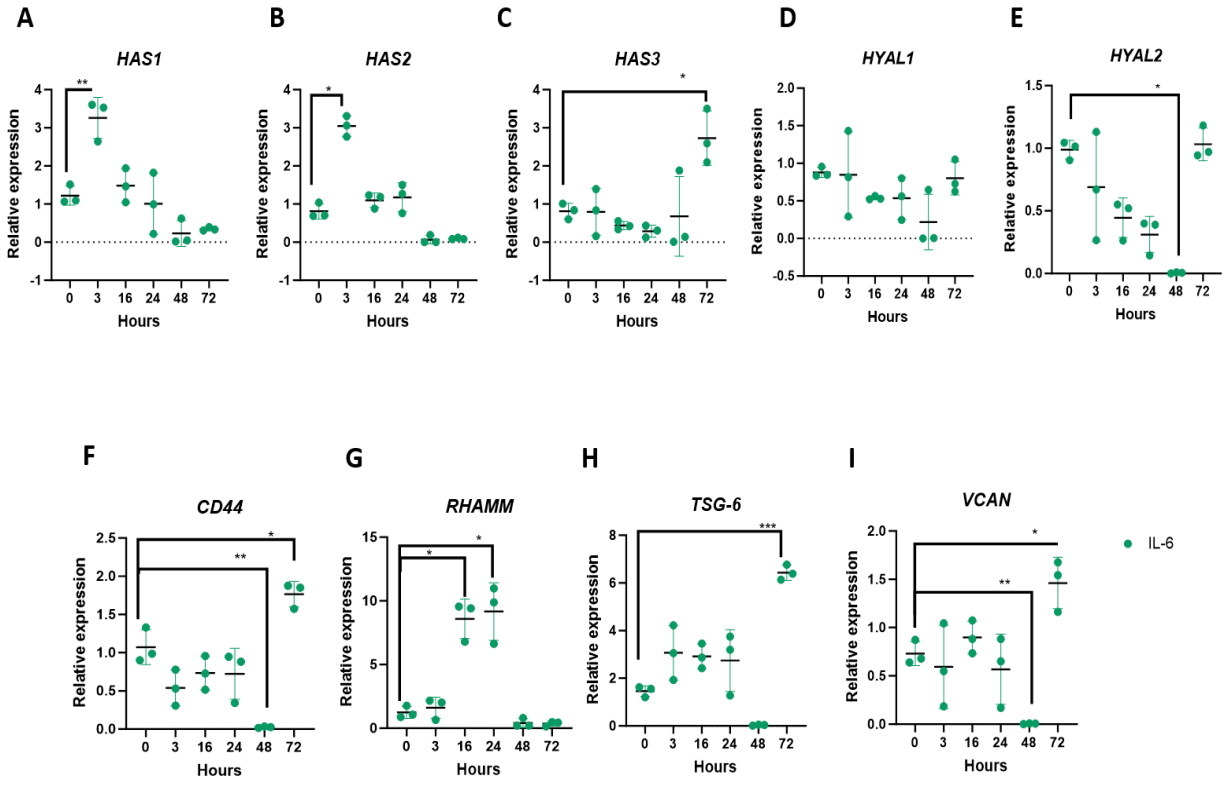

Figure 44 HA and related proteins mRNA expression in VSMCs stimulated with IL-6 in early time points

VSMCS were stimulated with normal medium with 10 ng/mL of IL-6 for up to 72 hours. mRNA was extracted at 0, 3, 16, 24, 48, and 72 h and HA and related proteins expression was assessed by RT-qPCR. β-actin was used as a standard reference gene. The comparative C_T method was used for relative quantification of gene expression and the results were represented as mean ± S.D. For the scatter dot plot, the median value obtained from each dot, are represented by a line. Each point in

the scatter dot plot denotes a single biological replicate. Data was analysed by Kruskal-Wallis test followed by Dunn's post hoc analysis (ns = p>0.05, * = p≤0.05, ** = p≤0.01, *** = p≤0.001).

For late time point expression analysis, VSMCs treated with IL-6 alone in normal growth medium, exhibited no significant change in HAS1 expression **Figure 45 [A]**. However, there was an upregulation in HAS2 mRNA expression observed at day 14 and day 21 **Figure 45 [B]**. Stimulation of VSMCs with normal growth medium + IL-6 led to an increase in HAS3 mRNA expression at all time points from day 7 to day 21, compared to the controls at 0 h **Figure 45 [C]**. HYAL1 displayed increased mRNA expression at days 14 and 21 **Figure 45 [C]**, while HYAL2 exhibited increased expression at day 21 when treated with normal growth medium + IL-6 **Figure 45 [D]**. CD44 demonstrated increased mRNA expression at day 14 and day 21 compared to control cells at 0 h when treated with IL-6 alone **Figure 45 [E]**. In contrast, RHAMM exhibited attenuation at all timepoints from day 7 days to 21 days when stimulated with IL-6 **Figure 45 [F]**. Stimulation with normal growth medium + IL-6 resulted in an attenuation of TSG-6 mRNA expression at day 7 **Figure 45 [H]**, whereas IL-6 stimulation did not alter the mRNA expression of VCAN at any timepoints from days 7 to 21 **Figure 45 [I]**.

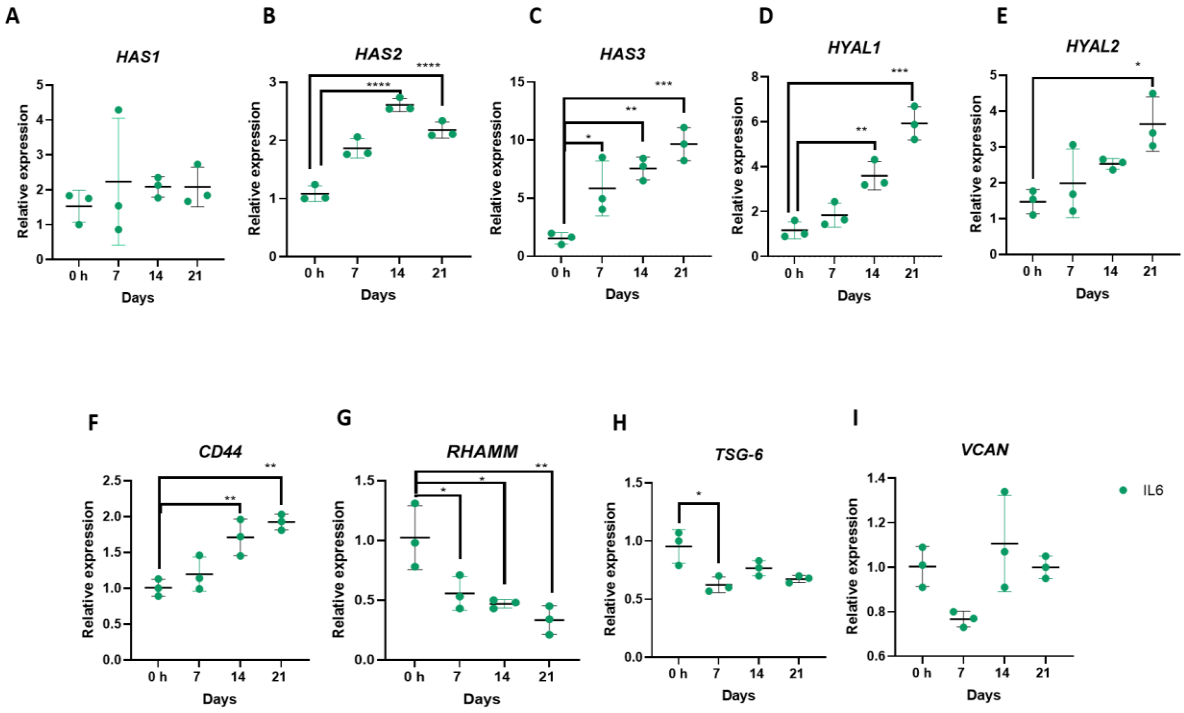

Figure 45 HA and related proteins mRNA expression in VSMCs stimulated with IL-6

VSMCS were stimulated with normal medium with 10 ng/mL of IL-6 for up to 21 days and HA and its related proteins expression was assessed by RT-qPCR. β-actin was used as a standard reference gene. The comparative C_T method was used for relative quantification of gene expression and the results were represented as mean ± S.D. For the scatter dot plot, the median value obtained from each dot, are represented by a line. Data was analysed by Kruskal-Wallis test followed by Dunn's post hoc analysis (ns = p>0.05, * = p≤0.05, ** = p≤0.01, *** = p≤0.001, **** = p≤0.0001).

4.2.3 HA modulation in VSMCs influences osteogenic differentiation and matrix calcification.

Inhibiting the synthesis of HA is an appealing strategy to investigate its role in conditions linked to changes in HA levels, such as atherosclerosis and VC[471,577]. Research has indicated that 4MU effectively hinders global HA synthesis and the creation of HA-rich matrices around cells in various cell types[580-582]. 4MU interferes with the production of HA by inhibiting the enzyme UDP-glucuronic acid: β-N-acetylglucosamine transferase which is involved in the biosynthetic pathway of HA. Without this enzyme's activity, the synthesis of HA is disrupted, leading to a decrease in HA levels[582].

Another means of modulating HA extracellular matrices is using exogenous treatment with hyaluronidase to remove HA matrices. HA degradation is possible with Strep-Hyal, a bacterial protein that possesses enzymatic activity capable of degrading HA[583]. Strep-Hyal degradation process involves the hydrolysis of the glycosidic linkages between the N-acetylglucosamine and glucuronic acid units that make up the HA polymer[584]. As a result, the size and structure of the HA molecule change, impacting its biological functions and properties.

The impact of 4MU and Strep-Hyal on VSMC calcification were investigated. After fixation, cells were stained with Alizarin Red and examined under a light microscope. To assess the calcification potential of 4MU/Strep-Hyal with OM, cells were exposed to OM+4MU **Figure 46 [E-H]** or OM-Strep-Hyal **Figure 46 [I-L]** and compared to OM-only treated cells **Figure 46 [A-D]**.

There was no calcium deposition detected at day 0 Figure **46 [A, E, & M]**. Subsequent Alizarin Red staining revealed increased calcium deposition at days 7, 14, and 21 with 4MU treatment **Figure 46 [F-H & M]**, compared to cells treated with osteogenic medium alone **Figure 46 [B-D & M]**.

To assess the impact of Step-Hyal, cells were exposed to OM+Strep-Hyal were compared to OM-treated cells. Alizarin Red staining was absent at day 0 **Figure 46 [E & N]** and **Figure 46 [A & N]**. OM-only treated cells showed emerging calcification at day 7, sporadic calcification at day 14, and widespread calcification at day 21 **Figure 46 [A-D].** By comparison, Strep-Hyal-treated cells exhibited complete attenuation of calcification at days 7, 14, and 21 **Figure 46 [I-L & N]**. These results were quantified and confirmed using the absorbance assay **Figure 46 [M & N].**

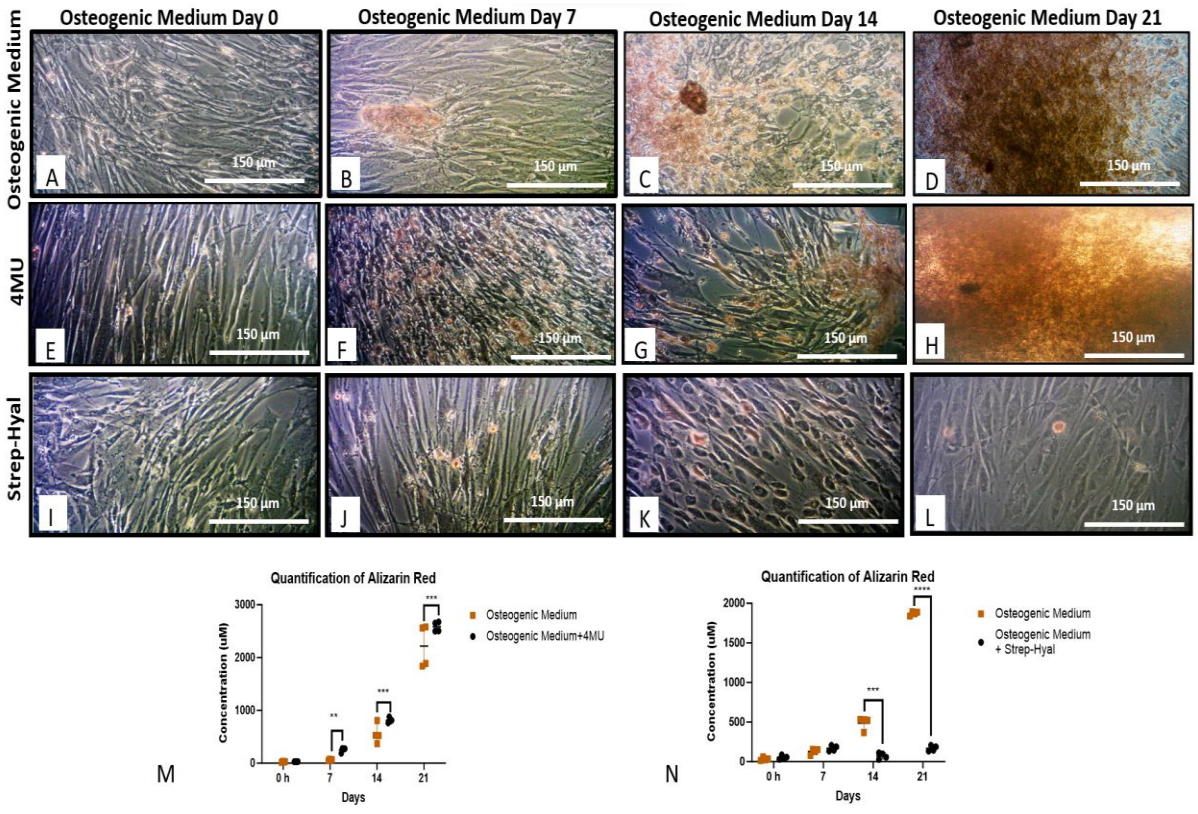

Figure 46 Alizarin red staining and quantification when VSMCs were stimulated with 4MU and Strep-Hyal

VSMCS were grown in normal media up to 80% confluence and were treated with 1mM 4MU for 48 hours or 1iU Streptococcus hyaluronidase for 1 hour. Then stimulated with osteogenic medium (A-D), osteogenic medium + 4MU (E-H), and osteogenic medium + Strep-Hyal (I-L) for up to 21 days.

They had been analysed at four different time points, day 0, 7, 14 and 21. The cells were fixed and stained with Alizarin Red (A-L) and extracted for quantitative measurement of absorbance at OD405 (M-N). The cells were analysed under a light microscope at magnification 100X. A digital eyepiece microscope camera was used to take pictures of the cells. Representative photographs of one of four independent experiments giving similar results Data was analysed by Kruskal-Wallis test followed by Dunn's post hoc analysis (= p≤0.01, *** = p≤0.001, **** = p≤0.0001).**

RT-qPCR was utilised to evaluate the impact of HA inhibition using 4MU on VSMC osteogenic differentiation. Incubation with 4MU induced an elevation in the mRNA expression of RunX2 at both day 14 and 21 **Figure 47 [A]**. On day 14, there was increased Osteopontin expression **Figure 47 [B]**. ALPL expression was enhanced on days 14 and 21 **Figure 47 [C]**. This data aligns with the outcome seen in the Alizarin Red staining, indicating increased calcium deposition.

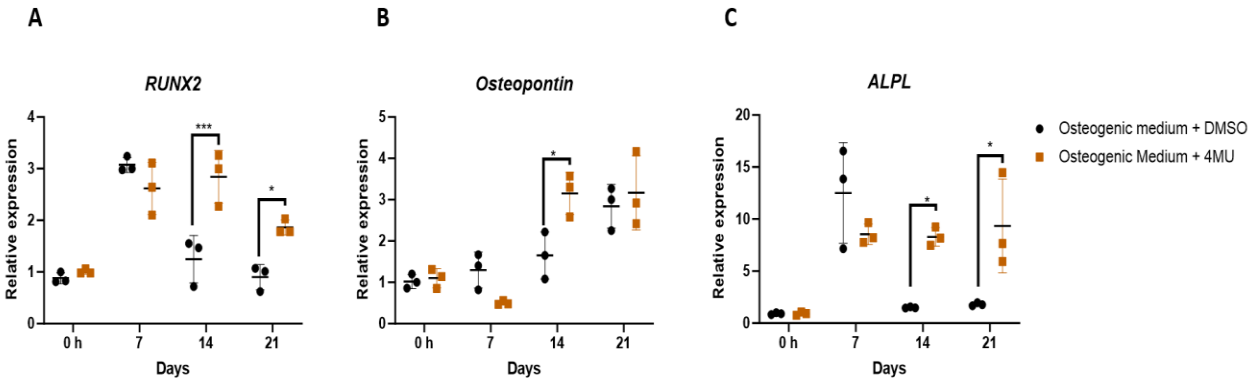

Figure 47 Differentiation markers in differentiated smooth muscle cells when stimulated with 4MU

VSMCS were grown in normal medium and were treated with DMSO or 1mM 4MU for 48 hours. Then stimulated with osteogenic medium for up to 21 days. mRNA was extracted at 0 hours, 7 days, 14 days, and 21 days. RunX2, Osteopontin and Alkaline Phosphatase mRNA expression was assessed by RT-qPCR. The comparative C_T method was used for relative quantification of gene expression and the results were represented as mean ± S.D. For the scatter dot plot, the median value obtained from each dot, are represented by a line. Each point in the scatter dot plot denotes a single biological replicate. Data was analysed by Kruskal-Wallis test followed by Dunn's post hoc analysis (* = p≤0.05, *** = p≤0.001).

The effects of HA degradation through Strep-Hyal on VSMC osteogenic differentiation using RT-qPCR were investigated. Across days 7 to 21, the expression of all osteogenic markers (RunX2, Osteopontin, and ALPL) exhibited significant attenuation, signifying a complete

inhibition of calcification **Figure 48 [A-C]**. This data correlates with the results observed from Strep-Hyal treatment for the Alizarin Red staining for calcium deposition.

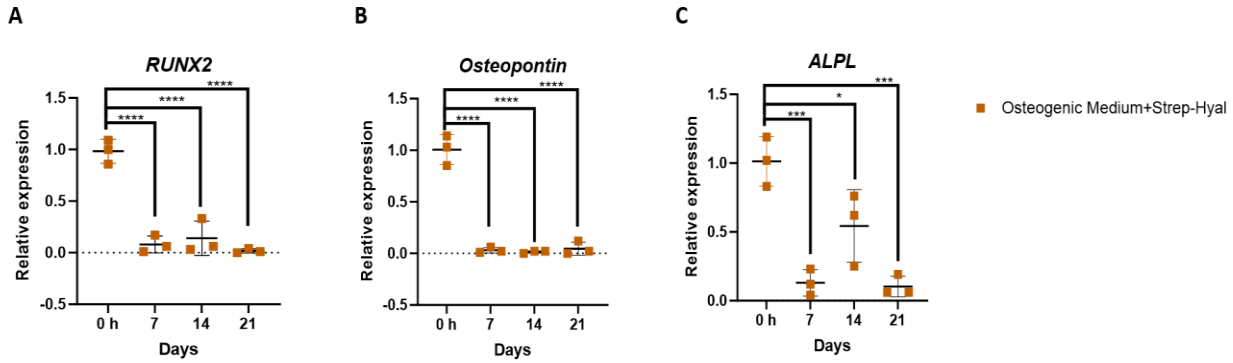

Figure 48 Investigating the effects of HA degradation using Hyaluronidase treatment on VSMC-osteogenic differentiation

VSMCS were grown in normal medium and were treated with 1iU Streptococcus hyaluronidase for 1 hour prior to stimulation with Osteogenic medium. mRNA was extracted at 0 hours, 7 days, 14 days, and 21 days. RunX2, Osteopontin and Alkaline Phosphatase mRNA expression was assessed by RT-qPCR. The comparative C_T method was used for relative quantification of gene expression and the results were represented as mean ± S.D. For the scatter dot plot, the median value obtained from each dot, are represented by a line. Each point in the scatter dot plot denotes a single biological replicate. Data was analysed by Kruskal-Wallis test followed by Dunn's post hoc analysis (* = p≤0.05, *** = p≤0.001).

The effects of HAS1/HAS2 plasmid overexpression on VSMC differentiation were explored next. Post-fixation, cells underwent Alizarin Red staining and were observed under a light microscope. To evaluate the calcification potential of HAS1/HAS2 over-expression alongside OM, cells were subjected to OM+ HAS1 plasmid **Figure 49 [E-H]** or OM-HAS2 plasmid **Figure 49 [I-L]** and compared to OM-treated only cells **Figure 49 [A-D]**.

Initial assessment at day 0 revealed no calcium deposition for both HAS1 plasmid-overexpressed cells and cells treated with OM **Figure 49 [A, E, & M]**. Subsequent Alizarin Red staining demonstrated complete suppression of calcium deposition at days 7, 14, and 21 for cells exposed to OM+HAS1 plasmid **Figure 49 [F-H & M]**, compared to cells treated with OM alone **Figure 49 [B-D & M]**.

To access the effects of HAS2 plasmid overexpression, cells treated with OM+HAS2 plasmid were compared to OM-only treated cells. Alizarin Red staining was absent at day 0 for OM+HAS2 plasmid **Figure 49 [E & N]**, as well as for cells treated with OM alone **Figure 49 [A & N]**. Similarly, to the HAS1 overexpression scenario, cells treated with OM+HAS2 plasmid exhibited complete suppression of calcification at days 7, 14, and 21 **Figure 49 [I-L & N]** compared to cells treated only with OM alone **Figure 49 [A-D & N].**

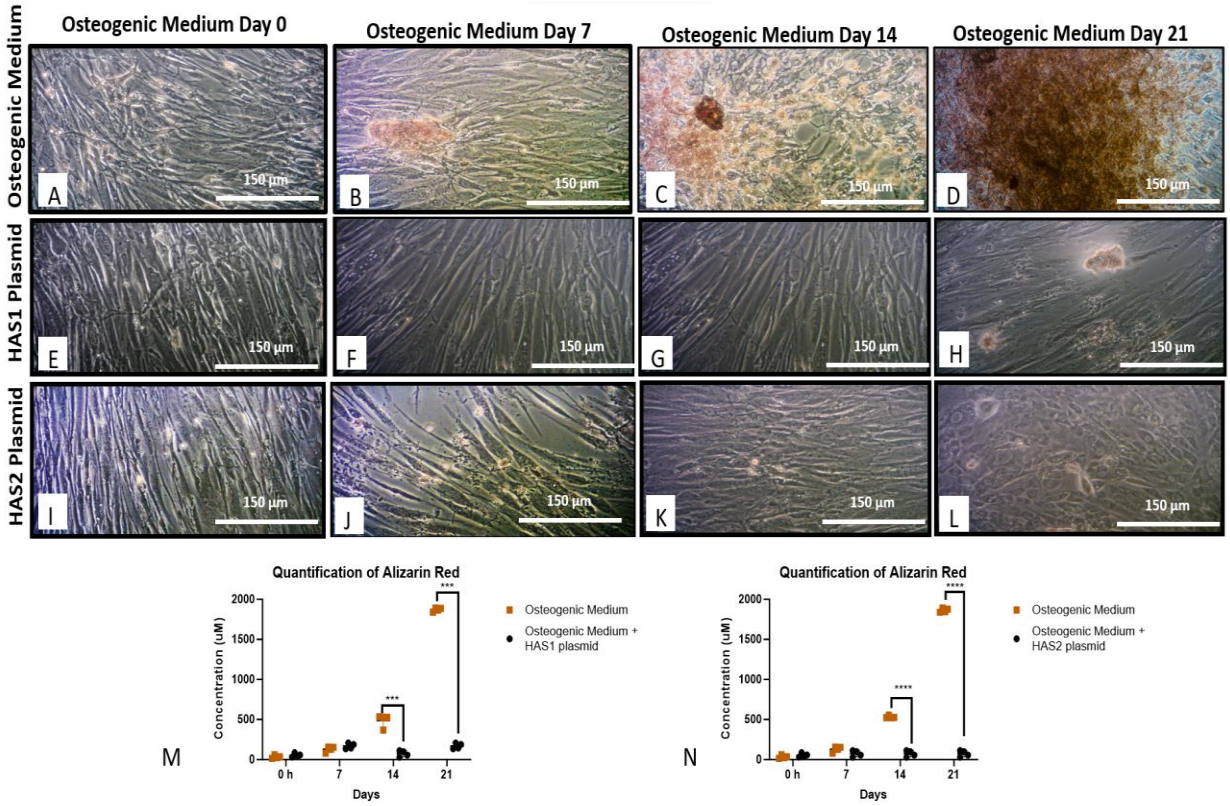

Figure 49 Alizarin red experiment and quantification in VSMCs when transfected with HAS1/HAS2 plasmid

VSMCS were grown in normal media up to 80% confluence and transfected with an empty pCR 3.1 plasmid or HAS1/HAS2 plasmid DNA for 72 hours. Then stimulated with osteogenic medium (A-D), osteogenic medium + HAS1 plasmid (E-H), and osteogenic medium + HAS2 plasmid (I-L) for up to 21 days. They had been analysed at four different time points, day 0, 7, 14 and 21. The cells were fixed and stained with Alizarin Red (A-L) and extracted for quantitative measurement of absorbance at OD405 (M-N). The cells were analysed under a light microscope at magnification 100X. A digital eyepiece microscope camera was used to take pictures of the cells. Representative photographs of one of four independent experiments giving similar results Data was analysed by Kruskal-Wallis test followed by Dunn's post hoc analysis (* = p≤0.001, **** = p≤0.0001). The data is expressed as mean ± S.D.**

The impact of HAS1 plasmid overexpression on VSMC osteogenic differentiation via RT-qPCR, were examined. Notably, there was a substantial reduction in RunX2 expression by day 21 **Figure 50 [A]**. Additionally, over days 7 to 21, the expression of Osteopontin and ALPL demonstrated significant attenuation, indicative of inhibition of osteogenic differentiation **Figure 50 [B & C]**. These findings align with the outcomes seen in the Alizarin Red staining, reflecting an absence of calcium deposition.

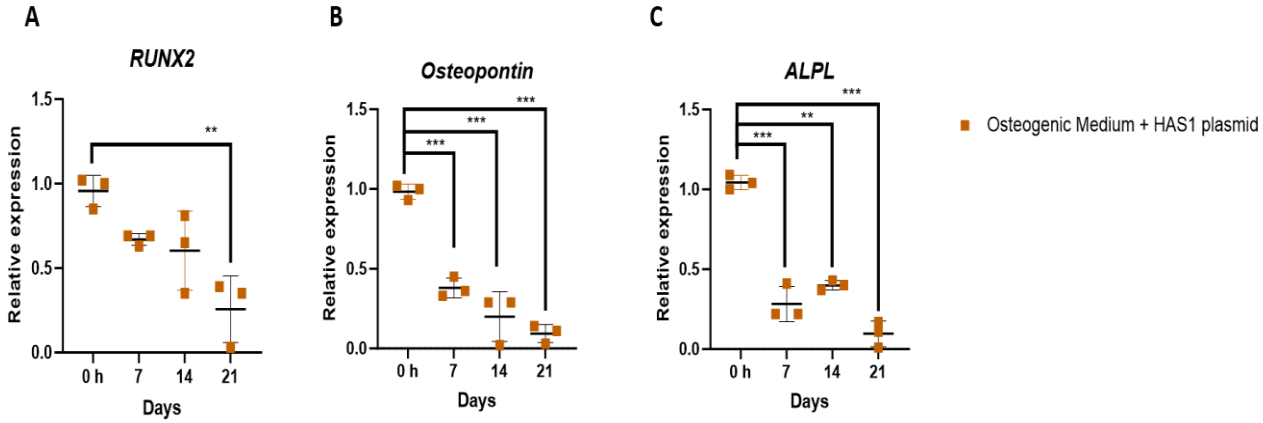

Figure 50 Differentiation markers in differentiated smooth muscle cells with HAS1 plasmid overexpression

VSMCS were grown in normal media up to 80% confluence and transfected with an empty pCR 3.1 plasmid or HAS1 plasmid DNA for 72 hours. Then stimulated with osteogenic medium for up to 21 days. mRNA was extracted at 0 hours, 7 days, 14 days, and 21 days RunX2, Osteopontin and Alkaline Phosphatase mRNA expression was assessed by RT-qPCR. The comparative C_T method was used for relative quantification of gene expression and the results were represented as mean ± S.D. For the scatter dot plot, the median value obtained from each dot, are represented by a line. Each point in the scatter dot plot denotes a single biological replicate. Each point in the scatter dot plot denotes a single biological replicate. Data was analysed by Kruskal-Wallis test followed by Dunn's post hoc analysis (= p≤0.01, **** = p≤0.0001).**

Similarly, the effects of HAS2 plasmid overexpression on VSMC osteogenic differentiation using RT-qPCR were evaluated. Over the interval of days 7 to 21, the expression of all osteogenic markers (RunX2, Osteopontin, and ALPL) exhibited marked attenuation, signifying an inhibition of osteogenic differentiation **Figure 51 [A-C]**. These findings are consistent with the results observed in the Alizarin Red staining, reflecting an absence of calcium deposition.

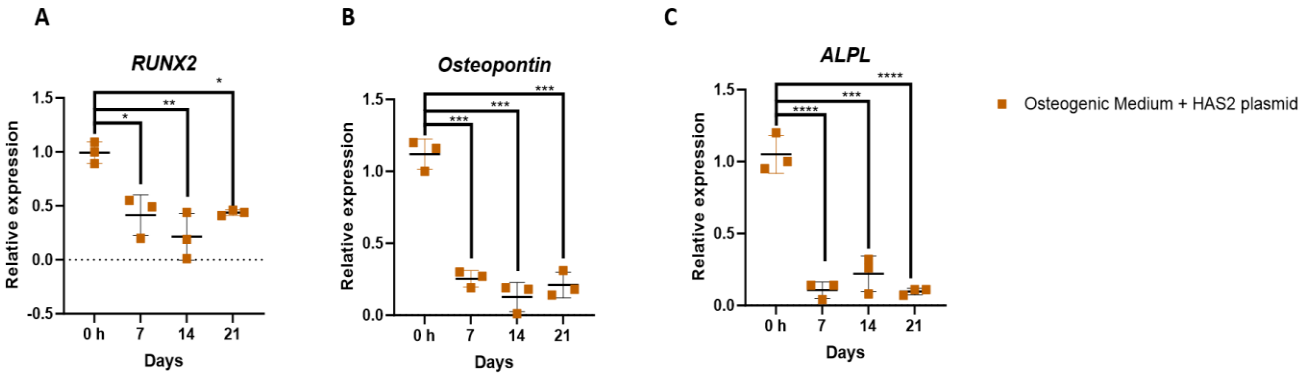

Figure 51 Differentiation markers in differentiated smooth muscle cells with HAS2 overexpression

VSMCS were grown in normal media up to 80% confluence and transfected with an empty pCR 3.1 plasmid or HAS2 plasmid DNA for 72 hours. Then stimulated with osteogenic medium for up to 21 days. mRNA was extracted at 0 hours, 7 days, 14 days, and 21 days RunX2, Osteopontin and Alkaline Phosphatase mRNA expression was assessed by RT-qPCR. The comparative C_T method was used for relative quantification of gene expression and the results were represented as mean ± S.D. For the scatter dot plot, the median value obtained from each dot, are represented by a line. Each point in the scatter dot plot denotes a single biological replicate. Each point in the scatter dot plot denotes a single biological replicate. Data was analysed by Kruskal-Wallis test followed by Dunn's post hoc analysis (* = p≤0.05, ** = p≤0.01, **** = p≤0.0001).

The effects of siRNA-mediated knock-down of HAS3 on VSMC osteogenic differentiation were evaluated using RT-qPCR. Over 7 to 21 **Figure 52 [A-C]** days the expression of OM + HAS3 siRNA remain constantly attenuated compared to OM + si negative controls.

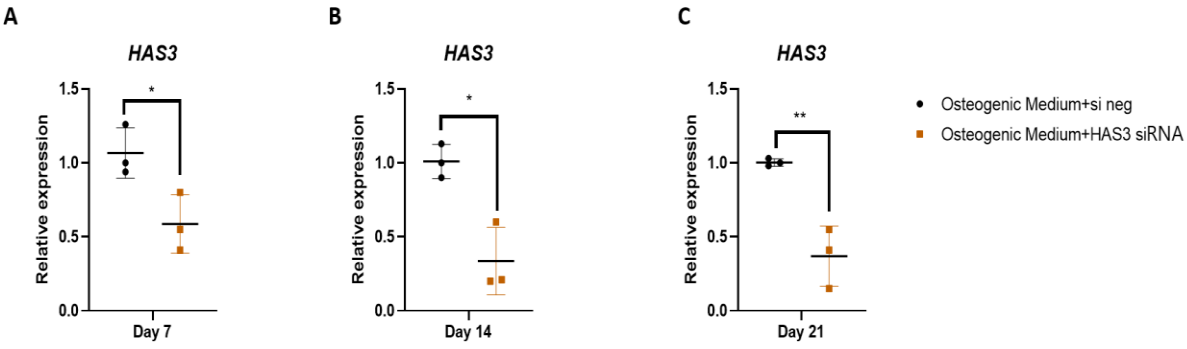

Figure 52 Characterizing HAS3 knock down when stimulated with Osteogenic medium

VSMCS were grown in osteogenic medium for up to 21 days and transfected overnight with a scrambled siRNA sequence or siRNA targeting HAS3 sequence. mRNA was extracted at 7 days, 14 days, and 21 days HAS3 mRNA expression was assessed by RT-qPCR. The comparative C_T method was used for relative quantification of gene expression and the results were represented as mean ± S.D. For the scatter dot plot, the median value obtained from each dot, are represented by a line.

Each point in the scatter dot plot denotes a single biological replicate. Data was analysed by Kruskal-Wallis test followed by Dunn's post hoc analysis (* = p≤0.05, ** = p≤0.01).

The impact of HAS3 siRNA on VSMC calcification was next investigated. Following fixation, cells were subjected to Alizarin Red staining and examined using a light microscope. Cells treated with OM+HAS3 siRNA **Figure 53 [E-H]** were contrasted with OM-only treated cells **Figure 53 [A-D]**. At day 0, Alizarin Red staining was absent **Figure 53 [A, E & I]**. However, cells treated with OM+HAS3 siRNA displayed heightened calcium deposition at day 7, in contrast to OM only treated cells **Figure 53 [B, F & I]**. Notably, from days 14 to 21, there was no alteration in calcium deposition for cells stimulated with HAS3 siRNA **Figure 53 [G-H & I]**, when compared to OM only treated cells **Figure 53 [C-D & I].**

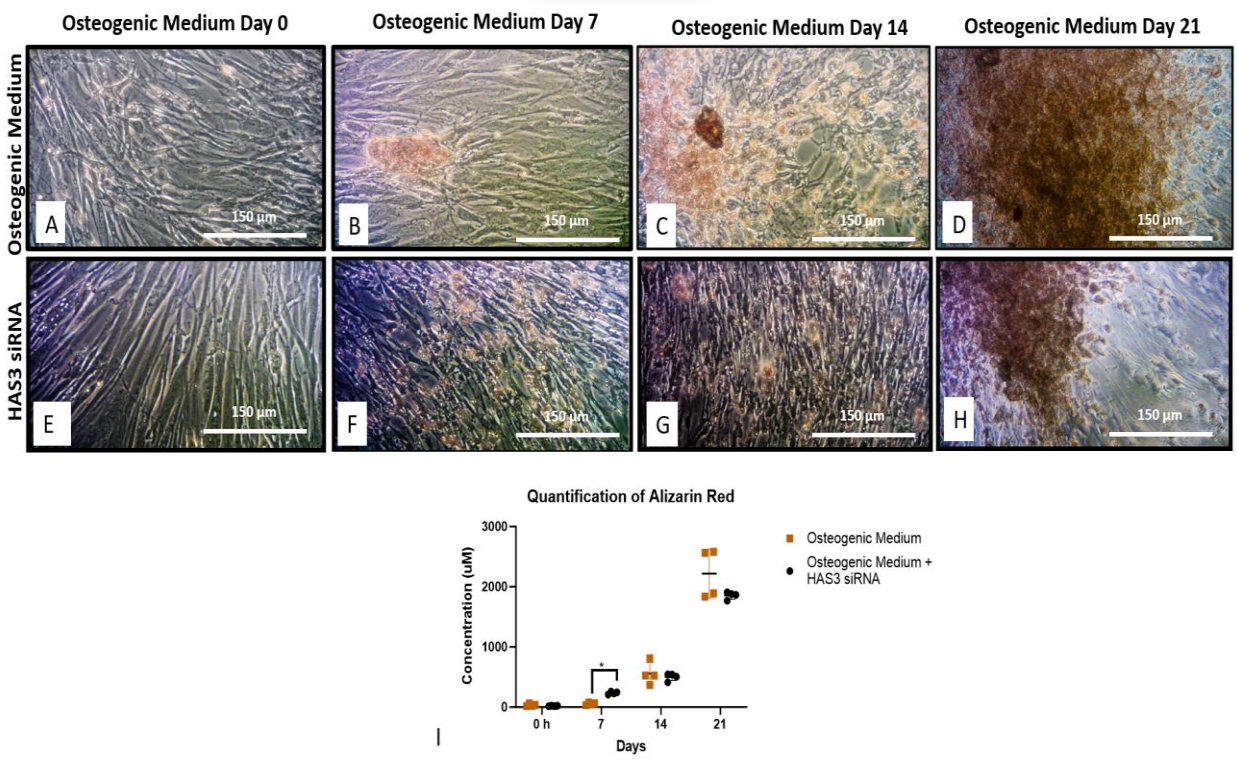

Figure 53 Alizarin red experiment and quantification in VSMCs when transfected with HAS3 siRNA sequence

VSMCS were grown in normal media up to 80% confluence and transfected with transfected with a scrambled siRNA sequence or siRNA targeting HAS3 sequence for 48 hours. Then stimulated with osteogenic medium (A-D), osteogenic medium + HAS3 siRNA (E-H) for up to 21 days. They had been analysed at four different time points, day 0, 7, 14 and 21. The cells were fixed and stained with Alizarin Red (A-H) and extracted for quantitative measurement of absorbance at OD405 (I). The cells

were analysed under a light microscope at magnification 100X. A digital eyepiece microscope camera was used to take pictures of the cells. Representative photographs of one of four independent experiments giving similar results Data was analysed by Kruskal-Wallis test followed by Dunn's post hoc analysis (* = p≤0.05).

RT-qPCR was then performed to assess the influence of HAS3 siRNA on VSMC osteogenic differentiation. Knockdown of HAS3 led to an increase in the mRNA expression of RunX2, Osteopontin, and ALPL at 7-day **Figure 54 [A-C]**. However, on days 14 and 21, there was no change in the mRNA expression of RunX2, Osteopontin, and ALPL **Figure 54 [A-C]**, when compared to cells treated with OM + si negative control.

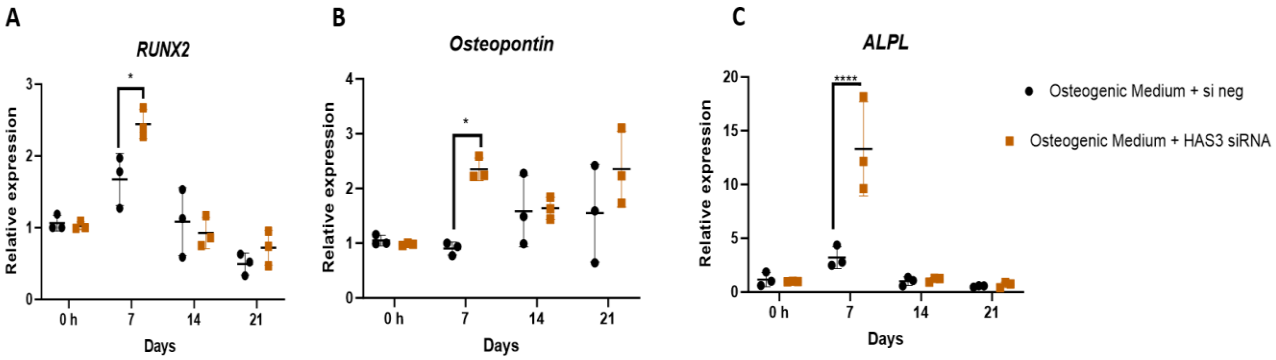

Figure 54 Differentiation markers in differentiated smooth muscle cells when HAS3 is knock down

VSMCS were grown in normal media up to 80% confluence and transfected with a scrambled siRNA sequence or siRNA targeting HAS3 sequence for 48 hours. Then stimulated with osteogenic medium for up to 21 days. mRNA was extracted at 0 hours, 7 days, 14 days, and 21 days RunX2, Osteopontin and Alkaline Phosphatase mRNA expression was assessed by RT-qPCR. The comparative C_T method was used for relative quantification of gene expression and the results were represented as mean ± S.D. For the scatter dot plot, the median value obtained from each dot, are represented by a line. Each point in the scatter dot plot denotes a single biological replicate. Each point in the scatter dot plot denotes a single biological replicate. Data was analysed by Kruskal-Wallis test followed by Dunn's post hoc analysis (* = p≤0.05, **** = p≤0.0001).

4.3 Discussion

My research has revolved around the modelling of VSMC osteogenic differentiation in vitro. Additionally, I have explored how cytokines elevated in CKD, such as TGF-β1 and IL-6, can stimulate osteogenic gene expression. This chapter delves into the profound alterations in HA linked to VSMC osteogenic differentiation, whether induced by OM or cytokines, highlighting the pivotal role of HA in this process. Further investigations, manipulating HA via using interventions like 4MU, Strep-Hyal, siRNA, and over-expression vectors, underscores its key importance in VSMC osteogenic differentiation. My data shows that VSMC to osteogenic differentiation is associated with marked alterations in HA matrices and associated gene expression. Specifically, the overall expression of HA was attenuated as the cells underwent osteogenic differentiation, suggesting that HA generation in this context is key to maintaining normal VSMC phenotype in arteries. However, whilst the amount of HA diminished, there was also a clear re-organisation of HA into HA cables, which may be a relevant factor in driving osteogenic differentiation.

HA is one of the major structural extracellular components and is an important regulator of cellular responses. However, the direct effects of HA on VSMC osteoblastic differentiation had not been previously explored. My results demonstrate that in VSMC that underwent osteogenic differentiation, there is a profound loss of HA evident within the cytoplasm and nucleus and instead HA is observed as newly forming long matrices, which were similar to previously described cables. When hyaluronan is bound to the cell surface, it can adopt two distinct structures: a pericellular coat situated near the plasma membrane, and hyaluronan chains that cluster into "cables" capable of spanning multiple cell lengths. It is noteworthy that these HA cables, induced by various inflammatory agents, have been previously associated with pro-inflammatory conditions[279]. Importantly, these HA cables have demonstrated the capacity to bind to leukocytes, subsequently leading to the release of inflammatory cytokines by these immune cells. Conversely, the HA present in the pericellular coat does not contribute to leukocyte binding. Our ICC research findings indicate that during the process of VSMC differentiation into an osteogenic state, there is an absence of the HA

coat, with HA predominantly existing in the form of HA cables. This structural transformation appears to hold significant relevance in the context of inflammation. HA binding proteins TSG-6 and Versican hold significant relevance in control of HA coats and cables. In the following discussion, we explored the expression patterns of TSG-6 and Versican in the context of VSMC osteogenic differentiation, with a specific focus on their potential roles in shaping the formation of HA coats and cables.

Prior studies have indicated a downregulation of TSG-6 during osteoblast differentiation[398], which is consistent with the expression patterns we observed in our model during VSMC osteogenic differentiation. Our data indeed confirms a reduction in both TSG-6 gene and protein expression as VSMCs transition towards an osteogenic phenotype. Interestingly, previous research involving the knockout of TSG-6 has underscored its importance in the formation of stable HA matrices[585] and emphasized its critical role in peri-cellular HA coat formation[360]. Our data indicates an initial increase in TSG-6 expression at an early time point, hinting a potential role in the formation of HA cables. However, it's noteworthy that TSG-6 expression diminishes at later time points when HA cables become prominent. This raises questions about whether TSG-6 directly contributes to cable formation in this context. Moreover, previous research, as indicated by studies in HK2 cells, suggests that inhibiting TSG-6 binding to HA does not significantly impact cable formation[276,586,587], suggesting that TSG-6 is not the sole factor responsible for the formation of HA cables. Therefore, while TSG-6 may have an initial role in cable formation, it is likely not the primary driver of HA cable formation during VSMC osteogenic differentiation. The presence of TSG6 is however critical for HA coat formation. To gain deeper insights into the specific role of TSG-6, our next steps will involve manipulating its expression during VSMC osteogenic differentiation for further investigation.

Versican's presence has been documented in the early stages of bone formation[401] aligning with our observations in our model. During VSMC osteogenic differentiation, our data shows a significant enhancement in Versican protein expression, as demonstrated through ICC. Interestingly, we have identified a correlation between increased Versican expression and the presence of HA cables, which are a prominent feature in our *in vitro* model. Previous research

has provided evidence of Versican co-localization within HA cable structures in smooth muscle cells[588] and proximal tubular epithelial cells[276]. These findings strongly suggest that Versican expression may play a pivotal role in promoting HA cable formation during VSMC osteogenic differentiation and subsequently drive the differentiation of VSMCs into an osteogenic phenotype.

While both TSG-6 and Versican can impact HA cable formation, prior literature revealed that Versican can efficiently compete with TSG-6 for binding to HA[589]. Versican serves as a potent inhibitor of HA binding to full length TSG-6[590]. These findings raise a possibility of the existence of counter-regulatory mechanisms between TSG-6 and Versican that modulate HA cable assembly. Considering the initial increase in TSG-6 expression at early time points, it's plausible that TSG-6 may have initiated the cable formation process, with Versican subsequently taking over in the later time points. This intricate interplay between TSG-6 and Versican underscores the complexity of HA cable assembly during VSMC osteogenic differentiation.

Next, we shift our focus to extracellular, intracellular, and pericellular HA alterations. The results demonstrated that there was an overall attenuation of extracellular and intracellular HA, and this is consistent with our ICC data, where we see marked attenuation of HA expression and intracellular HA when VSMCs become osteogenic. However, it's worth noting a distinct increase in pericellular HA at day 7. Correspondingly, our ICC data shows changes in cell morphology beginning at day 7, suggesting that these changes may be the initial steps necessary to promote VSMC osteogenic differentiation. Furthermore, despite this relocalisation of HA, the expression of all the HA markers experiences significant downregulation as VSMCs undergo osteogenic differentiation.

We know from previous studies[285,339,341,342,417,460,591,592] that it is not just expression but membrane distribution of the HA related proteins that dictate their function, particularly in relation to the HA receptor, CD44. The protein expression of CD44 showed no alteration while

the mRNA expression showed a downward trend as VSMC undergo osteogenic differentiation. Existing literature revealed that CD44-/- mice[337,593] demonstrated attenuated atherosclerotic arterial diseases. This may be specific to atherosclerotic disease and in the context of VC, HA may in fact be protective. The other receptor RHAMM showed marked attenuation of protein expression, and so does HYAL1/HYAL2, indicating they may have a protective role in VSMC osteogenic differentiation and require further investigation.

Next, we shift our focus to the alterations in HA in VSMCs when induced by cytokines relevant in CKD. IL-6 is a marker of severity of chronic inflammatory processes and TGF-β1 is a biomarker involved in VC[38]. Both cytokines are elevated in CKD. In dialysis patients, upregulation of IL-6 gene expression is associated with increased VC[573] and TGF-β1 is involved in the regulation of cell proliferation and can either stimulate or inhibit cell growth and is critical for maintaining immune cell homeostasis. Interestingly, both IL-6 and TGF-β1 demonstrated an ability to induce expression of a number of HA genes as VSMCs demonstrated enhanced osteoblast-like differentiation. TGF-β1 stimulation showed and upregulation of HAS1/HAS2, CD44, RHAMM and VCAN at early time points. An upregulation in HAS1 and TSG-6 and attenuation of RHAMM is observed at later time points with TGF-β1 stimulation. IL-6 stimulation showed and upregulation of HAS Synthase enzymes, CD44, RHAMM, TSG-6 and VCAN in early time points. An upregulation of HAS2/3, HYAL1/2 and CD44 was observed in later time points with stimulation with IL-6. RHAMM and TSG-6 were attenuated. Our results show differences when stimulated with OM/ IL-6/ TGF-β1. The outcome can be explained by considering the distinct effects of OM, IL-6, and TGF-β1 on VSMCs. Each of these factors activates unique signalling pathways in VSMCs, leading to diverse patterns of gene expression. These pathways can either intersect or counteract each other, resulting in varying consequences. In our in vitro model, IL-6 and TGF-β1 were found to increase the expression of osteogenic markers but failed to induce mineral deposition in the matrix. In contrast, OM stimulation not only upregulated the gene expression in VSMCs but also triggered mineral deposition. These observations suggests that HA changes observed with OM stimulation reflect the transition of VSMC towards an osteogenic phenotype. On the other hand, the HA alterations induced by IL-6 and TGF-β1 may signify an inclination towards the osteogenic pathway, but without inducing successful differentiation on their own. It

remains unclear why IL-6 and TGF-β1 increased HA related markers and this requires further study.

In interventional cell experiments, I aimed to establish a causal link between alterations in HA and VSMC trans-differentiation, using two distinct methods for HA degradation: 4MU and Strep-Hyal. While 4MU does not directly degrade HA but rather impacts its biosynthesis, leading to a global inhibition of HA synthesis levels in the extracellular matrix, Strep-Hyal specifically targets and breaks down glycosidic bonds within the HA molecule, resulting in its degradation into smaller fragments. Using the chemical inhibitor 4MU on VSMC osteogenic differentiation, we observed increased calcification at day 7, 14, and 21 compared to cells treated with only OM. Gene expression analysis revealed elevated expression of osteogenic markers at day 14 and 21, suggesting that HA in certain contexts plays a protective role in VC. High levels of likely high molecular weight intracellular and extracellular HA, driven by HAS activity, seem to protect the VSMCs' normal phenotype. This protection is diminished when 4MU is used to block HA generation, making the cells more susceptible to differentiation into bone cells. We also investigated the effects of Strep-Hyal, which cleaves HA enzymatically through a β-elimination process. Strep-Hyal treatment resulted in complete attenuation of calcification, confirmed by quantification, and exhibited a total suppression of osteogenic gene expression. As shown before, the organisation of HA in the matrix, possibly in the form of HA cables, may be a critical inducer of VSMC differentiation. The contrasting outcomes between 4MU and Strep-Hyal treatments could be attributed to the fact that Strep-Hyal specifically targets existing HA in the matrix (i.e., HA cables), rather than affecting HA synthesis. Furthermore, it appears that specific molecular weight HA, when bound to certain compositions of Hyaladherins, may promote a VSMC osteogenic phenotype. When Strep-Hyal breaks down HA, it generates smaller HA fragments around the cell, and these fragments seem to have the opposite effect, suggesting that the interaction between the HA matrix surrounding cells and its specific molecular weight may be a critical factor in driving VSMC osteogenic differentiation.

In our exploration of the role of HA in VSMC differentiation, we adopted a precise approach, individually manipulating the expression of HAS isoenzymes. We over-expressed HAS1 and HAS2 in VSMCs using plasmid over-expression vectors, while knocking down HAS3 using siRNA. Our finding unveiled a consistent reduction in mRNA levels of all the three HASes, suggesting a diminished HA production during VSMC osteogenic differentiation. Intriguingly, the protein expression of HAS1 and HAS2 mirrored their mRNA expression, implying a potential anti-inflammatory role during VSMC osteogenic differentiation. In contrast, HAS3 exhibited increased protein expression, implicating its contribution to VSMC osteogenic differentiation. To determine whether if HAS1 and HAS2 exclusively hold anti-inflammatory properties, we conducted individual overexpression experiments. Prior literature highlighted the role of HAS3 overexpression in the formation of HA coats and cables[276]. Building upon these insights, we hypothesized that knowing down HAS3 could potentially mitigate VSMC calcification, marking the next crucial step in our investigation. HAS1 overexpression yielded significant reduction in calcium deposition and osteogenic gene expression, suggesting a protective function for HAS1 in VSMC osteogenic differentiation. Similarly, HAS2 overexpression produced analogous results, implying a protective role of HAS2 as well. However, knock-down of HAS3 has complex effects; it appears to enhance osteogenic gene expression early on, yet it ultimately shows no significant change in calcification at later time points. Parallelly, calcium deposition assays reveal increased deposition on day 7, but this effect diminishes in later time points when VSMCs are exposed to HAS3 siRNA. One plausible explanation for these intricate results lies in the association of HAS3 with HA cable formation and its impact on HA coat dynamics. Overexpression of HAS3 has been linked to the induction of HA cable formation and increased incorporation of HA into pericellular coats[276]. Our findings suggest that as VSMCs undergo transdifferentiation into osteogenic-like cells, the HA coat disappears, and HA cables become more prominent. This transformation may be tightly regulated by HAS3. It's conceivable that knocking down HAS3 disrupted the delicate balance between HA coats and cables. This disruption could have led to the observed increase in expression of bone markers and enhanced calcium deposition at day 7, indicative of a potential protective role of HAS3 at early stages. However, the negligible effect on calcification at later time points raises intriguing questions that warrant further investigation. These findings underscore the need for comprehensive research to fully understand the

dynamic interplay between HAS3 and VSMC calcification, especially considering the complex association of HAS3 with HA cable formation.

In summary, this chapter's findings highlight significant alterations in HA associated with VSMC osteogenic differentiation, emphasizing the importance of the method used to remove HA from the cell. Hyaluronidase treatment indicated that pericellular HA is protective against VSMC osteogenic differentiation. HAS1, HAS2, and HA itself appear to be protective in VSMC osteogenic differentiation, while HAS3's role warrants further exploration. The next chapter aims to correlate these in vitro findings with two in vivo models of arterial disease, medial calcification, and atherosclerosis, in collaboration with VU in Amsterdam and UM in Maastricht.

Chapter 5

Characterising alterations in arterial HA in experimental rodent models of CKD specific cardiovascular disease

5.1 Introduction

In the preceding chapter, my research delved deep into the role of HA within my *in vitro* model of VC. I explored HA's effects by modifying it, seeking to understand its specific impact on osteogenic differentiation of VSMCs. Recognizing the complexity of cardiovascular health and diseases, it was crucial to investigate these changes through both *in vitro* and *in vivo* experiments. In this chapter, I delved into a comprehensive exploration of HA and its associated proteins within two *in vivo* models of CKD related cardiovascular disease. I have done this to compare and contrast the finding from my *in vitro* findings. The investigations begin by checking the level of calcification in each model. I then subsequently scrutinize HA alterations in these two models. I assess HA's potential role in VSMC osteogenic transformation and delve into the expressions of HAS1/2/3, HYAL2, CD44, TSG-6, and Versican to gain deeper insights into this intricate process. This effort is driven by the aim to unravel the multifaceted role of HA in maintaining cardiovascular health and its involvement in disease states based on different degrees of calcification. Animal models facilitate the investigation of human clinical observations within a controlled experimental setting, thereby enhancing our comprehension of the contributing factors and biological significance of arterial diseases in the context of CKD. The two *in vivo* models will explore the changes in the arterial media and specifically studies alterations in HA are Vitamin K deficient mice that develops medial VC and no intimal disease. My second model is a uraemic model that is predisposed to atherosclerosis. However, our specific focus in this model will be the impact of uraemia on the arterial media and identify alterations in HA here.

5.1.1 Vitamin K deficient Model

Medial VC is a distinctive characteristic of vascular aging in patients with CKD. In these patients, the biological age of their arterial vasculature surpasses their chronological age, as indicated by prior studies[594,595]. This phenomenon is characterised by pronounced VC, is prevalent in CKD patients[147,596,597] and serves as a strong predictor of cardiovascular morbidity

and mortality[598,599]. Those CKD patients demonstrating noticeable VC face an unfavourable prognosis compared to those with minimal or absent calcification[600,601]. Individuals with CKD prone to VC, often exhibits subclinical Vitamin K deficiency[602]. Numerous studies have explored the association between circulating Vitamin K status and the risk of CKD. Vitamin K deficiency has been identified as an independent predictor of CVD risk[603]. In both diabetes[604,605] and CKD[606] patients with insufficient total Vitamin K intake, there was an observed elevation in both cardiovascular and all-cause mortality compared to those with adequate intake. Notably, with a high estimated Vitamin K intake (exceeding 21.6 µg/day) reduction in coronary heart disease-related mortality as well as aortic calcification was found[607-609]. In line with this, Vitamin K supplementation might have the potential to decelerate vascular damage and act as a preventive measure against atherosclerosis, CVD, and stroke[610-613]. Ongoing interventional randomized clinical trials are expected to provide further insights into whether and at what dosage Vitamin K can effectively slow the progression of VC in CKD patients[614-617].

Prior research has highlighted the profound and lasting effects of Vitamin K deficiency, particularly in the development of medial calcification, aortic valve calcification, and increased vascular stiffness[618]. Vitamin K deficiency has significant implications for inhibiting the activation of tissue calcification inhibitors, such as Matrix Gla protein (MGP)[619] and Osteocalcin[620], thus promoting VC as observed in patients with CKD[621-624]. Additionally, the use of warfarin, which antagonizes Vitamin K, can lead to rapid arterial calcification[625,626]. Interestingly, a diet rich in Vitamin K has demonstrated the potential to reverse aortic calcification induced by warfarin treatment in experimental rat model[627]. Warfarin fed DBA/2 mice develop spontaneous ectopic heart calcification[618,628]. Furthermore, studies in rodents have elucidated that warfarin treatment not only exacerbates calcification but also fosters a transition of atherosclerotic plaques towards a more vulnerable phenotype[141]. Additionally, warfarin treatment has been associated with increased arterial stiffness and a decline in cardiac systolic function[629]. By utilizing Vitamin K deficient model, we aim to unravel the intricate mechanisms behind medial VC. This research model not only helps us to enhances our understanding of VC but also holds promise in guiding the development of novel therapeutic strategies for managing and preventing medial calcification-related conditions.

5.1.2 APO E-/- High-fat diet mice

The pursuit of a suitable mouse model that reflects the human pathology covering the entire spectrum of arterial lesions as seen in CKD patients led to the development of the apolipoprotein (APO) E -/- model. APO E, a glycoprotein found in all lipoproteins except LDL, acts as a ligand for receptors involved in clearing chylomicrons and remnants of very low-density lipoproteins (VLDL) from the bloodstream[630]. Deleting the APO E gene in mice results in a significant increase in plasma VLDL levels, and to a lesser extent, LDL levels and as well as a 45% reduction of the normal HDL levels, which contributes to the development of arterial lesions mainly localized in the aortic root and ascending aorta[631]. These lesions resemble their human counterparts and disease progression[632].

APO E-/- mice are widely utilized in research due to their inherent tendency to spontaneously develop arterial lesions even when maintained on a standard chow diet. In all instances of APO E deficiency, the onset of spontaneous atherosclerosis typically occurs at an age of 3–4 months in mice on a standard diet, primarily affecting the proximal aorta and involving lesions at the origins of the coronary artery and the pulmonary artery[633,634]. Notably, the consumption of a Western-type diet accelerates arterial lesion development in these mice[633]. To induce widespread and atherosclerotic plaque formation in these mice, a high-fat, high-cholesterol diet is essential. This dietary regimen has a profound impact on their cholesterol levels, leading to a remarkable threefold increase in total plasma cholesterol levels. Consequently, this dietary shift significantly accelerates the lesion formation and augments their size[635]. It's noteworthy that the level of hypercholesterolemia observed in APO E-/- mice surpasses that seen in the rare human cases of APO E deficiency[636-638]. The extensive analysis of lesions in APO E-/- mice has been meticulously documented in prior research[632,635,639]. Evidence suggests that disease progression is further intensified with prolonged exposure to such a diet. As APO E-/- mice age or are subjected to an extended high-fat/cholesterol diet, lesions become evident in the intimal layers of the arteries[632]. These lesions manifest various stages of development, ranging from the accumulation of foam cells to the formation of fibrous plaques, and even advanced lesions with necrotic cores and plaque calcification[640]. Moreover, with advanced age and prolonged exposure to an atherogenic diet, there is an

increased risk of fibrous cap disruption, often associated with plaque erosion[641,642]. Advanced lesions exhibit heightened inflammation contributing to an ongoing cycle of plaque development. Importantly, the lesions observed in APO E-/- mice are characterized by vascular inflammation, notably marked by the infiltration of macrophages and other immune cells. Considering these factors, APO E-/- mice are commonly used to study atherosclerosis[643,644]. CKD linked to metabolic syndrome, particularly due to an imbalanced high-fat diet, primarily involves factors like renal hemodynamic changes, endothelial dysfunction, chronic inflammation, and oxidative stress[645,646]. Yet, CKD's pathogenesis and its effect on VC remains complex and not entirely clear. Since atherosclerosis is a common complication in CKD patients, employing APO E -/- high-fat fed mice model provides an opportunity to explore any changes in the arterial media in atherosclerotic disease and compare this to what happens when this is combined with CKD and uraemia as described below.

5.1.2 The 5/6 Nephrectomy model of CKD

Kidney failure often coincide with conditions like hypertension, glucose intolerance, and cardiovascular disorders. These are driven by common mechanisms such as inflammation, oxidative stress, and dyslipidaemia, contributing to renal failure and associated disorders. Notably, there has been a rising interest in studying arterial calcification in patients with ESRD, as uraemic patients demonstrate a higher prevalence and more extensive calcification in both the intima and media layers of their arteries compared to nonuraemic individuals[80,150,647]. This VC serves as a predictor of heightened cardiovascular mortality and morbidity. When it comes to atheromatous plaques, the most notable disparity between uraemic and nonuraemic patients lies not in their size but in their composition, with a significant increase in calcium content[596,648]. To create uraemia models, many researchers have explored kidney disease by surgically reducing kidney mass. The 5/6th nephrectomy rat model, also known as the remnant kidney model, replicates experimental Chronic Renal Failure (CRF) by simulating the gradual loss of nephrons that occurs in human CRF. The reduction in renal mass typically involves a two-stage surgical procedure: partial nephrectomy of one kidney followed by total

nephrectomy of the contralateral kidney. This approach, referred to as 5/6th nephrectomy, is used to investigate the development of uraemia and complications related to CKD, resembling human condition[649]. Research into the progression of CKD in these uraemic models has revealed a striking consistency in phenotypes between animal models and humans. This consistency demonstrates a common pattern of increased plasma creatinine, elevated blood urea nitrogen levels, hyperparathyroidism, and hyperphosphatemia, reflecting the clinical features seen in CKD patients[597,650-652]. The 5/6th nephrectomy model has been observed to result in significantly elevated serum creatinine levels than control animals[653]. Additionally, these mice exhibit phosphorous levels that, eight weeks after the surgery, was significantly higher than those in control animals control animals[653]. The accumulation of uraemic toxins in CKD induces inflammation, and endothelial dysfunction, which are key factors contributing to the development of atherosclerosis[654]. In a specific study, the 5/6th nephrectomy model developed aortic calcification between 12 to 36 weeks when exposed to a diet containing phosphorus[650]. It has been demonstrated that uraemia accelerates both atherosclerosis and arterial calcification in APO E-/- mice following after 5/6th nephrectomy[652]. When nephrectomized rats were followed for 10 weeks while being fed a standard rodent diet with low phosphorus and high calcium, no calcification developed in aorta[655] except for the aortic arch[656] which is the site most prone for the onset of calcification.

In summary, this model is well suited for studying uraemia in the context of CKD. The rationale behind this lies in its capacity to replicate key features observed in CKD patients, including increased plasma creatinine, accelerated atherosclerosis and arterial calcification, mirroring the clinical manifestations of CKD. Therefore, the APO E -/- high-fat fed mice + 5/6th nephrectomy model stands as a well-suited choice for dissecting the intricate relationship between uraemia, VC, and CKD, offering a comprehensive platform for advancing our understanding of these interconnected conditions.

5.1.3 Peritoneal Fluid Exposure Model

PD is a vital kidney replacement therapy for uraemic patients with CKD, but a significant portion of CKD patients already have arterial calcification before starting dialysis[657]. Using animal models with uraemia and PD is essential to investigate whether PD in itself can exacerbate the progression of existing calcification.

To simulate clinical uraemia in PD animal models, the most common approach is through 5/6 nephrectomy[658-660]. Prolonged PD in these uraemic mice can lead to changes in peritoneal morphology and function[661,662], with the bioincompatibility of dialysis solutions suggested as a contributing factor to these alterations[663]. Using glucose-based PD solutions in a uraemic-PD rat model has been associated with morphological changes indicative of peritoneal fibrosis[664]. Notably, it's not just glucose but also other components in standard bioincompatible solutions, such as high levels of glucose degradation products (GDP), low pH, and low lactate content, that might contribute to peritoneal fibrosis[664]. However, one study showed stable blood values of creatinine and urea in uremic mice undergoing long-term PD[665]. It's important to highlight that continuous exposure of the peritoneal cavity to a catheter can also diminish local antibacterial defence mechanisms and result in heightened inflammation. A rat model demonstrated a rapid influx of neutrophilic granulocytes and exudate macrophages into the peritoneal cavity, indicating that exposure to PD fluid and the catheter itself can contribute to chronic inflammation[666]. The presence of a catheter in the peritoneal cavity of these exposed animals induced both structural and functional alterations of the peritoneum[667]. However, this inflammatory response tends to be more pronounced during the initial phase of PD and decreases significantly after 8 weeks of exposure[667]. Dialysis introduces additional inflammation due to the risk of infection within the peritoneal cavity[668]. Peritoneal dialysis contributes to the increase in inflammatory cytokine markers like IL-6 and TGF-β1[669].

Inflammation is a contributing cause of death in more than 10% of PD patients[670]. PD fluid exacerbates already existing systemic inflammation in CKD uraemic patients. This may

contribute to CVD in these patients and therefore this model of APO E -/- high-fat fed mice + 5/6th nephrectomy with PD infusions was used. In this model I will explore VC in the arterial media in the APO E -/- high-fat fed mice + 5/6th nephrectomy with PD infusions model and compare it to the Vitamin K deficient medial Calcification model, comparing HA alterations in both.

5.2 Results

5.2.1 Characterising calcium deposition within in vivo models of CKD related cardiovascular disease

Arterial calcification is a process in which calcium deposits accumulate in the walls of the arteries and disrupts the normal function of the arterial wall. This can lead to reduced elasticity and increased risk of cardiovascular complications. Arterial calcification can occur in two places, both intima and media. To assess calcium deposition in the aorta sections of two groups of mice, Alizarin Red and von Kossa Staining, two widely used techniques for detecting calcification were employed. Alizarin Red **Figure 55 [A-E],** and von Kossa Staining **Figure 55 [F-J],** revealed distinct patterns of calcium deposition in the aorta sections of the studied mouse groups.

Histological examination of Alizarin Red staining revealed no calcium depositions in the control mice **Figure 55 [A]**. Vitamin K-deficient mice displayed intense calcified lesions in the arterial media **Figure 55 [B] (arrows).** In APO E -/- high fat fed mice **Figure 55 [C]** there was an absence of calcium deposits at 24 weeks. Minor calcium lesions in arterial intima were detected in the aortas of the APO E -/- high-fat fed mice + 5/6th nephrectomy and APO E -/- high-fat fed mice + 5/6th nephrectomy with PD infusions group **Figure 55 [D & E] (arrows).**

Likewise, von Kossa staining of histological sections revealed no calcification in the control group **Figure 55 [F]**. Intense calcification confined to the arterial media was detected in Vitamin K deficient mice **Figure 55 [G] (arrows).** In the APO E -/- high-fat fed mice **Figure 55 [H] (arrows)**, von Kossa positive lesions were limited only to the plaque regions in the arterial intima at 24 weeks. In the aortas of the APO E -/- high-fat fed mice + 5/6th nephrectomy and APO E -/- high-fat fed mice+ 5/6th nephrectomy with PD infusions group, calcified lesions were detected in the arterial intima **Figure 55 [I & J] (arrows).**

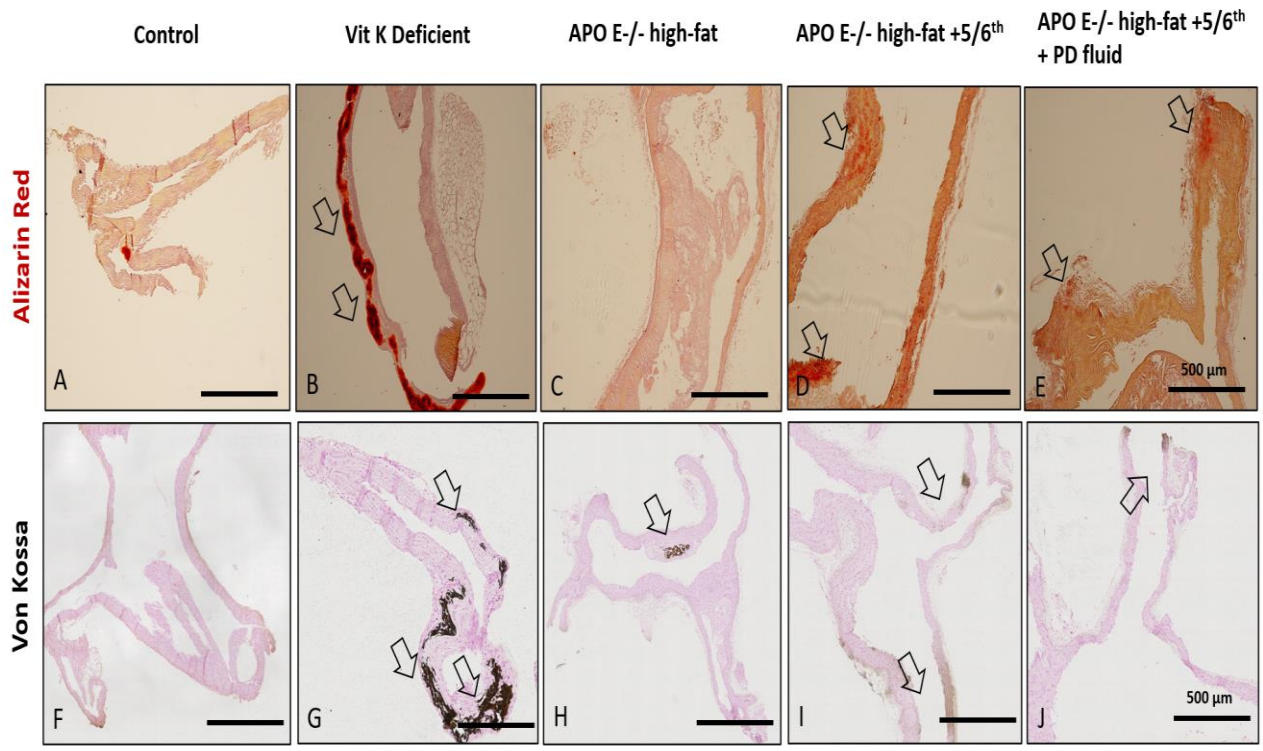

Figure 55 In vivo model of vascular calcification and atherosclerosis - Calcium Assays

Alizarin Red staining [A-E] and von Kossa staining [F-J] of the flat mounted aorta sections of Control [A, F], Vitamin K deficient [B, G], APO E knockout + high fat diet [C, H], APO E knockout + high fat diet + 5/6th Nephrectomy [D, I] and APO E knockout + high fat diet + 5/6th Nephrectomy + Peritoneal Dialysis fluid infusions mice [E, J] were performed. Scale bar is 500 µm. The images were analysed under a light microscope. A digital eyepiece microscope camera was used to take pictures of the tissue sections. These are representative images from 6 aorta sections in each group.

5.2.2 Characterising alteration in HA, HAS isoenzymes, Hyaluronidases and Hyaladherins in CKD related vascular disease

To visualise alteration in HA matrix in the in vivo arterial model of CKD-specific vascular disease, immunofluorescent staining was performed. Biotinylated HABP (Hyaluronan Binding Protein) was used to specifically stain for HA, represented by a green, fluorescent signal in the aortic sections. Immunofluorescence staining of HA effectively detected the presence of this GAG in the aortic sections **Figure 56 [A-F]**.

In control mice, HA was abundantly present both in arterial intima and media **Figure 56 [A]**. In the model of Vitamin K deficient mice, we observed a marked attenuation of HA in both arterial intima and media **Figure 56 [B & F]**, aligning with findings from our *in vitro* model of medial calcification. Interestingly, there was no significant change in HA expression in the APOE -/- high-fat fed mice **Figure 56 [C & F]** compared to the controls **Figure 56 [A]**. However, in the model with APO E -/- high-fat fed mice + 5/6th nephrectomy **Figure 56 [D & F]** as well as in the APO E -/- high-fat fed mice + 5/6th nephrectomy + Peritoneal Dialysis fluid infusion group **Figure 56 [E & F]** HA expression was upregulated in both intima and media, consistent with the existing literature on atherosclerosis[671,672]. In this model, noteworthy alterations were observed within the intimal layer of the arterial vasculature and in adventitia which are described in the subsequent section.

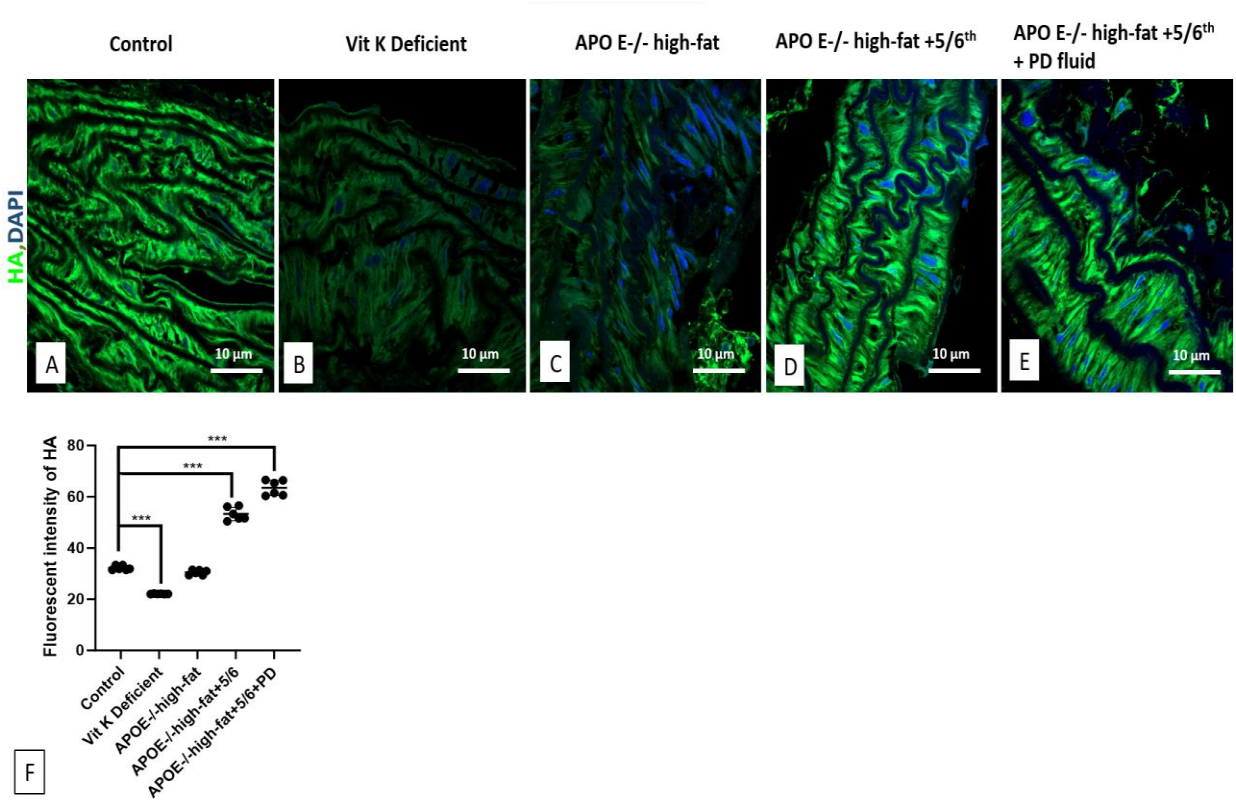

Figure 56 Alterations in HA matrix in an in vivo model of vascular calcification and atherosclerosis

Tissue staining of HA with biotinylated hyaluronan-binding protein was performed in the aorta sections of Control [A], Vitamin K deficient [B], APO E knockout + high fat diet [C], APO E knockout + high fat diet + 5/6th Nephrectomy [D] and APO E knockout + high fat diet + 5/6th Nephrectomy + Peritoneal Dialysis fluid infusions [E]. Scale bar is 10 µm. Secondary antibody alone served as a

negative control; sections were counterstained with DAPI (Nucleus). The images were taken with Laser Point scanning confocal microscope and the fluorescent intensity was measured using the ImageJ software [F]. For the scatter dot plot, the median value obtained from each dot, are represented by a line. All the values are expressed as means ± SD from 6 aorta sections in each group. Data was analysed by Kruskal-Wallis test followed by Dunn's post hoc analysis (* = p≤0.001).**

There were significant changes in VSMCs both in the intimal and medial layer of the arterial walls. Immunofluorescent staining of HA revealed distinct patterns of expression within the arterial intima in these three groups, the APO E-/- high-fat fed mice, APO E-/- high-fat fed mice + 5/6th nephrectomy, APO E -/- high-fat fed mice + 5/6th nephrectomy + Peritoneal Dialysis fluid infusion **Figure 57 [A-C]**. The intimal layer comprises a continuous endothelial monolayer and they are focally thickened by HA rich matrix and VSMCs. Increased HA deposition was observed particularly in the necrotic cores of the plaques in the arterial intima **(white arrow heads)**. These necrotic cores are characterized by the presence of foam cells (macrophages and lipids), VSMCs, collagen matrix, and cytokines, displayed abundant HA expression **Figure 57 [A-C]**. Moving outward from the necrotic cores, the tunica media, primarily consisting of VSMCs, also exhibited elevated HA deposition along the layer adjacent to the atherosclerotic plaques in the higher magnified images **Figure 57 [D-F] (denoted by white dotted line)**. This localized deposition suggested a potential role for HA in the interaction between VSMCs and the developing arterial lesions. Interestingly, in the outermost layer of the vessel, adventitia, which are mainly fibroblasts and loose connective tissues, a significant HA deposition was observed **Figure 57 [G]**, indicating the involvement of HA even in regions away from the plaque sites.

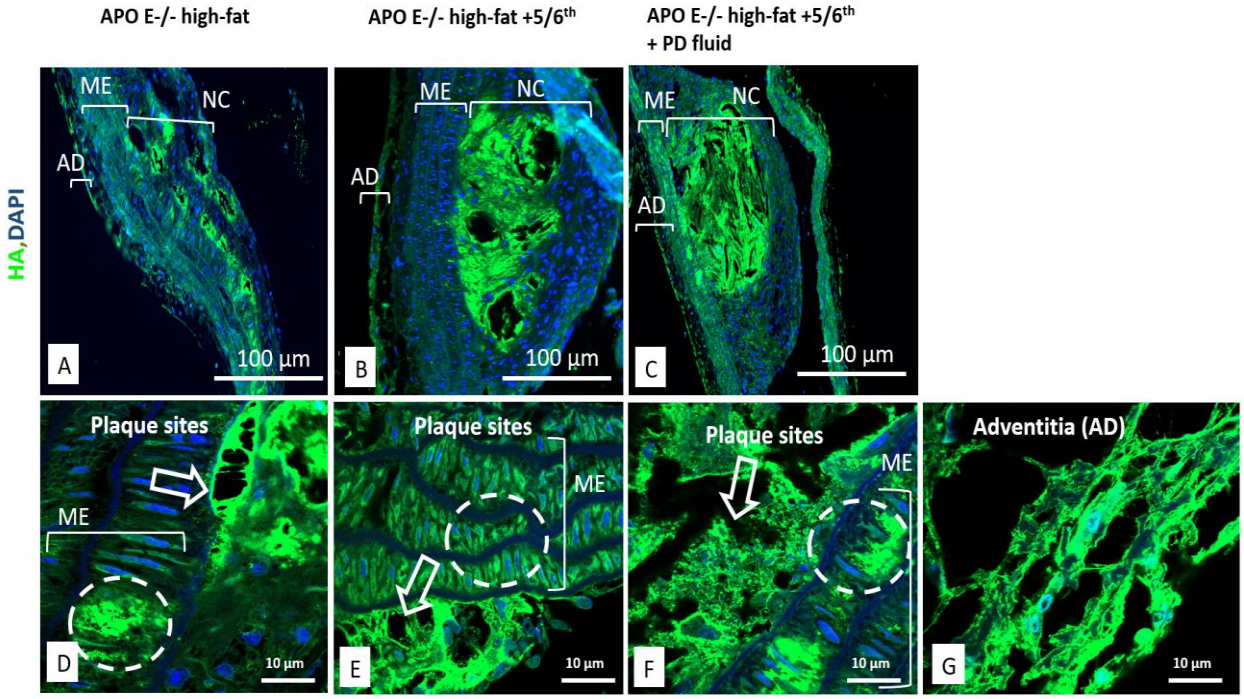

Figure 57 HA matrix alteration at the plaque sites and adventitia in an in vivo model of atherosclerosis

Tissue staining of HA with biotinylated hyaluronan-binding protein was performed in the plaque containing aorta sections of APO E knockout + high fat diet [A, D], APO E knockout + high fat diet + 5/6th Nephrectomy [B, E], APO E knockout + high fat diet + 5/6th Nephrectomy + Peritoneal Dialysis fluid infusions [C, F] and Adventitia [G]. AD, ME, and NC represents Adventitia, Medial layer and Necrotic core containing plaques respectively [A-C], scale bar is 100 µm. Magnified images of the plaques and adventitia are shown in the lower panel, scale bar is 10 µm [D-G]. Plaque sites are marked with an arrow [D-F]. Brightly stained vascular smooth muscle cells in the medial layer are marked with dotted white line [D-F]. Secondary antibody alone served as a negative control; sections were counterstained with DAPI (Nucleus). The images were taken with Laser Point scanning confocal microscope. These are representative images of n=6 aorta sections in each group.

HAS1 is one of the three isoenzymes responsible for cellular HA synthesis[231]. Immunofluorescent staining targeting HAS1 successfully detected the presence of this enzyme in both tunica intima and media of the arterial wall **Figure 58 [A-E]**. The HAS1 expression exhibited a punctate pattern and seemed to be present in both the nucleus and cell cytoplasm across all the groups **Figure 58 [A-E]**. Comparing the images with the control mice **Figure 58 [A]**, a remarkable attenuation of HAS1 expression both in arterial intima and media was observed in the Vitamin K deficient mice **Figure 58 [B & F]**, mirroring the changes

seen in HA expression. However, HAS1 was absent in the adventitia across both the groups **Figure 58 [A-B]**.

No significant alterations in HAS1 expression were observed in the model of APO E -/- high-fat fed mice **Figure 58 [C & F]** and APO E -/- high-fat fed mice + 5/6th nephrectomy **Figure 58 [D & F]** groups in tunica intima and media. Interestingly, in the model of APO E -/- high-fat fed mice + 5/6th nephrectomy + Peritoneal Dialysis fluid infusions, HAS1 expression was markedly upregulated in both intima and media **Figure 58 [E & F].** HAS1 is upregulated in VSMCs during arterial lesions in VSMCs during atherosclerosis, which is in line with the previous literature[673]. There was no HAS1 staining observed in the adventitia.

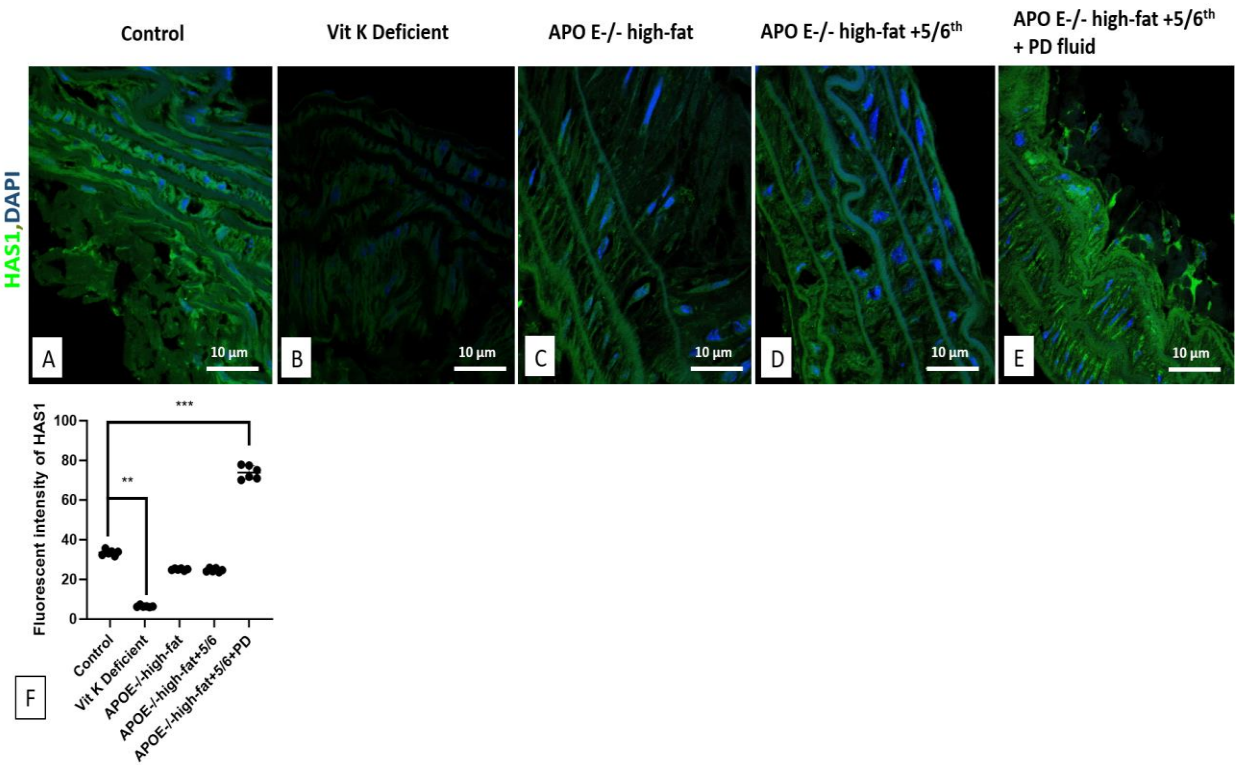

Figure 58 Alterations in HAS1 in an in vivo model of vascular calcification and atherosclerosis

Tissue staining of HAS1 was performed in the aorta sections of Control [A], Vitamin K deficient [B], APO E knockout + high fat diet [C], APO E knockout + high fat diet + 5/6th Nephrectomy [D] and APO E knockout + high fat diet + 5/6th Nephrectomy + Peritoneal Dialysis fluid infusions [E]. Magnification is x630 and the scale bar is 10 µm. Secondary antibody alone served as a negative control; sections were counterstained with DAPI (DNA). The images were taken with Laser Point scanning confocal

microscope and the fluorescent intensity was measured using the ImageJ software [F]. For the scatter dot plot, the median value obtained from each dot, are represented by a line. All the values are expressed as means ± SD from 6 aorta sections in each group. Data was analysed by Kruskal-Wallis test followed by Dunn's post hoc analysis (= p≤0.01, *** = p≤0.001).**

The expression pattern of HAS2 was investigated in various experimental models, shedding light on its potential role in medial calcification and atherosclerosis. Similarities and distinctions in the expression profile of HAS2 among the different groups, highlights its significance in these pathophysiological conditions. In line with HAS1, HAS2 exhibited subcellular localization within the nucleus and cytoplasm, characterized by punctate staining across the different experimental groups **Figure 59 [A-E]**. HAS2 was abundantly expressed in control mice in both arterial intima and media **Figure 59 [A].** Notably, Vitamin K deficient mice displayed a pronounced attenuation of HAS2 expression in both intimal and medial layers **Figure 59 [B & F]**, which is in line with the previous literature[577]. HAS2 was not detected in the adventitia across both the groups **Figure 59 [A-B]**.

In the model of APO E -/- high-fat fed mice **Figure 59 [C & F]** no significant alterations in HAS2 expression were observed compared to the control mice **Figure 59 [A]**. Conversely, an upregulation of HAS2 expression in the arterial intima and media was detected in the model of APO E -/- high-fat fed mice + 5/6th nephrectomy **Figure 59 [D & F]** and the APO E -/- high-fat fed mice + 5/6th nephrectomy + Peritoneal Dialysis fluid infusions groups **Figure 59 [E & F]**. Upregulation of HAS2 is observed in VSMCs during arterial diseases in the previous literature[407]. Furthermore, HAS2 was absent from the adventitia across all the groups **Figure 59 [C-D]**.

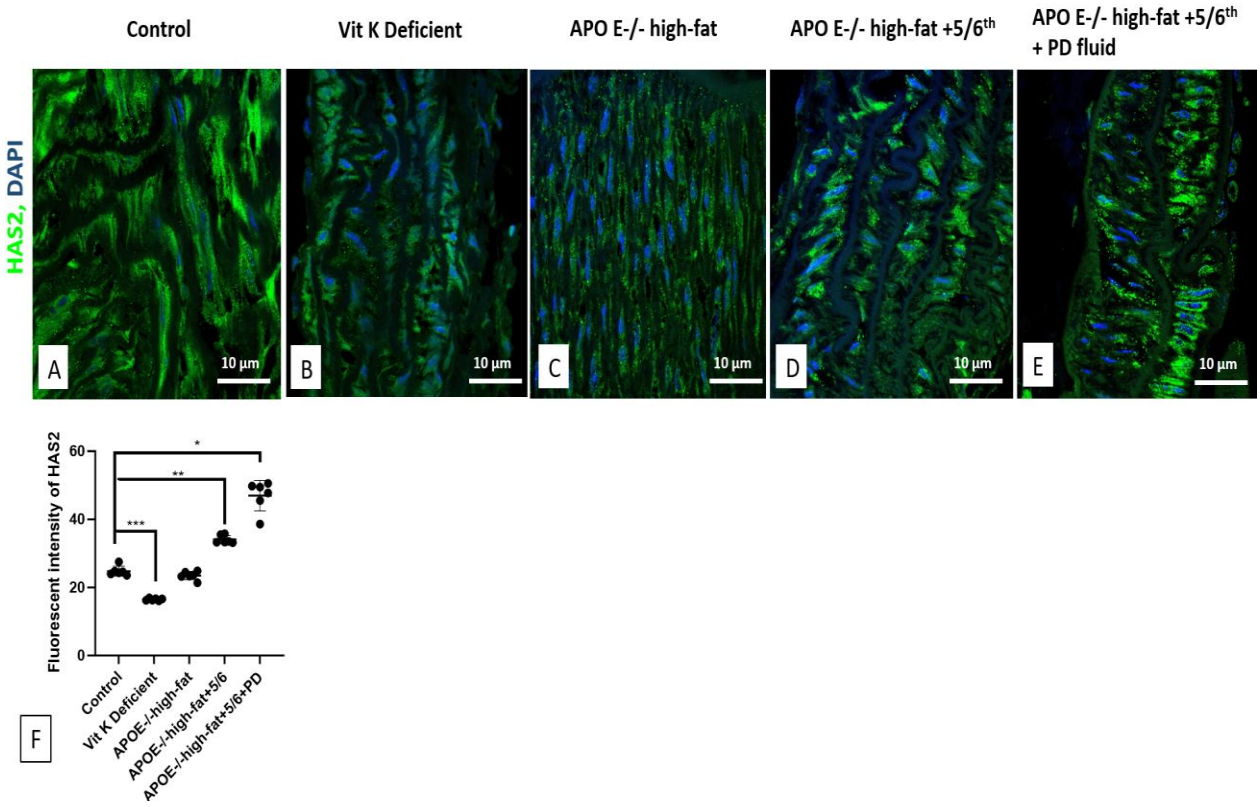

Figure 59 Alterations in HAS2 in an in vivo model of vascular calcification and atherosclerosis

Tissue staining of HAS2 was performed in the aorta sections of Control [A], Vitamin K deficient [B], APO E knockout + high fat diet [C], APO E knockout + high fat diet + 5/6th Nephrectomy [D] and APO E knockout + high fat diet + 5/6th Nephrectomy + Peritoneal Dialysis fluid infusions [E] mice. Scale bar is 10 µm. Secondary antibody alone served as a negative control; sections were counterstained with DAPI (DNA). The images were taken with Laser Point scanning confocal microscope and the fluorescent intensity was measured using the ImageJ software [F]. For the scatter dot plot, the median value obtained from each dot, are represented by a line. All the values are expressed as means ± SD from 6 aorta sections in each group. Data was analysed by Kruskal-Wallis test followed by Dunn's post hoc analysis (* = p≤0.05, ** = p≤0.01, *** = p≤0.001).

We investigated the immunofluorescence staining pattern of HAS3 and its expression levels in two experimental models across different groups, aiming to gain insights into its potential role in VC. The immunofluorescence staining for HAS3 revealed a distinct punctate expression pattern and seemed to be localizing primarily within the cell cytoplasm across all experimental groups **Figure 60 [A-E]**. In contrast to the expression of HA, HAS1/2, in the control group, low expression of HAS3 was detected both in arterial intima and media **Figure 60 [A]**. The model

of Vitamin K deficient mice exhibited a notable exaggeration in HAS3 expression in tunica intima and media **Figure 60 [B & F]**. Interestingly, this upregulation of HAS3 in the context of vitamin K deficiency stands in contrast to the expression profiles of other HAS isoforms and HA. HAS3 was absent from adventitia across both the groups **Figure 60 [A-B]**.

APO E -/- high-fat fed mice show increased expression of HAS3 in arterial intima and media **Figure 60 [C & F]**. In accordance with the results observed for HAS2, APO E -/- high-fat fed mice + 5/6th nephrectomy, and APO E -/- high-fat fed mice + 5/6th nephrectomy + Peritoneal Dialysis fluid infusions groups also displayed heightened expression of HAS3 both in tunica intima and media **Figure 60 [D-F]**. Earlier literature suggests that HAS3 promotes atheroprogression[413]. HAS3 was not detected in the adventitia across all the three groups **Figure 60 [C-E]**.

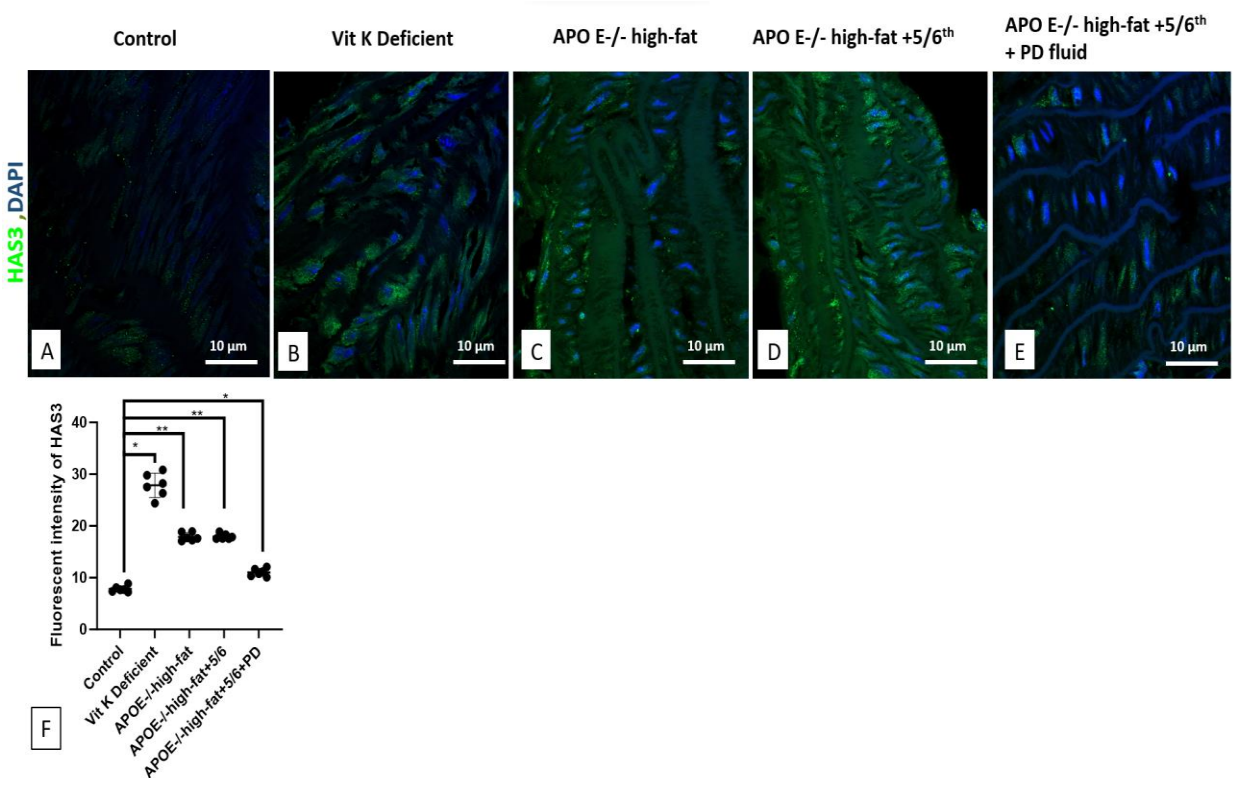

Figure 60 Alterations in HAS3 in an in vivo model of vascular calcification and atherosclerosis

Tissue staining of HAS3 was performed in the aorta sections of Control [A], Vitamin K deficient [B], APO E knockout + high fat diet [C], APO E knockout + high fat diet + 5/6th Nephrectomy [D] and APO E knockout + high fat diet + 5/6th Nephrectomy + Peritoneal Dialysis fluid infusions [E] mice. Scale bar is 10 µm. Secondary antibody alone served as a negative control; sections were counterstained with DAPI (DNA). The images were taken with Laser Point scanning confocal microscope and the fluorescent intensity was measured using the ImageJ software [F]. For the scatter dot plot, the

median value obtained from each dot, are represented by a line. All the values are expressed as means ± SD from 6 aorta sections in each group. Data was analysed by Kruskal-Wallis test followed by Dunn's post hoc analysis (* = p≤0.05, ** = p≤0.01).

Immunofluorescence staining for HYAL2 revealed a characteristic punctate expression pattern, prominently localized within both the cytoplasm and nucleus across all experimental groups **Figure 61 [A-E]**. In correlation with the expression patterns of HA and HAS1/2, HYAL2 displayed attenuated expression in the Vitamin K-deficient mice group in both arterial intima and media **Figure 61 [B & F]**. HYAL2 was not detected in the adventitia across both the groups **Figure 61 [A & B]**.

Conversely, HYAL2 expression exhibited exaggerated expression in both arterial intima and arterial media in all the groups, APO E -/- high-fat fed mice, APO E -/- high-fat fed mice + 5/6th nephrectomy, and APO E -/- high-fat fed mice + 5/6th nephrectomy + Peritoneal Dialysis fluid infusions **Figure 61 [C-F]**. This consistent increase in HYAL2 expression is observed in VSMCs in previous atherosclerotic literature[674]. HYAL2 was not detected in adventitia across all the three groups **Figure 61 [C-F]**.

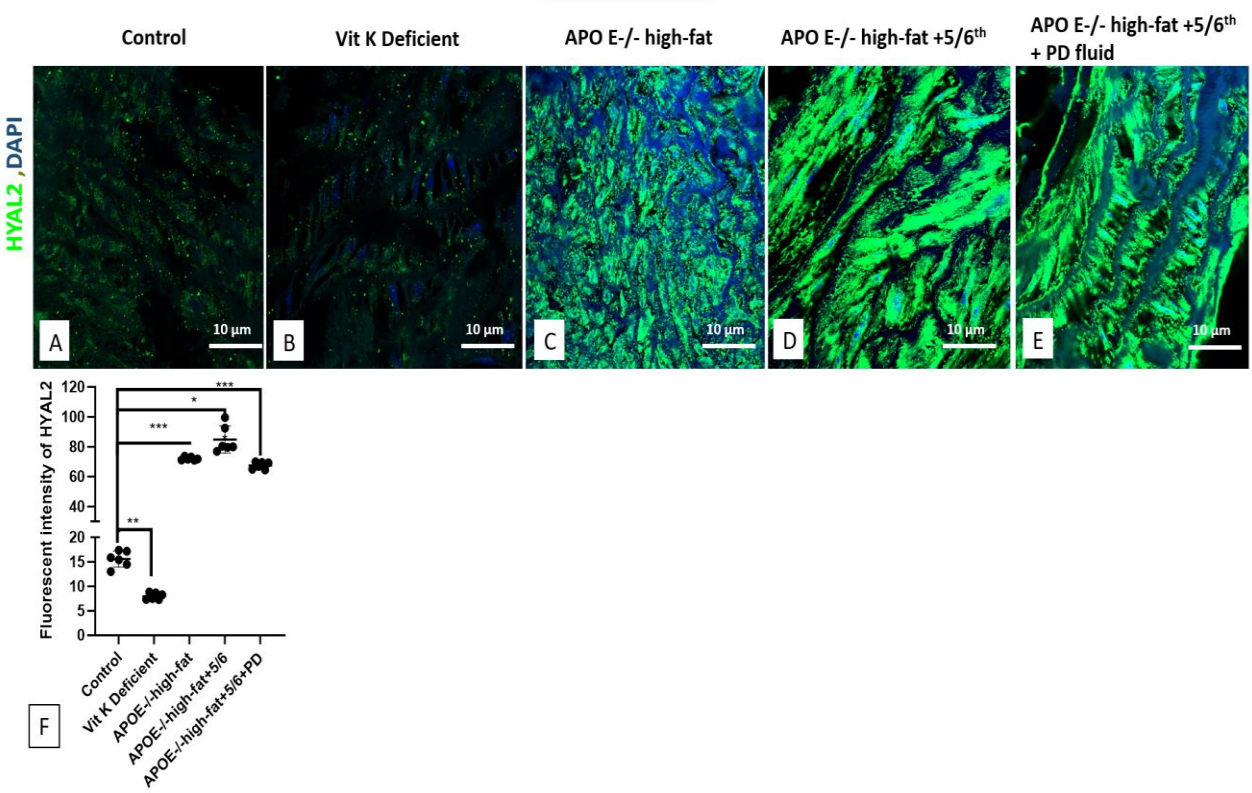

Figure 61 Alterations in HYAL2 in an in vivo model of vascular calcification and atherosclerosis

Tissue staining of HYAL2 was performed in the aorta sections of Control [A], Vitamin K deficient [B], APO E knockout + high fat diet [C], APO E knockout + high fat diet + 5/6th Nephrectomy [D] and APO E knockout + high fat diet + 5/6th Nephrectomy + Peritoneal Dialysis fluid infusions [E] mice. Scale bar is 10 µm. Secondary antibody alone served as a negative control; sections were counterstained with DAPI (DNA). The images were taken with Laser Point scanning confocal microscope and the fluorescent intensity was measured using the ImageJ software [F]. For the scatter dot plot, the median value obtained from each dot, are represented by a line. All the values are expressed as means ± SD from 6 aorta sections in each group. Data was analysed by Kruskal-Wallis test followed by Dunn's post hoc analysis (* = p≤0.05, ** = p≤0.01, *** = p≤0.001).

CD44 is a cell-surface glycoprotein involved in cell-cell interactions, cell proliferation, cell differentiation[675]. Immunofluorescence staining for CD44, represented in red, exhibited a diffuse expression pattern surrounding the cells, within the cell membrane, and the cytoplasm across all experimental groups **Figure 62 [A-E]**. In the controls, CD44 was abundantly present in arterial intima and media **Figure 62 [A].** In the Vitamin K deficient mice model, no alteration in CD44 expression was detected compared to controls **Figure 62 [B & F]**. CD44 was absent from adventitia across both the groups **Figure 62 [A & B]**.

APO E -/- high-fat fed mice demonstrated reduction in expression of CD44 in both arterial intima and media **Figure 62 [C & F]**. In the model of APO E -/- high-fat fed mice + 5/6th nephrectomy, no significant change in CD44 expression was observed compared to the controls **Figure 62 [D & F]**. The APO E -/- high-fat fed mice + 5/6th nephrectomy + Peritoneal Dialysis fluid infusions group exhibited marked attenuated expression of CD44 in both arterial intima and media **Figure 62 [E & F]**. CD44 was not detected in the adventitia across all the three groups **Figure 62 [C-E]**.

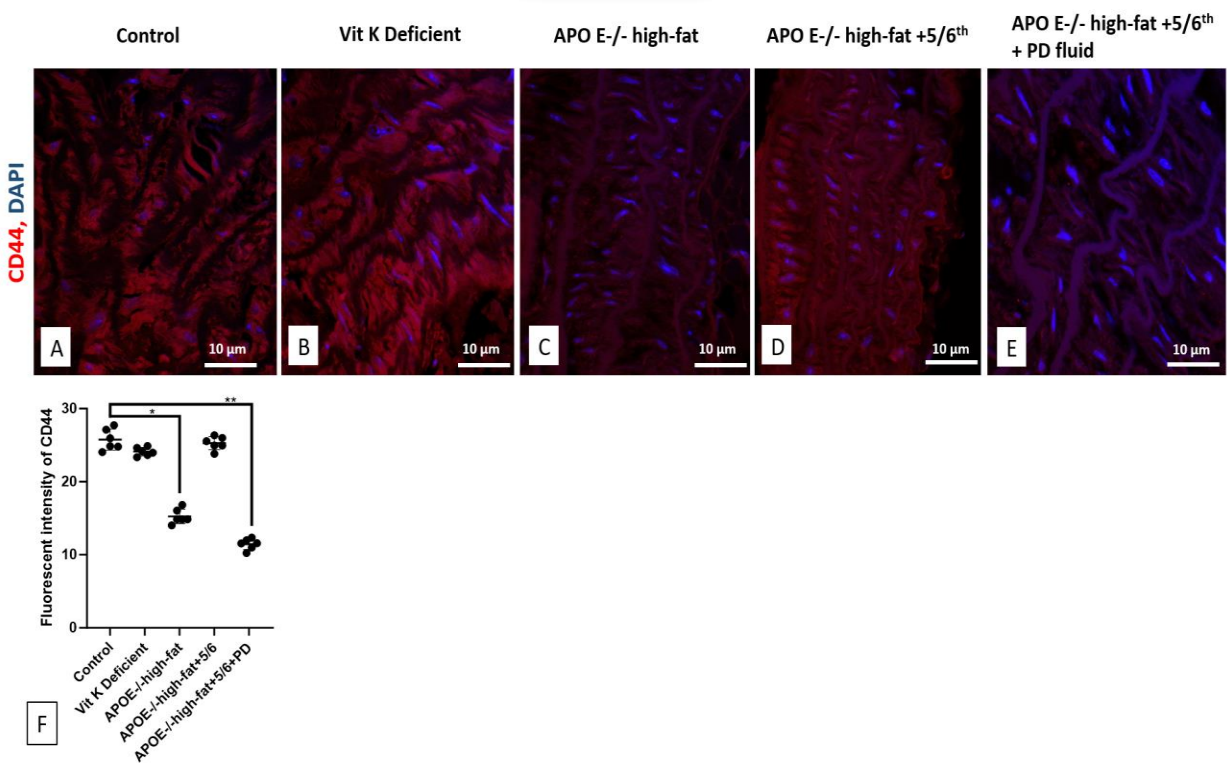

Figure 62 Alterations in CD44 in an in vivo model of vascular calcification and atherosclerosis

Tissue staining of CD44 was performed in the aorta sections of Control [A], Vitamin K deficient [B], APO E knockout + high fat diet [C], APO E knockout + high fat diet + 5/6th Nephrectomy [D] and APO E knockout + high fat diet + 5/6th Nephrectomy + Peritoneal Dialysis fluid infusions [E] mice. Scale bar is 10 µm. Secondary antibody alone served as a negative control; sections were counterstained with DAPI (DNA). The images were taken with Laser Point scanning confocal microscope and the fluorescent intensity was measured using the ImageJ software [F]. For the scatter dot plot, the median value obtained from each dot, are represented by a line. All the values are expressed as

means ± SD from 6 aorta sections in each group. Data was analysed by Kruskal-Wallis test followed by Dunn's post hoc analysis (* = p≤0.05, ** = p≤0.01).

Immunofluorescence staining for TSG-6, represented by a green, fluorescent signal, revealed an intracellular punctate expression pattern across all experimental groups **Figure 63 [A-H]**. TSG-6 is moderately expressed in the tunica intima and media in the controls **Figure 63 [A].** Consistent with the expression patterns of HA, HAS1, HAS2, and HYAL2, the Vitamin K deficient mice exhibited an attenuated expression of TSG-6 in both arterial intima and media **Figure 63 [B]**. TSG-6 was not detected in the adventitia across both the groups **Figure 63 [A & B]**.

Attenuated expression of TSG-6 was observed in the APO E -/- high-fat fed mice **Figure 63 [C & I]**. Conversely, APO E -/- high-fat fed mice + 5/6th nephrectomy **Figure 63 [D & I]** displayed high expression of TSG-6 in both tunica intima and media. Diminished expression of TSG-6 in arterial intima and media was detected in APO E -/- high-fat fed mice + 5/6th nephrectomy + Peritoneal Dialysis fluid infusion group **Figure 63 [E & I].** TSG-6 was found to be expressed also at plaque sites in the arterial media **Figure 63 [F-H]**, resembling the expression pattern of HA. TSG-6 was not found in the adventitia across the three different groups **Figure 63 [C-H]**.

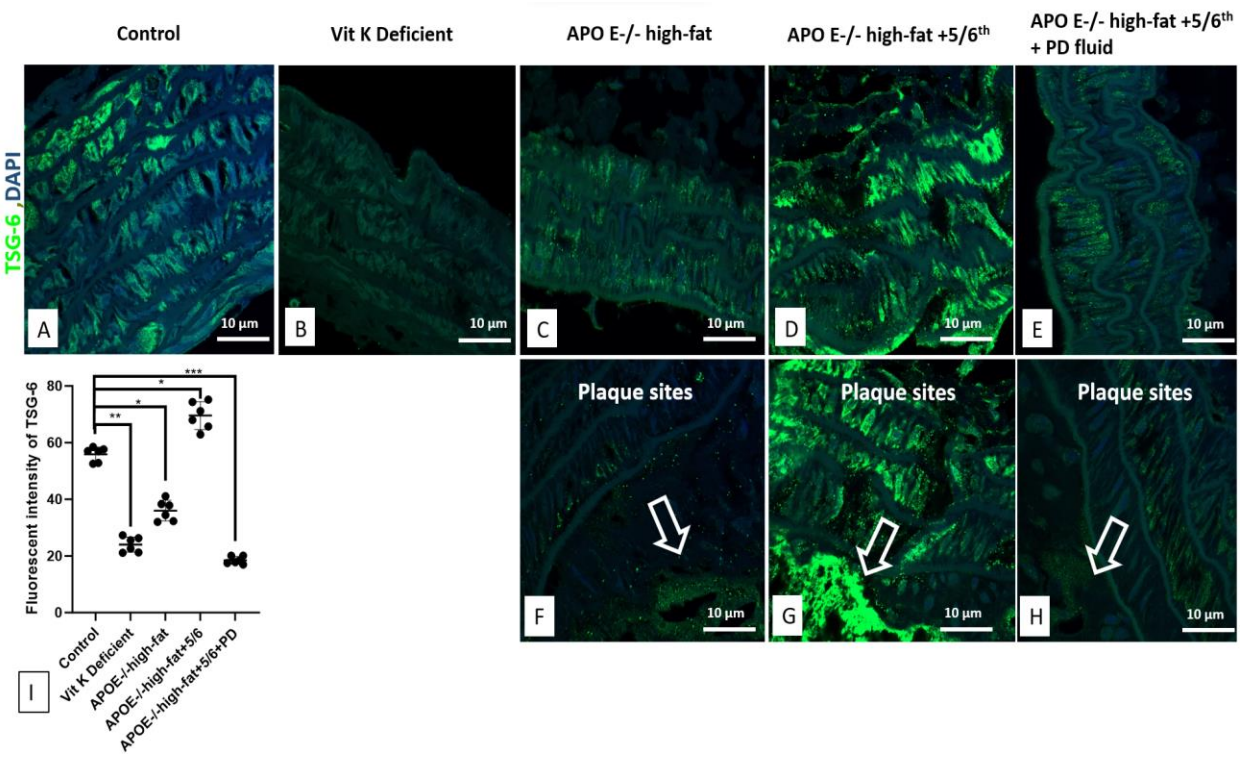

Figure 63 Alterations in TSG-6 in an in vivo model of vascular calcification and atherosclerosis

Tissue staining of TSG-6 was performed in the aorta sections of Control [A], Vitamin K deficient [B], APO E knockout + high fat diet [C], APO E knockout + high fat diet + 5/6th Nephrectomy [D] and APO E knockout + high fat diet + 5/6th Nephrectomy + Peritoneal Dialysis fluid infusions [E] mice. Images of the plaques are shown in the lower panel [F-H], marked with an arrow. Magnification is x630 and scale bar is 10 µm. Secondary antibody alone served as a negative control; sections were counterstained with DAPI (DNA). The images were taken with Laser Point scanning confocal microscope and the fluorescent intensity was measured using the ImageJ software [I]. For the scatter dot plot, the median value obtained from each dot, are represented by a line. All the values are expressed as means ± SD from 6 aorta sections in each group. Data was analysed by Kruskal-Wallis test followed by Dunn's post hoc analysis (* = p≤0.05, ** = p≤0.01, *** = p≤0.001).

To visualize the expression of VCAN labelled with red, fluorescent stain, we employed immunofluorescence techniques. In control group, VCAN exhibited both intracellular and pericellular presence in arterial intima and media **Figure 64 [A]**. Conversely, in the Vitamin K deficient model, VCAN displayed elevated expression, solely as pericellular localization in both arterial intima and media **Figure 64 [B & I]**. The attenuation in VCAN expression parallels that of HA, HAS1, HAS2 and HYAL2. VCAN was also detected in the adventitia, similar to the expression of HA **Figure 64 [B] (arrows)**.

VCAN expression was attenuated in both arterial intima and media, with exclusive pericellular localization observed in all three experimental models **Figure 64 [C-H & I]**. This reduced expression pattern was consistently observed across different experimental groups, APO E -/- high-fat fed mice, APO E -/- high-fat fed mice + 5/6th nephrectomy, APO E -/- high-fat fed mice + 5/6th nephrectomy + Peritoneal Dialysis fluid infusion **Figure 64 [C-H & I]**. Furthermore, similar to HA and TSG-6, VCAN was detected at the plaque sites in the arterial intima **Figure 64 [F-H] (indicated by white arrows).** Similar to HA, VCAN was also in the adventitia **Figure 64 [D] (indicated by white arrows).**

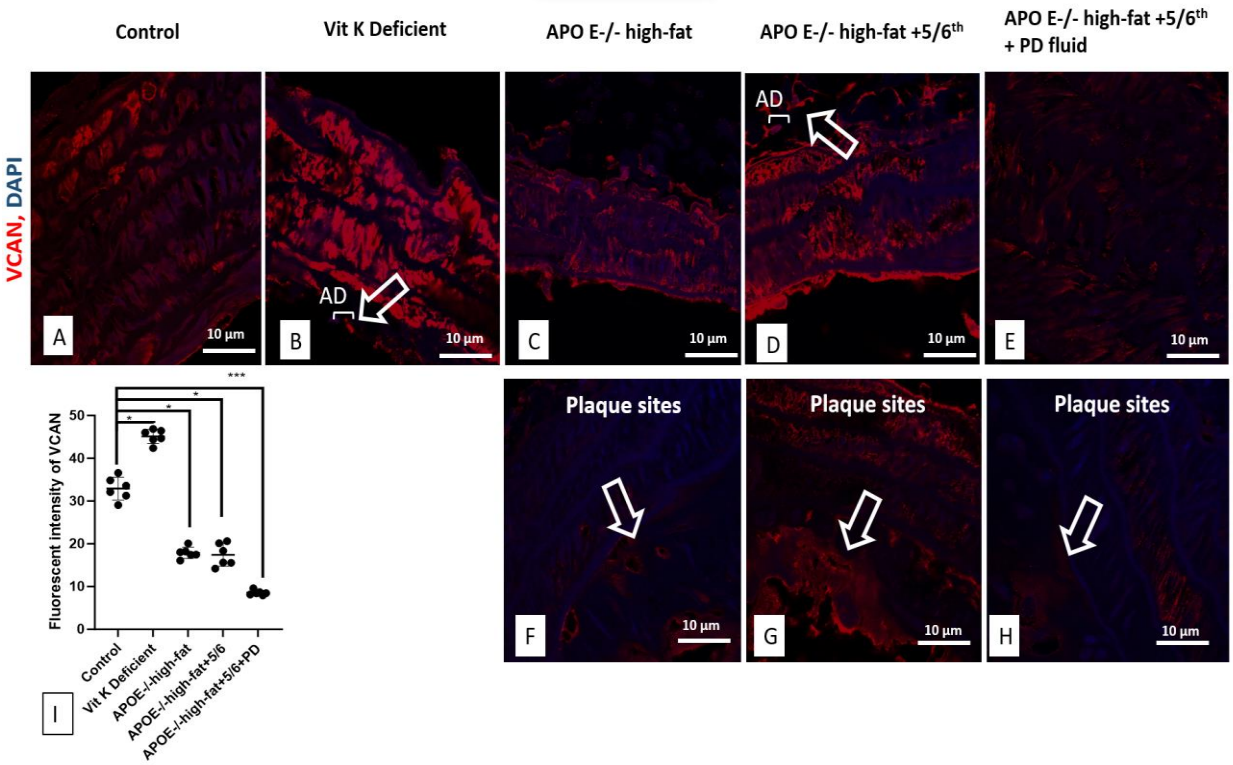

Figure 64 Alterations in Versican in an in vivo model of vascular calcification and atherosclerosis

Tissue staining of VCAN was performed in the aorta sections of Control [A], Vitamin K deficient [B], APO E knockout + high fat diet [C], APO E knockout + high fat diet + 5/6th Nephrectomy [D] and APO E knockout + high fat diet + 5/6th Nephrectomy + Peritoneal Dialysis fluid infusions [E] mice. Images of the plaques are shown in the lower panel [F-H], marked with an arrow. Magnification is x630 and the scale bar is 10 µm. Secondary antibody alone served as a negative control; sections were counterstained with DAPI (DNA). The images were taken with Laser Point scanning confocal microscope and the fluorescent intensity was measured using the ImageJ software [I]. For the scatter dot plot, the median value obtained from each dot, are represented by a line. All the values

are expressed as means ± SD from 6 aorta sections in each group. Data was analysed by Kruskal-Wallis test followed by Dunn's post hoc analysis (* = p≤0.05, *** = p≤0.001).

5.3 Discussion

In the preceding chapter, I extensively characterized HA alterations in an *in vitro* model of VC, underscoring the significance of HA inhibition and the modulation of HA-related proteins in calcification progression. Our findings revealed a substantial downregulation of HA expression and its related markers during VSMC osteogenic differentiation, suggesting HA generation is the key to maintaining normal VSMC phenotype. We observed changes in the organization of HA, resembling newly forming cell-cell contact spindles, which resembled HA cables. Furthermore, when we degraded HA generation using 4MU, the VSMCs were more easily calcified. While treatment with Strep-Hyal, whose role is to breakdown HA within the matrix (HA cables) completely mitigated VSMC osteogenic differentiation, suggesting HA cable might act as inducers of VSMC osteogenic differentiation. Building upon these pivotal findings, the current chapter aimed to investigate the *in vivo* relevance of these *in vitro* observations. In this study, we collaborated with VU Amsterdam and MU Maastricht to develop distinct mouse models characterized by the development of medial calcification and specific cardiovascular complications associated with CKD. Cardiovascular disease stands as the predominant cause of mortality among CKD patients. VC induced by calcium and phosphate excess and uraemia, represents a significant risk factor that is independently linked to cardiovascular events and mortality. Utilizing Alizarin Red and von Kossa Staining, we gained valuable insights into the extent and localization of calcium deposition within the aorta sections of the studied mouse groups.

In our Vitamin K deficient model of medial calcification, we observed extensive calcification within the tunica media throughout the entire vascular tree, while no calcification was evident in the intima. It's worth noting that medial calcification has been identified as a more robust predictor of CVD events[676]. Our findings align with previous research that has established a correlation between Vitamin K deficiency and an increased predisposition to calcification in VSMCs residing within the tunica media[135]. Notably, subclinical Vitamin K deficiency is commonly observed in CKD[602,677,678] and dialysis[679-681] patients rendering them susceptible to VC. Medial calcification is particularly associated with uraemic risk factors. It's essential to recognize that the mechanisms underlying these two types of VC (media vs. intima) are distinct and represent different aspects of the calcification process[682,683].

In our APO E-/- high-fat fed mouse model, we observed the presence of calcification specifically within the atherosclerotic plaques, with no evidence of calcification observed in other arterial regions. It is plausible that the APO E-/- high-fat fed mice were not maintained for a duration sufficient to induce significant intimal calcification, aside from the calcification observed within the plaques in our model. Significantly, plaque calcification is known to markedly increase the risk of acute vascular events, including myocardial infarction and ischemic stroke[684]. Moreover, this type of calcification has been associated with the advancement of atherosclerotic lesions[92]. It is noteworthy that previous research has indicated that APO E-/- mice on a C57BL/6 background tend to develop atherosclerosis when subjected to a Western-type diet but exhibit limited development of significant medial calcification[141]. This characteristic may explain the absence of medial calcification in our model.

Shifting our focus to the subsequent *in vivo* uraemia model, we have detected sporadic calcification within the arterial intima. Previous investigations have demonstrated that the induction of uraemia through 5/6th nephrectomy in APO E-/- mice leads to accelerated atherosclerosis and calcification within the arterial intima[61,685]. Indeed, while the uraemic model effectively replicates the clinical conditions observed in CKD patients, it's noteworthy that various studies have consistently reported the occurrence of atherosclerosis and intimal calcification in these uraemic models. However, substantial medial calcification has remained notably absent in these models, as documented in multiple studies[653,686-688]. This collective observation aligns with our own findings, providing a plausible explanation for our inability to detect medial calcification in our model.

In our uraemia model with added inflammation, we also noted sporadic calcification in the arterial intima. When kidneys are dysfunctional, there is a buildup of retained solutes that can reach harmful levels. While dialysis is employed to alleviate this condition, it unexpectedly exacerbates inflammation. Although detecting differences in calcium deposition between uraemia and the uraemia model with added inflammation was challenging, distinctions emerged when examining the HA profiles of these *in vivo* models.

In our investigation of HA alterations within *in vivo* models of medial calcification and CKD specific CVD, we have garnered valuable insights into the pivotal role HA plays in these

pathological processes. Notably, in Vitamin K deficient mice, we observed a significant reduction in HA expression, finding congruent with our *in vitro* model results that indicate a marked decrease in HA expression during VSMC osteogenic differentiation. Alterations in HA were different in the intima and media depending on the type of calcification. In the media, certain forms of HA demonstrated a protective effect, while in the intima, it was consistently linked to worsened disease. This highlights the need for a deeper understanding of the molecular weight and interactions of HA within these two distinct forms of calcification.

There is an increase in HA expression only in the plaques in APO E -/- high-fat fed mice, whereas an increase in HA expression is evident in both arterial intima and media in uraemic models and uraemic models with added inflammation. In the context of APO E -/- high-fat fed mice, it is plausible that their state corresponds to an early stage of lesion development, wherein HA expression in the arterial layers remains comparable to that of control subjects. Given that this stage primarily manifests as plaque calcification, the observed increase in HA expression within the plaque implies a potential association between HA and lesion progression in this particular model of arterial diseases. Notably, the heightened HA expression in arterial intima and media in models featuring uraemia and uraemia with added inflammation reveals an intriguing correlation with arterial disease advancement[689]. Additionally, HA possesses unique properties that enable its interaction with lipid-rich plaques residing within arterial walls[405], which may explain the accumulation of HA within lipid-laden necrotic cores and the layer of VSMCs adjacent to the plaque. These findings collectively suggest that HA assumes distinct roles within different arterial layers, depending upon the type and location of calcification, thereby underscoring its pivotal role in the intricately orchestrated process of VC. It is worth noting that HA is also present in the adventitia, a layer primarily composed of fibroblasts and collagen fibers. Within the adventitia, HA is thought to contribute to maintaining the structural integrity of outermost blood vessel layer and provides a gel-like matrix that enhances the flexibility and elasticity of the blood vessel wall. However, its role in the adventitia has not yet been explored.

Moving on to the enzymes that makes HA, HAS1 and HAS2 exhibited significant downregulation in the medial calcification model involving Vitamin K deficient mice, corroborating our *in vitro* findings that revealed a notable decrease in HAS1 and HAS2 expression during VSMCs osteogenic differentiation. Furthermore, this observation aligns

with earlier literature demonstrating that HAS2 overexpression can inhibit calcification, further substantiating the protective role of HAS2 against medial calcification[577]. Consequently, our findings collectively highlight that both HAS enzymes, along with HA itself, undergo attenuation during medial calcification, underscoring their potential significance in the pathological process. Within the CKD-specific CVD models, our examination of HAS1 expression revealed relatively stable levels in APO E -/- high-fat fed mice and the uraemia model compared to the control group. However, HAS1 expression exhibited an augmentation in both arterial intima and media in the uraemia model with added inflammation, consistent with our prior data indicating an increase in HAS1 expression in response to inflammatory cytokines. Existing literature also supports elevated HAS1 expression in arterial diseases[690]. Similarly, HAS2 expression showed no significant difference between APO E -/- high-fat fed mice and the control group. This phenomenon might be attributed to these mice being in an early developmental stage of arterial diseases. Conversely, HAS2 expression in arterial intima and media was notably elevated in both the uraemia and uraemia with added inflammation models, aligning with our *in vitro* model of VSMCs stimulated with cytokines, where an increase in HAS2 expression was observed. Importantly, a connection between HAS2 and arterial disease progression is evident. Earlier literature demonstrated that overexpression of HAS2 in mice has led to increased arterial disease development[415], and high levels of HAS2 have been observed in advanced atherosclerosis model[691]. Collectively, our findings suggest that while HAS1 and HAS2 may promote arterial diseases in CKD-specific CVD models, they concurrently play a protective role in preventing medial calcification.

In contrast to HAS1 and HAS2, the third HAS isoenzyme, HAS3, exhibited significant upregulation in the medial calcification model involving Vitamin K deficient mice. This observation corresponds with our *in vitro* model, where we observed an increase in HAS3 protein expression during VSMC osteogenic differentiation. HAS3 is involved in the formation of HA cables[276], which may play a role in VSMC osteogenic transdifferentiation. Furthermore, all the three HAS isoenzymes are located on different chromosomes and have different levels of activity and expression patterns and biological roles[250,261]. To explore the roles of HAS isoenzymes in medial calcification more in depth exploration is required. In the atherosclerosis, uraemia, and uraemia with added inflammation model we observed increased expression of HAS3 in both arterial intima and media in all groups. Previous studies

have indicated that the knockdown of HAS3 in mice inhibits atherosclerosis[413], indicating an atherogenic role of HAS3 in the development and progression of atherosclerosis. HAS3 is expressed more strongly in comparison to HAS1 and HAS2 in during atheroprogression in mice[413]. The distinctive expression pattern of HAS3, prominently upregulated in both intimal and medial calcification[413], raises intriguing questions about its functional significance and potential as a therapeutic target. Unravelling the underlying molecular mechanisms responsible for HAS3's role in these cardiovascular disorders and understanding the downstream effects of increased HA synthesis mediated by HAS3 will be essential for future research.

In our *in vivo* medial calcification model of Vitamin K deficient mice, HYAL2 was downregulated in the arterial media, consistent with our *in vitro* VC model where both gene and protein expression of HYAL2 diminished as VSMCs underwent osteogenic transformation. The role of HYAL2 in medial calcification has not been previously studied. Conversely, HYAL2 expression was heightened both in arterial intima and media in the atherosclerosis, uraemia, and uraemia with added inflammation models. In the medial calcification model, CD44 expression in arterial media remained unchanged, mirroring our *in vitro* findings. CD44 serves as the primary receptor for HA, and its role in medial calcification warrants further investigation. In APO E -/- high-fat fed mice model, CD44 expression was attenuated in both arterial intima and media and subsequently increased in uraemia model, only to be attenuated again in added inflammation model. Existing literature suggests that CD44-/- mice exhibit reduced atherosclerotic lesions[417]. It fluctuations in expression seen in the in atherosclerosis, uraemia and inflammation models, suggests that the regulation of CD44 is complex and likely is influenced by various factors. CD44 have different splice variants and can exist as multiple isoforms[692]. Prior studies showed specific molecular weight HA-interaction with CD44 is also a determinant factor for its behaviour. Literature suggests that LMW HA-CD44 interactions promote VSMC proliferation whereas HMW HA-CD44 interactions had an opposite effect[417,460], it might be certain molecular weight HA and it's interaction in different mice group is affecting its expression. In the Vitamin K deficient model, TSG-6 expression was attenuated in the arterial media aligning with our *in vitro* results of VC where TSG-6 protein expression was attenuated as VSMCs become osteogenic. TSG-6 is enhanced at early time points in our *in vitro* model, and we know that TSG-6 is associated

with formation of HA coats, which are disappears when VSMCs become osteogenic. The TSG-6 and HA interactions are of vital importance and this needs to be investigated further in medial calcification model. In APO E -/- high-fat fed mice model there was a low expression of TSG-6 in both arterial intima and media, it was increased in the uraemia model and decreased again in added inflammation model. The expression of TSG-6 was also found in the plaques alongside HA in all these CKD-specific CVD mice groups. Previous literature found TSG-6 expression in atherosclerotic plaques[426,430,693], which is in line with our observations of TSG-6 expression in the plaque regions. The presence of TSG-6 corresponds with vascular inflammation and macrophages[693]. Our *in vitro* data indicated that inflammatory cytokines boost TSG-6 expression.

In our *in vivo* model of medial VC, Versican expression was enhanced in the arterial media, correlating with protein expression in our *in vitro* VC model where Versican expression was enhanced when VSMCs become osteogenic. Versican in medial calcification has not been studied so further interventional experiments are required to elucidate the precise role of Versican in medial calcification. Conversely, in the APO E -/- high-fat fed mice model, uraemia and added inflammation model, we get attenuation of Versican in the medial layer. Nevertheless, Versican was present in the plaques in arterial intima and also in the adventitia, alongside HA. Existing literature supports the presence of Versican in the necrotic cores and plaques in arterial intima[432]. Versican is also known to bind to LDL, supporting its presence in the plaque sites[431]. Versican plays a pivotal role in various biological processes. It contributes significantly to bone formation[401], influences the progression of arterial diseases[432], and plays a crucial role in regulating cell phenotype[694]. Versican seems to be a key factor responsible for the process of VSMCs osteogenic differentiation and this needs further investigations.

In summary, our study has illuminated the complex roles of HA and its related proteins in VC across various *in vivo* models. Consistent findings between the medial calcification model *in vivo* and *in vitro* further validate our observations and pinpoint crucial targets in VSMC osteogenic differentiation. The alterations in HA observed in models with CKD-specific CVD mirror existing literature on arterial diseases. In essence, these two types of calcifications represent distinct entities, and our research paves the way for further exploration to mitigate VC.

Chapter 6

General Discussion

The thesis comprehensively investigates the pathology of arterial calcification in CKD. The two main pathologies that exist in CKD are exaggerated atherosclerosis and VC of arteries[695]. The prevalence of aortic calcification is 81% in patients with diabetes[696] and 100% with ESRD[697], associating with their co-morbidities[698]. Moreover, VC is such a strong indicator of plaque progression and vunerability[699,700], that is it routinely used as a marker for designing cardiovascular treatment plans[701,702]. VC can be observed in two distinct anatomical locations: the medial and intimal layers[682,703]. Although clinical studies have demonstrated that distinguishing between intimal and medial calcification is not a straightforward binary categorization, this classification is still relevant for clinical treatment and diagnosis due to their distinct clinical consequences[704]. These locations of calcification represent separate entities within the context of CKD. Within the arterial intima, calcifications are frequently found a as a notable component of atherosclerotic plaque. Previously considered a late-stage phenomenon, it is now understood that intimal calcification is an active process that commences relatively early in atherosclerotic plaque development[705]. Local inflammation likely serves as the trigger for atherosclerotic calcification[706]. The presence of calcifications, regardless of their origin (intima or media), can exacerbate the inflammatory process in CVD, creating a positive feedback loop[707]. Medial calcification, on the other hand, is distinct in phenotype from arterial intimal calcification and can occur independently of intimal calcification[45]. Both systemic and localized inflammation play critical roles in the formation and progression of arterial calcification[704,708]. Although VC is so common and so strikingly linked to poor cardiovascular health, we are still only recently learning that morphology specific outcomes may exist, let alone nearing the development of a specific VC treatment to adjust these morphologies[56].

To comprehensively investigate this process, we established an *in vitro* model of medial VC in **Chapter 3.** This model aimed to replicate the process of medial calcification, mirroring the conditions observed in CKD patients who are susceptible to developing medial VC. Specific stimuli, including elevated calcium or phosphate levels, trigger a transition in VSMCs towards an osteogenic phenotype[103]. Individuals with CKD suffer from hyperphosphatemia which represents a risk factor for increased mortality[709]. Additionally, there is a strong correlation

between elevated phosphate levels and the accelerated progression of VC[710]. Utilizing human VSMCs, we exposed them to three distinct culture media, each with varying phosphate compositions. Particularly noteworthy was the medium enriched with sodium orthophosphate, which emerged as the most conducive environment, eliciting heightened gene expression of bone markers, and promoting the deposition of calcium hydroxyapatite within our *in vitro* model. Notably, our observations indicated that VSMCs did not undergo complete transformation into fully bone-like cells, rather, they exhibited certain characteristics reminiscent of bone cells while still retaining some of their intrinsic VSMC properties[501]. Most notably, they reduced their ability to contract, signifying a significant phenotypic switching. Given that, increased arterial stiffness is often associated with presence of VC, our next step is to explore this relationship further.

In order to gain insights into the intricate molecular mechanisms underpinning VC, we deemed it essential to investigate an *in vivo* model of medial VC in **Chapter 5**. In pursuit of this objective, we employed warfarin fed Vitamin K-deficient mice. Previous research has established medial calcification as a late-stage remodeling feature, contributing to ectopic heart calcification, vulvar calcification, and aortic medial calcification[711-713]. In our Vitamin K-deficient mouse model, we specifically directed our attention to the aorta and observed the occurrence of distinctive medial calcification extending throughout the entire segment of the medial layer. Whereas, in our uraemia and uraemia with added inflammation we observed calcification in the arterial intima.

VC is an active gene regulated process resembling osteogenesis where both osteogenic gene expression and mineralisation are crucial[714,715]. Specifically, HA has been demonstrated an important factor regulating mineralisation[716,717], with evidence of its regulatory role in human VSMC calcification[718]. In **Chapter 4 and 5** of our study, we conducted an examination of the two models, with a specific focus on HA. Notably, we observed remarkable parallels between our *in vivo* and *in vitro* VC models in terms of alterations in HA and its associated proteins. It's worth noting that while there have been numerous studies examining the role of HA in CVD or intimal calcification, there has been limited research into its role in medial calcification. This uncharted territory offered us a unique opportunity to explore a novel aspect of VC and to validate the accuracy of our observations by comparing the two models.

In our *in vivo* model involving Vitamin K deficient mice which exhibits medial calcification, we observed a significant reduction in HA content. Similarly, our *in vitro* model exhibited substantial reductions in both gene and protein expression related to HA when VSMCs underwent osteogenic differentiation. These observations align with previous studies where HA treatments prevent osteogenic differentiation of VSMCs[577,719]. Moreover, prior research demonstrated calcification-mitigating role of the HA grafts on the biomaterial[717]. Similarly, in our *in vitro* model, ICC analysis revealed a profound loss of HA in the nucleus and cytoplasm of VSMCs during osteogenic transformation. Interestingly, HA morphology changed, transitioning from a traditional HA coat to the formation of HA cables capable of spanning multiple cell lengths during osteogenic differentiation. From previous studies we know that these cables were found to be associated with inflammation, as they possessed the capability to bind to leukocytes and facilitate the release of inflammatory cytokines[276].

To gain a deeper understanding of HA's role, we employed interventional approaches to investigate the impact of HA degradation on osteogenic differentiation in **Chapter 4**. Two modulation methods were utilized: 4MU, which globally inhibited HA, resulted in increased calcification, suggesting a protective role for HA in the osteogenic differentiation process. The second degradation method, cleaving HA into smaller disaccharides, led to complete attenuation of calcification, highlighting the significance of how HA is spatially organised in the ECM is critical to its function in inducing VSMC differentiation. These findings align with previous research demonstrating that HMW-HA inhibits osteogenic differentiation and calcification of rat VSMCs and arterial calcification[577]. Intriguingly, LMW-HA also reduces calcification of rat VSMCs and arterial calcification[577]. This suggests that the molecular mass of HA might not be the primary determinant influencing medial VC, instead, it could be the influence of HA-binding partners that drives the transdifferentiation of VSMCs into an osteogenic phenotype. We hypothesize that the formation of HA cables could be the driving factor behind the differentiation of VSMCs into an osteogenic phenotype. Considering all these observations, HA strongly indicates an inhibitory role in medial VC. To get more insights about this inhibitory role future work involves examining the effects of 4MU in a Vitamin K deficient model.

In our models, the expression patterns of HA binding proteins in **Chapter 4 and 5** emerged as of utmost significance, displaying remarkable similarities that further validate their importance. Notably, we observed a reduction in the expression of TSG-6 in both our *in vivo* and *in vitro* models of medial VC. This finding aligns with our understanding of TSG-6's association with HA coat formation, which diminishes as VSMCs transition into an osteogenic state. This reduction in both HA coat and TSG-6 during this transdifferentiation process resonates with our observations[271]. Conversely, Versican displayed increased expression when VSMCs underwent osteogenic differentiation in both the *in vivo* and *in vitro* models. Prior research has established a connection between Versican and HA cable formation[720]. It is plausible that Versican plays a role in promoting HA cable formation, thereby driving VSMCs towards an osteogenic phenotype. These findings strongly suggest a dynamic interplay between HA-binding proteins, such as TSG-6 and Versican, in modulating HA coat and cable formation during VSMC osteogenic differentiation, as evidenced by ICC in our *in vitro* model. Notably, previous studies have underscored the importance of Versican in bone and cartilage formation during fetal rat development[400] as well as its involvement in the development of rat mandible and hind limbs[401], implying that Versican play an important role in osteogenesis. Versican also shows its importance in arterial diseases progression[432] and there are evidences of increased Versican deposition in VSMCs after injury[721-723]. Additionally, Versican has a role in regulation of cell phenotype and can influence the ability of the cells to proliferate, migrate, adhere, and remodel the ECM[694], suggests its potential significance in the phenotypic switch of VSMCs. These multifaceted roles of Versican in various contexts raise the possibility that it may also be a critical factor in VSMC osteogenic differentiation, warranting further investigation. To investigate the specific roles of these HA binding proteins the next step is to knockdown TSG-6 and Versican individually in our *in vitro* model of VSMC osteogenic differentiation and use ICC to see what impacts it has in the formation of HA coats and cables along with its impact on calcification.

In our examination of HAS isoenzymes, we observed notable similarities between our *in vivo* and *in vitro* models. Both HAS1 and HAS2 demonstrated diminished expression in both models when VSMCs underwent osteogenic differentiation, suggesting a potential protective role in this specific context. To substantiate these findings, we conducted interventional cell experiments involving the individual overexpression of HAS1 and HAS2, which resulted in a

complete attenuation of calcification at both the gene and protein expression levels, further validating our observations. HAS2 is the major enzyme responsible for HA synthesis in VSMC[364]. Prior study shows HAS2 overexpression attenuates medial calcification process which further confirms its protective role[577]. All these results related HAS2 opens up new areas to mitigate calcification and the next step is to test this in the Vitamin K deficient model to see if it actually cures calcification.

All the three HAS isoenzymes are located on different chromosomes and have been reported to have different biological roles[250,261]. HAS3 exhibited intriguing expression patterns which was different from the other two HASes. Protein expression of HAS3 was increased in both *in vivo* and *in vitro* models, suggesting it induces VSMC osteogenic differentiation. Despite this increase in its protein expression, the outcome of knocking down HAS3 was unexpected. In our *in vitro* model, HAS3 knockdown led to an early increase (day 7) in both calcium deposition and osteogenic markers, followed by a lack of subsequent changes in calcium deposition or bone marker expression in the later time points. It is worth noting that HAS3 is a recognized critical regulator of HA coat and cables. This suggests a potential disruption in the delicate balance between HA coats and cables when HAS3 is suppressed. To gain deeper insights into the specific role of HAS3 in VSMC osteogenic differentiation, our future research endeavours will involve utilizing an *in vivo* model of HAS3-/- Vitamin K deficient mice.

The intricate relationship between inflammation and VC is not completely understood. Following our comparative analysis of VC in the media in both our *in vivo* and *in vitro* models, our focus shifted towards examining the influence inflammation and CKD in the arterial media. Our *in vivo* model in **Chapter 5** specifically mimic VC under conditions related to inflammation, as observed in CKD-related CVD. These unique *in vivo* models incorporated uraemia and uraemia coupled with induced peritoneal inflammation, providing a platform to explore VC in greater detail.

In these models, we observed a notable increase in HA expression, which stands in contrast to the dynamics of HA expression typically associated with Vitamin K model. This elevated HA expression was predominantly localized within the plaque regions of the arterial intima, aligning with prior research findings in arterial diseases, particularly atherosclerosis plaque,

where increased HA levels have been documented[405,437,438]. Remarkably, although the observations in the *in vivo* inflammation model differed from those in Vitamin K model, we identified striking similarities with our *in vitro* model induced with inflammatory cytokines, notably IL-6 and TGF-β1 in **Chapter 4**. These cytokines, while not inducing calcification directly, demonstrated the ability to stimulate markers associated with osteogenesis. Furthermore, our examination of the HAS profiles in both *in vivo* and *in vitro* models revealed a consistent pattern of exaggerated HAS expression under conditions of induced inflammation. This heightened expression of HAS isoenzymes aligns with previous research that has linked HAS1, HAS2, and HAS3 to the progression of atherosclerosis within the arterial intima[413,415,724]. The observation of increased HYAL2 expression in both our *in vivo* and *in vitro* models of inflammation represents a noteworthy departure from our findings in models of medial calcification. Given the limited exploration of HYAL's role in CVD progression within CKD patients, this discovery opens up a promising new avenue for further investigation. Similar to HA, TSG-6 was also present at the plaque sites in our study in **Chapter 5**. Prior studies have documented the presence of TSG-6 in atherosclerotic plaques[426,427]. Notably, in our uraemia model, we observed an increase in TSG-6 expression, followed by attenuation in the uraemia with added inflammation model. Previous studies show that TSG-6 may increase to counteract the progression of atherosclerosis and stabilize plaques[693]. However, it's worth noting that there is also evidence suggesting that high serum TSG-6 levels can serve as a biomarker for the severity of arterial diseases[725]. From previous data we know that TSG-6 is tightly controlled by growth factors and cytokines in VSMCs[358] which might explain the difference of expression between the *in vivo* models. We also observed contrasting expression of TSG-6 in our *in vitro* model of inflammation in **Chapter 4**, where TSG-6 expression was increased at day 21 when stimulated with TGF-β1, in contrast it showed attenuated expression when stimulated with IL-6 by day 21. This divergence requires further investigation to fully understand the regulatory mechanisms at play in different inflammatory contexts.

Shifting our attention to the HA-binding protein Versican, which has been emphasized as crucial in medial calcification models due to its association with HA cables, we observed a contrasting expression pattern in our *in vivo* model of inflammation in **Chapter 5**. The expression of Versican is attenuated in the *in vivo* models of inflammation. Intriguingly,

Versican was detected in the regions of the necrotic core along with HA, implying a potential connection with increased Versican deposition in areas associated with plaque development. Prior studies have provided insights into Versican's role in arterial diseases. It's been shown that Versican is prominent at the borders of lipid-filled necrotic cores and the plaque-thrombus interface, indicating its involvement in lipid accumulation and inflammation[726].

In summary **Figure 65**, our research demonstrates that HA and its associated proteins are downregulated as VSMCs undergo osteogenic transformation in medial VC models. The consistent findings observed both *in vivo* and *in vitro* models further support our conclusions, suggesting a shared mechanism governing HA changes during medial calcification. We propose that the formation of HA cables is a key driver in the differentiation of VSMCs into an osteogenic phenotype. Our focus on HAS3 and Versican, both associated with HA cable formation, reveals their upregulation during VSMC osteogenic transformation, highlighting them as critical targets in this process. In light of these findings, HA appears to play an inhibitory role in medial VC. To gain deeper insights into this inhibition, our next research step involves investigating the effects of 4MU in a Vitamin K deficient model and manipulating HAS3 and Versican in both *in vivo* and *in vitro* medial VC models. Furthermore, the alterations in HA exhibit variability in the intima and media, depending on the type of calcification. Notably, certain forms of HA in the media appear to have a protective effect, while consistently, in the intima, HA is associated with worsened disease. This underscores the necessity for a more profound comprehension of HA's interactions within these two distinct forms of calcification. In summary, our study serves as a bridge between *in vitro* and *in vivo* investigations, offering valuable insights into the intricate roles of HA and its related proteins in medial calcification and CKD-specific CVD.

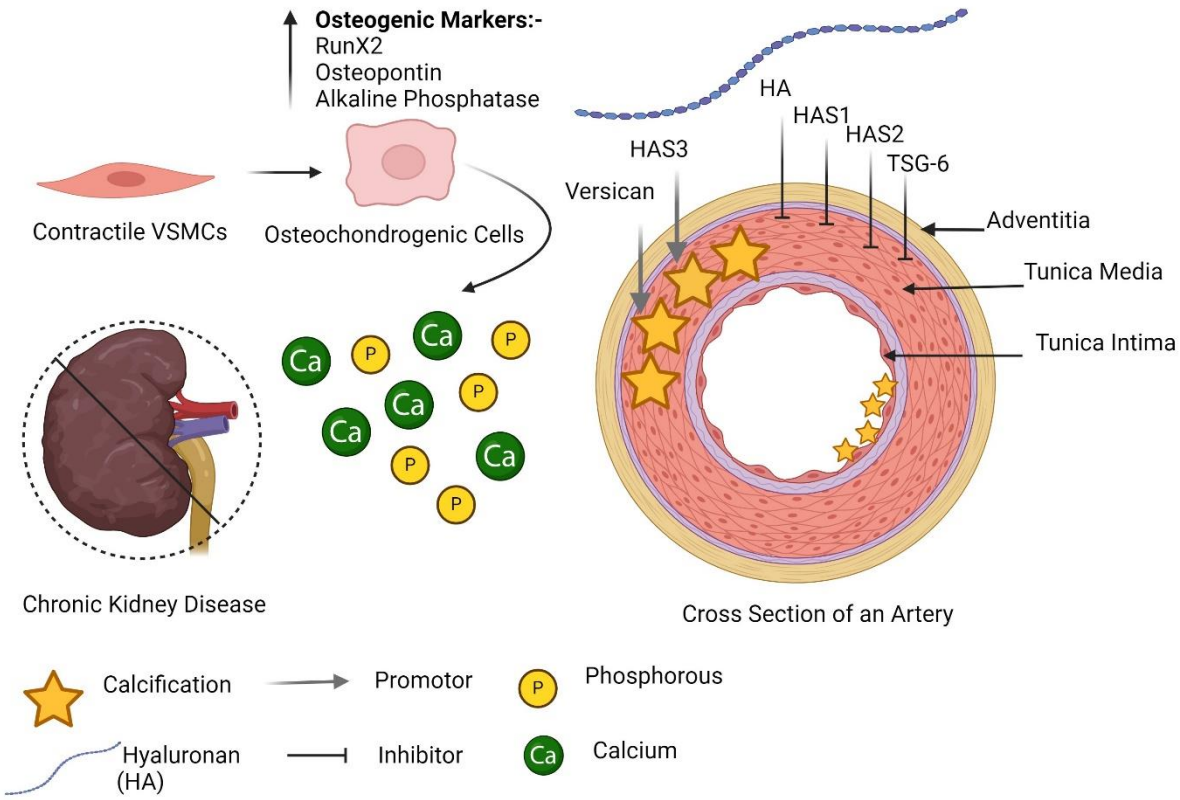

Figure 65 Key aspects of Vascular Calcification (VC) in chronic kidney disease (CKD) patients

In patients with chronic kidney disease (CKD), both medial and intimal calcification can occur. Dysfunction of the kidneys leads to the initiation of calcification, primarily mediated by the deposition of hydroxyapatite crystals in the matrix. This process is initiated by the influx of calcium (green) ions and phosphate (yellow) ions into vascular smooth muscle cells (VSMCs). In response, VSMCs undergo a phenotypic change from a contractile state to an osteochondrogenic cell type, accompanied by the upregulation of bone markers such as RunX2, Osteopontin, and Alkaline phosphatase. Hyaluronan (HA) present in the extracellular matrix plays a crucial role in regulating cell phenotype. Specifically, HA, along with the enzymes, HAS1 and HAS2, inhibits calcification in the medial layer. Conversely, HAS3, along with HA-binding proteins such as TSG-6 and Versican, modulates and influences the differentiation of VSMCs, potentially impacting calcification processes.

Reference

1. Hill NR, Fatoba ST, Oke JL, et al. Global Prevalence of Chronic Kidney Disease - A Systematic Review and Meta-Analysis. *PloS one*. 2016;11(7):e0158765-e0158765. doi:10.1371/journal.pone.0158765
2. Crews DC, Bello AK, Saadi G, et al. Burden, access and disparities in kidney disease. Editorial Material. *Clinical Kidney Journal*. Apr 2019;12(2):160-166. doi:10.1093/ckj/sfy128
3. Harris DCH, Davies SJ, Finkelstein FO, et al. Increasing access to integrated ESKD care as part of universal health coverage. Review. *Kidney International*. Apr 2019;95(4):S1-S33. doi:10.1016/j.kint.2018.12.005
4. Luyckx VA, Tonelli M, Stanifer JW. The global burden of kidney disease and the sustainable development goals. *Bulletin of the World Health Organization*. 2018;96(6):414-422D. doi:10.2471/BLT.17.206441
5. Wang HD, Naghavi M, Allen C, et al. Global, regional, and national life expectancy, all-cause mortality, and cause-specific mortality for 249 causes of death, 1980-2015: a systematic analysis for the Global Burden of Disease Study 2015. *Lancet*. Oct 2016;388(10053):1459-1544. doi:10.1016/s0140-6736(16)31012-1
6. Wright J, Hutchison A. Cardiovascular disease in patients with chronic kidney disease. *Vascular health and risk management*. 2009;5:713-722. doi:10.2147/vhrm.s6206
7. Bagshaw SM, Cruz DN, Aspromonte N, et al. Epidemiology of cardio-renal syndromes: workgroup statements from the 7th ADQI Consensus Conference. *Nephrology Dialysis Transplantation*. 2010;25(5):1406-1416. doi:10.1093/ndt/gfq066
8. Segall L, Nistor I, Covic A. Heart Failure in Patients with Chronic Kidney Disease: A Systematic Integrative Review. *BioMed Research International*. 2014/05/15 2014;2014:937398. doi:10.1155/2014/937398
9. Foley RN, Parfrey PS, Sarnak MJ. Clinical epidemiology of cardiovascular disease in chronic renal disease. *American Journal of Kidney Diseases*. Nov 1998;32(5):S112-S119. doi:10.1053/ajkd.1998.v32.pm9820470
10. Garimella PS, Sarnak MJ. Cardiovascular disease in CKD in 2012: moving forward, slowly but surely. *Nat Rev Nephrol*. Feb 2013;9(2):69-70. doi:10.1038/nrneph.2012.285
11. Stevens PE, Levin A. Evaluation and management of chronic kidney disease: synopsis of the kidney disease: improving global outcomes 2012 clinical practice guideline. *Ann Intern Med*. Jun 4 2013;158(11):825-30. doi:10.7326/0003-4819-158-11-201306040-00007
12. K/DOQI clinical practice guidelines for chronic kidney disease: evaluation, classification, and stratification. *Am J Kidney Dis*. Feb 2002;39(2 Suppl 1):S1-266.
13. Levey AS, de Jong PE, Coresh J, et al. The definition, classification, and prognosis of chronic kidney disease: a KDIGO Controversies Conference report. *Kidney Int*. 2011:17-28. vol. 1.
14. Wang YN, Ma SX, Chen YY, et al. Chronic kidney disease: Biomarker diagnosis to therapeutic targets. *Clin Chim Acta*. Dec 2019;499:54-63. doi:10.1016/j.cca.2019.08.030
15. Webster AC, Nagler EV, Morton RL, Masson P. Chronic Kidney Disease. *Lancet*. Mar 25 2017;389(10075):1238-1252. doi:10.1016/s0140-6736(16)32064-5
16. Fathallah-Shaykh SA. Proteinuria and progression of pediatric chronic kidney disease: lessons from recent clinical studies. *Pediatr Nephrol*. May 2017;32(5):743-751. doi:10.1007/s00467-016-3448-8
17. Lin HY, Niu SW, Kuo IC, et al. Hematuria and Renal Outcomes in Patients With Diabetic Chronic KidneyDisease. *Am J Med Sci*. Sep 2018;356(3):268-276. doi:10.1016/j.amjms.2018.06.005
18. Andrassy KM. Comments on 'KDIGO 2012 clinical practice guideline for the evaluation and management of chronic kidney disease'. *Kidney International*. Sep 2013;84(3):622-623. doi:10.1038/ki.2013.243

19. Bailie GR, Uhlig K, Levey AS. Clinical practice guidelines in nephrology: Evaluation, classification, and stratification of chronic kidney disease. Article. *Pharmacotherapy*. Apr 2005;25(4):491-502. doi:10.1592/phco.25.4.491.61034
20. Valdivielso José M, Rodríguez-Puyol D, Pascual J, et al. Atherosclerosis in Chronic Kidney Disease. *Arteriosclerosis, Thrombosis, and Vascular Biology*. 2019/10/01 2019;39(10):1938-1966. doi:10.1161/ATVBAHA.119.312705
21. Sharples E, Casula A, Byrne C. UK Renal Registry 19th Annual Report: Chapter 3 Demographic and Biochemistry Profile of Kidney Transplant Recipients in the UK in 2015: National and Centre-specific Analyses. *Nephron*. 09/01 2017;137:73-102. doi:10.1159/000481365
22. Berger JR, Jaikaransingh V, Hedayati SS. End-Stage Kidney Disease in the Elderly: Approach to Dialysis Initiation, Choosing Modality, and Predicting Outcomes. *Advances in Chronic Kidney Disease*. Jan 2016;23(1):36-43. doi:10.1053/j.ackd.2015.08.005
23. Wilkie M. Choosing Dialysis Modality-Patient Choice or Physician Bias? *Peritoneal Dialysis International*. Jul-Aug 2016;36(4):357-358. doi:10.3747/pdi.2016.00073
24. Abecassis M, Bartlett ST, Collins AJ, et al. Kidney transplantation as primary therapy for end-stage renal disease: A National Kidney Foundation/Kidney Disease Outcomes Quality Initiative (NKF/KDOQI (TM)) conference. *Clinical Journal of the American Society of Nephrology*. Mar 2008;3(2):471-480. doi:10.2215/cjn.05021107
25. Garcia GG, Harden P, Chapman J, World Kidney Day Steering C. The Global Role of Kidney Transplantation. *Nephrology Dialysis Transplantation*. Aug 2013;28(8):E1-E5. doi:10.1093/ndt/gfs013
26. Cianciolo G, Capelli I, Angelini ML, et al. Importance of Vascular Calcification in Kidney Transplant Recipients. *American Journal of Nephrology*. 2014;39(5):418-426. doi:10.1159/000362492
27. Kramer A, Pippias M, Noordzij M, et al. The European Renal Association - European Dialysis and Transplant Association (ERA-EDTA) Registry Annual Report 2016: a summary. Article. *Clinical Kidney Journal*. Oct 2019;12(5):702-720. doi:10.1093/ckj/sfz011
28. Nongnuch A, Assanatham M, Panorchan K, Davenport A. Strategies for preserving residual renal function in peritoneal dialysis patients. *Clinical kidney journal*. 2015;8(2):202-211. doi:10.1093/ckj/sfu140
29. Chanouzas D, Ng KP, Fallouh B, Baharani J. What influences patient choice of treatment modality at the pre-dialysis stage? *Nephrol Dial Transplant*. Apr 2012;27(4):1542-7. doi:10.1093/ndt/gfr452
30. Stack AG. Determinants of modality selection among incident US dialysis patients: results from a national study. *J Am Soc Nephrol*. May 2002;13(5):1279-87.
31. Vonesh EF, Snyder JJ, Foley RN, Collins AJ. Mortality studies comparing peritoneal dialysis and hemodialysis: What do they tell us? *Kidney International*. Nov 2006;70:S3-S11. doi:10.1038/sj.ki.5001910
32. Briggs V, Pitcher D, Braddon F, Fogarty D, Wilkie M. UK Renal Registry 15th annual report: Chapter 8 UK multisite peritoneal dialysis access catheter audit for first PD catheters 2011. *Nephron Clinical Practice*. 2013;123(Suppl. 1):165-181.
33. Renal A. UK Renal Registry: 21st annual report. Bristol; 2019.
34. El Shamy O, Sharma S, Winston J, Uribarri J. Peritoneal Dialysis During the Coronavirus 2019 (COVID-19) Pandemic: Acute Inpatient and Maintenance Outpatient Experiences. *Kidney Med*. 2020.
35. Yung S, Chan TM. Preventing peritoneal fibrosis - Insights from the laboratory. *Peritoneal Dialysis International*. 2003;23:S37-S41.
36. Lima SMA, Otoni A, Sabino AD, et al. Inflammation, neoangiogenesis and fibrosis in peritoneal dialysis. *Clinica Chimica Acta*. Jun 2013;421:46-50. doi:10.1016/j.cca.2013.02.027
37. Mou X, Zhou DY, Ma JR, et al. Serum TGF-β1 as a Biomarker for Type 2 Diabetic Nephropathy: A Meta-Analysis of Randomized Controlled Trials. *PLoS One*. 2016;11(2):e0149513. doi:10.1371/journal.pone.0149513

38. Podolec J, Baran J, Siedlinski M, et al. Serum rantes, transforming growth factor-β1 and interleukin-6 levels correlate with cardiac muscle fibrosis in patients with aortic valve stenosis. *J Physiol Pharmacol*. Aug 2018;69(4)doi:10.26402/jpp.2018.4.12
39. López-Hernández FJ, López-Novoa JM. Role of TGF-β in chronic kidney disease: an integration of tubular, glomerular and vascular effects. *Cell Tissue Res*. Jan 2012;347(1):141-54. doi:10.1007/s00441-011-1275-6
40. Loeffler I, Wolf G. Transforming growth factor-β and the progression of renal disease. *Nephrology Dialysis Transplantation*. 2014;29(suppl_1):i37-i45. doi:10.1093/ndt/gft267
41. Su H, Lei C-T, Zhang C. Interleukin-6 Signaling Pathway and Its Role in Kidney Disease: An Update. *Frontiers in immunology*. 2017;8:405-405. doi:10.3389/fimmu.2017.00405
42. Barreto DV, Barreto FC, Liabeuf S, et al. Plasma interleukin-6 is independently associated with mortality in both hemodialysis and pre-dialysis patients with chronic kidney disease. *Kidney International*. 2010/03/02/ 2010;77(6):550-556. doi:https://doi.org/10.1038/ki.2009.503
43. Magno AL, Herat LY, Carnagarin R, Schlaich MP, Matthews VB. Current Knowledge of IL-6 Cytokine Family Members in Acute and Chronic Kidney Disease. *Biomedicines*. 2019;7(1):19. doi:10.3390/biomedicines7010019
44. Fernandes N, Bastos MG, Cassi HV, et al. The Brazilian Peritoneal Dialysis Multicenter Study (BRAZPD) : characterization of the cohort. *Kidney Int Suppl*. Apr 2008;(108):S145-51. doi:10.1038/sj.ki.5002616
45. Liu M, Li XC, Lu L, et al. Cardiovascular disease and its relationship with chronic kidney disease. *Eur Rev Med Pharmacol Sci*. Oct 2014;18(19):2918-26.
46. Glassock RJ, Pecoits-Filho R, Barberato SH. Left ventricular mass in chronic kidney disease and ESRD. *Clin J Am Soc Nephrol*. Dec 2009;4 Suppl 1:S79-91. doi:10.2215/cjn.04860709
47. Heywood JT, Fonarow GC, Costanzo MR, Mathur VS, Wigneswaran JR, Wynne J. High prevalence of renal dysfunction and its impact on outcome in 118,465 patients hospitalized with acute decompensated heart failure: a report from the ADHERE database. *J Card Fail*. Aug 2007;13(6):422-30. doi:10.1016/j.cardfail.2007.03.011
48. Anavekar NS, McMurray JJ, Velazquez EJ, et al. Relation between renal dysfunction and cardiovascular outcomes after myocardial infarction. *N Engl J Med*. Sep 23 2004;351(13):1285-95. doi:10.1056/NEJMoa041365
49. Tonelli M, Muntner P, Lloyd A, et al. Risk of coronary events in people with chronic kidney disease compared with those with diabetes: a population-level cohort study. *Lancet*. Sep 1 2012;380(9844):807-14. doi:10.1016/s0140-6736(12)60572-8
50. Latif F, Kleiman NS, Cohen DJ, et al. In-hospital and 1-year outcomes among percutaneous coronary intervention patients with chronic kidney disease in the era of drug-eluting stents: a report from the EVENT (Evaluation of Drug Eluting Stents and Ischemic Events) registry. *JACC Cardiovasc Interv*. Jan 2009;2(1):37-45. doi:10.1016/j.jcin.2008.06.012
51. Roghi A, Savonitto S, Cavallini C, et al. Impact of acute renal failure following percutaneous coronary intervention on long-term mortality. *J Cardiovasc Med (Hagerstown)*. Apr 2008;9(4):375-81. doi:10.2459/JCM.0b013e3282eee979
52. Waheed S, Matsushita K, Sang Y, et al. Combined association of albuminuria and cystatin C-based estimated GFR with mortality, coronary heart disease, and heart failure outcomes: the Atherosclerosis Risk in Communities (ARIC) Study. *Am J Kidney Dis*. Aug 2012;60(2):207-16. doi:10.1053/j.ajkd.2012.03.011
53. Gracia M, Betriu À, Martínez-Alonso M, et al. Predictors of Subclinical Atheromatosis Progression over 2 Years in Patients with Different Stages of CKD. *Clin J Am Soc Nephrol*. Feb 5 2016;11(2):287-96. doi:10.2215/cjn.01240215
54. Attman PO, Samuelsson O. Dyslipidemia of kidney disease. *Curr Opin Lipidol*. Aug 2009;20(4):293-9. doi:10.1097/MOL.0b013e32832dd832

55. McCullough PA, Agrawal V, Danielewicz E, Abela GS. Accelerated atherosclerotic calcification and Monckeberg's sclerosis: a continuum of advanced vascular pathology in chronic kidney disease. *Clin J Am Soc Nephrol*. Nov 2008;3(6):1585-98. doi:10.2215/cjn.01930408
56. Karwowski W, Naumnik B, Szczepański M, Myśliwiec M. The mechanism of vascular calcification - a systematic review. *Med Sci Monit*. Jan 2012;18(1):Ra1-11. doi:10.12659/msm.882181
57. K/DOQI clinical practice guidelines for cardiovascular disease in dialysis patients. *Am J Kidney Dis*. Apr 2005;45(4 Suppl 3):S1-153.
58. Palmer SC, Gardner S, Tonelli M, et al. Phosphate-binding agents in adults with CKD: a network meta-analysis of randomized trials. *American Journal of Kidney Diseases*. 2016;68(5):691-702.
59. Amann K, Wiest G, Zimmer G, Gretz N, Ritz E, Mall G. Reduced capillary density in the myocardium of uremic rats--a stereological study. *Kidney Int*. Nov 1992;42(5):1079-85. doi:10.1038/ki.1992.390
60. Bro S, Bentzon JF, Falk E, Andersen CB, Olgaard K, Nielsen LB. Chronic renal failure accelerates atherogenesis in apolipoprotein E-deficient mice. *J Am Soc Nephrol*. Oct 2003;14(10):2466-74. doi:10.1097/01.asn.0000088024.72216.2e
61. Massy ZA, Ivanovski O, Nguyen-Khoa T, et al. Uremia accelerates both atherosclerosis and arterial calcification in apolipoprotein E knockout mice. *J Am Soc Nephrol*. Jan 2005;16(1):109-16. doi:10.1681/asn.2004060495
62. Coresh J, Longenecker JC, Young HJ, Klag MJ. Epidemiology of cardiovascular risk factors in chronic renal disease. *Journal of the American Society of Nephrology: JASN*. 1998;9(12 Suppl):S24-30.
63. van Dokkum RP, Eijkelkamp WB, Kluppel AC, et al. Myocardial infarction enhances progressive renal damage in an experimental model for cardio-renal interaction. *J Am Soc Nephrol*. Dec 2004;15(12):3103-10. doi:10.1097/01.asn.0000145895.62896.98
64. Raine AE, Seymour AM, Roberts AF, Radda GK, Ledingham JG. Impairment of cardiac function and energetics in experimental renal failure. *J Clin Invest*. Dec 1993;92(6):2934-40. doi:10.1172/jci116916
65. Amann K, Neusüss R, Ritz E, Irzyniec T, Wiest G, Mall G. Changes of vascular architecture independent of blood pressure in experimental uremia. *Am J Hypertens*. Apr 1995;8(4 Pt 1):409-17. doi:10.1016/0895-7061(94)00248-a
66. Stein EA, Raal F. Future Directions to Establish Lipoprotein(a) as a Treatment for Atherosclerotic Cardiovascular Disease. *Cardiovascular Drugs and Therapy*. 2016/02/01 2016;30(1):101-108. doi:10.1007/s10557-016-6654-5
67. Miao B, Hernandez AV, Alberts MJ, Mangiafico N, Roman YM, Coleman CI. Incidence and Predictors of Major Adverse Cardiovascular Events in Patients With Established Atherosclerotic Disease or Multiple Risk Factors. *Journal of the American Heart Association*. 2020/01/21 2020;9(2):e014402. doi:10.1161/JAHA.119.014402
68. Schantl AE, Ivarsson ME, Leroux J-C. Investigational Pharmacological Treatments for Vascular Calcification. *Advanced Therapeutics*. 2019/01/01 2019;2(1):1800094. doi:https://doi.org/10.1002/adtp.201800094
69. Gourgas O, Marulanda J, Zhang P, Murshed M, Cerruti M. Multidisciplinary Approach to Understand Medial Arterial Calcification. *Arteriosclerosis, Thrombosis, and Vascular Biology*. 2018/02/01 2018;38(2):363-372. doi:10.1161/ATVBAHA.117.309808
70. Wu B, Elmariah S, Kaplan FS, Cheng G, Mohler Iii ER. Paradoxical effects of statins on aortic valve myofibroblasts and osteoblasts: implications for end-stage valvular heart disease. *Arteriosclerosis, thrombosis, and vascular biology*. 2005;25(3):592-597.
71. Osman L, Yacoub MH, Latif N, Amrani M, Chester AH. Role of human valve interstitial cells in valve calcification and their response to atorvastatin. *Circulation*. 2006;114(1_supplement):I-547.
72. Rajamannan NM, Subramaniam M, Stock SR, et al. Atorvastatin inhibits calcification and enhances nitric oxide synthase production in the hypercholesterolaemic aortic valve. *Heart*. 2005;91(6):806-810.

73. Rajamannan NM, Subramaniam M, Springett M, et al. Atorvastatin inhibits hypercholesterolemia-induced cellular proliferation and bone matrix production in the rabbit aortic valve. *Circulation*. 2002;105(22):2660-2665.
74. Caira FC, Stock SR, Gleason TG, et al. Human degenerative valve disease is associated with up-regulation of low-density lipoprotein receptor-related protein 5 receptor-mediated bone formation. *Journal of the American College of Cardiology*. 2006;47(8):1707-1712.
75. Moura LM, Ramos SF, Zamorano JL, et al. Rosuvastatin affecting aortic valve endothelium to slow the progression of aortic stenosis. *Journal of the American College of Cardiology*. 2007;49(5):554-561.
76. Cowell SJ, Newby DE, Prescott RJ, et al. A randomized trial of intensive lipid-lowering therapy in calcific aortic stenosis. *New England Journal of Medicine*. 2005;352(23):2389-2397.
77. Rossebo AB, Pedersen TR, Boman K, et al. Gohlke-390 Barwolf C, Holme I, Kesaniemi YA, Malbecq W, Nienaber CA, Ray S, Skjaerpe T, Wachtell 391 K, Willenheimer R. Intensive lipid lowering with simvastatin and ezetimibe in aortic stenosis. *N Engl J Med*. 2008;359:1343-1356.
78. Tsai PH, Chung CH, Chien WC, Chu P. Effects of calcium-containing phosphate binders on cardiovascular events and mortality in predialysis CKD stage 5 patients. *PLoS One*. 2020;15(10):e0241435. doi:10.1371/journal.pone.0241435
79. Moe SM. Attenuating Progression of Cardiovascular Calcification Due to Hemodialysis Treatment in ESRD Patients: Vascular Calcification. 2020.
80. Blacher J, Guerin AP, Pannier B, Marchais SJ, London GM. Arterial calcifications, arterial stiffness, and cardiovascular risk in end-stage renal disease. *Hypertension*. Oct 2001;38(4):938-42. doi:10.1161/hy1001.096358
81. Neven E, D'Haese PC. Vascular Calcification in Chronic Renal Failure. *Circulation Research*. 2011/01/21 2011;108(2):249-264. doi:10.1161/CIRCRESAHA.110.225904
82. Paloian NJ, Giachelli CM. A current understanding of vascular calcification in CKD. *American Journal of Physiology-Renal Physiology*. Oct 2014;307(8):F891-F900. doi:10.1152/ajprenal.00163.2014
83. Davies MR, Hruska KA. Pathophysiological mechanisms of vascular calcification in end-stage renal disease. *Kidney International*. Aug 2001;60(2):472-479. doi:10.1046/j.1523-1755.2001.060002472.x
84. Wada T, McKee MD, Steitz S, Giachelli CM. Calcification of vascular smooth muscle cell cultures inhibition by osteopontin. *Circulation Research*. Feb 1999;84(2):166-178. doi:10.1161/01.res.84.2.166
85. Chertow GM, Block GA, Correa-Rotter R, et al. Effect of Cinacalcet on Cardiovascular Disease in Patients Undergoing Dialysis. *New England Journal of Medicine*. Dec 2012;367(26):2482-2494. doi:10.1056/NEJMoa1205624
86. Edmonds ME. Medial arterial calcification and diabetes mellitus. *Z Kardiol*. 2000;89 Suppl 2:101-4. doi:10.1007/s003920070107
87. Covic A, Kanbay M, Voroneanu L, et al. Vascular calcification in chronic kidney disease. *Clin Sci (Lond)*. Apr 28 2010;119(3):111-21. doi:10.1042/cs20090631
88. Dai L, Qureshi AR, Witasp A, Lindholm B, Stenvinkel P. Early Vascular Ageing and Cellular Senescence in Chronic Kidney Disease. *Comput Struct Biotechnol J*. 2019;17:721-729. doi:10.1016/j.csbj.2019.06.015
89. Blumenthal HT, Lansing AI, Wheeler PA. Calcification of the Media of the Human Aorta and Its Relation to Intimal Arteriosclerosis, Ageing and Disease. *Am J Pathol*. Jul 1944;20(4):665-87.
90. Giachelli CM. Vascular calcification mechanisms. *J Am Soc Nephrol*. Dec 2004;15(12):2959-64. doi:10.1097/01.asn.0000145894.57533.c4
91. Clarke MC, Littlewood TD, Figg N, et al. Chronic apoptosis of vascular smooth muscle cells accelerates atherosclerosis and promotes calcification and medial degeneration. *Circ Res*. Jun 20 2008;102(12):1529-38. doi:10.1161/circresaha.108.175976

92. Shioi A, Ikari Y. Plaque Calcification During Atherosclerosis Progression and Regression. *J Atheroscler Thromb*. Apr 1 2018;25(4):294-303. doi:10.5551/jat.RV17020
93. Greenland P, Bonow RO, Brundage BH, et al. ACCF/AHA 2007 clinical expert consensus document on coronary artery calcium scoring by computed tomography in global cardiovascular risk assessment and in evaluation of patients with chest pain: a report of the American College of Cardiology Foundation Clinical Expert Consensus Task Force (ACCF/AHA Writing Committee to Update the 2000 Expert Consensus Document on Electron Beam Computed Tomography) developed in collaboration with the Society of Atherosclerosis Imaging and Prevention and the Society of Cardiovascular Computed Tomography. *J Am Coll Cardiol*. Jan 23 2007;49(3):378-402. doi:10.1016/j.jacc.2006.10.001
94. Terry JG, Carr JJ, Kouba EO, et al. Effect of simvastatin (80 mg) on coronary and abdominal aortic arterial calcium (from the coronary artery calcification treatment with zocor [CATZ] study). *Am J Cardiol*. Jun 15 2007;99(12):1714-7. doi:10.1016/j.amjcard.2007.01.060
95. Räber L, Taniwaki M, Zaugg S, et al. Effect of high-intensity statin therapy on atherosclerosis in non-infarct-related coronary arteries (IBIS-4): a serial intravascular ultrasonography study. *Eur Heart J*. Feb 21 2015;36(8):490-500. doi:10.1093/eurheartj/ehu373
96. Chen Z, Qureshi AR, Parini P, et al. Does statins promote vascular calcification in chronic kidney disease? *Eur J Clin Invest*. Feb 2017;47(2):137-148. doi:10.1111/eci.12718
97. Stary HC. Natural history of calcium deposits in atherosclerosis progression and regression. *Z Kardiol*. 2000;89 Suppl 2:28-35. doi:10.1007/s003920070097
98. Ehara S, Kobayashi Y, Yoshiyama M, et al. Spotty calcification typifies the culprit plaque in patients with acute myocardial infarction: an intravascular ultrasound study. *Circulation*. 2004;110(22):3424-3429.
99. Criqui MH, Knox JB, Denenberg JO, et al. Coronary Artery Calcium Volume and Density: Potential Interactions and Overall Predictive Value: The Multi-Ethnic Study of Atherosclerosis. *JACC Cardiovasc Imaging*. Aug 2017;10(8):845-854. doi:10.1016/j.jcmg.2017.04.018
100. Li ZY, Howarth S, Tang T, Graves M, J UK-I, Gillard JH. Does calcium deposition play a role in the stability of atheroma? Location may be the key. *Cerebrovasc Dis*. 2007;24(5):452-9. doi:10.1159/000108436
101. Gimbrone MA, Jr., García-Cardeña G. Endothelial Cell Dysfunction and the Pathobiology of Atherosclerosis. *Circ Res*. Feb 19 2016;118(4):620-36. doi:10.1161/circresaha.115.306301
102. Hadi HAR, Carr CS, Al Suwaidi J. Endothelial dysfunction: cardiovascular risk factors, therapy, and outcome. *Vascular health and risk management*. 2005;1(3):183-198.
103. Iyemere VP, Proudfoot D, Weissberg PL, Shanahan CM. Vascular smooth muscle cell phenotypic plasticity and the regulation of vascular calcification. Review. *Journal of Internal Medicine*. Sep 2006;260(3):192-210. doi:10.1111/j.1365-2796.2006.01692.x
104. Adeney KL, Siscovick DS, Ix JH, et al. Association of Serum Phosphate with Vascular and Valvular Calcification in Moderate CKD. *Journal of the American Society of Nephrology*. Feb 2009;20(2):381-387. doi:10.1681/asn.2008040349
105. Marreiros C, Viegas C, Simes D. Targeting a Silent Disease: Vascular Calcification in Chronic Kidney Disease. *International Journal of Molecular Sciences*. 2022;23(24). doi:10.3390/ijms232416114
106. Tyson J, Bundy K, Roach C, et al. Mechanisms of the Osteogenic Switch of Smooth Muscle Cells in Vascular Calcification: WNT Signaling, BMPs, Mechanotransduction, and EndMT. *Bioengineering (Basel)*. Aug 6 2020;7(3)doi:10.3390/bioengineering7030088
107. Byon CH, Javed A, Dai Q, et al. Oxidative stress induces vascular calcification through modulation of the osteogenic transcription factor Runx2 by AKT signaling. *J Biol Chem*. May 30 2008;283(22):15319-27. doi:10.1074/jbc.M800021200
108. Wu M, Rementer C, Giachelli CM. Vascular calcification: an update on mechanisms and challenges in treatment. *Calcified tissue international*. 2013;93:365-373.

109. Brini M, Ottolini D, Calì T, Carafoli E. Calcium in health and disease. *Met Ions Life Sci*. 2013;13:81-137. doi:10.1007/978-94-007-7500-8_4
110. Nordin BE. Calcium and osteoporosis. *Nutrition*. Jul-Aug 1997;13(7-8):664-86. doi:10.1016/s0899-9007(97)83011-0
111. Jono S, Nishizawa Y, Shioi A, Morii H. 1,25-Dihydroxyvitamin D3 Increases In Vitro Vascular Calcification by Modulating Secretion of Endogenous Parathyroid Hormone–Related Peptide. *Circulation*. 1998/09/29 1998;98(13):1302-1306. doi:10.1161/01.CIR.98.13.1302
112. Copp DH. Calcium and phosphorus metabolism. *Am J Med*. Feb 1957;22(2):275-85. doi:10.1016/0002-9343(57)90011-6
113. Moe SM, Chen NX. Mechanisms of vascular calcification in chronic kidney disease. *J Am Soc Nephrol*. Feb 2008;19(2):213-6. doi:10.1681/asn.2007080854
114. Steitz SA, Speer MY, Curinga G, et al. Smooth muscle cell phenotypic transition associated with calcification: upregulation of Cbfa1 and downregulation of smooth muscle lineage markers. *Circ Res*. Dec 7 2001;89(12):1147-54. doi:10.1161/hh2401.101070
115. Proudfoot D, Skepper JN, Shanahan CM, Weissberg PL. Calcification of human vascular cells in vitro is correlated with high levels of matrix Gla protein and low levels of osteopontin expression. *Arterioscler Thromb Vasc Biol*. Mar 1998;18(3):379-88. doi:10.1161/01.atv.18.3.379
116. Coll B, Betriu A, Martínez-Alonso M, et al. Large Artery Calcification on Dialysis Patients Is Located in the Intima and Related to Atherosclerosis. *Clinical Journal of the American Society of Nephrology*. 2011;6(2):303. doi:10.2215/CJN.04290510
117. Wilson PWF, Kauppila LI, O'Donnell CJ, et al. Abdominal aortic calcific deposits are an important predictor of vascular morbidity and mortality. *Circulation*. Mar 2001;103(11):1529-1534. doi:10.1161/01.cir.103.11.1529
118. Abou-Hassan N, Tantisattamo E, D'Orsi ET, O'Neill WC. The clinical significance of medial arterial calcification in end-stage renal disease in women. *Kidney International*. Jan 2015;87(1):195-199. doi:10.1038/ki.2014.187
119. McCarty MF, DiNicolantonio JJ. The Molecular Biology and Pathophysiology of Vascular Calcification. Article. *Postgraduate Medicine*. Mar 2014;126(2):54-64. doi:10.3810/pgm.2014.03.2740
120. Thompson GR, Partridge J. Coronary calcification score: the coronary-risk impact factor. *Lancet*. Feb 14 2004;363(9408):557-9. doi:10.1016/s0140-6736(04)15544-x
121. Detrano R, Guerci AD, Carr JJ, et al. Coronary calcium as a predictor of coronary events in four racial or ethnic groups. *N Engl J Med*. Mar 27 2008;358(13):1336-45. doi:10.1056/NEJMoa072100
122. Rennenberg RJ, Kessels AG, Schurgers LJ, van Engelshoven JM, de Leeuw PW, Kroon AA. Vascular calcifications as a marker of increased cardiovascular risk: a meta-analysis. *Vasc Health Risk Manag*. 2009;5(1):185-97. doi:10.2147/vhrm.s4822
123. Ferro CJ, Chue CD, Steeds RP, Townend JN. Is lowering phosphate exposure the key to preventing arterial stiffening with age? *Heart*. Nov 2009;95(21):1770-2. doi:10.1136/hrt.2008.162594
124. Fox CS, Vasan RS, Parise H, et al. Mitral annular calcification predicts cardiovascular morbidity and mortality: the Framingham Heart Study. *Circulation*. Mar 25 2003;107(11):1492-6. doi:10.1161/01.cir.0000058168.26163.bc
125. Fox CS, Parise H, Vasan RS, et al. Mitral annular calcification is a predictor for incident atrial fibrillation. *Atherosclerosis*. Apr 2004;173(2):291-4. doi:10.1016/j.atherosclerosis.2003.12.018
126. Potpara TS, Vasiljevic ZM, Vujisic-Tesic BD, et al. Mitral annular calcification predicts cardiovascular morbidity and mortality in middle-aged patients with atrial fibrillation: the Belgrade Atrial Fibrillation Study. *Chest*. Oct 2011;140(4):902-910. doi:10.1378/chest.10-2963
127. De Marco M, Gerdts E, Casalnuovo G, et al. Mitral annular calcification and incident ischemic stroke in treated hypertensive patients: the LIFE study. *Am J Hypertens*. Apr 2013;26(4):567-73. doi:10.1093/ajh/hps082

128. Singh DK, Winocour P, Summerhayes B, et al. Prevalence and progression of peripheral vascular calcification in type 2 diabetes subjects with preserved kidney function. *Diabetes Res Clin Pract*. Jul 2012;97(1):158-65. doi:10.1016/j.diabres.2012.01.038
129. Reynolds JL, Joannides AJ, Skepper JN, et al. Human vascular smooth muscle cells undergo vesicle-mediated calcification in response to changes in extracellular calcium and phosphate concentrations: a potential mechanism for accelerated vascular calcification in ESRD. *J Am Soc Nephrol*. Nov 2004;15(11):2857-67. doi:10.1097/01.asn.0000141960.01035.28
130. Vervloet M, Cozzolino M. Vascular calcification in chronic kidney disease: different bricks in the wall? *Kidney Int*. Apr 2017;91(4):808-817. doi:10.1016/j.kint.2016.09.024
131. Raposo G, Stoorvogel W. Extracellular vesicles: exosomes, microvesicles, and friends. *J Cell Biol*. Feb 18 2013;200(4):373-83. doi:10.1083/jcb.201211138
132. Schurgers LJ, Akbulut AC, Kaczor DM, Halder M, Koenen RR, Kramann R. Initiation and Propagation of Vascular Calcification Is Regulated by a Concert of Platelet- and Smooth Muscle Cell-Derived Extracellular Vesicles. 10.3389/fcvm.2018.00036. *Frontiers in Cardiovascular Medicine*. 2018;5:36.
133. Shroff RC, Shanahan CM. VASCULAR CALCIFICATION IN PATIENTS WITH KIDNEY DISEASE: The Vascular Biology of Calcification. *Seminars in Dialysis*. 2007/03/01 2007;20(2):103-109. doi:10.1111/j.1525-139X.2007.00255.x
134. Jahnen-Dechent W, Heiss A, Schäfer C, Ketteler M. Fetuin-A regulation of calcified matrix metabolism. *Circ Res*. Jun 10 2011;108(12):1494-509. doi:10.1161/circresaha.110.234260
135. Schurgers LJ, Uitto J, Reutelingsperger CP. Vitamin K-dependent carboxylation of matrix Gla-protein: a crucial switch to control ectopic mineralization. *Trends Mol Med*. Apr 2013;19(4):217-26. doi:10.1016/j.molmed.2012.12.008
136. Köppert S, Büscher A, Babler A, et al. Cellular Clearance and Biological Activity of Calciprotein Particles Depend on Their Maturation State and Crystallinity. *Front Immunol*. 2018;9:1991. doi:10.3389/fimmu.2018.01991
137. Schinke T, Amendt C, Trindl A, Pöschke O, Müller-Esterl W, Jahnen-Dechent W. The serum protein alpha2-HS glycoprotein/fetuin inhibits apatite formation in vitro and in mineralizing calvaria cells. A possible role in mineralization and calcium homeostasis. *J Biol Chem*. Aug 23 1996;271(34):20789-96. doi:10.1074/jbc.271.34.20789
138. Schafer C, Heiss A, Schwarz A, et al. The serum protein alpha 2-Heremans-Schmid glycoprotein/fetuin-A is a systemically acting inhibitor of ectopic calcification. *J Clin Invest*. Aug 2003;112(3):357-66. doi:10.1172/jci17202
139. Ketteler M, Bongartz P, Westenfeld R, et al. Association of low fetuin-A (AHSG) concentrations in serum with cardiovascular mortality in patients on dialysis: a cross-sectional study. *Lancet*. Mar 8 2003;361(9360):827-33. doi:10.1016/s0140-6736(03)12710-9
140. Luo G, Ducy P, McKee MD, et al. Spontaneous calcification of arteries and cartilage in mice lacking matrix GLA protein. *Nature*. Mar 6 1997;386(6620):78-81. doi:10.1038/386078a0
141. Schurgers LJ, Joosen IA, Laufer EM, et al. Vitamin K-antagonists accelerate atherosclerotic calcification and induce a vulnerable plaque phenotype. *PLoS One*. 2012;7(8):e43229. doi:10.1371/journal.pone.0043229
142. Yao Y, Bennett BJ, Wang X, et al. Inhibition of bone morphogenetic proteins protects against atherosclerosis and vascular calcification. *Circ Res*. Aug 20 2010;107(4):485-94. doi:10.1161/circresaha.110.219071
143. Tanimura A, McGregor DH, Anderson HC. Matrix vesicles in atherosclerotic calcification. *Proc Soc Exp Biol Med*. Feb 1983;172(2):173-7. doi:10.3181/00379727-172-41542
144. Shanahan CM, Cary NR, Metcalfe JC, Weissberg PL. High expression of genes for calcification-regulating proteins in human atherosclerotic plaques. *J Clin Invest*. Jun 1994;93(6):2393-402. doi:10.1172/jci117246

145. Naik V, Leaf EM, Hu JH, et al. Sources of cells that contribute to atherosclerotic intimal calcification: an in vivo genetic fate mapping study. *Cardiovasc Res*. Jun 1 2012;94(3):545-54. doi:10.1093/cvr/cvs126
146. Block GA. Prevalence and clinical consequences of elevated Ca x P product in hemodialysis patients. *Clin Nephrol*. Oct 2000;54(4):318-24.
147. Goodman WG, Goldin J, Kuizon BD, et al. Coronary-artery calcification in young adults with end-stage renal disease who are undergoing dialysis. *N Engl J Med*. May 18 2000;342(20):1478-83. doi:10.1056/nejm200005183422003
148. Honaryar MK, Allodji R, Ferrières J, et al. Early Coronary Artery Calcification Progression over Two Years in Breast Cancer Patients Treated with Radiation Therapy: Association with Cardiac Exposure (BACCARAT Study). *Cancers*. 2022;14(23). doi:10.3390/cancers14235724
149. Oh J, Wunsch R, Turzer M, et al. Advanced coronary and carotid arteriopathy in young adults with childhood-onset chronic renal failure. *Circulation*. Jul 2 2002;106(1):100-5. doi:10.1161/01.cir.0000020222.63035.c0
150. Raggi P, Boulay A, Chasan-Taber S, et al. Cardiac calcification in adult hemodialysis patients. A link between end-stage renal disease and cardiovascular disease? *J Am Coll Cardiol*. Feb 20 2002;39(4):695-701. doi:10.1016/s0735-1097(01)01781-8
151. Speer MY, Giachelli CM. Regulation of cardiovascular calcification. *Cardiovasc Pathol*. Mar-Apr 2004;13(2):63-70. doi:10.1016/s1054-8807(03)00130-3
152. Mohler ER, 3rd, Gannon F, Reynolds C, Zimmerman R, Keane MG, Kaplan FS. Bone formation and inflammation in cardiac valves. *Circulation*. Mar 20 2001;103(11):1522-8. doi:10.1161/01.cir.103.11.1522
153. Levy RJ, Schoen FJ, Levy JT, Nelson AC, Howard SL, Oshry LJ. Biologic determinants of dystrophic calcification and osteocalcin deposition in glutaraldehyde-preserved porcine aortic valve leaflets implanted subcutaneously in rats. *Am J Pathol*. Nov 1983;113(2):143-55.
154. Jono S, McKee MD, Murry CE, et al. Phosphate regulation of vascular smooth muscle cell calcification. *Circ Res*. Sep 29 2000;87(7):E10-7. doi:10.1161/01.res.87.7.e10
155. Parhami F, Basseri B, Hwang J, Tintut Y, Demer LL. High-Density Lipoprotein Regulates Calcification of Vascular Cells. *Circulation Research*. 2002/10/04 2002;91(7):570-576. doi:10.1161/01.RES.0000036607.05037.DA
156. Tintut Y, Patel J, Parhami F, Demer LL. Tumor necrosis factor-α promotes in vitro calcification of vascular cells via the cAMP pathway. *Circulation*. 2000;102(21):2636-2642.
157. Schoen FJ, Tsao JW, Levy RJ. Calcification of bovine pericardium used in cardiac valve bioprostheses. Implications for the mechanisms of bioprosthetic tissue mineralization. *Am J Pathol*. Apr 1986;123(1):134-45.
158. Oh J, Wunsch R, Turzer M, et al. Advanced coronary and carotid arteriopathy in young adults with childhood-onset chronic renal failure. *Circulation*. 2002;106(1):100-105.
159. Schulick AH, Taylor AJ, Zuo W, et al. Overexpression of transforming growth factor β1 in arterial endothelium causes hyperplasia, apoptosis, and cartilaginous metaplasia. *Proceedings of the National Academy of Sciences*. 1998;95(12):6983-6988.
160. Jian B, Narula N, Li Q-y, Mohler Iii ER, Levy RJ. Progression of aortic valve stenosis: TGF-β1 is present in calcified aortic valve cusps and promotes aortic valve interstitial cell calcification via apoptosis. *The Annals of thoracic surgery*. 2003;75(2):457-465.
161. Jeziorska M. Transforming growth factor-βs and CD105 expression in calcification and bone formation in human atherosclerotic lesions. *Zeitschrift für Kardiologie*. 2001;90:23-26.
162. Lieben L, Carmeliet G. Vitamin D signaling in osteocytes: effects on bone and mineral homeostasis. *Bone*. 2013;54(2):237-243.
163. Olauson H, Vervloet MG, Cozzolino M, Massy ZA, Ureña Torres P, Larsson TE. New insights into the FGF23-Klotho axis. *Semin Nephrol*. Nov 2014;34(6):586-97. doi:10.1016/j.semnephrol.2014.09.005

164. Norman PE, Powell JT. Vitamin D and cardiovascular disease. *Circ Res*. Jan 17 2014;114(2):379-93. doi:10.1161/circresaha.113.301241
165. Nakatani T, Ohnishi M, Shawkat Razzaque M. Inactivation of klotho function induces hyperphosphatemia even in presence of high serum fibroblast growth factor 23 levels in a genetically engineered hypophosphatemic (Hyp) mouse model. https://doi.org/10.1096/fj.08-123992. *The FASEB Journal*. 2009/11/01 2009;23(11):3702-3711. doi:https://doi.org/10.1096/fj.08-123992
166. Quarles LD. Role of FGF23 in vitamin D and phosphate metabolism: implications in chronic kidney disease. *Experimental cell research*. 2012;318(9):1040-1048.
167. Mazzaferro S, Pasquali M, Pirrò G, Rotondi S, Tartaglione L. The bone and the kidney. *Archives of biochemistry and biophysics*. 2010;503(1):95-102.
168. Olauson H, Larsson TE. FGF23 and Klotho in chronic kidney disease. *Current opinion in nephrology and hypertension*. 2013;22(4):397-404.
169. Tyson KL, Reynolds JL, McNair R, Zhang Q, Weissberg PL, Shanahan CM. Osteo/chondrocytic transcription factors and their target genes exhibit distinct patterns of expression in human arterial calcification. *Arteriosclerosis, thrombosis, and vascular biology*. 2003;23(3):489-494.
170. Román-García P, Rodríguez-García M, Cabezas-Rodríguez I, López-Ongil S, Díaz-López B, Cannata-Andía JB. Vascular calcification in patients with chronic kidney disease: types, clinical impact and pathogenesis. *Medical Principles and Practice*. 2011;20(3):203-212.
171. Moe SM, Chen NX. Mechanisms of vascular calcification in chronic kidney disease. *Journal of the American Society of Nephrology*. 2008;19(2):213-216.
172. Lin M-E, Chen T, Leaf EM, Speer MY, Giachelli CM. Runx2 expression in smooth muscle cells is required for arterial medial calcification in mice. *The American journal of pathology*. 2015;185(7):1958-1969.
173. Teplyuk NM, Haupt LM, Ling L, et al. The osteogenic transcription factor Runx2 regulates components of the fibroblast growth factor/proteoglycan signaling axis in osteoblasts. *Journal of cellular biochemistry*. 2009;107(1):144-154.
174. Shioi A, Katagi M, Okuno Y, et al. Induction of bone-type alkaline phosphatase in human vascular smooth muscle cells: roles of tumor necrosis factor-α and oncostatin M derived from macrophages. *Circulation research*. 2002;91(1):9-16.
175. Demer LL, Tintut Y. Vascular calcification: pathobiology of a multifaceted disease. *Circulation*. 2008;117(22):2938-2948.
176. Bone turnover markers. *Australian Journal for General Practitioners*. 04/29 2013;42:285-287.
177. Shioi A, Katagi M, Okuno Y, et al. Induction of bone-type alkaline phosphatase in human vascular smooth muscle cells: roles of tumor necrosis factor-alpha and oncostatin M derived from macrophages. *Circ Res*. Jul 12 2002;91(1):9-16. doi:10.1161/01.res.0000026421.61398.f2
178. Yeniyol S, Ricci JL. Alkaline phosphatase levels of murine pre-osteoblastic cells on anodized and annealed titanium surfaces. *Eur Oral Res*. Jan 2018;52(1):12-19. doi:10.26650/eor.2018.78387
179. Sharma U, Pal D, Prasad R. Alkaline phosphatase: an overview. *Indian J Clin Biochem*. Jul 2014;29(3):269-78. doi:10.1007/s12291-013-0408-y
180. Bucay N, Sarosi I, Dunstan CR, et al. Osteoprotegerin-deficient mice develop early onset osteoporosis and arterial calcification. *Genes & development*. 1998;12(9):1260-1268.
181. Aubin JE, Bonnelye E. Osteoprotegerin and its ligand: a new paradigm for regulation of osteoclastogenesis and bone resorption. *Osteoporosis international*. 2000;11:905-913.
182. Banks LM, Lees B, MacSweeney JE, Stevenson JC. Effect of degenerative spinal and aortic calcification on bone density measurements in post-menopausal women: links between osteoporosis and cardiovascular disease? *European journal of clinical investigation*. 1994;24(12):813-817.
183. Price PA, June HH, Buckley JR, Williamson MK. Osteoprotegerin inhibits artery calcification induced by warfarin and by vitamin D. *Arteriosclerosis, thrombosis, and vascular biology*. 2001;21(10):1610-1616.

184. Price PA, Faus SA, Williamson MK. Bisphosphonates alendronate and ibandronate inhibit artery calcification at doses comparable to those that inhibit bone resorption. *Arteriosclerosis, thrombosis, and vascular biology*. 2001;21(5):817-824.
185. Price PA, June HH, Buckley JR, Williamson MK. SB 242784, a selective inhibitor of the osteoclastic V-H+-ATPase, inhibits arterial calcification in the rat. *Circulation research*. 2002;91(6):547-552.
186. Price PA, Caputo JM, Williamson MK. Bone origin of the serum complex of calcium, phosphate, fetuin, and matrix Gla protein: biochemical evidence for the cancellous bone-remodeling compartment. *Journal of bone and mineral research*. 2002;17(7):1171-1179.
187. Tanimura A, McGregor DH, Anderson HC. Matrix vesicles in atherosclerotic calcification. *Proceedings of the Society for Experimental Biology and Medicine*. 1983;172(2):173-177.
188. Proudfoot D, Skepper JN, Hegyi L, Bennett MR, Shanahan CM, Weissberg PL. Apoptosis regulates human vascular calcification in vitro: evidence for initiation of vascular calcification by apoptotic bodies. *Circulation research*. 2000;87(11):1055-1062.
189. Metz RP, Patterson JL, Wilson E. Vascular smooth muscle cells: isolation, culture, and characterization. *Methods Mol Biol*. 2012;843:169-76. doi:10.1007/978-1-61779-523-7_16
190. Owens GK, Kumar MS, Wamhoff BR. Molecular regulation of vascular smooth muscle cell differentiation in development and disease. *Physiol Rev*. Jul 2004;84(3):767-801. doi:10.1152/physrev.00041.2003
191. Ponticos M, Smith BD. Extracellular matrix synthesis in vascular disease: hypertension, and atherosclerosis. *J Biomed Res*. Jan 2014;28(1):25-39. doi:10.7555/jbr.27.20130064
192. Alexander MR, Owens GK. Epigenetic control of smooth muscle cell differentiation and phenotypic switching in vascular development and disease. *Annu Rev Physiol*. 2012;74:13-40. doi:10.1146/annurev-physiol-012110-142315
193. Sinha S, Iyer D, Granata A. Embryonic origins of human vascular smooth muscle cells: implications for in vitro modeling and clinical application. *Cell Mol Life Sci*. Jun 2014;71(12):2271-88. doi:10.1007/s00018-013-1554-3
194. Rensen SS, Doevendans PA, van Eys GJ. Regulation and characteristics of vascular smooth muscle cell phenotypic diversity. *Neth Heart J*. 2007;15(3):100-8. doi:10.1007/bf03085963
195. Shanahan CM, Crouthamel MH, Kapustin A, Giachelli CM. Arterial calcification in chronic kidney disease: key roles for calcium and phosphate. *Circ Res*. Sep 2 2011;109(6):697-711. doi:10.1161/circresaha.110.234914
196. Swirski FK, Nahrendorf M. Do vascular smooth muscle cells differentiate to macrophages in atherosclerotic lesions? *Circ Res*. 2014:605-6. vol. 7.
197. Samouillan V, Dandurand J, Nasarre L, Badimon L, Lacabanne C, Llorente-Cortés V. Lipid loading of human vascular smooth muscle cells induces changes in tropoelastin protein levels and physical structure. *Biophys J*. Aug 8 2012;103(3):532-540. doi:10.1016/j.bpj.2012.06.034
198. Davies JD, Carpenter KL, Challis IR, et al. Adipocytic differentiation and liver x receptor pathways regulate the accumulation of triacylglycerols in human vascular smooth muscle cells. *J Biol Chem*. Feb 4 2005;280(5):3911-9. doi:10.1074/jbc.M410075200
199. Gomez D, Swiatlowska P, Owens GK. Epigenetic Control of Smooth Muscle Cell Identity and Lineage Memory. *Arterioscler Thromb Vasc Biol*. Dec 2015;35(12):2508-16. doi:10.1161/atvbaha.115.305044
200. Marra KG, Brayfield CA, Rubin JP. Adipose stem cell differentiation into smooth muscle cells. *Methods Mol Biol*. 2011;702:261-8. doi:10.1007/978-1-61737-960-4_19
201. Allahverdian S, Chehroudi AC, McManus BM, Abraham T, Francis GA. Contribution of intimal smooth muscle cells to cholesterol accumulation and macrophage-like cells in human atherosclerosis. *Circulation*. Apr 15 2014;129(15):1551-9. doi:10.1161/circulationaha.113.005015
202. Loebel C, Czekanska EM, Bruderer M, Salzmann G, Alini M, Stoddart MJ. In vitro osteogenic potential of human mesenchymal stem cells is predicted by Runx2/Sox9 ratio. *Tissue Eng Part A*. Jan 2015;21(1-2):115-23. doi:10.1089/ten.TEA.2014.0096

203. Komori T. Regulation of bone development and extracellular matrix protein genes by RUNX2. *Cell Tissue Res*. Jan 2010;339(1):189-95. doi:10.1007/s00441-009-0832-8
204. Tsuji K, Bandyopadhyay A, Harfe BD, et al. BMP2 activity, although dispensable for bone formation, is required for the initiation of fracture healing. *Nat Genet*. Dec 2006;38(12):1424-9. doi:10.1038/ng1916
205. Nguyen N, Naik V, Speer MY. Diabetes mellitus accelerates cartilaginous metaplasia and calcification in atherosclerotic vessels of LDLr mutant mice. *Cardiovasc Pathol*. Mar-Apr 2013;22(2):167-75. doi:10.1016/j.carpath.2012.06.007
206. Hutcheson JD, Goettsch C, Bertazzo S, et al. Genesis and growth of extracellular-vesicle-derived microcalcification in atherosclerotic plaques. *Nat Mater*. Mar 2016;15(3):335-43. doi:10.1038/nmat4519
207. Otsuka F, Sakakura K, Yahagi K, Joner M, Virmani R. Has our understanding of calcification in human coronary atherosclerosis progressed? *Arterioscler Thromb Vasc Biol*. Apr 2014;34(4):724-36. doi:10.1161/atvbaha.113.302642
208. Bobryshev YV. Transdifferentiation of smooth muscle cells into chondrocytes in atherosclerotic arteries in situ: implications for diffuse intimal calcification. *J Pathol*. Apr 2005;205(5):641-50. doi:10.1002/path.1743
209. Pittenger MF, Mackay AM, Beck SC, et al. Multilineage potential of adult human mesenchymal stem cells. *Science*. Apr 2 1999;284(5411):143-7. doi:10.1126/science.284.5411.143
210. Kleinman HK, Philp D, Hoffman MP. Role of the extracellular matrix in morphogenesis. *Curr Opin Biotechnol*. Oct 2003;14(5):526-32. doi:10.1016/j.copbio.2003.08.002
211. Breitkreutz D, Mirancea N, Nischt R. Basement membranes in skin: unique matrix structures with diverse functions? *Histochem Cell Biol*. Jul 2009;132(1):1-10. doi:10.1007/s00418-009-0586-0
212. Huber M, Trattnig S, Lintner F. Anatomy, biochemistry, and physiology of articular cartilage. *Invest Radiol*. Oct 2000;35(10):573-80. doi:10.1097/00004424-200010000-00003
213. Kuure S, Vuolteenaho R, Vainio S. Kidney morphogenesis: cellular and molecular regulation. *Mech Dev*. Mar 15 2000;92(1):31-45. doi:10.1016/s0925-4773(99)00323-8
214. Ottani V, Martini D, Franchi M, Ruggeri A, Raspanti M. Hierarchical structures in fibrillar collagens. *Micron*. 2002;33(7-8):587-96. doi:10.1016/s0968-4328(02)00033-1
215. Van Der Rest M, Garrone R. Collagen family of proteins. https://doi.org/10.1096/fasebj.5.13.1916105. *The FASEB Journal*. 1991/10/01 1991;5(13):2814-2823. doi:https://doi.org/10.1096/fasebj.5.13.1916105
216. Raines EW. The extracellular matrix can regulate vascular cell migration, proliferation, and survival: relationships to vascular disease. *Int J Exp Pathol*. Jun 2000;81(3):173-82. doi:10.1046/j.1365-2613.2000.00155.x
217. Ratcliffe A. Tissue engineering of vascular grafts. *Matrix Biol*. Aug 2000;19(4):353-7. doi:10.1016/s0945-053x(00)00080-9
218. Laurent GJ, Chambers RC, Hill MR, McAnulty RJ. Regulation of matrix turnover: fibroblasts, forces, factors and fibrosis. *Biochem Soc Trans*. Aug 2007;35(Pt 4):647-51. doi:10.1042/bst0350647
219. Sasisekharan R, Raman R, Prabhakar V. Glycomics approach to structure-function relationships of glycosaminoglycans. *Annu Rev Biomed Eng*. 2006;8:181-231. doi:10.1146/annurev.bioeng.8.061505.095745
220. Hwang NS, Varghese S, Lee HJ, et al. Response of zonal chondrocytes to extracellular matrix-hydrogels. *FEBS Lett*. Sep 4 2007;581(22):4172-8. doi:10.1016/j.febslet.2007.07.049
221. Tognana E, Borrione A, De Luca C, Pavesio A. Hyalograft C: hyaluronan-based scaffolds in tissue-engineered cartilage. *Cells Tissues Organs*. 2007;186(2):97-103. doi:10.1159/000102539
222. Varghese S, Hwang NS, Canver AC, Theprungsirikul P, Lin DW, Elisseeff J. Chondroitin sulfate based niches for chondrogenic differentiation of mesenchymal stem cells. *Matrix Biol*. Jan 2008;27(1):12-21. doi:10.1016/j.matbio.2007.07.002
223. White ES, Baralle FE, Muro AF. New insights into form and function of fibronectin splice variants. *J Pathol*. Sep 2008;216(1):1-14. doi:10.1002/path.2388

224. Schwarzbauer JE, DeSimone DW. Fibronectins, their fibrillogenesis, and in vivo functions. *Cold Spring Harb Perspect Biol*. Jul 1 2011;3(7)doi:10.1101/cshperspect.a005041
225. Kubota Y, Kleinman HK, Martin GR, Lawley TJ. Role of laminin and basement membrane in the morphological differentiation of human endothelial cells into capillary-like structures. *J Cell Biol*. Oct 1988;107(4):1589-98. doi:10.1083/jcb.107.4.1589
226. Tzu J, Marinkovich MP. Bridging structure with function: structural, regulatory, and developmental role of laminins. *Int J Biochem Cell Biol*. 2008;40(2):199-214. doi:10.1016/j.biocel.2007.07.015
227. Humphries SM, Lu Y, Canty EG, Kadler KE. Active negative control of collagen fibrillogenesis in vivo. Intracellular cleavage of the type I procollagen propeptides in tendon fibroblasts without intracellular fibrils. *J Biol Chem*. May 2 2008;283(18):12129-35. doi:10.1074/jbc.M708198200
228. Kanagawa M, Michele DE, Satz JS, et al. Disruption of perlecan binding and matrix assembly by post-translational or genetic disruption of dystroglycan function. *FEBS Letters*. 2005/08/29/ 2005;579(21):4792-4796. doi:https://doi.org/10.1016/j.febslet.2005.07.059
229. Meyer K, Palmer JW. The polysaccharide of the vitreous humor. *Journal of Biological Chemistry*. Dec 1934;107(3):629-634.
230. Fraser JRE, Laurent TC, Laurent UBG. Hyaluronan: Its nature, distribution, functions and turnover. *Journal of Internal Medicine*. Jul 1997;242(1):27-33. doi:10.1046/j.1365-2796.1997.00170.x
231. Itano N, Kimata K. Mammalian hyaluronan synthases. *Iubmb Life*. Oct 2002;54(4):195-199. doi:10.1080/15216540214929
232. Weigel PH, Hascall VC, Tammi M. Hyaluronan synthases. *J Biol Chem*. May 30 1997;272(22):13997-4000. doi:10.1074/jbc.272.22.13997
233. McAtee CO, Barycki JJ, Simpson MA. Emerging roles for hyaluronidase in cancer metastasis and therapy. *Adv Cancer Res*. 2014;123:1-34. doi:10.1016/b978-0-12-800092-2.00001-0
234. Toole BP. Hyaluronan is not just a goo! *The Journal of Clinical Investigation*. 08/01/ 2000;106(3):335-336. doi:10.1172/JCI10706
235. Blundell CD, DeAngelis PL, Almond A. Hyaluronan: the absence of amide-carboxylate hydrogen bonds and the chain conformation in aqueous solution are incompatible with stable secondary and tertiary structure models. *Biochemical Journal*. Jun 2006;396:487-498. doi:10.1042/bj20060085
236. Cowman MK, Matsuoka S. Experimental approaches to hyaluronan structure. *Carbohydrate Research*. Apr 2005;340(5):791-809. doi:10.1016/j.carres.2005.01.022
237. Lee JY, Spicer AP. Hyaluronan: a multifunctional, megaDalton, stealth molecule. *Curr Opin Cell Biol*. Oct 2000;12(5):581-6. doi:10.1016/s0955-0674(00)00135-6
238. Spicer AP, Tien JY. Hyaluronan and morphogenesis. *Birth Defects Res C Embryo Today*. Mar 2004;72(1):89-108. doi:10.1002/bdrc.20006
239. Tien JY, Spicer AP. Three vertebrate hyaluronan synthases are expressed during mouse development in distinct spatial and temporal patterns. *Dev Dyn*. May 2005;233(1):130-41. doi:10.1002/dvdy.20328
240. Turley EA. Hyaluronan and cell locomotion. *Cancer Metastasis Rev*. Mar 1992;11(1):21-30. doi:10.1007/bf00047600
241. Turley EA, Austen L, Vandeligt K, Clary C. Hyaluronan and a cell-associated hyaluronan binding protein regulate the locomotion of ras-transformed cells. *J Cell Biol*. Mar 1991;112(5):1041-7. doi:10.1083/jcb.112.5.1041
242. Nettelbladt O, Bergh J, Schenholm M, Tengblad A, Hällgren R. Accumulation of hyaluronic acid in the alveolar interstitial tissue in bleomycin-induced alveolitis. *Am Rev Respir Dis*. Mar 1989;139(3):759-62. doi:10.1164/ajrccm/139.3.759
243. Waldenström A, Martinussen HJ, Gerdin B, Hällgren R. Accumulation of hyaluronan and tissue edema in experimental myocardial infarction. *J Clin Invest*. Nov 1991;88(5):1622-8. doi:10.1172/jci115475

244. Weigel PH, Fuller GM, LeBoeuf RD. A model for the role of hyaluronic acid and fibrin in the early events during the inflammatory response and wound healing. *J Theor Biol*. Mar 21 1986;119(2):219-34. doi:10.1016/s0022-5193(86)80076-5
245. Evanko SP, Tammi MI, Tammi RH, Wight TN. Hyaluronan-dependent pericellular matrix. *Advanced Drug Delivery Reviews*. Nov 2007;59(13):1351-1365. doi:10.1016/j.addr.2007.08.008
246. Vigetti D, Karousou E, Viola M, Deleonibus S, De Luca G, Passi A. Hyaluronan: Biosynthesis and signaling. *Biochimica Et Biophysica Acta-General Subjects*. Aug 2014;1840(8):2452-2459. doi:10.1016/j.bbagen.2014.02.001
247. de Oliveira JD, Carvalho LS, Gomes AMV, Queiroz LR, Magalhães BS, Parachin NS. Genetic basis for hyper production of hyaluronic acid in natural and engineered microorganisms. *Microbial Cell Factories*. 2016/07/01 2016;15(1):119. doi:10.1186/s12934-016-0517-4
248. Spicer AP, McDonald JA. Characterization and molecular evolution of a vertebrate hyaluronan synthase gene family. *J Biol Chem*. Jan 23 1998;273(4):1923-32. doi:10.1074/jbc.273.4.1923
249. Meyer MF, Kreil G. Cells expressing the DG42 gene from early Xenopus embryos synthesize hyaluronan. *Proc Natl Acad Sci U S A*. May 14 1996;93(10):4543-7. doi:10.1073/pnas.93.10.4543
250. Spicer AP, Seldin MF, Olsen AS, et al. Chromosomal localization of the human and mouse hyaluronan synthase genes. *Genomics*. May 1 1997;41(3):493-7. doi:10.1006/geno.1997.4696
251. Tammi MI, Day AJ, Turley EA. Hyaluronan and homeostasis: a balancing act. *J Biol Chem*. Feb 15 2002;277(7):4581-4. doi:10.1074/jbc.R100037200
252. Kypta RM, Goldberg Y, Ulug ET, Courtneidge SA. Association between the PDGF receptor and members of the src family of tyrosine kinases. *Cell*. 1990/08/10/ 1990;62(3):481-492. doi:https://doi.org/10.1016/0092-8674(90)90013-5
253. Jones S, Phillips AO. Regulation of renal proximal tubular epithelial cell hyaluronan generation: implications for diabetic nephropathy. *Kidney Int*. May 2001;59(5):1739-49. doi:10.1046/j.1523-1755.2001.0590051739.x
254. Kennedy CI, Diegelmann RF, Haynes JH, Yager DR. Proinflammatory cytokines differentially regulate hyaluronan synthase isoforms in fetal and adult fibroblasts. *J Pediatr Surg*. Jun 2000;35(6):874-9. doi:10.1053/jpsu.2000.6869
255. Monslow J, Williams JD, Guy CA, et al. Identification and analysis of the promoter region of the human hyaluronan synthase 2 gene. *J Biol Chem*. May 14 2004;279(20):20576-81. doi:10.1074/jbc.M312666200
256. Monslow J, Williams JD, Norton N, et al. The human hyaluronan synthase genes: genomic structures, proximal promoters and polymorphic microsatellite markers. *Int J Biochem Cell Biol*. Aug 2003;35(8):1272-83. doi:10.1016/s1357-2725(03)00048-7
257. Yamada Y, Itano N, Zako M, et al. The gene structure and promoter sequence of mouse hyaluronan synthase 1. *Biochem J*. Mar 15 1998;330 (Pt 3)(Pt 3):1223-7. doi:10.1042/bj3301223
258. Chao H, Spicer AP. Natural antisense mRNAs to hyaluronan synthase 2 inhibit hyaluronan biosynthesis and cell proliferation. *J Biol Chem*. Jul 29 2005;280(30):27513-22. doi:10.1074/jbc.M411544200
259. Momberger TS, Levick JR, Mason RM. Hyaluronan secretion by synoviocytes is mechanosensitive. *Matrix Biol*. Dec 2005;24(8):510-9. doi:10.1016/j.matbio.2005.08.006
260. Itano N, Sawai T, Yoshida M, et al. Three isoforms of mammalian hyaluronan synthases have distinct enzymatic properties. *J Biol Chem*. Aug 27 1999;274(35):25085-92. doi:10.1074/jbc.274.35.25085
261. Spicer AP, McDonald JA. Characterization and molecular evolution of a vertebrate hyaluronan synthase gene family. *Journal of Biological Chemistry*. 1998;273(4):1923-1932.
262. Camenisch TD, Spicer AP, Brehm-Gibson T, et al. Disruption of hyaluronan synthase-2 abrogates normal cardiac morphogenesis and hyaluronan-mediated transformation of epithelium to mesenchyme. *J Clin Invest*. Aug 2000;106(3):349-60. doi:10.1172/jci10272

263. Spicer AP, Tien JL, Joo A, Bowling RA, Jr. Investigation of hyaluronan function in the mouse through targeted mutagenesis. *Glycoconj J*. May-Jun 2002;19(4-5):341-5. doi:10.1023/a:1025321105691
264. Camenisch TD, Schroeder JA, Bradley J, Klewer SE, McDonald JA. Heart-valve mesenchyme formation is dependent on hyaluronan-augmented activation of ErbB2-ErbB3 receptors. *Nat Med*. Aug 2002;8(8):850-5. doi:10.1038/nm742
265. Stock AE, Bouchard N, Brown K, et al. Induction of hyaluronan synthase 2 by human chorionic gonadotropin in mural granulosa cells of equine preovulatory follicles. *Endocrinology*. Nov 2002;143(11):4375-84. doi:10.1210/en.2002-220563
266. Toole BP, Zoltan-Jones A, Misra S, Ghatak S. Hyaluronan: A Critical Component of Epithelial-Mesenchymal and Epithelial-Carcinoma Transitions. *Cells Tissues Organs*. 2005;179(1-2):66-72. doi:10.1159/000084510
267. Desmoulière A, Geinoz A, Gabbiani F, Gabbiani G. Transforming growth factor-beta 1 induces alpha-smooth muscle actin expression in granulation tissue myofibroblasts and in quiescent and growing cultured fibroblasts. *J Cell Biol*. Jul 1993;122(1):103-11. doi:10.1083/jcb.122.1.103
268. Midgley AC, Duggal L, Jenkins R, et al. Hyaluronan Regulates Bone Morphogenetic Protein-7-dependent Prevention and Reversal of Myofibroblast Phenotype. *Journal of Biological Chemistry*. May 2015;290(18):11218-11234. doi:10.1074/jbc.M114.625939
269. Simpson RM, Meran S, Thomas D, et al. Age-related changes in pericellular hyaluronan organization leads to impaired dermal fibroblast to myofibroblast differentiation. *Am J Pathol*. Nov 2009;175(5):1915-28. doi:10.2353/ajpath.2009.090045
270. Vaughan MB, Howard EW, Tomasek JJ. Transforming growth factor-beta1 promotes the morphological and functional differentiation of the myofibroblast. *Exp Cell Res*. May 25 2000;257(1):180-9. doi:10.1006/excr.2000.4869
271. Webber J, Meran S, Steadman R, Phillips A. Hyaluronan Orchestrates Transforming Growth Factor-beta 1-dependent Maintenance of Myofibroblast Phenotype. *Journal of Biological Chemistry*. Apr 2009;284(14):9083-9092. doi:10.1074/jbc.M806989200
272. Webber J, Jenkins RH, Meran S, Phillips A, Steadman R. Modulation of TGF beta 1-Dependent Myofibroblast Differentiation by Hyaluronan. *American Journal of Pathology*. Jul 2009;175(1):148-160. doi:10.2353/ajpath.2009.080837
273. Kosaki R, Watanabe K, Yamaguchi Y. Overproduction of hyaluronan by expression of the hyaluronan synthase Has2 enhances anchorage-independent growth and tumorigenicity. *Cancer Res*. Mar 1 1999;59(5):1141-5.
274. Huey G, Moiin A, Stern R. Levels of [3H]glucosamine incorporation into hyaluronic acid by fibroblasts is modulated by culture conditions. *Matrix*. May 1990;10(2):75-83. doi:10.1016/s0934-8832(11)80173-3
275. Selbi W, Day AJ, Rugg MS, et al. Overexpression of hyaluronan synthase 2 alters hyaluronan distribution and function in proximal tubular epithelial cells. *J Am Soc Nephrol*. Jun 2006;17(6):1553-67. doi:10.1681/asn.2005080879
276. Selbi W, de la Motte CA, Hascall VC, Day AJ, Bowen T, Phillips AO. Characterization of hyaluronan cable structure and function in renal proximal tubular epithelial cells. *Kidney Int*. Oct 2006;70(7):1287-95. doi:10.1038/sj.ki.5001760
277. Evanko SP, Wight TN. Intracellular localization of hyaluronan in proliferating cells. *J Histochem Cytochem*. Oct 1999;47(10):1331-42. doi:10.1177/002215549904701013
278. de la Motte CA, Hascall VC, Drazba J, Bandyopadhyay SK, Strong SA. Mononuclear leukocytes bind to specific hyaluronan structures on colon mucosal smooth muscle cells treated with polyinosinic acid:polycytidylic acid: inter-alpha-trypsin inhibitor is crucial to structure and function. *Am J Pathol*. Jul 2003;163(1):121-33. doi:10.1016/s0002-9440(10)63636-x
279. Petrey AC, de la Motte CA. Hyaluronan, a crucial regulator of inflammation. *Front Immunol*. 2014;5:101. doi:10.3389/fimmu.2014.00101

280. Iijima J, Konno K, Itano N. Inflammatory alterations of the extracellular matrix in the tumor microenvironment. *Cancers (Basel)*. Aug 9 2011;3(3):3189-205. doi:10.3390/cancers3033189
281. De la Motte CA, Hascall VC, Drazba J, Bandyopadhyay SK, Strong SA. Mononuclear leukocytes bind to specific hyaluronan structures on colon mucosal smooth muscle cells treated with polyinosinic acid: polycytidylic acid: inter-α-trypsin inhibitor is crucial to structure and function. *The American journal of pathology*. 2003;163(1):121-133.
282. Day AJ, de la Motte CA. Hyaluronan cross-linking: a protective mechanism in inflammation? *Trends in immunology*. 2005;26(12):637-643.
283. Selbi W, de la Motte C, Hascall V, Phillips A. BMP-7 modulates hyaluronan-mediated proximal tubular cell-monocyte interaction. *J Am Soc Nephrol*. May 2004;15(5):1199-211. doi:10.1097/01.asn.0000125619.27422.8e
284. Knudson W, Chow G, Knudson CB. CD44-mediated uptake and degradation of hyaluronan. *Matrix Biol*. Jan 2002;21(1):15-23. doi:10.1016/s0945-053x(01)00186-x
285. Knudson CB. Hyaluronan and CD44: strategic players for cell-matrix interactions during chondrogenesis and matrix assembly. *Birth Defects Res C Embryo Today*. May 2003;69(2):174-96. doi:10.1002/bdrc.10013
286. Banerji S, Ni J, Wang SX, et al. LYVE-1, a new homologue of the CD44 glycoprotein, is a lymph-specific receptor for hyaluronan. *J Cell Biol*. Feb 22 1999;144(4):789-801. doi:10.1083/jcb.144.4.789
287. Zhou B, Weigel JA, Fauss L, Weigel PH. Identification of the hyaluronan receptor for endocytosis (HARE). *J Biol Chem*. Dec 1 2000;275(48):37733-41. doi:10.1074/jbc.M003030200
288. Rodén L, Campbell P, Fraser JRE, Laurent TC, Pertoft H, Thompson JN. Enzymic Pathways of Hyaluronan Catabolism. *Ciba Foundation Symposium 143 - The Biology of Hyaluronan*. 2007:60-86. *Novartis Foundation Symposia*.
289. Csóka AB, Scherer SW, Stern R. Expression analysis of six paralogous human hyaluronidase genes clustered on chromosomes 3p21 and 7q31. *Genomics*. Sep 15 1999;60(3):356-61. doi:10.1006/geno.1999.5876
290. Baggenstoss BA, Harris EN, Washburn JL, Medina AP, Nguyen L, Weigel PH. Hyaluronan synthase control of synthesis rate and hyaluronan product size are independent functions differentially affected by mutations in a conserved tandem B-X7-B motif. *Glycobiology*. Jan 2017;27(2):154-164. doi:10.1093/glycob/cww089
291. Cherr GN, Yudin AI, Overstreet JW. The dual functions of GPI-anchored PH-20: hyaluronidase and intracellular signaling. *Matrix Biol*. Dec 2001;20(8):515-25. doi:10.1016/s0945-053x(01)00171-8
292. Nawy SS, Csóka AB, Mio K, Stern R. Hyaluronidase activity and hyaluronidase inhibitors. Assay using a microtiter-based system. *Methods Mol Biol*. 2001;171:383-9. doi:10.1385/1-59259-209-0:383
293. Csóka AB, Frost GI, Wong T, Stern R. Purification and microsequencing of hyaluronidase isozymes from human urine. *FEBS Lett*. Nov 17 1997;417(3):307-10. doi:10.1016/s0014-5793(97)01309-4
294. Tokita Y, Ohshima K, Okamoto A. Degradation of hyaluronic acid during freeze drying. *Polymer Degradation and Stability*. 1997/01/01/ 1997;55(2):159-164. doi:https://doi.org/10.1016/S0141-3910(96)00128-0
295. Gakunga P, Frost G, Shuster S, Cunha G, Formby B, Stern R. Hyaluronan is a prerequisite for ductal branching morphogenesis. *Development*. Oct 1997;124(20):3987-97. doi:10.1242/dev.124.20.3987
296. El-Safory N, Fazary A, Lee C-K. Hyaluronidases, a group of glycosidases: Current and future perspectives. *Carbohydrate Polymers*. 06/01 2010;81:165-181. doi:10.1016/j.carbpol.2010.02.047
297. Colombaro V, Jadot I, Declèves AE, et al. Hyaluronidase 1 and hyaluronidase 2 are required for renal hyaluronan turnover. *Acta Histochem*. Jan 2015;117(1):83-91. doi:10.1016/j.acthis.2014.11.007

298. Chowdhury B, Hemming R, Hombach-Klonisch S, Flamion B, Triggs-Raine B. Murine hyaluronidase 2 deficiency results in extracellular hyaluronan accumulation and severe cardiopulmonary dysfunction. *J Biol Chem*. Jan 4 2013;288(1):520-8. doi:10.1074/jbc.M112.393629
299. Muggenthaler MM, Chowdhury B, Hasan SN, et al. Mutations in HYAL2, Encoding Hyaluronidase 2, Cause a Syndrome of Orofacial Clefting and Cor Triatriatum Sinister in Humans and Mice. *PLoS Genet*. Jan 2017;13(1):e1006470. doi:10.1371/journal.pgen.1006470
300. Stern R, Jedrzejas MJ. Hyaluronidases: their genomics, structures, and mechanisms of action. *Chem Rev*. Mar 2006;106(3):818-39. doi:10.1021/cr050247k
301. Midgley AC, Oltean S, Hascall V, et al. Nuclear hyaluronidase 2 drives alternative splicing of CD44 pre-mRNA to determine profibrotic or antifibrotic cell phenotype. *Sci Signal*. Nov 21 2017;10(506)doi:10.1126/scisignal.aao1822
302. Csoka AB, Frost GI, Stern R. The six hyaluronidase-like genes in the human and mouse genomes. *Matrix biology*. 2001;20(8):499-508.
303. Erickson M, Stern R. Chain gangs: new aspects of hyaluronan metabolism. *Biochem Res Int*. 2012;2012:893947. doi:10.1155/2012/893947
304. Rai SK, Duh F-M, Vigdorovich V, Danilkovitch-Miagkova A, Lerman MI, Miller AD. Candidate tumor suppressor HYAL2 is a glycosylphosphatidylinositol (GPI)-anchored cell-surface receptor for jaagsiekte sheep retrovirus, the envelope protein of which mediates oncogenic transformation. *Proceedings of the National Academy of Sciences*. 2001;98(8):4443. doi:10.1073/pnas.071572898
305. Stair-Nawy S, Csóka AB, Stern R. Hyaluronidase expression in human skin fibroblasts. *Biochem Biophys Res Commun*. Dec 9 1999;266(1):268-73. doi:10.1006/bbrc.1999.1802
306. Stern R. Devising a pathway for hyaluronan catabolism: are we there yet? *Glycobiology*. Dec 2003;13(12):105r-115r. doi:10.1093/glycob/cwg112
307. Hemming R, Martin DC, Slominski E, et al. Mouse Hyal3 encodes a 45- to 56-kDa glycoprotein whose overexpression increases hyaluronidase 1 activity in cultured cells. *Glycobiology*. Apr 2008;18(4):280-9. doi:10.1093/glycob/cwn006
308. Atmuri V, Martin DC, Hemming R, et al. Hyaluronidase 3 (HYAL3) knockout mice do not display evidence of hyaluronan accumulation. *Matrix Biol*. Oct 2008;27(8):653-60. doi:10.1016/j.matbio.2008.07.006
309. Yoshida H, Nagaoka A, Kusaka-Kikushima A, et al. KIAA1199, a deafness gene of unknown function, is a new hyaluronan binding protein involved in hyaluronan depolymerization. *Proceedings of the National Academy of Sciences*. 2013;110(14):5612-5617.
310. Nagaoka A, Yoshida H, Nakamura S, et al. Regulation of hyaluronan (HA) metabolism mediated by HYBID (hyaluronan-binding protein involved in HA depolymerization, KIAA1199) and HA synthases in growth factor-stimulated fibroblasts. *Journal of Biological Chemistry*. 2015;290(52):30910-30923.
311. Sato S, Mizutani Y, Yoshino Y, et al. Pro-inflammatory cytokines suppress HYBID (hyaluronan (HA)-binding protein involved in HA depolymerization/KIAA1199/CEMIP)-mediated HA metabolism in human skin fibroblasts. *Biochemical and Biophysical Research Communications*. 2021;539:77-82.
312. Deroyer C, Charlier E, Neuville S, et al. CEMIP (KIAA1199) induces a fibrosis-like process in osteoarthritic chondrocytes. *Cell Death Dis*. Feb 4 2019;10(2):103. doi:10.1038/s41419-019-1377-8
313. Yamamoto H, Tobisawa Y, Inubushi T, Irie F, Ohyama C, Yamaguchi Y. A mammalian homolog of the zebrafish transmembrane protein 2 (TMEM2) is the long-sought-after cell-surface hyaluronidase. *Journal of Biological Chemistry*. 2017;292(18):7304-7313.
314. Yoshino Y, Goto M, Hara H, Inoue S. The role and regulation of TMEM2 (transmembrane protein 2) in HYBID (hyaluronan (HA)-binding protein involved in HA depolymerization/ KIAA1199/CEMIP)-mediated HA depolymerization in human skin fibroblasts. *Biochem Biophys Res Commun*. Oct 20 2018;505(1):74-80. doi:10.1016/j.bbrc.2018.09.097
315. Smith KA, Lagendijk AK, Courtney AD, et al. Transmembrane protein 2 (Tmem2) is required to regionally restrict atrioventricular canal boundary and endocardial cushion development. *Development*. 2011;138(19):4193-4198.

316. Totong R, Schell T, Lescroart F, et al. The novel transmembrane protein Tmem2 is essential for coordination of myocardial and endocardial morphogenesis. *Development*. 2011;138(19):4199-4205.
317. Heldin P. Importance of hyaluronan biosynthesis and degradation in cell differentiation and tumor formation. *Braz J Med Biol Res*. Aug 2003;36(8):967-73. doi:10.1590/s0100-879x2003000800002
318. Knudson CB, Knudson W. Hyaluronan-binding proteins in development, tissue homeostasis, and disease. *Faseb j*. Oct 1993;7(13):1233-41.
319. Day AJ, Prestwich GD. Hyaluronan-binding proteins: tying up the giant. *J Biol Chem*. Feb 15 2002;277(7):4585-8. doi:10.1074/jbc.R100036200
320. Hascall V, Esko JD. Hyaluronan. In: Varki A, Cummings RD, Esko JD, et al, eds. *Essentials of Glycobiology*. Cold Spring Harbor Laboratory Press

 2015:197-206.
321. Turley EA, Noble PW, Bourguignon LY. Signaling properties of hyaluronan receptors. *J Biol Chem*. Feb 15 2002;277(7):4589-92. doi:10.1074/jbc.R100038200
322. Entwistle J, Hall CL, Turley EA. HA receptors: regulators of signalling to the cytoskeleton. *J Cell Biochem*. Jun 15 1996;61(4):569-77. doi:10.1002/(sici)1097-4644(19960616)61:4<569::aid-jcb10>3.0.co;2-b
323. Sleeman J, Rudy W, Hofmann M, Moll J, Herrlich P, Ponta H. Regulated clustering of variant CD44 proteins increases their hyaluronate binding capacity. *J Cell Biol*. Nov 1996;135(4):1139-50. doi:10.1083/jcb.135.4.1139
324. Bourguignon LY, Lokeshwar VB, He J, Chen X, Bourguignon GJ. A CD44-like endothelial cell transmembrane glycoprotein (GP116) interacts with extracellular matrix and ankyrin. *Mol Cell Biol*. Oct 1992;12(10):4464-71. doi:10.1128/mcb.12.10.4464-4471.1992
325. Li H, Guo L, Li J-W, Liu N, Qi R, Liu J. Expression of hyaluronan receptors CD44 and RHAMM in stomach cancers: relevance with tumor progression. *International journal of oncology*. 2000;17(5):927-959.
326. Ito T, Williams JD, Al-Assaf S, Phillips GO, Phillips AO. Hyaluronan and proximal tubular cell migration. *Kidney Int*. Mar 2004;65(3):823-33. doi:10.1111/j.1523-1755.2004.00457.x
327. Bourguignon LY, Singleton PA, Zhu H, Diedrich F. Hyaluronan-mediated CD44 interaction with RhoGEF and Rho kinase promotes Grb2-associated binder-1 phosphorylation and phosphatidylinositol 3-kinase signaling leading to cytokine (macrophage-colony stimulating factor) production and breast tumor progression. *J Biol Chem*. Aug 8 2003;278(32):29420-34. doi:10.1074/jbc.M301885200
328. Bourguignon LY, Zhu D, Zhu H. CD44 isoform-cytoskeleton interaction in oncogenic signaling and tumor progression. *Front Biosci*. Jul 1 1998;3:d637-49. doi:10.2741/a308
329. Bourguignon LY, Zhu H, Shao L, Chen YW. CD44 interaction with c-Src kinase promotes cortactin-mediated cytoskeleton function and hyaluronic acid-dependent ovarian tumor cell migration. *J Biol Chem*. Mar 9 2001;276(10):7327-36. doi:10.1074/jbc.M006498200
330. Ponta H, Sherman L, Herrlich PA. CD44: from adhesion molecules to signalling regulators. *Nat Rev Mol Cell Biol*. Jan 2003;4(1):33-45. doi:10.1038/nrm1004
331. Tsukita S, Oishi K, Sato N, Sagara J, Kawai A. ERM family members as molecular linkers between the cell surface glycoprotein CD44 and actin-based cytoskeletons. *J Cell Biol*. Jul 1994;126(2):391-401. doi:10.1083/jcb.126.2.391
332. Lesley J, Hyman R, Kincade PW. CD44 and its interaction with extracellular matrix. *Adv Immunol*. 1993;54:271-335. doi:10.1016/s0065-2776(08)60537-4
333. Knudson CB, Knudson W. Hyaluronan and CD44: modulators of chondrocyte metabolism. *Clin Orthop Relat Res*. Oct 2004;(427 Suppl):S152-62.

334. Ohno S, Ohno-Nakahara M, Knudson CB, Knudson W. Induction of MMP-3 by hyaluronan oligosaccharides in temporomandibular joint chondrocytes. *J Dent Res*. Nov 2005;84(11):1005-9. doi:10.1177/154405910508401107
335. Girish KS, Kemparaju K. The magic glue hyaluronan and its eraser hyaluronidase: a biological overview. *Life Sci*. May 1 2007;80(21):1921-43. doi:10.1016/j.lfs.2007.02.037
336. Bourguignon LY, Singleton PA, Zhu H, Zhou B. Hyaluronan promotes signaling interaction between CD44 and the transforming growth factor beta receptor I in metastatic breast tumor cells. *J Biol Chem*. Oct 18 2002;277(42):39703-12. doi:10.1074/jbc.M204320200
337. Ito T, Williams JD, Fraser DJ, Phillips AO. Hyaluronan regulates transforming growth factor-beta1 receptor compartmentalization. *J Biol Chem*. Jun 11 2004;279(24):25326-32. doi:10.1074/jbc.M403135200
338. Turley EA, Harrison R. RHAMM, a member of the hyaladherins. *Science of hyaluronan today http://www glycoforum gr jp/science/hyaluronan/HA11/HA11E html (accessed November 1, 2006)*. 1999;
339. Nedvetzki S, Gonen E, Assayag N, et al. RHAMM, a receptor for hyaluronan-mediated motility, compensates for CD44 in inflamed CD44-knockout mice: a different interpretation of redundancy. *Proceedings of the National Academy of Sciences*. 2004;101(52):18081-18086.
340. Lovvorn HN, 3rd, Cass DL, Sylvester KG, et al. Hyaluronan receptor expression increases in fetal excisional skin wounds and correlates with fibroplasia. *J Pediatr Surg*. Jul 1998;33(7):1062-9; discussion 1069-70. doi:10.1016/s0022-3468(98)90532-2
341. Tolg C, Hamilton SR, Nakrieko KA, et al. Rhamm-/- fibroblasts are defective in CD44-mediated ERK1,2 motogenic signaling, leading to defective skin wound repair. *J Cell Biol*. Dec 18 2006;175(6):1017-28. doi:10.1083/jcb.200511027
342. Zaman A, Cui Z, Foley JP, et al. Expression and role of the hyaluronan receptor RHAMM in inflammation after bleomycin injury. *Am J Respir Cell Mol Biol*. Nov 2005;33(5):447-54. doi:10.1165/rcmb.2004-0333OC
343. Hirose J, Kawashima H, Yoshie O, Tashiro K, Miyasaka M. Versican interacts with chemokines and modulates cellular responses. *J Biol Chem*. Feb 16 2001;276(7):5228-34. doi:10.1074/jbc.M007542200
344. Kawashima H, Hirose M, Hirose J, Nagakubo D, Plaas AH, Miyasaka M. Binding of a large chondroitin sulfate/dermatan sulfate proteoglycan, versican, to L-selectin, P-selectin, and CD44. *J Biol Chem*. Nov 10 2000;275(45):35448-56. doi:10.1074/jbc.M003387200
345. Lemire JM, Braun KR, Maurel P, Kaplan ED, Schwartz SM, Wight TN. Versican/PG-M isoforms in vascular smooth muscle cells. *Arterioscler Thromb Vasc Biol*. Jul 1999;19(7):1630-9. doi:10.1161/01.atv.19.7.1630
346. Martin J, Midgley A, Meran S, et al. Tumor Necrosis Factor-stimulated Gene 6 (TSG-6)-mediated Interactions with the Inter-α-inhibitor Heavy Chain 5 Facilitate Tumor Growth Factor β1 (TGFβ1)-dependent Fibroblast to Myofibroblast Differentiation. *J Biol Chem*. Jun 24 2016;291(26):13789-801. doi:10.1074/jbc.M115.670521
347. Wight TN, Kang I, Merrilees MJ. Versican and the control of inflammation. *Matrix Biology*. 2014;35:152-161.
348. Petrey AC, de la Motte CA. Hyaluronan in inflammatory bowel disease: cross-linking inflammation and coagulation. *Matrix Biology*. 2019;78:314-323.
349. Evanko SP, Potter-Perigo S, Bollyky PL, Nepom GT, Wight TN. Hyaluronan and versican in the control of human T-lymphocyte adhesion and migration. *Matrix Biology*. 2012;31(2):90-100.
350. Wight TN. Arterial remodeling in vascular disease: a key role for hyaluronan and versican. *Frontiers in Bioscience-Landmark*. 2008;13(13):4933-4937.
351. Viola M, Karousou E, D'Angelo ML, et al. Regulated Hyaluronan Synthesis by Vascular Cells. *International journal of cell biology*. 2015;2015:208303-208303. doi:10.1155/2015/208303

352. Gill S, Wight TN, Frevert CW. Proteoglycans: key regulators of pulmonary inflammation and the innate immune response to lung infection. *The Anatomical Record: Advances in Integrative Anatomy and Evolutionary Biology*. 2010;293(6):968-981.
353. Frevert CW, Felgenhauer J, Wygrecka M, Nastase MV, Schaefer L. Danger-associated molecular patterns derived from the extracellular matrix provide temporal control of innate immunity. *Journal of Histochemistry & Cytochemistry*. 2018;66(4):213-227.
354. Wight TN, Kang I, Evanko SP, et al. Versican-A Critical Extracellular Matrix Regulator of Immunity and Inflammation. *Front Immunol*. 2020;11:512. doi:10.3389/fimmu.2020.00512
355. Lang R, Patel D, Morris JJ, Rutschman RL, Murray PJ. Shaping gene expression in activated and resting primary macrophages by IL-10. *The Journal of Immunology*. 2002;169(5):2253-2263.
356. Martinez FO, Gordon S, Locati M, Mantovani A. Transcriptional profiling of the human monocyte-to-macrophage differentiation and polarization: new molecules and patterns of gene expression. *The Journal of immunology*. 2006;177(10):7303-7311.
357. Chang MY, Tanino Y, Vidova V, et al. A rapid increase in macrophage-derived versican and hyaluronan in infectious lung disease. *Matrix Biology*. 2014;34:1-12.
358. Ye L, Mora R, Akhayani N, Haudenschild CC, Liau G. Growth factor and cytokine-regulated hyaluronan-binding protein TSG-6 is localized to the injury-induced rat neointima and confers enhanced growth in vascular smooth muscle cells. *Circ Res*. Sep 1997;81(3):289-96. doi:10.1161/01.res.81.3.289
359. Coombes BK, Mahony JB. cDNA array analysis of altered gene expression in human endothelial cells in response to Chlamydia pneumoniae infection. *Infect Immun*. Mar 2001;69(3):1420-7. doi:10.1128/iai.69.3.1420-1427.2001
360. Bommaya G, Meran S, Krupa A, Phillips AO, Steadman R. Tumour necrosis factor-stimulated gene (TSG)-6 controls epithelial-mesenchymal transition of proximal tubular epithelial cells. *Int J Biochem Cell Biol*. Dec 2011;43(12):1739-46. doi:10.1016/j.biocel.2011.08.009
361. de La Motte CA, Hascall VC, Calabro A, Yen-Lieberman B, Strong SA. Mononuclear leukocytes preferentially bind via CD44 to hyaluronan on human intestinal mucosal smooth muscle cells after virus infection or treatment with poly(I.C). *J Biol Chem*. Oct 22 1999;274(43):30747-55. doi:10.1074/jbc.274.43.30747
362. Camenisch TD, Spicer AP, Brehm-Gibson T, et al. Disruption of hyaluronan synthase-2 abrogates normal cardiac morphogenesis and hyaluronan-mediated transformation of epithelium to mesenchyme. *The Journal of Clinical Investigation*. 08/01/ 2000;106(3):349-360. doi:10.1172/JCI10272
363. Evanko Stephen P, Angello John C, Wight Thomas N. Formation of Hyaluronan- and Versican-Rich Pericellular Matrix Is Required for Proliferation and Migration of Vascular Smooth Muscle Cells. *Arteriosclerosis, Thrombosis, and Vascular Biology*. 1999/04/01 1999;19(4):1004-1013. doi:10.1161/01.ATV.19.4.1004
364. Evanko SP, Johnson PY, Braun KR, Underhill CB, Dudhia J, Wight TN. Platelet-derived growth factor stimulates the formation of versican–hyaluronan aggregates and pericellular matrix expansion in arterial smooth muscle cells. *Archives of biochemistry and biophysics*. 2001;394(1):29-38.
365. Nishida Y, Knudson CB, Nietfeld JJ, Margulis A, Knudson W. Antisense inhibition of hyaluronan synthase-2 in human articular chondrocytes inhibits proteoglycan retention and matrix assembly. *J Biol Chem*. Jul 30 1999;274(31):21893-9. doi:10.1074/jbc.274.31.21893
366. Mjaatvedt CH, Yamamura H, Capehart AA, Turner D, Markwald RR. The Cspg2 gene, disrupted in the hdf mutant, is required for right cardiac chamber and endocardial cushion formation. *Dev Biol*. Oct 1 1998;202(1):56-66. doi:10.1006/dbio.1998.9001
367. Ausprunk DH, Boudreau CL, Nelson DA. Proteoglycans in the microvascular. II. Histochemical localization in proliferating capillaries of the rabbit cornea. *Am J Pathol*. Jun 1981;103(3):367-75.
368. Anttila MA, Tammi RH, Tammi MI, Syrjänen KJ, Saarikoski SV, Kosma V-M. High Levels of Stromal Hyaluronan Predict Poor Disease Outcome in Epithelial Ovarian Cancer. *Cancer Research*. 2000;60(1):150.

369. West DC, Hampson IN, Arnold F, Kumar S. Angiogenesis induced by degradation products of hyaluronic acid. *Science*. Jun 14 1985;228(4705):1324-6. doi:10.1126/science.2408340
370. Hayen W, Goebeler M, Kumar S, Riessen R, Nehls V. Hyaluronan stimulates tumor cell migration by modulating the fibrin fiber architecture. *J Cell Sci*. Jul 1999;112 (Pt 13):2241-51.
371. Midgley AC, Rogers M, Hallett MB, et al. Transforming Growth Factor-beta 1 (TGF-beta 1)-stimulated Fibroblast to Myofibroblast Differentiation Is Mediated by Hyaluronan (HA)-facilitated Epidermal Growth Factor Receptor (EGFR) and CD44 Co-localization in Lipid Rafts. *Journal of Biological Chemistry*. May 2013;288(21):14824-14838. doi:10.1074/jbc.M113.451336
372. Jenkins RH, Thomas GJ, Williams JD, Steadman R. Myofibroblastic differentiation leads to hyaluronan accumulation through reduced hyaluronan turnover. *J Biol Chem*. Oct 1 2004;279(40):41453-60. doi:10.1074/jbc.M401678200
373. Cohen M, Klein E, Geiger B, Addadi L. Organization and adhesive properties of the hyaluronan pericellular coat of chondrocytes and epithelial cells. *Biophysical journal*. 2003;85(3):1996-2005.
374. Meran S, Thomas DW, Stephens P, et al. Hyaluronan facilitates transforming growth factor-beta(1)-mediated fibroblast proliferation. *Journal of Biological Chemistry*. Mar 2008;283(10):6530-6545. doi:10.1074/jbc.M704819200
375. Simpson RML, Meran S, Thomas D, et al. Age-Related Changes in Pericellular Hyaluronan Organization Leads to Impaired Dermal Fibroblast to Myofibroblast Differentiation. *American Journal of Pathology*. Nov 2009;175(5):1915-1928. doi:10.2353/ajpath.2009.090045
376. Bommaya G, Meran S, Krupa A, Phillips AO, Steadman R. Tumour necrosis factor-stimulated gene (TSG)-6 controls epithelial-mesenchymal transition of proximal tubular epithelial cells. *International Journal of Biochemistry & Cell Biology*. Dec 2011;43(12):1739-1746. doi:10.1016/j.biocel.2011.08.009
377. Meran S, Martin J, Luo DD, Steadman R, Phillips A. Interleukin-1 beta Induces Hyaluronan and CD44-Dependent Cell Protrusions That Facilitate Fibroblast-Monocyte Binding. *American Journal of Pathology*. Jun 2013;182(6):2223-2240. doi:10.1016/j.ajpath.2013.02.038
378. Sagliyan A, Han MC, Karabulut E, Ozkaraca M. Research of the effects of autologous cancellous bone graft and hyaluronic acid on the healing of bone defects experimentally induced in rabbits. *Turkish Journal of Veterinary & Animal Sciences*. 2016;40(4):374-381. doi:10.3906/vet-1511-30
379. Yamasaki S, Hashimoto Y, Takigami J, et al. Effect of the direct injection of bone marrow mesenchymal stem cells in hyaluronic acid and bone marrow stimulation to treat chondral defects in the canine model. *Regenerative Therapy*. Dec 2015;2:42-48. doi:10.1016/j.reth.2015.10.003
380. Aebli N, Stich H, Schawalder P, Theis JC, Krebs J. Effects of bone morphogenetic protein-2 and hyaluronic acid on the osseointegration of hydroxyapatite-coated implants: An experimental study in sheep. *Journal of Biomedical Materials Research Part A*. Jun 2005;73A(3):295-302. doi:10.1002/jbm.a.30299
381. Parfitt AM, Drezner MK, Glorieux FH, et al. Bone histomorphometry: standardization of nomenclature, symbols, and units. Report of the ASBMR Histomorphometry Nomenclature Committee. *J Bone Miner Res*. Dec 1987;2(6):595-610. doi:10.1002/jbmr.5650020617
382. Mohamed AM. An overview of bone cells and their regulating factors of differentiation. *Malays J Med Sci*. Jan 2008;15(1):4-12.
383. Boskey AL, Dick BL. Hyaluronan interactions with hydroxyapatite do not alter in vitro hydroxyapatite crystal proliferation and growth. *Matrix*. Dec 1991;11(6):442-6. doi:10.1016/s0934-8832(11)80198-8
384. Huang L, Cheng YY, Koo PL, et al. The effect of hyaluronan on osteoblast proliferation and differentiation in rat calvarial-derived cell cultures. *J Biomed Mater Res A*. Sep 15 2003;66(4):880-4. doi:10.1002/jbm.a.10535
385. Bornes TD, Jomha NM, Mulet-Sierra A, Adesida AB. Hypoxic culture of bone marrow-derived mesenchymal stromal stem cells differentially enhances in vitro chondrogenesis within cell-seeded

collagen and hyaluronic acid porous scaffolds. *Stem Cell Research & Therapy*. 2015/04/23 2015;6(1):84. doi:10.1186/s13287-015-0075-4
386. Bastow ER, Byers S, Golub SB, Clarkin CE, Pitsillides AA, Fosang AJ. Hyaluronan synthesis and degradation in cartilage and bone. *Cell Mol Life Sci*. Feb 2008;65(3):395-413. doi:10.1007/s00018-007-7360-z
387. Pilloni A, Bernard GW. The effect of hyaluronan on mouse intramembranous osteogenesis in vitro. *Cell Tissue Res*. Nov 1998;294(2):323-33. doi:10.1007/s004410051182
388. Nagahata M, Tsuchiya T, Ishiguro T, et al. A novel function of N-cadherin and Connexin43: marked enhancement of alkaline phosphatase activity in rat calvarial osteoblast exposed to sulfated hyaluronan. *Biochem Biophys Res Commun*. Mar 12 2004;315(3):603-11. doi:10.1016/j.bbrc.2004.01.098
389. Zou L, Zou X, Chen L, et al. Effect of hyaluronan on osteogenic differentiation of porcine bone marrow stromal cells in vitro. *J Orthop Res*. May 2008;26(5):713-20. doi:10.1002/jor.20539
390. Stancíková M, Svík K, Istok R, Rovenský J, Velebný V. The effects of hyaluronan on bone resorption and bone mineral density in a rat model of estrogen deficiency-induced osteopenia. *Int J Tissue React*. 2004;26(1-2):9-16.
391. Ariyoshi W, Takahashi T, Kanno T, et al. Mechanisms involved in enhancement of osteoclast formation and function by low molecular weight hyaluronic acid. *J Biol Chem*. May 13 2005;280(19):18967-72. doi:10.1074/jbc.M412740200
392. Larjava H, Mielityinen H, Tenovuo J, Jalkanen M, Paunio K. The effect of human dental plaque on bone resorption and hyaluronic acid synthesis in in-vitro cultures of fetal rat calvaria. *Arch Oral Biol*. 1982;27(2):147-50. doi:10.1016/0003-9969(82)90135-2
393. Puissant E, Boonen M. Monocytes/Macrophages Upregulate the Hyaluronidase HYAL1 and Adapt Its Subcellular Trafficking to Promote Extracellular Residency upon Differentiation into Osteoclasts. *PLoS One*. 2016;11(10):e0165004. doi:10.1371/journal.pone.0165004
394. Hayer S, Steiner G, Görtz B, et al. CD44 is a determinant of inflammatory bone loss. *The Journal of experimental medicine*. 04/01 2005;201:903-14. doi:10.1084/jem.20040852
395. Prince CW. Roles of hyaluronan in bone resorption. *BMC Musculoskeletal Disorders*. 2004/04/29 2004;5(1):12. doi:10.1186/1471-2474-5-12
396. Cao JJ, Singleton PA, Majumdar S, et al. Hyaluronan increases RANKL expression in bone marrow stromal cells through CD44. *J Bone Miner Res*. Jan 2005;20(1):30-40. doi:10.1359/jbmr.041014
397. Maxwell CA, Rasmussen E, Zhan F, et al. RHAMM expression and isoform balance predict aggressive disease and poor survival in multiple myeloma. *Blood*. 2004;104(4):1151-1158. doi:10.1182/blood-2003-11-4079
398. Chou CH, Attarian DE, Wisniewski HG, Band PA, Kraus VB. TSG-6 - a double-edged sword for osteoarthritis (OA). *Osteoarthritis Cartilage*. Feb 2018;26(2):245-254. doi:10.1016/j.joca.2017.10.019
399. Broeren MGA, Di Ceglie I, Bennink MB, et al. Treatment of collagenase-induced osteoarthritis with a viral vector encoding TSG-6 results in ectopic bone formation. *PeerJ*. 2018;6:e4771. doi:10.7717/peerj.4771
400. Shibata S, Fukada K, Suzuki S, Ogawa T, Yamashita Y. Histochemical localisation of versican, aggrecan and hyaluronan in the developing condylar cartilage of the fetal rat mandible. *J Anat*. Feb 2001;198(Pt 2):129-35. doi:10.1046/j.1469-7580.2001.19820129.x
401. Nakamura M, Sone S, Takahashi I, Mizoguchi I, Echigo S, Sasano Y. Expression of versican and ADAMTS1, 4, and 5 during bone development in the rat mandible and hind limb. *J Histochem Cytochem*. Dec 2005;53(12):1553-62. doi:10.1369/jhc.5A6669.2005
402. Heickendorff L, Ledet T, Rasmussen LM. Glycosaminoglycans in the human aorta in diabetes mellitus: a study of tunica media from areas with and without atherosclerotic plaque. *Diabetologia*. 1994;37:286-292.

403. Riessen R, Wight TN, Pastore C, Henley C, Isner JM. Distribution of hyaluronan during extracellular matrix remodeling in human restenotic arteries and balloon-injured rat carotid arteries. *Circulation*. 1996;93(6):1141-1147.
404. Turley EA. Extracellular matrix remodeling: multiple paradigms in vascular disease. Am Heart Assoc; 2001. p. 2-4.
405. Stephens EH, Chu C-K, Grande-Allen KJ. Valve proteoglycan content and glycosaminoglycan fine structure are unique to microstructure, mechanical load and age: Relevance to an age-specific tissue-engineered heart valve. *Acta biomaterialia*. 2008;4(5):1148-1160.
406. Nakashima Y, Fujii H, Sumiyoshi S, Wight TN, Sueishi K. Early human atherosclerosis: accumulation of lipid and proteoglycans in intimal thickenings followed by macrophage infiltration. *Arteriosclerosis, thrombosis, and vascular biology*. 2007;27(5):1159-1165.
407. Sussmann M, Sarbia M, Meyer-Kirchrath J, Nusing RM, Schror K, Fischer JW. Induction of hyaluronic acid synthase 2 (HAS2) in human vascular smooth muscle cells by vasodilatory prostaglandins. *Circulation research*. 2004;94(5):592-600.
408. Papakonstantinou E, Roth M, Block LH, Mirtsou-Fidani V, Argiriadis P, Karakiulakis G. The differential distribution of hyaluronic acid in the layers of human atheromatic aortas is associated with vascular smooth muscle cell proliferation and migration. *Atherosclerosis*. 1998/05/01/ 1998;138(1):79-89. doi:https://doi.org/10.1016/S0021-9150(98)00006-9
409. Levesque H, Girard N, Maingonnat C, et al. Localization and solubilization of hyaluronan and of the hyaluronan-binding protein hyaluronectin in human normal and arteriosclerotic arterial walls. *Atherosclerosis*. 1994;105(1):51-62.
410. Itoh S, Matubara M, Kawauchi T, et al. Enhancement of bone ingrowth in a titanium fiber mesh implant by rhBMP-2 and hyaluronic acid. *Journal of Materials Science: Materials in Medicine*. 2001;12:575-581.
411. Kim HD, Valentini RF. Retention and activity of BMP-2 in hyaluronic acid-based scaffolds in vitro. *Journal of Biomedical Materials Research: An Official Journal of The Society for Biomaterials, The Japanese Society for Biomaterials, and The Australian Society for Biomaterials and the Korean Society for Biomaterials*. 2002;59(3):573-584.
412. Nagy N, Freudenberger T, Melchior-Becker A, et al. Inhibition of hyaluronan synthesis accelerates murine atherosclerosis: novel insights into the role of hyaluronan synthesis. *Circulation*. Nov 30 2010;122(22):2313-22. doi:10.1161/circulationaha.110.972653
413. Homann S, Grandoch M, Kiene LS, et al. Hyaluronan synthase 3 promotes plaque inflammation and atheroprogression. *Matrix Biology*. 2018;66:67-80.
414. Kiene LS, Homann S, Suvorava T, et al. Deletion of hyaluronan synthase 3 inhibits neointimal hyperplasia in mice. *Arteriosclerosis, thrombosis, and vascular biology*. 2016;36(2):e9-e16.
415. Chai S, Chai Q, Danielsen Carl C, et al. Overexpression of Hyaluronan in the Tunica Media Promotes the Development of Atherosclerosis. *Circulation Research*. 2005/03/18 2005;96(5):583-591. doi:10.1161/01.RES.0000158963.37132.8b
416. Zhao L, Lee E, Zukas AM, et al. CD44 expressed on both bone marrow–derived and non–bone marrow–derived cells promotes atherogenesis in ApoE-deficient mice. *Arteriosclerosis, thrombosis, and vascular biology*. 2008;28(7):1283-1289.
417. Cuff CA, Kothapalli D, Azonobi I, et al. The adhesion receptor CD44 promotes atherosclerosis by mediating inflammatory cell recruitment and vascular cell activation. *J Clin Invest*. Oct 2001;108(7):1031-40. doi:10.1172/jci12455
418. Kolodgie FD, Burke AP, Wight TN, Virmani R. The accumulation of specific types of proteoglycans in eroded plaques: a role in coronary thrombosis in the absence of rupture. *Current opinion in lipidology*. 2004;15(5):575-582.
419. Kolodgie FD, Burke AP, Farb A, et al. Differential accumulation of Proteoglycans and hyaluronan in culprit lesions - Insights into plaque erosion. *Arteriosclerosis Thrombosis and Vascular Biology*. Oct 2002;22(10):1642-1648. doi:10.1161/01.atv.0000034021.92658.4c

420. Zhao L, A. Hall J, Levenkova N, et al. CD44 regulates vascular gene expression in a proatherogenic environment. *Arteriosclerosis, thrombosis, and vascular biology*. 2007;27(4):886-892.
421. Hägg D, Sjöberg S, Hultén LM, et al. Augmented levels of CD44 in macrophages from atherosclerotic subjects: A possible IL-6–CD44 feedback loop? *Atherosclerosis*. 2007;190(2):291-297.
422. Krettek A, Sukhova GK, Schönbeck U, Libby P. Enhanced expression of CD44 variants in human atheroma and abdominal aortic aneurysm: possible role for a feedback loop in endothelial cells. *The American journal of pathology*. 2004;165(5):1571-1581.
423. Matsui Y, Rittling SR, Okamoto H, et al. Osteopontin deficiency attenuates atherosclerosis in female apolipoprotein E–deficient mice. *Arteriosclerosis, thrombosis, and vascular biology*. 2003;23(6):1029-1034.
424. Baugh L, Watson MC, Kemmerling EC, Hinds PW, Huggins GS, Black LD. Knockdown of CD44 expression decreases valve interstitial cell calcification in vitro. *American Journal of Physiology-Heart and Circulatory Physiology*. 2019/07/01 2019;317(1):H26-H36. doi:10.1152/ajpheart.00123.2018
425. Krupinski J, Ethirajan P, Font MA, et al. Changes in Hyaluronan Metabolism and RHAMM Receptor Expression Accompany Formation of Complicated Carotid Lesions and May be Pro-Angiogenic Mediators of Intimal Neovessel Growth. *Biomark Insights*. May 12 2008;2:361-7.
426. Tuomisto TT, Lumivuori H, Kansanen E, et al. Simvastatin has an anti-inflammatory effect on macrophages via upregulation of an atheroprotective transcription factor, Kruppel-like factor 2. *Cardiovasc Res*. Apr 1 2008;78(1):175-84. doi:10.1093/cvr/cvn007
427. Ye L, Mora R, Akhayani N, Haudenschild CC, Liau G. Growth factor and cytokine-regulated hyaluronan-binding protein TSG-6 is localized to the injury-induced rat neointima and confers enhanced growth in vascular smooth muscle cells. *Circulation Research*. Sep 1997;81(3):289-296. doi:10.1161/01.res.81.3.289
428. Wang S-s, Hu S-w, Zhang Q-h, Xia A-x, Jiang Z-x, Chen X-m. Mesenchymal stem cells stabilize atherosclerotic vulnerable plaque by anti-inflammatory properties. *PLoS One*. 2015;10(8):e0136026.
429. Watanabe R, Sato Y, Ozawa N, Takahashi Y, Koba S, Watanabe T. Emerging roles of tumor necrosis factor-stimulated gene-6 in the pathophysiology and treatment of atherosclerosis. *International Journal of Molecular Sciences*. 2018;19(2):465.
430. Wang SK, Xie J, Green LA, et al. TSG-6 is highly expressed in human abdominal aortic aneurysms. *Journal of Surgical Research*. 2017;220:311-319.
431. Wu YJ, Pierre DPLA, Wu J, Yee AJ, Yang BB. The interaction of versican with its binding partners. *Cell Research*. 2005/07/01 2005;15(7):483-494. doi:10.1038/sj.cr.7290318
432. Kenagy RD, Plaas AH, Wight TN. Versican degradation and vascular disease. *Trends Cardiovasc Med*. Aug 2006;16(6):209-15. doi:10.1016/j.tcm.2006.03.011
433. Asplund A, Fridén V, Stillemark-Billton P, Camejo G, Bondjers G. Macrophages exposed to hypoxia secrete proteoglycans for which LDL has higher affinity. *Atherosclerosis*. 2011;215(1):77-81.
434. Asplund A, Östergren-Lundén G, Camejo G, Stillemark-Billton P, Bondjers G. Hypoxia increases macrophage motility, possibly by decreasing the heparan sulfate proteoglycan biosynthesis. *Journal of Leukocyte Biology*. 2009;86(2):381-388.
435. Wingrove JA, Daniels SE, Sehnert AJ, et al. Correlation of peripheral-blood gene expression with the extent of coronary artery stenosis. *Circulation: Cardiovascular Genetics*. 2008;1(1):31-38.
436. Toeda K, Nakamura K, Hirohata S, et al. Versican is induced in infiltrating monocytes in myocardial infarction. *Molecular and cellular biochemistry*. 2005;280:47-56.
437. Mine S, Okada Y, Kawahara C, Tabata T, Tanaka Y. Serum hyaluronan concentration as a marker of angiopathy in patients with diabetes mellitus. *Endocr J*. Dec 2006;53(6):761-6. doi:10.1507/endocrj.k05-119
438. Andresen JL, Rasmussen LM, Ledet T. Diabetic macroangiopathy and atherosclerosis. *Diabetes*. 1996;45(Supplement_3):S91-S94.
439. Järvisalo MJ, Jartti L, Näntö-Salonen K, et al. Increased aortic intima-media thickness: a marker of preclinical atherosclerosis in high-risk children. *Circulation*. 2001;104(24):2943-2947.

440. Jarvisalo MJ, Putto-Laurila A, Jartti L, et al. Carotid artery intima-media thickness in children with type 1 diabetes. *Diabetes*. 2002;51(2):493-498.
441. Nieuwdorp M, Holleman F, de Groot E, et al. Perturbation of hyaluronan metabolism predisposes patients with type 1 diabetes mellitus to atherosclerosis. *Diabetologia*. 2007/06/01 2007;50(6):1288-1293. doi:10.1007/s00125-007-0666-4
442. Nieuwdorp M, van Haeften TW, Gouverneur MCLG, et al. Loss of endothelial glycocalyx during acute hyperglycemia coincides with endothelial dysfunction and coagulation activation in vivo. *Diabetes*. 2006;55(2):480-486.
443. Nagy N, Freudenberger T, Melchior-Becker A, et al. Inhibition of hyaluronan synthesis accelerates murine atherosclerosis: novel insights into the role of hyaluronan synthesis. *Circulation*. 2010;122(22):2313-2322.
444. Dogné S, Rath G, Jouret F, Caron N, Dessy C, Flamion B. Hyaluronidase 1 Deficiency Preserves Endothelial Function and Glycocalyx Integrity in Early Streptozotocin-Induced Diabetes. *Diabetes*. 2016;65(9):2742-2753. doi:10.2337/db15-1662
445. Mahadevan P, Larkins RG, Fraser JR, Fosang AJ, Dunlop ME. Increased hyaluronan production in the glomeruli from diabetic rats: a link between glucose-induced prostaglandin production and reduced sulphated proteoglycan. *Diabetologia*. Mar 1995;38(3):298-305. doi:10.1007/bf00400634
446. Chajara A, Raoudi M, Delpech B, Leroy M, Basuyau JP, Levesque H. Circulating hyaluronan and hyaluronidase are increased in diabetic rats. *Diabetologia*. Mar 2000;43(3):387-8. doi:10.1007/s001250050061
447. Ikegami-Kawai M, Okuda R, Nemoto T, Inada N, Takahashi T. Enhanced activity of serum and urinary hyaluronidases in streptozotocin-induced diabetic Wistar and GK rats. *Glycobiology*. 2004;14(1):65-72.
448. Moretto P, Karousou E, Viola M, et al. Regulation of Hyaluronan Synthesis in Vascular Diseases and Diabetes. *Journal of Diabetes Research*. 2015;167283. doi:10.1155/2015/167283
449. Roccabianca S, Bellini C, Humphrey JD. Computational modelling suggests good, bad and ugly roles of glycosaminoglycans in arterial wall mechanics and mechanobiology. *Journal of the Royal Society Interface*. Aug 2014;11(97)20140397. doi:10.1098/rsif.2014.0397
450. Chajara A, Delpech B, Levesque H. Effect of aging on neointima formation and hyaluronan, hyaluronidase and hyaluronectin production in injured rat aorta. *Journal of Vascular Research*. Aug 1998;35:98-98.
451. Weiss L, Slavin S, Reich S, et al. Induction of resistance to diabetes in non-obese diabetic mice by targeting CD44 with a specific monoclonal antibody. *Proc Natl Acad Sci U S A*. Jan 4 2000;97(1):285-90. doi:10.1073/pnas.97.1.285
452. Basatemur GL, Jørgensen HF, Clarke MCH, Bennett MR, Mallat Z. Vascular smooth muscle cells in atherosclerosis. *Nature reviews cardiology*. 2019;16(12):727-744.
453. Ross R. George Lyman Duff Memorial Lecture. Atherosclerosis: a problem of the biology of arterial wall cells and their interactions with blood components. *Arteriosclerosis*. Sep-Oct 1981;1(5):293-311. doi:10.1161/01.atv.1.5.293
454. Evanko SP, Angello JC, Wight TN. Formation of hyaluronan- and versican-rich pericellular matrix is required for proliferation and migration of vascular smooth muscle cells. *Arteriosclerosis Thrombosis and Vascular Biology*. Apr 1999;19(4):1004-1013. doi:10.1161/01.atv.19.4.1004
455. Brecht M, Mayer U, Schlosser E, Prehm P. Increased hyaluronate synthesis is required for fibroblast detachment and mitosis. *Biochemical Journal*. 1986;239(2):445-450.
456. Papakonstantinou E, Karakiulakis G, Roth M, Block LH. Platelet-derived growth factor stimulates the secretion of hyaluronic acid by proliferating human vascular smooth muscle cells. *Proceedings of the National Academy of Sciences*. 1995;92(21):9881-9885.
457. Vigetti D, Rizzi M, Viola M, et al. The effects of 4-methylumbelliferone on hyaluronan synthesis, MMP2 activity, proliferation, and motility of human aortic smooth muscle cells. *Glycobiology*. 2009;19(5):537-546.

458. Vigetti D, Rizzi M, Moretto P, et al. Glycosaminoglycans and glucose prevent apoptosis in 4-methylumbelliferone-treated human aortic smooth muscle cells. *Journal of Biological Chemistry*. 2011;286(40):34497-34503.
459. Kothapalli D, Zhao L, Hawthorne EA, et al. Hyaluronan and CD44 antagonize mitogen-dependent cyclin D1 expression in mesenchymal cells. *The Journal of cell biology*. 2007;176(4):535-544.
460. Jain M, He Q, Lee W-S, et al. Role of CD44 in the reaction of vascular smooth muscle cells to arterial wall injury. *The Journal of clinical investigation*. 1996;97(3):596-603.
461. Maier KG, Sadowitz B, Cullen S, Han X, Gahtan V. Thrombospondin-1–induced vascular smooth muscle cell migration is dependent on the hyaluronic acid receptor CD44. *The American journal of surgery*. 2009;198(5):664-669.
462. Yao LY, Moody C, Schönherr E, Wight TN, Sandell LJ. Identification of the proteoglycan versican in aorta and smooth muscle cells by DNA sequence analysis, in situ hybridization and immunohistochemistry. *Matrix Biology*. 1994;14(3):213-225.
463. LeBaron RG, Zimmermann DR, Ruoslahti E. Hyaluronate binding properties of versican. *Journal of Biological Chemistry*. 1992;267(14):10003-10010.
464. Chang Y, Yanagishita M, Hascall VC, Wight TN. Proteoglycans synthesized by smooth muscle cells derived from monkey (Macaca nemestrina) aorta. *Journal of Biological Chemistry*. 1983;258(9):5679-5688.
465. Schönherr E, Järveläinen HT, Sandell LJ, Wight TN. Effects of platelet-derived growth factor and transforming growth factor-beta 1 on the synthesis of a large versican-like chondroitin sulfate proteoglycan by arterial smooth muscle cells. *Journal of Biological Chemistry*. 1991;266(26):17640-17647.
466. Wilkinson TS, Bressler SL, Evanko SP, Braun KR, Wight TN. Overexpression of hyaluronan synthases alters vascular smooth muscle cell phenotype and promotes monocyte adhesion. *Journal of cellular physiology*. 2006;206(2):378-385.
467. Caon I, Bartolini B, Moretto P, et al. Sirtuin 1 reduces hyaluronan synthase 2 expression by inhibiting nuclear translocation of NF-κB and expression of the long-noncoding RNA HAS2–AS1. *Journal of Biological Chemistry*. 2020;295(11):3485-3496.
468. Vigetti D, Viola M, Karousou E, et al. Hyaluronan-CD44-ERK1/2 regulate human aortic smooth muscle cell motility during aging. *Journal of Biological Chemistry*. Feb 2008;283(7):4448-4458. doi:10.1074/jbc.M709051200
469. Kashima Y, Takahashi M, Shiba Y, et al. Crucial Role of Hyaluronan in Neointimal Formation after Vascular Injury. *Plos One*. Mar 2013;8(3)e58760. doi:10.1371/journal.pone.0058760
470. Kiene LS, Homann S, Suvorava T, et al. Deletion of Hyaluronan Synthase 3 Inhibits Neointimal Hyperplasia in Mice. *Arteriosclerosis Thrombosis and Vascular Biology*. Feb 2016;36(2):E9-E16. doi:10.1161/atvbaha.115.306607
471. Fischer JW, Schrör K. Regulation of hyaluronan synthesis by vasodilatory prostaglandins. Implications for atherosclerosis. *Thromb Haemost*. Aug 2007;98(2):287-95.
472. Savani RC, Wang C, Yang B, et al. Migration of bovine aortic smooth muscle cells after wounding injury. The role of hyaluronan and RHAMM. *The Journal of clinical investigation*. 1995;95(3):1158-1168.
473. Gerdin B, Hällgren R. Dynamic role of hyaluronan (HYA) in connective tissue activation and inflammation. *Journal of Internal Medicine*. 1997/07/01 1997;242(1):49-55. doi:10.1046/j.1365-2796.1997.00173.x
474. Laurent TC, Laurent UB, Fraser JR. Serum hyaluronan as a disease marker. *Ann Med*. Jun 1996;28(3):241-53. doi:10.3109/07853899609033126
475. Marutsuka K, Woodcock-Mitchell J, Sakamoto T, Sobel BE, Fujii S. Pathogenetic implications of hyaluronan-induced modification of vascular smooth muscle cell fibrinolysis in diabetes. *Coron Artery Dis*. 1998;9(4):177-84. doi:10.1097/00019501-199809040-00002

476. Soulié P, Chassot A, Ernandez T, Montesano R, Féraille E. Spatially restricted hyaluronan production by Has2 drives epithelial tubulogenesis in vitro. *Am J Physiol Cell Physiol*. Oct 15 2014;307(8):C745-59. doi:10.1152/ajpcell.00047.2014
477. Nishikawa K, Andres G, Bhan AK, et al. Hyaluronate is a component of crescents in rat autoimmune glomerulonephritis. *Lab Invest*. Feb 1993;68(2):146-53.
478. Yung S, Tsang RC, Leung JK, Chan TM. Increased mesangial cell hyaluronan expression in lupus nephritis is mediated by anti-DNA antibody-induced IL-1beta. *Kidney Int*. Jan 2006;69(2):272-80. doi:10.1038/sj.ki.5000042
479. Mummert ME, Mohamadzadeh M, Mummert DI, Mizumoto N, Takashima A. Development of a peptide inhibitor of hyaluronan-mediated leukocyte trafficking. *The Journal of experimental medicine*. 2000;192(6):769-779. doi:10.1084/jem.192.6.769
480. Teder P, Vandivier RW, Jiang D, et al. Resolution of lung inflammation by CD44. *Science*. Apr 5 2002;296(5565):155-8. doi:10.1126/science.1069659
481. DeGrendele HC, Estess P, Picker LJ, Siegelman MH. CD44 and its ligand hyaluronate mediate rolling under physiologic flow: a novel lymphocyte-endothelial cell primary adhesion pathway. *J Exp Med*. Mar 1 1996;183(3):1119-30. doi:10.1084/jem.183.3.1119
482. Mohamadzadeh M, DeGrendele H, Arizpe H, Estess P, Siegelman M. Proinflammatory stimuli regulate endothelial hyaluronan expression and CD44/HA-dependent primary adhesion. *J Clin Invest*. Jan 1 1998;101(1):97-108. doi:10.1172/jci1604
483. Majors AK, Austin RC, de la Motte CA, et al. Endoplasmic reticulum stress induces hyaluronan deposition and leukocyte adhesion. *J Biol Chem*. Nov 21 2003;278(47):47223-31. doi:10.1074/jbc.M304871200
484. Yang J, Jin K, Xiao J, Ma J, Ma D. Endogenous tissue factor pathway inhibitor in vascular smooth muscle cells inhibits arterial thrombosis. *Front Med*. Sep 2017;11(3):403-409. doi:10.1007/s11684-017-0522-y
485. Hays TT, Ma B, Zhou N, Stoll S, Pearce WJ, Qiu H. Vascular smooth muscle cells direct extracellular dysregulation in aortic stiffening of hypertensive rats. *Aging Cell*. Jun 2018;17(3):e12748. doi:10.1111/acel.12748
486. Orekhov AN, Andreeva ER, Mikhailova IA, Gordon D. Cell proliferation in normal and atherosclerotic human aorta: proliferative splash in lipid-rich lesions. *Atherosclerosis*. Jul 1998;139(1):41-8. doi:10.1016/s0021-9150(98)00044-6
487. Yap C, Mieremet A, de Vries CJM, Micha D, de Waard V. Six Shades of Vascular Smooth Muscle Cells Illuminated by KLF4 (Krüppel-Like Factor 4). *Arteriosclerosis, Thrombosis, and Vascular Biology*. 2021/11/01 2021;41(11):2693-2707. doi:10.1161/ATVBAHA.121.316600
488. Rensen SSM, Doevendans P, Van Eys G. Regulation and characteristics of vascular smooth muscle cell phenotypic diversity. *Netherlands Heart Journal*. 2007;15:100-108.
489. Rzucidlo EM, Martin KA, Powell RJ. Regulation of vascular smooth muscle cell differentiation. *Journal of Vascular Surgery*. 2007/06/01/ 2007;45(6, Supplement):A25-A32. doi:https://doi.org/10.1016/j.jvs.2007.03.001
490. Owens GK. Regulation of differentiation of vascular smooth muscle cells. *Physiol Rev*. Jul 1995;75(3):487-517. doi:10.1152/physrev.1995.75.3.487
491. Speer MY, Yang HY, Brabb T, et al. Smooth muscle cells give rise to osteochondrogenic precursors and chondrocytes in calcifying arteries. *Circ Res*. Mar 27 2009;104(6):733-41. doi:10.1161/circresaha.108.183053
492. Durham AL, Speer MY, Scatena M, Giachelli CM, Shanahan CM. Role of smooth muscle cells in vascular calcification: implications in atherosclerosis and arterial stiffness. *Cardiovasc Res*. Mar 15 2018;114(4):590-600. doi:10.1093/cvr/cvy010
493. Woldt E, Terrand J, Mlih M, et al. The nuclear hormone receptor PPARγ counteracts vascular calcification by inhibiting Wnt5a signalling in vascular smooth muscle cells. *Nature Communications*. 2012/09/25 2012;3(1):1077. doi:10.1038/ncomms2087

494. Cozzolino M, Brancaccio D, Gallieni M, Slatopolsky E. Pathogenesis of vascular calcification in chronic kidney disease. *Kidney international*. 2005;68(2):429-436.
495. Johnson RC, Leopold JA, Loscalzo J. Vascular calcification: pathobiological mechanisms and clinical implications. *Circulation research*. 2006;99(10):1044-1059.
496. Lian JB, Stein GS. The developmental stages of osteoblast growth and differentiation exhibit selective responses of genes to growth factors (TGF beta 1) and hormones (vitamin D and glucocorticoids). *J Oral Implantol*. 1993;19(2):95-105; discussion 136-7.
497. Shanahan CM, Cary NR, Salisbury JR, Proudfoot D, Weissberg PL, Edmonds ME. Medial localization of mineralization-regulating proteins in association with Mönckeberg's sclerosis: evidence for smooth muscle cell-mediated vascular calcification. *Circulation*. Nov 23 1999;100(21):2168-76. doi:10.1161/01.cir.100.21.2168
498. Lanzer P, Boehm M, Sorribas V, et al. Medial vascular calcification revisited: review and perspectives. *European Heart Journal*. 2014;35(23):1515-1525. doi:10.1093/eurheartj/ehu163
499. Patel JJ, Bourne LE, Davies BK, et al. Differing calcification processes in cultured vascular smooth muscle cells and osteoblasts. *Experimental cell research*. 2019;380(1):100-113.
500. Essalihi R, Ouellette V, Dao HH, McKee MD, Moreau P. Phenotypic modulation of vascular smooth muscle cells during medial arterial calcification: a role for endothelin? *Journal of cardiovascular pharmacology*. 2004;44:S147-S150.
501. Alves R, Eijken M, van de Peppel J, van Leeuwen J. Calcifying vascular smooth muscle cells and osteoblasts: independent cell types exhibiting extracellular matrix and biomineralization-related mimicries. *Bmc Genomics*. Nov 2014;15965. doi:10.1186/1471-2164-15-965
502. Boström K. Insights into the mechanism of vascular calcification. *Am J Cardiol*. Jul 19 2001;88(2a):20e-22e. doi:10.1016/s0002-9149(01)01718-0
503. Giachelli CM. Vascular calcification: in vitro evidence for the role of inorganic phosphate. *Journal of the American Society of Nephrology*. 2003;14(suppl_4):S300-S304.
504. Persy V, D'Haese P. Vascular calcification and bone disease: the calcification paradox. *Trends Mol Med*. Sep 2009;15(9):405-16. doi:10.1016/j.molmed.2009.07.001
505. Lin H, Zhou Y, Lei Q, Lin D, Chen J, Wu C. Effect of inorganic phosphate on migration and osteogenic differentiation of bone marrow mesenchymal stem cells. *BMC Developmental Biology*. 2021/01/06 2021;21(1):1. doi:10.1186/s12861-020-00229-x
506. Yang H, Curinga G, Giachelli CM. Elevated extracellular calcium levels induce smooth muscle cell matrix mineralization in vitro. *Kidney Int*. Dec 2004;66(6):2293-9. doi:10.1111/j.1523-1755.2004.66015.x
507. Zoccali C. Traditional and emerging cardiovascular and renal risk factors: an epidemiologic perspective. *Kidney Int*. Jul 2006;70(1):26-33. doi:10.1038/sj.ki.5000417
508. Stenvinkel P, Ketteler M, Johnson RJ, et al. IL-10, IL-6, and TNF-alpha: central factors in the altered cytokine network of uremia--the good, the bad, and the ugly. *Kidney Int*. Apr 2005;67(4):1216-33. doi:10.1111/j.1523-1755.2005.00200.x
509. Zoccali C, Mallamaci F, Tripepi G. Inflammatory proteins as predictors of cardiovascular disease in patients with end-stage renal disease. *Nephrol Dial Transplant*. Aug 2004;19 Suppl 5:V67-72. doi:10.1093/ndt/gfh1059
510. Barreto DV, Barreto FC, Liabeuf S, et al. Plasma interleukin-6 is independently associated with mortality in both hemodialysis and pre-dialysis patients with chronic kidney disease. *Kidney Int*. Mar 2010;77(6):550-6. doi:10.1038/ki.2009.503
511. Tripepi G, Mallamaci F, Zoccali C. Inflammation markers, adhesion molecules, and all-cause and cardiovascular mortality in patients with ESRD: searching for the best risk marker by multivariate modeling. *J Am Soc Nephrol*. Mar 2005;16 Suppl 1:S83-8. doi:10.1681/asn.2004110972
512. Honda H, Qureshi AR, Heimbürger O, et al. Serum albumin, C-reactive protein, interleukin 6, and fetuin a as predictors of malnutrition, cardiovascular disease, and mortality in patients with ESRD. *Am J Kidney Dis*. Jan 2006;47(1):139-48. doi:10.1053/j.ajkd.2005.09.014

513. Mehta T, Buzkova P, Kizer JR, et al. Higher plasma transforming growth factor (TGF)-β is associated with kidney disease in older community dwelling adults. *BMC Nephrology*. 2017/03/21 2017;18(1):98. doi:10.1186/s12882-017-0509-6
514. Fisman EZ, Benderly M, Esper RJ, et al. Interleukin-6 and the risk of future cardiovascular events in patients with angina pectoris and/or healed myocardial infarction. *The American journal of cardiology*. 2006;98(1):14-18.
515. Roig E, Orús J, Paré C, et al. Serum interleukin-6 in congestive heart failure secondary to idiopathic dilated cardiomyopathy. *American Journal of Cardiology*. 1998;82(5):688-690.
516. Kraśniak A, Drożdż M, Pasowicz M, et al. Factors involved in vascular calcification and atherosclerosis in maintenance haemodialysis patients. *Nephrology Dialysis Transplantation*. 2007;22(2):515-521.
517. Lee C-T, Chua S, Hsu C-Y, et al. Biomarkers associated with vascular and valvular calcification in chronic hemodialysis patients. *Disease markers*. 2013;34(4):229-235.
518. Schuett H, Luchtefeld M, Grothusen C, Grote K, Schieffer B. How much is too much? Interleukin-6 and its signalling in atherosclerosis. *Thrombosis and haemostasis*. 2009;102(08):215-222.
519. Wassmann S, Stumpf M, Strehlow K, et al. Interleukin-6 induces oxidative stress and endothelial dysfunction by overexpression of the angiotensin II type 1 receptor. *Circulation research*. 2004;94(4):534-541.
520. Kurozumi A, Nakano K, Yamagata K, Okada Y, Nakayamada S, Tanaka Y. IL-6 and sIL-6R induces STAT3-dependent differentiation of human VSMCs into osteoblast-like cells through JMJD2B-mediated histone demethylation of RUNX2. *Bone*. 2019;124:53-61.
521. Collin-Osdoby P. Regulation of vascular calcification by osteoclast regulatory factors RANKL and osteoprotegerin. *Circulation research*. 2004;95(11):1046-1057.
522. Deuell KA, Callegari A, Giachelli CM, Rosenfeld ME, Scatena M. RANKL enhances macrophage paracrine pro-calcific activity in high phosphate-treated smooth muscle cells: dependence on IL-6 and TNF-α. *Journal of vascular research*. 2012;49(6):510-521.
523. Yokota K, Sato K, Miyazaki T, et al. Characterization and Function of Tumor Necrosis Factor and Interleukin-6–Induced Osteoclasts in Rheumatoid Arthritis. *Arthritis & Rheumatology*. 2021;73(7):1145-1154.
524. Lee G-L, Yeh C-C, Wu J-Y, et al. TLR2 promotes vascular smooth muscle cell chondrogenic differentiation and consequent calcification via the concerted actions of osteoprotegerin suppression and IL-6–mediated RANKL induction. *Arteriosclerosis, Thrombosis, and Vascular Biology*. 2019;39(3):432-445.
525. Chen G, Deng C, Li Y-P. TGF-β and BMP Signaling in Osteoblast Differentiation and Bone Formation. Review. *International Journal of Biological Sciences*. 2012;8(2):272-288. doi:10.7150/ijbs.2929
526. Hu X-j, Wu W-c-h, Dong N-g, et al. Role of TGF-β1 Signaling in Heart Valve Calcification Induced by Abnormal Mechanical Stimulation in a Tissue Engineering Model. *Current Medical Science*. 2018/10/01 2018;38(5):765-775. doi:10.1007/s11596-018-1943-9
527. Wang N, Wang X, Xing C, et al. Role of TGF-β1 in Bone Matrix Production in Vascular Smooth Muscle Cells Induced by a High-Phosphate Environment. *Nephron Experimental Nephrology*. 2010;115(3):e60-e68. doi:10.1159/000313831
528. He F, Li L, Li P-P, et al. Cyclooxygenase-2/sclerostin mediates TGF-β1-induced calcification in vascular smooth muscle cells and rats undergoing renal failure. *Aging (Albany NY)*. 2020;12(21):21220.
529. Alam MU, Kirton JP, Wilkinson FL, et al. Calcification is associated with loss of functional calcium-sensing receptor in vascular smooth muscle cells. *Cardiovasc Res*. Feb 1 2009;81(2):260-8. doi:10.1093/cvr/cvn279
530. Wada T, McKee MD, Steitz S, Giachelli CM. Calcification of Vascular Smooth Muscle Cell Cultures. *Circulation Research*. 1999/02/05 1999;84(2):166-178. doi:10.1161/01.RES.84.2.166

531. da Silva RA, da SFG, da CFCJ, Zambuzzi WF. Osteogenic gene markers are epigenetically reprogrammed during contractile-to-calcifying vascular smooth muscle cell phenotype transition. *Cell Signal*. Feb 2020;66:109458. doi:10.1016/j.cellsig.2019.109458
532. Chen Y, Zhao X, Wu H. Transcriptional Programming in Arteriosclerotic Disease. *Arteriosclerosis, Thrombosis, and Vascular Biology*. 2021/01/01 2021;41(1):20-34. doi:10.1161/ATVBAHA.120.313791
533. Sun Y, Byon CH, Yuan K, et al. Smooth muscle cell-specific runx2 deficiency inhibits vascular calcification. *Circ Res*. Aug 17 2012;111(5):543-52. doi:10.1161/circresaha.112.267237
534. Thiagarajan L, Abu-Awwad HA-DM, Dixon JE. Osteogenic Programming of Human Mesenchymal Stem Cells with Highly Efficient Intracellular Delivery of RUNX2. *Stem cells translational medicine*. 2017;6(12):2146-2159. doi:10.1002/sctm.17-0137
535. Zohar R, Cheifetz S, McCulloch CA, Sodek J. Analysis of intracellular osteopontin as a marker of osteoblastic cell differentiation and mesenchymal cell migration. *Eur J Oral Sci*. Jan 1998;106 Suppl 1:401-7. doi:10.1111/j.1600-0722.1998.tb02206.x
536. De Fusco C, Messina A, Monda V, et al. Osteopontin: Relation between Adipose Tissue and Bone Homeostasis. *Stem Cells International*. 2017/01/17 2017;2017:4045238. doi:10.1155/2017/4045238
537. Nakamura T, Nakamura-Takahashi A, Kasahara M, Yamaguchi A, Azuma T. Tissue-nonspecific alkaline phosphatase promotes the osteogenic differentiation of osteoprogenitor cells. *Biochemical and Biophysical Research Communications*. 2020/04/09/ 2020;524(3):702-709. doi:https://doi.org/10.1016/j.bbrc.2020.01.136
538. Prins H-J, Braat AK, Gawlitta D, et al. In vitro induction of alkaline phosphatase levels predicts in vivo bone forming capacity of human bone marrow stromal cells. *Stem Cell Research*. 2014/03/01/ 2014;12(2):428-440. doi:https://doi.org/10.1016/j.scr.2013.12.001
539. Skalli O, Pelte MF, Peclet MC, et al. Alpha-smooth muscle actin, a differentiation marker of smooth muscle cells, is present in microfilamentous bundles of pericytes. *J Histochem Cytochem*. Mar 1989;37(3):315-21. doi:10.1177/37.3.2918221
540. Fatigati V, Murphy RA. Actin and tropomyosin variants in smooth muscles. Dependence on tissue type. *J Biol Chem*. Dec 10 1984;259(23):14383-8.
541. Wang J, Zohar R, McCulloch CA. Multiple roles of alpha-smooth muscle actin in mechanotransduction. *Exp Cell Res*. Feb 1 2006;312(3):205-14. doi:10.1016/j.yexcr.2005.11.004
542. Jaminon A, Reesink K, Kroon A, Schurgers L. The Role of Vascular Smooth Muscle Cells in Arterial Remodeling: Focus on Calcification-Related Processes. *International journal of molecular sciences*. 2019;20(22):5694. doi:10.3390/ijms20225694
543. Dominguez R, Holmes KC. Actin Structure and Function. *Annual Review of Biophysics*. 2011/06/09 2011;40(1):169-186. doi:10.1146/annurev-biophys-042910-155359
544. Wang N. Mechanical interactions among cytoskeletal filaments. *Hypertension*. Jul 1998;32(1):162-5. doi:10.1161/01.hyp.32.1.162
545. Okuda S, Languino LR, Ruoslahti E, Border WA. Elevated expression of transforming growth factor-beta and proteoglycan production in experimental glomerulonephritis. Possible role in expansion of the mesangial extracellular matrix. *J Clin Invest*. Aug 1990;86(2):453-62. doi:10.1172/jci114731
546. Rees JR, Onwuegbusi BA, Save VE, Alderson D, Fitzgerald RC. In vivo and in vitro evidence for transforming growth factor-beta1-mediated epithelial to mesenchymal transition in esophageal adenocarcinoma. *Cancer Res*. Oct 1 2006;66(19):9583-90. doi:10.1158/0008-5472.can-06-1842
547. Moses HL, Roberts AB, Derynck R. The Discovery and Early Days of TGF-β: A Historical Perspective. *Cold Spring Harbor perspectives in biology*. 2016;8(7):a021865. doi:10.1101/cshperspect.a021865
548. Border WA, Ruoslahti E. Transforming growth factor-beta 1 induces extracellular matrix formation in glomerulonephritis. *Cell Differ Dev*. Dec 2 1990;32(3):425-31. doi:10.1016/0922-3371(90)90059-6

549. Baune BT, Rothermundt M, Ladwig KH, Meisinger C, Berger K. Systemic inflammation (Interleukin 6) predicts all-cause mortality in men: results from a 9-year follow-up of the MEMO Study. *AGE*. 2011/06/01 2011;33(2):209-217. doi:10.1007/s11357-010-9165-5
550. Zhu D, Mackenzie NC, Millán JL, Farquharson C, MacRae VE. The appearance and modulation of osteocyte marker expression during calcification of vascular smooth muscle cells. *PLoS One*. 2011;6(5):e19595. doi:10.1371/journal.pone.0019595
551. Ponnusamy A, Sinha S, Hyde GD, et al. FTI-277 inhibits smooth muscle cell calcification by up-regulating PI3K/Akt signaling and inhibiting apoptosis. *PLoS One*. 2018;13(4):e0196232. doi:10.1371/journal.pone.0196232
552. Patel JJ, Zhu D, Opdebeeck B, et al. Inhibition of arterial medial calcification and bone mineralization by extracellular nucleotides: The same functional effect mediated by different cellular mechanisms. *J Cell Physiol*. Apr 2018;233(4):3230-3243. doi:10.1002/jcp.26166
553. Willems BA, Furmanik M, Caron MMJ, et al. Ucma/GRP inhibits phosphate-induced vascular smooth muscle cell calcification via SMAD-dependent BMP signalling. *Sci Rep*. Mar 21 2018;8(1):4961. doi:10.1038/s41598-018-23353-y
554. Shioi A, Nishizawa Y, Jono S, Koyama H, Hosoi M, Morii H. Beta-glycerophosphate accelerates calcification in cultured bovine vascular smooth muscle cells. *Arterioscler Thromb Vasc Biol*. Nov 1995;15(11):2003-9. doi:10.1161/01.atv.15.11.2003
555. Alesutan I, Moritz F, Haider T, et al. Impact of β-glycerophosphate on the bioenergetic profile of vascular smooth muscle cells. *J Mol Med (Berl)*. Jul 2020;98(7):985-997. doi:10.1007/s00109-020-01925-8
556. Ciceri P, Volpi E, Brenna I, et al. Combined effects of ascorbic acid and phosphate on rat VSMC osteoblastic differentiation. *Nephrology Dialysis Transplantation*. 2012;27(1):122-127. doi:10.1093/ndt/gfr284
557. Tzaphlidou M. Bone architecture: collagen structure and calcium/phosphorus maps. *J Biol Phys*. Apr 2008;34(1-2):39-49. doi:10.1007/s10867-008-9115-y
558. Mori K, Shioi A, Jono S, Nishizawa Y, Morii H. Dexamethasone enhances In vitro vascular calcification by promoting osteoblastic differentiation of vascular smooth muscle cells. *Arterioscler Thromb Vasc Biol*. Sep 1999;19(9):2112-8. doi:10.1161/01.atv.19.9.2112
559. Li Q-x, Li Z-y, Liu L, et al. Dexamethasone causes calcium deposition and degeneration in human anterior cruciate ligament cells through endoplasmic reticulum stress. *Biochemical Pharmacology*. 2020/05/01/ 2020;175:113918. doi:https://doi.org/10.1016/j.bcp.2020.113918
560. Idelevich A, Rais Y, Monsonego-Ornan E. Bone Gla protein increases HIF-1alpha-dependent glucose metabolism and induces cartilage and vascular calcification. *Arterioscler Thromb Vasc Biol*. Sep 2011;31(9):e55-71. doi:10.1161/atvbaha.111.230904
561. Orriss IR, Taylor SE, Arnett TR. Rat osteoblast cultures. *Methods Mol Biol*. 2012;816:31-41. doi:10.1007/978-1-61779-415-5_3
562. Proudfoot D, Skepper JN, Hegyi L, Bennett MR, Shanahan CM, Weissberg PL. Apoptosis Regulates Human Vascular Calcification In Vitro. *Circulation Research*. 2000/11/24 2000;87(11):1055-1062. doi:10.1161/01.RES.87.11.1055
563. Clausen MJ, Poulsen H. Sodium/Potassium homeostasis in the cell. *Met Ions Life Sci*. 2013;12:41-67. doi:10.1007/978-94-007-5561-1_3
564. Pivovarov AS, Calahorro F, Walker RJ. Na(+)/K(+)-pump and neurotransmitter membrane receptors. *Invert Neurosci*. Nov 28 2018;19(1):1. doi:10.1007/s10158-018-0221-7
565. Blair HC, Larrouture QC, Tourkova IL, et al. Support of bone mineral deposition by regulation of pH. *American Journal of Physiology-Cell Physiology*. 2018/10/01 2018;315(4):C587-C597. doi:10.1152/ajpcell.00056.2018
566. Galow AM, Rebl A, Koczan D, Bonk SM, Baumann W, Gimsa J. Increased osteoblast viability at alkaline pH in vitro provides a new perspective on bone regeneration. *Biochem Biophys Rep*. Jul 2017;10:17-25. doi:10.1016/j.bbrep.2017.02.001

567. Zhao Y, Sun Q, Wang S, Huo B. Spreading Shape and Area Regulate the Osteogenesis of Mesenchymal Stem Cells. *Tissue Eng Regen Med*. Dec 2019;16(6):573-583. doi:10.1007/s13770-019-00213-y
568. Ciceri P, Elli F, Braidotti P, et al. Iron citrate reduces high phosphate-induced vascular calcification by inhibiting apoptosis. *Atherosclerosis*. Nov 2016;254:93-101. doi:10.1016/j.atherosclerosis.2016.09.071
569. Huang J, Huang H, Wu M, et al. Connective tissue growth factor induces osteogenic differentiation of vascular smooth muscle cells through ERK signaling. *Int J Mol Med*. Aug 2013;32(2):423-9. doi:10.3892/ijmm.2013.1398
570. Patel JJ, Bourne LE, Davies BK, et al. Differing calcification processes in cultured vascular smooth muscle cells and osteoblasts. *Experimental cell research*. 2019;380(1):100-113. doi:10.1016/j.yexcr.2019.04.020
571. Wasteson P, Johansson BR, Jukkola T, et al. Developmental origin of smooth muscle cells in the descending aorta in mice. *Development*. May 2008;135(10):1823-32. doi:10.1242/dev.020958
572. Kilian KA, Bugarija B, Lahn BT, Mrksich M. Geometric cues for directing the differentiation of mesenchymal stem cells. *Proc Natl Acad Sci U S A*. Mar 16 2010;107(11):4872-7. doi:10.1073/pnas.0903269107
573. Desjardins M-P, Sidibé A, Fortier C, et al. Association of interleukin-6 with aortic stiffness in end-stage renal disease. *Journal of the American Society of Hypertension*. 2018/01/01/ 2018;12(1):5-13. doi:https://doi.org/10.1016/j.jash.2017.09.013
574. Jian B, Narula N, Li QY, Mohler ER, 3rd, Levy RJ. Progression of aortic valve stenosis: TGF-beta1 is present in calcified aortic valve cusps and promotes aortic valve interstitial cell calcification via apoptosis. *Ann Thorac Surg*. Feb 2003;75(2):457-65; discussion 465-6. doi:10.1016/s0003-4975(02)04312-6
575. Watson KE, Boström K, Ravindranath R, Lam T, Norton B, Demer LL. TGF-beta 1 and 25-hydroxycholesterol stimulate osteoblast-like vascular cells to calcify. *The Journal of clinical investigation*. 1994;93(5):2106-2113.
576. Grainger DJ, Metcalfe JC, Grace AA, Mosedale DE. Transforming growth factor-beta dynamically regulates vascular smooth muscle differentiation in vivo. *J Cell Sci*. Oct 1998;111 (Pt 19):2977-88. doi:10.1242/jcs.111.19.2977
577. Kong Y, Liang Q, Chen Y, et al. Hyaluronan negatively regulates vascular calcification involving BMP2 signaling. *Laboratory Investigation*. 2018/10/01 2018;98(10):1320-1332. doi:10.1038/s41374-018-0076-x
578. Lauer ME, Cheng G, Swaidani S, Aronica MA, Weigel PH, Hascall VC. Tumor necrosis factor-stimulated gene-6 (TSG-6) amplifies hyaluronan synthesis by airway smooth muscle cells. *J Biol Chem*. Jan 4 2013;288(1):423-31. doi:10.1074/jbc.M112.389882
579. Ang LC, Zhang Y, Cao L, et al. Versican enhances locomotion of astrocytoma cells and reduces cell adhesion through its G1 domain. *J Neuropathol Exp Neurol*. Jun 1999;58(6):597-605. doi:10.1097/00005072-199906000-00004
580. Nakamura T, Takagaki K, Shibata S, Tanaka K, Higuchi T, Endo M. Hyaluronic-acid-deficient extracellular matrix induced by addition of 4-methylumbelliferone to the medium of cultured human skin fibroblasts. *Biochem Biophys Res Commun*. Mar 17 1995;208(2):470-5. doi:10.1006/bbrc.1995.1362
581. Morohashi H, Kon A, Nakai M, et al. Study of hyaluronan synthase inhibitor, 4-methylumbelliferone derivatives on human pancreatic cancer cell (KP1-NL). *Biochem Biophys Res Commun*. Jul 14 2006;345(4):1454-9. doi:10.1016/j.bbrc.2006.05.037
582. Yoshihara S, Kon A, Kudo D, et al. A hyaluronan synthase suppressor, 4-methylumbelliferone, inhibits liver metastasis of melanoma cells. *FEBS Lett*. May 9 2005;579(12):2722-6. doi:10.1016/j.febslet.2005.03.079

583. Kolar SL, Kyme P, Tseng CW, et al. Group B Streptococcus Evades Host Immunity by Degrading Hyaluronan. *Cell Host Microbe*. Dec 9 2015;18(6):694-704. doi:10.1016/j.chom.2015.11.001
584. Li S, Kelly SJ, Lamani E, Ferraroni M, Jedrzejas MJ. Structural basis of hyaluronan degradation by Streptococcus pneumoniae hyaluronate lyase. *Embo j*. Mar 15 2000;19(6):1228-40. doi:10.1093/emboj/19.6.1228
585. Fülöp C, Szántó S, Mukhopadhyay D, et al. Impaired cumulus mucification and female sterility in tumor necrosis factor-induced protein-6 deficient mice. *Development*. May 2003;130(10):2253-61. doi:10.1242/dev.00422
586. Lesley J, English NM, Gál I, Mikecz K, Day AJ, Hyman R. Hyaluronan binding properties of a CD44 chimera containing the link module of TSG-6. *J Biol Chem*. Jul 19 2002;277(29):26600-8. doi:10.1074/jbc.M201068200
587. Ochsner SA, Day AJ, Rugg MS, Breyer RM, Gomer RH, Richards JS. Disrupted function of tumor necrosis factor-alpha-stimulated gene 6 blocks cumulus cell-oocyte complex expansion. *Endocrinology*. Oct 2003;144(10):4376-84. doi:10.1210/en.2003-0487
588. de la Motte CA, Hascall VC, Drazba JA, Strong SA. Poly I: C induces mononuclear leukocyte-adhesive hyaluronan structures on colon smooth muscle cells: IαI and versican facilitate adhesion. *Hyaluronan*. Elsevier; 2002:381-388.
589. Parkar AA, Day AJ. Overlapping sites on the Link module of human TSG-6 mediate binding to hyaluronan and chrondroitin-4-sulphate. *FEBS Lett*. Jun 30 1997;410(2-3):413-7. doi:10.1016/s0014-5793(97)00621-2
590. Wisniewski HG, Snitkin ES, Mindrescu C, Sweet MH, Vilcek J. TSG-6 protein binding to glycosaminoglycans: formation of stable complexes with hyaluronan and binding to chondroitin sulfates. *J Biol Chem*. Apr 15 2005;280(15):14476-84. doi:10.1074/jbc.M411734200
591. Li H, Guo L, Li JW, Liu N, Qi R, Liu J. Expression of hyaluronan receptors CD44 and RHAMM in stomach cancers: relevance with tumor progression. *Int J Oncol*. Nov 2000;17(5):927-32.
592. Culty M, Nguyen HA, Underhill CB. The hyaluronan receptor (CD44) participates in the uptake and degradation of hyaluronan. *J Cell Biol*. Feb 1992;116(4):1055-62. doi:10.1083/jcb.116.4.1055
593. Nurwidya F, Takahashi F, Kato M, et al. CD44 silencing decreases the expression of stem cell-related factors induced by transforming growth factor β1 and tumor necrosis factor α in lung cancer: Preliminary findings. *Bosnian journal of basic medical sciences*. 2017;17(3):228-234. doi:10.17305/bjbms.2017.1966
594. Kooman JP, Kotanko P, Schols AM, Shiels PG, Stenvinkel P. Chronic kidney disease and premature ageing. *Nat Rev Nephrol*. Dec 2014;10(12):732-42. doi:10.1038/nrneph.2014.185
595. Shanahan CM. Mechanisms of vascular calcification in CKD-evidence for premature ageing? *Nat Rev Nephrol*. Nov 2013;9(11):661-70. doi:10.1038/nrneph.2013.176
596. Schwarz U, Buzello M, Ritz E, et al. Morphology of coronary atherosclerotic lesions in patients with end-stage renal failure. *Nephrol Dial Transplant*. Feb 2000;15(2):218-23. doi:10.1093/ndt/15.2.218
597. Ibels LS, Alfrey AC, Huffer WE, Craswell PW, Anderson JT, Weil R, 3rd. Arterial calcification and pathology in uremic patients undergoing dialysis. *Am J Med*. May 1979;66(5):790-6. doi:10.1016/0002-9343(79)91118-5
598. London GM, Guérin AP, Marchais SJ, Métivier F, Pannier B, Adda H. Arterial media calcification in end-stage renal disease: impact on all-cause and cardiovascular mortality. *Nephrol Dial Transplant*. Sep 2003;18(9):1731-40. doi:10.1093/ndt/gfg414
599. Mizobuchi M, Towler D, Slatopolsky E. Vascular calcification: the killer of patients with chronic kidney disease. *J Am Soc Nephrol*. Jul 2009;20(7):1453-64. doi:10.1681/asn.2008070692
600. Rosenhek R, Binder T, Porenta G, et al. Predictors of outcome in severe, asymptomatic aortic stenosis. *N Engl J Med*. Aug 31 2000;343(9):611-7. doi:10.1056/nejm200008313430903

601. Raggi P, Shaw LJ, Berman DS, Callister TQ. Prognostic value of coronary artery calcium screening in subjects with and without diabetes. *J Am Coll Cardiol*. May 5 2004;43(9):1663-9. doi:10.1016/j.jacc.2003.09.068
602. Cozzolino M, Mangano M, Galassi A, Ciceri P, Messa P, Nigwekar S. Vitamin K in Chronic Kidney Disease. *Nutrients*. Jan 14 2019;11(1)doi:10.3390/nu11010168
603. Popa DS, Bigman G, Rusu ME. The Role of Vitamin K in Humans: Implication in Aging and Age-Associated Diseases. *Antioxidants (Basel)*. Apr 6 2021;10(4)doi:10.3390/antiox10040566
604. Dalmeijer GW, van der Schouw YT, Magdeleyns EJ, et al. Circulating desphospho-uncarboxylated matrix γ-carboxyglutamate protein and the risk of coronary heart disease and stroke. *J Thromb Haemost*. Jul 2014;12(7):1028-34. doi:10.1111/jth.12609
605. Dalmeijer GW, van der Schouw YT, Magdeleyns EJ, et al. Matrix Gla protein species and risk of cardiovascular events in type 2 diabetic patients. *Diabetes Care*. Nov 2013;36(11):3766-71. doi:10.2337/dc13-0065
606. Vissers LET, Dalmeijer GW, Boer JMA, Verschuren WMM, van der Schouw YT, Beulens JWJ. The relationship between vitamin K and peripheral arterial disease. *Atherosclerosis*. Sep 2016;252:15-20. doi:10.1016/j.atherosclerosis.2016.07.915
607. Geleijnse JM, Vermeer C, Grobbee DE, et al. Dietary intake of menaquinone is associated with a reduced risk of coronary heart disease: the Rotterdam Study. *The Journal of nutrition*. 2004;134(11):3100-3105.
608. Efsa Panel on Dietetic Products NaA, Turck D, Bresson JL, et al. Dietary reference values for vitamin K. *EFSA Journal*. 2017;15(5):e04780.
609. Cundiff DK, Agutter PS. Cardiovascular Disease Death Before Age 65 in 168 Countries Correlated Statistically with Biometrics, Socioeconomic Status, Tobacco, Gender, Exercise, Macronutrients, and Vitamin K. *Cureus*. Aug 24 2016;8(8):e748. doi:10.7759/cureus.748
610. Harshman SG, Shea MK. The Role of Vitamin K in Chronic Aging Diseases: Inflammation, Cardiovascular Disease, and Osteoarthritis. *Curr Nutr Rep*. Jun 2016;5(2):90-98. doi:10.1007/s13668-016-0162-x
611. Braam LA, Hoeks AP, Brouns F, Hamulyák K, Gerichhausen MJ, Vermeer C. Beneficial effects of vitamins D and K on the elastic properties of the vessel wall in postmenopausal women: a follow-up study. *Thromb Haemost*. Feb 2004;91(2):373-80. doi:10.1160/th03-07-0423
612. Vaccaro JA, Huffman FG. Phylloquinone (vitamin K1) intake and pulse pressure as a measure of arterial stiffness in older adults. *Journal of nutrition in gerontology and geriatrics*. 2013;32(3):244-257.
613. Provenzano M, Coppolino G, Faga T, Garofalo C, Serra R, Andreucci M. Epidemiology of cardiovascular risk in chronic kidney disease patients: the real silent killer. *Reviews in cardiovascular medicine*. 2019;20(4):209-220.
614. Roumeliotis S, Duni A, Vaios V, Kitsos A, Liakopoulos V, Dounousi E. Vitamin K Supplementation for Prevention of Vascular Calcification in Chronic Kidney Disease Patients: Are We There Yet? *Nutrients*. Feb 22 2022;14(5)doi:10.3390/nu14050925
615. Holden RM, Booth SL, Day AG, et al. Inhibiting the Progression of Arterial Calcification with Vitamin K in HemoDialysis Patients (iPACK-HD) Trial: Rationale and Study Design for a Randomized Trial of Vitamin K in Patients with End Stage Kidney Disease. *Canadian Journal of Kidney Health and Disease*. 2015/01/01 2015;2:53. doi:10.1186/s40697-015-0053-x
616. Haroon SW, Tai BC, Ling LH, et al. Treatment to reduce vascular calcification in hemodialysis patients using vitamin K (Trevasc-HDK): A study protocol for a randomized controlled trial. *Medicine (Baltimore)*. Sep 4 2020;99(36):e21906. doi:10.1097/md.0000000000021906
617. Krueger T, Schlieper G, Schurgers L, et al. Vitamin K1 to slow vascular calcification in haemodialysis patients (VitaVasK trial): a rationale and study protocol. *Nephrology Dialysis Transplantation*. 2014;29(9):1633-1638. doi:10.1093/ndt/gft459

618. Krüger T, Oelenberg S, Kaesler N, et al. Warfarin Induces Cardiovascular Damage in Mice. *Arteriosclerosis, Thrombosis, and Vascular Biology*. 2013/11/01 2013;33(11):2618-2624. doi:10.1161/ATVBAHA.113.302244
619. Wallin R, Wajih N, Greenwood GT, Sane DC. Arterial calcification: a review of mechanisms, animal models, and the prospects for therapy. *Med Res Rev*. Jul 2001;21(4):274-301. doi:10.1002/med.1010
620. SuttlE JW. Warfarin and vitamin K. *Clinical Cardiology*. 1990;13(S6):VI-16.
621. Fusaro M, Cianciolo G, Evenepoel P, Schurgers L, Plebani M. Vitamin K in CKD Bone Disorders. *Calcif Tissue Int*. Apr 2021;108(4):476-485. doi:10.1007/s00223-020-00792-2
622. van Ballegooijen AJ, Beulens JW. The Role of Vitamin K Status in Cardiovascular Health: Evidence from Observational and Clinical Studies. *Curr Nutr Rep*. 2017;6(3):197-205. doi:10.1007/s13668-017-0208-8
623. Shioi A, Morioka T, Shoji T, Emoto M. The Inhibitory Roles of Vitamin K in Progression of Vascular Calcification. *Nutrients*. Feb 23 2020;12(2)doi:10.3390/nu12020583
624. Gallieni M, Fusaro M. Vitamin K and cardiovascular calcification in CKD: is patient supplementation on the horizon? *Kidney Int*. Aug 2014;86(2):232-4. doi:10.1038/ki.2014.24
625. Price PA, Faus SA, Williamson MK. Warfarin causes rapid calcification of the elastic lamellae in rat arteries and heart valves. *Arterioscler Thromb Vasc Biol*. Sep 1998;18(9):1400-7. doi:10.1161/01.atv.18.9.1400
626. Beulens JW, Booth SL, van den Heuvel EG, Stoecklin E, Baka A, Vermeer C. The role of menaquinones (vitamin K_2) in human health. *Br J Nutr*. Oct 2013;110(8):1357-68. doi:10.1017/s0007114513001013
627. Schurgers LJ, Spronk HM, Soute BA, Schiffers PM, DeMey JG, Vermeer C. Regression of warfarin-induced medial elastocalcinosis by high intake of vitamin K in rats. *Blood*. Apr 1 2007;109(7):2823-31. doi:10.1182/blood-2006-07-035345
628. Van den Broek FAR, Beynen AC. The influence of dietary phosphorus and magnesium concentrations on the calcium content of heart and kidneys of DBA/2 and NMRI mice. *Laboratory animals*. 1998;32(4):483-491.
629. Eggebrecht L, Prochaska JH, Schulz A, et al. Intake of Vitamin K Antagonists and Worsening of Cardiac and Vascular Disease: Results From the Population-Based Gutenberg Health Study. *J Am Heart Assoc*. Sep 4 2018;7(17):e008650. doi:10.1161/jaha.118.008650
630. Ishibashi S, Herz J, Maeda N, Goldstein JL, Brown MS. The two-receptor model of lipoprotein clearance: tests of the hypothesis in" knockout" mice lacking the low density lipoprotein receptor, apolipoprotein E, or both proteins. *Proceedings of the National Academy of Sciences*. 1994;91(10):4431-4435.
631. Jawien J, Nastalek P, Korbut R. Mouse models of experimental atherosclerosis. *Journal of physiology and pharmacology*. 2004;55(3):503-517.
632. Reddick RL, Zhang SH, Maeda N. Atherosclerosis in mice lacking apo E. Evaluation of lesional development and progression. *Arteriosclerosis and thrombosis: a journal of vascular biology*. 1994;14(1):141-147.
633. Plump AS, Smith JD, Hayek T, et al. Severe hypercholesterolemia and atherosclerosis in apolipoprotein E-deficient mice created by homologous recombination in ES cells. *Cell*. 1992;71(2):343-353.
634. Zhang SH, Reddick RL, Piedrahita JA, Maeda N. Spontaneous hypercholesterolemia and arterial lesions in mice lacking apolipoprotein E. *Science*. 1992;258(5081):468-471.
635. Nakashima Y, Plump AS, Raines EW, Breslow JL, Ross R. ApoE-deficient mice develop lesions of all phases of atherosclerosis throughout the arterial tree. *Arteriosclerosis and thrombosis: a journal of vascular biology*. 1994;14(1):133-140.
636. Feussner G. Severe xanthomatosis associated with familial apolipoprotein E deficiency. *Journal of clinical pathology*. 1996;49(12):985-989.

637. Lohse P, Brewer 3rd HB, Meng MS, Skarlatos SI, LaRosa JC, Brewer Jr HB. Familial apolipoprotein E deficiency and type III hyperlipoproteinemia due to a premature stop codon in the apolipoprotein E gene. *Journal of lipid research*. 1992;33(11):1583-1590.
638. Mabuchi H, Itoh H, Takeda M, et al. A young type III hyperlipoproteinemic patient associated with apolipoprotein E deficiency. *Metabolism*. 1989;38(2):115-119.
639. Zhang SH, Reddick RL, Burkey B, Maeda N. Diet-induced atherosclerosis in mice heterozygous and homozygous for apolipoprotein E gene disruption. *The Journal of clinical investigation*. 1994;94(3):937-945.
640. Paigen B, Holmes PA, Mitchell D, Albee D. Comparison of atherosclerotic lesions and HDL-lipid levels in male, female, and testosterone-treated female mice from strains C57BL/6, BALB/c, and C3H. *Atherosclerosis*. Apr 1987;64(2-3):215-21. doi:10.1016/0021-9150(87)90249-8
641. Rosenfeld ME, Polinsky P, Virmani R, Kauser K, Rubanyi G, Schwartz SM. Advanced atherosclerotic lesions in the innominate artery of the ApoE knockout mouse. *Arteriosclerosis, thrombosis, and vascular biology*. 2000;20(12):2587-2592.
642. Bond AR, Jackson CL. The fat-fed apolipoprotein E knockout mouse brachiocephalic artery in the study of atherosclerotic plaque rupture. *Journal of Biomedicine and Biotechnology*. 2010;2011
643. Stylianou IM, Bauer RC, Reilly MP, Rader DJ. Genetic basis of atherosclerosis: insights from mice and humans. *Circulation research*. 2012;110(2):337-355.
644. Hopkins PN. Molecular biology of atherosclerosis. *Physiological reviews*. 2013;
645. Du J, Li J-M. BAS/BSCR23 apocynin treatment reduces high-fat diet-induced obesity and hypertension but has no significant effect on hyperglycaemia. *Heart*. 2010;96(17):e19-e19.
646. Giraud Billoud MG, Fader Kaiser CM, Agüero R, Ezquer F, Ezquer EM. Diabetic nephropathy, autophagy and proximal tubule protein endocytic transport: a potentially harmful relationship. 2018;
647. Wang AY, Wang M, Woo J, et al. Cardiac valve calcification as an important predictor for all-cause mortality and cardiovascular mortality in long-term peritoneal dialysis patients: a prospective study. *J Am Soc Nephrol*. Jan 2003;14(1):159-68. doi:10.1097/01.asn.0000038685.95946.83
648. Moe SM, O'Neill KD, Duan D, et al. Medial artery calcification in ESRD patients is associated with deposition of bone matrix proteins. *Kidney Int*. Feb 2002;61(2):638-47. doi:10.1046/j.1523-1755.2002.00170.x
649. Ejerblad S, Eriksson I, Johansson H. Uraemic arterial disease: an experimental study with special reference to the effect of parathyroidectomy. *Scandinavian journal of urology and nephrology*. 1979;13(2):161-169.
650. Ejerblad S, Eriksson I, Johansson H. Uraemic arterial disease. An experimental study with special reference to the effect of parathyroidectomy. *Scand J Urol Nephrol*. 1979;13(2):161-9. doi:10.3109/00365597909181172
651. Giachelli CM. Mechanisms of vascular calcification in uremia. Elsevier; 401-402.
652. Massy ZA, Ivanovski O, Nguyen-Khoa T, et al. Uremia Accelerates both Atherosclerosis and Arterial Calcification in Apolipoprotein E Knockout Mice. *Journal of the American Society of Nephrology*. 2005;16(1)
653. Shobeiri N, Adams MA, Holden RM. Vascular Calcification in Animal Models of CKD: A Review. *American Journal of Nephrology*. 2010;31(6):471-481. doi:10.1159/000299794
654. Huang M, Wei R, Wang Y, Su T, Li P, Chen X. The uremic toxin hippurate promotes endothelial dysfunction via the activation of Drp1-mediated mitochondrial fission. *Redox Biol*. Jun 2018;16:303-313. doi:10.1016/j.redox.2018.03.010
655. Mizobuchi M, Ogata H, Hatamura I, et al. Up-regulation of Cbfa1 and Pit-1 in calcified artery of uraemic rats with severe hyperphosphataemia and secondary hyperparathyroidism. *Nephrology Dialysis Transplantation*. 2006;21(4):911-916.
656. Koleganova N, Piecha G, Ritz E, Schmitt CP, Gross M-L. A calcimimetic (R-568), but not calcitriol, prevents vascular remodeling in uremia. *Kidney international*. 2009;75(1):60-71.

657. Zoccali C, Benedetto FA, Mallamaci F, et al. Inflammation is associated with carotid atherosclerosis in dialysis patients. Creed Investigators. Cardiovascular Risk Extended Evaluation in Dialysis Patients. *J Hypertens*. Sep 2000;18(9):1207-13. doi:10.1097/00004872-200018090-00006
658. Ferrantelli E, Liappas G, Keuning ED, et al. A Novel Mouse Model of Peritoneal Dialysis: Combination of Uraemia and Long-Term Exposure to PD Fluid. *Biomed Res Int*. 2015;2015:106902. doi:10.1155/2015/106902
659. Vlahu CA, Aten J, de Graaff M, et al. New Insights into the Effects of Chronic Kidney Failure and Dialysate Exposure on the Peritoneum. *Perit Dial Int*. 11-12 2016;36(6):614-622. doi:10.3747/pdi.2015.00204
660. Van Biesen W, Faict D, Boer W, Lameire N. Further animal and human experience with a 0.6% amino acid/1.4% glycerol peritoneal dialysis solution. *Perit Dial Int*. 1997;17 Suppl 2:S56-62.
661. Williams JD, Craig KJ, Topley N, et al. Morphologic changes in the peritoneal membrane of patients with renal disease. *J Am Soc Nephrol*. Feb 2002;13(2):470-9.
662. Krediet RT, Struijk DG. Peritoneal changes in patients on long-term peritoneal dialysis. *Nat Rev Nephrol*. Jul 2013;9(7):419-29. doi:10.1038/nrneph.2013.99
663. Dobbie JW. Peritoneal ultrastructure and changes with continuous ambulatory peritoneal dialysis. *Peritoneal dialysis international*. 1993;13(2_suppl):585-587.
664. Yao Q, Pawlaczyk K, Ayala ER, et al. The role of the TGF/Smad signaling pathway in peritoneal fibrosis induced by peritoneal dialysis solutions. *Nephron Exp Nephrol*. 2008;109(2):e71-8. doi:10.1159/000142529
665. Miller TE, Findon G, Rowe L. Characterization of an animal model of continuous peritoneal dialysis in chronic renal impairment. *Clinical nephrology*. 1992;37(1):42-47.
666. Bos HJ, Meijer F, De Veld JC, Beelen RHJ. Peritoneal dialysis ffuid induces an elicitation of mononuclear phagocytes in the rat peritoneal cavity. A cytochemical and immunological study. *Kidney Int*. 1989;36:20-26.
667. Flessner MF, Credit K, Henderson K, et al. Peritoneal changes after exposure to sterile solutions by catheter. *J Am Soc Nephrol*. Aug 2007;18(8):2294-302. doi:10.1681/asn.2006121417
668. Lai KN, Leung JCK. Inflammation in Peritoneal Dialysis. *Nephron Clinical Practice*. 2010;116(1):c11-c18. doi:10.1159/000314544
669. Li PK-T, Ng JK-C, McIntyre CW. Inflammation and Peritoneal Dialysis. *Seminars in Nephrology*. 2017/01/01/ 2017;37(1):54-65. doi:https://doi.org/10.1016/j.semnephrol.2016.10.007
670. Pajek J, Hutchison AJ, Bhutani S, et al. Outcomes of peritoneal dialysis patients and switching to hemodialysis: a competing risks analysis. *Perit Dial Int*. May 2014;34(3):289-98. doi:10.3747/pdi.2012.00248
671. Sadowitz B, Seymour K, Gahtan V, Maier KG. The role of hyaluronic acid in atherosclerosis and intimal hyperplasia. *J Surg Res*. Apr 2012;173(2):e63-72. doi:10.1016/j.jss.2011.09.025
672. Fischer JW. Role of hyaluronan in atherosclerosis: Current knowledge and open questions. *Matrix Biol*. May 2019;78-79:324-336. doi:10.1016/j.matbio.2018.03.003
673. Siiskonen H, Oikari S, Pasonen-Seppänen S, Rilla K. Hyaluronan synthase 1: a mysterious enzyme with unexpected functions. *Front Immunol*. 2015;6:43. doi:10.3389/fimmu.2015.00043
674. Pedicino D, Vinci R, Giglio Ada F, et al. Alterations of Hyaluronan Metabolism in Acute Coronary Syndrome. *Journal of the American College of Cardiology*. 2018/09/25 2018;72(13):1490-1503. doi:10.1016/j.jacc.2018.06.072
675. Senbanjo LT, Chellaiah MA. CD44: A Multifunctional Cell Surface Adhesion Receptor Is a Regulator of Progression and Metastasis of Cancer Cells. *Front Cell Dev Biol*. 2017;5:18. doi:10.3389/fcell.2017.00018
676. Bartstra JW, Mali WPTM, Spiering W, de Jong PA. Abdominal aortic calcification: from ancient friend to modern foe. *European Journal of Preventive Cardiology*. 2021;28(12):1386-1391. doi:10.1177/2047487320919895
677. Bellone F, Cinquegrani M, Nicotera R, et al. Role of Vitamin K in Chronic Kidney Disease: A Focus on Bone and Cardiovascular Health. *Int J Mol Sci*. May 9 2022;23(9)doi:10.3390/ijms23095282

678. Holden RM, Morton AR, Garland JS, Pavlov A, Day AG, Booth SL. Vitamins K and D status in stages 3–5 chronic kidney disease. *Clinical journal of the American Society of Nephrology: CJASN*. 2010;5(4):590.
679. Pilkey RM, Morton AR, Boffa MB, et al. Subclinical vitamin K deficiency in hemodialysis patients. *American journal of kidney diseases*. 2007;49(3):432-439.
680. Holden RM, Iliescu E, Morton AR, Booth SL. Vitamin K status of Canadian peritoneal dialysis patients. *Peritoneal dialysis international*. 2008;28(4):415-418.
681. Kohlmeier M, Saupe J, Shearer MJ, Schaefer K, Asmus G. Bone health of adult hemodialysis patients is related to vitamin K status. *Kidney international*. 1997;51(4):1218-1221.
682. Amann K. Media calcification and intima calcification are distinct entities in chronic kidney disease. *Clin J Am Soc Nephrol*. Nov 2008;3(6):1599-605. doi:10.2215/cjn.02120508
683. Doherty TM, Fitzpatrick LA, Inoue D, et al. Molecular, endocrine, and genetic mechanisms of arterial calcification. *Endocr Rev*. Aug 2004;25(4):629-72. doi:10.1210/er.2003-0015
684. Zhu D, Mackenzie NCW, Farquharson C, MacRae VE. Mechanisms and clinical consequences of vascular calcification. *Frontiers in endocrinology*. 2012;3:95.
685. Bro S. Cardiovascular effects of uremia in apolipoprotein E-deficient mice. *Dan Med Bull*. Nov 2009;56(4):177-92.
686. Lopez I, Aguilera-Tejero E, Mendoza FJ, et al. Calcimimetic R-568 decreases extraosseous calcifications in uremic rats treated with calcitriol. *Journal of the American Society of Nephrology*. 2006;17(3):795-804.
687. Noonan W, Koch K, Nakane M, et al. Differential effects of vitamin D receptor activators on aortic calcification and pulse wave velocity in uraemic rats. *Nephrology Dialysis Transplantation*. 2008;23(12):3824-3830.
688. Cozzolino M, Staniforth ME, Liapis H, et al. Sevelamer hydrochloride attenuates kidney and cardiovascular calcifications in long-term experimental uremia. *Kidney international*. 2003;64(5):1653-1661.
689. Kucur M, Karadag B, Isman FK, et al. Plasma hyaluronidase activity as an indicator of atherosclerosis in patients with coronary artery disease. *Bratisl Lek Listy*. 2009;110(1):21-6.
690. Marzoll A, Nagy N, Wördehoff L, et al. Cyclooxygenase inhibitors repress vascular hyaluronan-synthesis in murine atherosclerosis and neointimal thickening. *Journal of Cellular and Molecular Medicine*. 2009;13(9b):3713-3719.
691. Zhu L, Li Q, Qi D, et al. Atherosclerosis-associated endothelial cell apoptosis by miRNA let7-b-mediated downregulation of HAS-2. *Journal of Cellular Biochemistry*. 2020/08/01 2020;121(8-9):3961-3972. doi:https://doi.org/10.1002/jcb.29537
692. Ruiz P, Schwärzler C, Günthert U. CD44 isoforms during differentiation and development. *BioEssays*. 1995/01/01 1995;17(1):17-24. doi:https://doi.org/10.1002/bies.950170106
693. Watanabe R, Sato Y, Ozawa N, Takahashi Y, Koba S, Watanabe T. Emerging Roles of Tumor Necrosis Factor-Stimulated Gene-6 in the Pathophysiology and Treatment of Atherosclerosis. *Int J Mol Sci*. Feb 5 2018;19(2)doi:10.3390/ijms19020465
694. Wight TN. Provisional matrix: A role for versican and hyaluronan. *Matrix biology : journal of the International Society for Matrix Biology*. 2017;60-61:38-56. doi:10.1016/j.matbio.2016.12.001
695. Polonsky TS, McClelland RL, Jorgensen NW, et al. Coronary artery calcium score and risk classification for coronary heart disease prediction. *Jama*. Apr 28 2010;303(16):1610-6. doi:10.1001/jama.2010.461
696. Reaven PD, Sacks J. Coronary artery and abdominal aortic calcification are associated with cardiovascular disease in type 2 diabetes. *Diabetologia*. Feb 2005;48(2):379-85. doi:10.1007/s00125-004-1640-z
697. Kraus MA, Kalra PA, Hunter J, Menoyo J, Stankus N. The prevalence of vascular calcification in patients with end-stage renal disease on hemodialysis: a cross-sectional observational study. *Ther Adv Chronic Dis*. May 2015;6(3):84-96. doi:10.1177/2040622315578654

698. Rocha-Singh KJ, Zeller T, Jaff MR. Peripheral arterial calcification: prevalence, mechanism, detection, and clinical implications. *Catheter Cardiovasc Interv*. May 1 2014;83(6):E212-20. doi:10.1002/ccd.25387
699. Kataoka Y, Puri R, Hammadah M, et al. Spotty calcification and plaque vulnerability in vivo: frequency-domain optical coherence tomography analysis. *Cardiovasc Diagn Ther*. Dec 2014;4(6):460-9. doi:10.3978/j.issn.2223-3652.2014.11.06
700. Kataoka Y, Wolski K, Uno K, et al. Spotty calcification as a marker of accelerated progression of coronary atherosclerosis: insights from serial intravascular ultrasound. *J Am Coll Cardiol*. May 1 2012;59(18):1592-7. doi:10.1016/j.jacc.2012.03.012
701. Sangiorgi G, Rumberger JA, Severson A, et al. Arterial calcification and not lumen stenosis is highly correlated with atherosclerotic plaque burden in humans: a histologic study of 723 coronary artery segments using nondecalcifying methodology. *J Am Coll Cardiol*. Jan 1998;31(1):126-33. doi:10.1016/s0735-1097(97)00443-9
702. Arad Y, Goodman KJ, Roth M, Newstein D, Guerci AD. Coronary calcification, coronary disease risk factors, C-reactive protein, and atherosclerotic cardiovascular disease events: the St. Francis Heart Study. *J Am Coll Cardiol*. Jul 5 2005;46(1):158-65. doi:10.1016/j.jacc.2005.02.088
703. Willems BA, Vermeer C, Reutelingsperger CP, Schurgers LJ. The realm of vitamin K dependent proteins: shifting from coagulation toward calcification. *Mol Nutr Food Res*. Aug 2014;58(8):1620-35. doi:10.1002/mnfr.201300743
704. Lee HY, Lim S, Park S. Role of Inflammation in Arterial Calcification. *Korean Circ J*. Feb 2021;51(2):114-125. doi:10.4070/kcj.2020.0517
705. Roijers RB, Debernardi N, Cleutjens JP, Schurgers LJ, Mutsaers PH, van der Vusse GJ. Microcalcifications in early intimal lesions of atherosclerotic human coronary arteries. *Am J Pathol*. Jun 2011;178(6):2879-87. doi:10.1016/j.ajpath.2011.02.004
706. Voelkl J, Egli-Spichtig D, Alesutan I, Wagner CA. Inflammation: a putative link between phosphate metabolism and cardiovascular disease. *Clin Sci (Lond)*. Jan 15 2021;135(1):201-227. doi:10.1042/cs20190895
707. Nadra I, Mason JC, Philippidis P, et al. Proinflammatory activation of macrophages by basic calcium phosphate crystals via protein kinase C and MAP kinase pathways: a vicious cycle of inflammation and arterial calcification? *Circ Res*. Jun 24 2005;96(12):1248-56. doi:10.1161/01.RES.0000171451.88616.c2
708. Al-Aly Z. Medial vascular calcification in diabetes mellitus and chronic kidney disease: the role of inflammation. *Cardiovasc Hematol Disord Drug Targets*. Mar 2007;7(1):1-6. doi:10.2174/187152907780059047
709. Bai W, Li J, Liu J. Serum phosphorus, cardiovascular and all-cause mortality in the general population: A meta-analysis. *Clin Chim Acta*. Oct 1 2016;461:76-82. doi:10.1016/j.cca.2016.07.020
710. Bellasi A, Mandreoli M, Baldrati L, et al. Chronic kidney disease progression and outcome according to serum phosphorus in mild-to-moderate kidney dysfunction. *Clin J Am Soc Nephrol*. Apr 2011;6(4):883-91. doi:10.2215/cjn.07810910
711. Koos R, Mahnken AH, Mühlenbruch G, et al. Relation of oral anticoagulation to cardiac valvular and coronary calcium assessed by multislice spiral computed tomography. *Am J Cardiol*. Sep 15 2005;96(6):747-9. doi:10.1016/j.amjcard.2005.05.014
712. Chatrou ML, Winckers K, Hackeng TM, Reutelingsperger CP, Schurgers LJ. Vascular calcification: the price to pay for anticoagulation therapy with vitamin K-antagonists. *Blood Rev*. Jul 2012;26(4):155-66. doi:10.1016/j.blre.2012.03.002
713. Peeters F, Dudink E, Kimenai DM, et al. Vitamin K Antagonists, Non-Vitamin K Antagonist Oral Anticoagulants, and Vascular Calcification in Patients with Atrial Fibrillation. *TH Open*. Oct 2018;2(4):e391-e398. doi:10.1055/s-0038-1675578
714. Chang JR, Guo J, Wang Y, et al. Intermedin1-53 attenuates vascular calcification in rats with chronic kidney disease by upregulation of α-Klotho. *Kidney Int*. Mar 2016;89(3):586-600. doi:10.1016/j.kint.2015.12.029

715. Lin ME, Chen TM, Wallingford MC, et al. Runx2 deletion in smooth muscle cells inhibits vascular osteochondrogenesis and calcification but not atherosclerotic lesion formation. *Cardiovasc Res*. Nov 1 2016;112(2):606-616. doi:10.1093/cvr/cvw205
716. Lovekamp J, Vyavahare N. Periodate-mediated glycosaminoglycan stabilization in bioprosthetic heart valves. *J Biomed Mater Res*. Sep 15 2001;56(4):478-86. doi:10.1002/1097-4636(20010915)56:4<478::aid-jbm1119>3.0.co;2-c
717. Ohri R, Hahn SK, Hoffman AS, Stayton PS, Giachelli CM. Hyaluronic acid grafting mitigates calcification of glutaraldehyde-fixed bovine pericardium. *J Biomed Mater Res A*. Aug 1 2004;70(2):328-34. doi:10.1002/jbm.a.30088
718. Yan J, Stringer SE, Hamilton A, et al. Decorin GAG synthesis and TGF-β signaling mediate Ox-LDL-induced mineralization of human vascular smooth muscle cells. *Arterioscler Thromb Vasc Biol*. Mar 2011;31(3):608-15. doi:10.1161/atvbaha.110.220749
719. Kaneko K, Higuchi C, Kunugiza Y, et al. Hyaluronan inhibits BMP-induced osteoblast differentiation. *FEBS Lett*. Feb 13 2015;589(4):447-54. doi:10.1016/j.febslet.2014.12.031
720. Nandadasa S, O'Donnell A, Murao A, et al. The versican-hyaluronan complex provides an essential extracellular matrix niche for Flk1(+) hematoendothelial progenitors. *Matrix biology : journal of the International Society for Matrix Biology*. 2021;97:40-57. doi:10.1016/j.matbio.2021.01.002
721. Nikkari ST, Järveläinen HT, Wight TN, Ferguson M, Clowes AW. Smooth muscle cell expression of extracellular matrix genes after arterial injury. *Am J Pathol*. Jun 1994;144(6):1348-56.
722. Matsuura R, Isaka N, Imanaka-Yoshida K, Yoshida T, Sakakura T, Nakano T. Deposition of PG-M/versican is a major cause of human coronary restenosis after percutaneous transluminal coronary angioplasty. *J Pathol*. Nov 1996;180(3):311-6. doi:10.1002/(sici)1096-9896(199611)180:3<311::aid-path657>3.0.co;2-b
723. Wight TN, Lara S, Riessen R, Le Baron R, Isner J. Selective deposits of versican in the extracellular matrix of restenotic lesions from human peripheral arteries. *Am J Pathol*. Oct 1997;151(4):963-73.
724. Papakonstantinou E, Kouri FM, Karakiulakis G, Klagas I, Eickelberg O. Increased hyaluronic acid content in idiopathic pulmonary arterial hypertension. *Eur Respir J*. Dec 2008;32(6):1504-12. doi:10.1183/09031936.00159507
725. Tian X, Wang X, Shi Z, et al. Tumor necrosis factor-stimulated gene-6-a new serum identification marker to identify severe and symptomatic carotid artery stenosis. *Pathol Res Pract*. Apr 2022;232:153838. doi:10.1016/j.prp.2022.153838
726. Wight TN, Merrilees MJ. Proteoglycans in atherosclerosis and restenosis: key roles for versican. *Circ Res*. May 14 2004;94(9):1158-67. doi:10.1161/01.res.0000126921.29919.51